CASCADE - A framework for modeling fluvial sediment connectivity and its application for designing low impact hydropower portfolios

Politecnico di Milano
Doctoral Progam in Information Technology

Doctoral Dissertation of
Rafael J. P. Schmitt

Supervisor
Andrea Castelletti

Co-Supervisor
Simone Bizzi

POLITECNICO
MILANO 1863

SCHMITT CASCADE - A framework for modeling fluvial sediment connectivity

Chi
Mun
Thailand
Cambodia
Lao
Cambodia
Mekong
Tonle Sap
Sen
Se Kong
Se San
Sre Pok
Cambodia
Vietnam

POLITECNICO DI MILANO
DEPARTMENT OF ELECTRONICS, INFORMATION, AND BIOENGINEERING
DOCTORAL PROGRAM IN INFORMATION TECHNOLOGY

CASCADE - A FRAMEWORK FOR MODELING FLUVIAL SEDIMENT CONNECTIVITY AND ITS APPLICATION FOR DESIGNING LOW IMPACT HYDROPOWER PORTFOLIOS

Doctoral Dissertation of:
Rafael J. P. Schmitt

Supervisor:
Prof. Dr. Andrea F. Castelletti
Co-Supervisor:
Dr. Simone Bizzi

Tutor:
Prof. Dr. Paolo Bolzern

The Chair of the Doctoral Program:
Prof. Dr. Andrea Bonarini

Title Page: Visualizing sediment connectivity for the Se Kong, Se San, Sre Pok (3S) River basin, a major tributary system of the Mekong River. Sediment connectivity was modelled for that basin applying the CASCADE modeling framework (see chapter 3) using an inverse approach for model initialization (see chapter 5). Each curved line represents the transport of sediment from one of many sediment sources through the river network to the basin outlet. Colors from blue to yellow indicate different, increasing, sediment fluxes from each source. The 3S basin is currently subject to major hydroelectric dam developments, likely to trap the majority of sediment changing the pattern and magnitude of sediment connectivity in the 3S basin, and sediment delivery to the lower Mekong River, the Tonle Sap lake, and the Mekong Delta (see chapter 6).

Abstract

Human activities, and especially dam constructions, have altered water and sediment fluxes in river basins with an unprecedented rate over the last decades. The resulting changes in river and delta processes pose a risk to river, floodplain, and coastal ecosystems and human livelihoods. While fluvial sediment transfers act on network-scales, impact assessments of dam sediment trapping (regarding downstream impacts and storage loss in reservoirs) and economic benefits focus commonly on single dam sites. Such local approaches omit the connected functioning of fluvial sediment transfers and the resulting network-scale trade-offs between dam economic benefits and cumulative sediment trapping of dams. Such analyses would require sediment data and models to evaluate future impacts of dams on network-scale sediment transport. However, neither sediment data nor numerical sediment transport models are commonly available on network scales.

Within this context, the thesis sets out to answer the research questions of what would be optimal trade-offs between dam sediment trapping and economic hydropower benefits in large river systems? To answer this research question, the objectives of this thesis are 1) developing a network-scale sediment transport and connectivity model, 2) test its application for various, data scarce river basins with various initialization strategies and evaluate the robustness of results, and, 3) apply the model for quantifying cumulative dam sediment trapping and network-scale trade-offs between sediment trapping and hydroelectric production.

First, we introduce a numerical modeling framework for connected sediment transfers on the scale of large river networks. The CASCADE (CAtchment Sediment Connectivity and DElivery) framework is a parsimonious statistical framework coupling network scale, grain-size specific sediment

budgets with recent concepts of sediment connectivity. Analyzing sediment connectivity in two major Asian river basins (Da River, 50570 km^2 and Se Kong, Se San, Sre Pok (3S) Rivers, 82500 km^2) quantified how sediment connectivity is a multi-scale, multi-domain property of river systems driven by the spatial distribution and properties of sediment supply and fluvial transport processes. Such information was so far available in qualitative terms, mostly, and only for smaller, well monitored rivers. CASCADE can be parameterized deterministically based on remotely sensed data using hydro-morphologic equilibrium considerations for large and data-scarce river systems. However, we also show how CASCADE allows to implement network-scale stochastic modeling for the 3S basin. Such stochastic modeling allows to dis-aggregate point observations of sediment flux and grain size into spatially distributed estimates of grain sizes and supply from many sediment sources to the river network via an inverse Monte Carlo Approach. This source information is used to model sediment flux and grain size composition in the entire river network .

One key result is that sediment transport is spatially highly heterogeneous. This heterogeneity, which is derived from the CASCADE framework and validated with other lines of evidence, is observed for both case studies. This poses the opportunity to minimize dam sediment trapping by placing dams in parts of the networks where sediment transport is naturally low compared to the hydro-power potential. To analyse impacts of hydropower developments, we add a simplified model of reservoir hydraulics to CASCADE and analyze actual and hypothetical hydro-power development strategies for the 3S rivers. Developing all hydro-power dams will reduce total sediment flux from the 3S by more than 90 %. Nearly 60 % of this reduction are attributable to a single dam site. We then introduce a network scale analysis of dam portfolios (i.e., different combinations of the proposed dam sites). The aim of this analysis is to identify optimal trade-offs between dam hydro-power production, production costs, and sediment trapping. We find that, because of the spatial heterogeneity in sediment transfers, very similar hydropower production levels can be reached for very different levels of sediment trapping in function of how dams are placed within the river network. In the basin under study, up to 70 % of the hydro-power potential could have been developed with a minor (20 %) reduction in sediment flux. Additionally, using an empirical model for hydro-power production costs, we find that there is a strong synergy between providing cheap hydro-power and reducing dam sediment trapping on network scales.

To conclude, CASCADE enables analysing and quantifying connected sediment transfers from a whole-network perspective. We provide evidence for how this novel information can be used to identify optimal dam portfolios

that minimize trade-offs between hydropower production and sediment trapping in dams. Such a strategic planning of hydropower portfolios is advantageous from an environmental and economic perspective, and poses major potential for reducing impacts of future hydro-power developments on large river systems.

Parts of this thesis have appeared or are about to appear in the following publications:

- Schmitt, R.J.P., Bizzi, S., Castelletti, A., 2016. Tracking multiple sediment cascades at the river network scale identifies controls and emerging patterns of sediment connectivity. Water Resour. Res. 3941–3965. doi:10.1002/2015WR018097
- Schmitt, R.J.P., Bizzi, S., Castelletti, A., , 2015. Process based classification of sediment connectivity at the river basin scale. In: Novel Approaches to Assess and Rehabilitate Modified Rivers. Proceedings of the REFORM International Conference on River and Stream Restoration, Wageningen, NL.
- Schmitt, R.J.P., Bizzi, S., Castelletti, A., Kondolf, G.M., (IN REVIEW). Inverse connectivity modeling for reconstructing sediment provenance and sediment fluxes in unmonitored river tributaries. Journal of Geophysical Research: Earth Surface.
- Schmitt, R.J.P., Bizzi, S., Castelletti, A., Kondolf, G.M., (IN PREPARATION). Strategic hydro-power planning trades-off network sediment connectivity and hydro-power generation in the transboundary Se Kong,Se San, Sre Pok River Basin.

Acknowledgments

Foremost, I would like to thank my supervisors at Politecnico di Milano, Professor. Dr. Andrea Castelletti and Dr. Simone Bizzi. Professor Castelletti enabled this work at the intersection of river morphology and water resources management. I highly appreciate the guidance and resources he provided. My sincere gratitude is expressed to Dr. Simone Bizzi for his invaluable inputs shaping this research and his mentoring and deep involvement in my work. Both made this research truly inspirational.

In addition, I would like to express my appreciation to Professor Dr. G. Mathias Kondolf for the research opportunity at the University of California, Berkeley. His inputs and wide perspective on river management were crucial to develop the final two chapters of this thesis. I would like to thank Dr. Zan Rubin for our discussion and his constructive critique during my stay at UC Berkeley.

Prof. Dr. John Pitlick, University of Colorado, Boulder, and Prof. Dr. Peter Molnar, ETH Zurich, are acknowledged for their insightful and constructive reviews that were of great value for finalizing this thesis.

This research was made possible in part by a scholarship of the German National Academic foundation. The project *"Integrated and sustainable water Management of Red-Thai Binh Rivers System in changing climate"* (IMRR) provided data for the case study on the Da River. Professor. Dr. Tom Cochrane and his group is acknowledged for making their data and results publicly available, which enabled extending my work to the Mekong River Basin.

Lastly, I would like to thank my parents and grandparents who always supported my pursuits and Zelda and all my dear friends who encouraged me during this research.

Thesis summary and overview

THIS thesis expands approaches such as integrated water resources or river basin management (IWRM, IRMB) to include river hydro-morphology to the scale of major river basins. We focus on large river basins in emerging economies. It is in these settings, where increasing populations, climate change, and progressing industrialization results in an increasing water and energy demand. A typical response to these challenges is the construction of dams and reservoirs. While dams have direct economic benefits, they can also trigger negative environmental externalities that exert additional pressure on fluvial systems and water resources. One key impact of dams on rivers systems is the trapping of sediment. Trapping of sediment changes river morphologic and delta processes, resulting in considerable impacts on eco-systems and water users. Dam impacts on network sediment transfers are rarely anticipated or included into basin scale water resources planning. This is largely because numerical models that are used to model river hydro-morphology on local scales cannot be applied to network scale planning because of data-scarcity and high computational costs.

This thesis introduces a new network scale modelling framework to overcome these limitations and to introduce sediment transport and the resulting river hydro-morphology into basin-scale water resources management and planning. The modeling framework is based on a simplified, but process-based description of sediment transfers to achieve computational efficiency. This efficiency is a prerequisite to handle the large uncertainty in input data via stochastic methods and for allowing the integration into multi-objective approaches. Because of the fundamental role of sediment transport for fluvial processes, we hope that this integration will make IWRM more transparent regarding negative effects of dams on fluvial systems and resulting

negative environmental externalities. This transparency should then enable finding better trade-offs between direct economic benefits and environmental impacts of dams. Towards this aim, the thesis is structured as follows:
Hydro-morphology or sediment transport is not commonly considered in IWRM or IRBM. Therefore, an introductory chapter introduces the intrinsic link between hydro-morphology and IWRM and current hindrances in terms of process understanding and modelling for the successful integration of both fields.
The relevance of making this link is shown for a concrete case study in chapter 2, where also background information on geographic setting and challenges in water resources management for included case-studies is presented.
In Chapter 3, we introduce a numerical modeling framework that quantifies network-scale transport of sediment mixtures originating from multiple sources. The framework, named CASCADE (**CA**tchment **S**ediment **C**onnectivity **A**nd **DE**livery) is based on a simplified description of grain size specific transport rates in a modelling environment that is based in graph-theory and recent concepts of network sediment connectivity. We demonstrate, how the new modelling framework can describe trajectories of deposition as sediment travels from multiple sources through the fluvial network. This allows to derive a spatially explicit representation of how any sediment source in a river network is connected to specific downstream sinks. In turn, it identifies which upstream sources contribute to the sediment budget of any downstream sink.
Chapter 4 introduces how the derived multi-dimensional, multi-scale information progresses the understanding of connected fluvial sediment transfers. Results clarify how sediment connectivity is a nested property that spans from local to whole-network scales. Each part of the river network has a specific connectivity to upstream sediment sources, and a certain function in network sediment routing and storage.
Chapter 5 approaches the problem of how a network connectivity model can be initialized for a concrete planning case study. We propose that the developed modeling approach does not only increase the fidelity of network sediment transfer models, but can also help reducing uncertainty and accuracy of network sediment modeling. To provide evidence for this, we apply the modelling framework to an inverse problem in a major river system. The inverse problem is posed as the availability of few point sediment data mismatches the task of planning reservoir cascades on network scales. Based on the inverse problem, we disaggregate single sediment measures into spatially distributed estimates of sediment source characteristics. Sediment source characteristics are then transferred into network estimates of sediment fluxes

and uncertainty via forward modeling. We compare model results with available lithologic and remote sensing evidence. The inverse modelling extracts network scale patterns of sediment transport that are in line with, but much more detailed, than traditional data-sources and that indicate a high heterogeneity in sediment fluxes driven by the underlying lithology in the basin under study.
In Chapter 6, results of the inverse modeling are applied for the network-scale planning of hydro-power dams in a major South-East Asian river basin. As methodological contribution, we expand the spatially distributed model-structure to describe also the routing of sediment in reservoirs. As reservoir development is already well progressed in the river basin under study, we perform first an ex-post analysis of existing developments. This demonstrates how the impact of single reservoirs can vary by orders of magnitude in function of their location in the river basin, but also their location within a reservoir cascade. The historic analysis shows also how a network scale sediment transport model can be used as tool for integrated assessments of reservoir siltation and downstream reservoir impacts. We expand this analysis to many different reservoir portfolios that could have been developed based on the available dam sites. Each portfolio is evaluated regarding its impacts on network sediment connectivity and economic performance in terms of total production and unit production costs. Results indicate that the river network had a high carrying capacity for hydro-power, i.e., most of the hydro-power potential could have been developed without strongly compromising sediment connectivity. We then compare the results to the actual trajectory of reservoir development. Results are a cautionary tale showing how lacking consideration of fluvial processes and missing trans-national integration of the planning process results in development strategies that incur over-proportional damage to the fluvial eco-system in comparison to economic benefits. This finding holds especially for large main-stem dams.

As a vision for future research, we stipulate that integrating network-scale planning tools for river hydro-morphology and sediment transport into dam portfolio analysis will allow balancing dam construction and hydro-electric production without overly compromising river sediment connectivity and related eco-system services and eco-system integrity.

Contents

List of Figures

List of Tables

CHAPTER 1

Introduction

1.1 Linking Sediment and Water Resources Management

RIVERS are key connectors in global geo-chemical and hydrological cycle, redistributing water and sediment from the sources of precipitation and erosion to downstream oceanic or continental sinks (*Milliman and Meade*, 1983; *Syvitski et al.*, 2003; *Syvitski and Milliman*, 2007). For millennia, human economic activities focused on rivers environments (*Gallup et al.*, 1999; *James*, 2015). Human use of resources in riverine landscapes expanded beyond the river channels to include diverse landscape features and biomes, for example, flood-plain forests, lakes, and wetlands. Until today, fluvial landscapes provide a wide array of resources for extractive and none-extractive use (*Brismar*, 2002; *Gilvear et al.*, 2013), above all water for agricultural, industrial, and domestic use. Extractive uses include food in form of fish or other aquatic species, timber from floodplain forests (*Gren et al.*, 1995; *Horner et al.*, 2010), or aggregate sediment for construction (*Kondolf*, 1994). Rivers provided connectors along which goods and people moved, and sources of mechanical energy. Fertile floodplains and deltas, regularly resupplied with water and sediment-bound nutrients, were where agricultural civilizations were born and flourished (*James*, 2015). Floodplain and coastal forest provided protection from hydrological extremes and sta-

bilized river banks. Many of these fluvial ecosystem services - benefits to human societies derived from the functioning of fluvial ecosystems - are related to the interplay between water and sediment transport in rivers (*Gilvear et al.*, 2013). This dynamic interplay between hydraulic forces, geomorphic elements in channels and floodplains, and their dynamic co-evolution over time is commonly concluded under the term "hydro-morphology" (*Vaughan et al.*, 2009; *Vogel*, 2011).

Over millennia, human use of fluvial systems went hand in hand with the construction of fluvial infrastructures. Dams were erected to store and divert water for agricultural or domestic purposes as well as for flood protection. Reports of major dams in the Nile, Euphrates and Tigris catchments reach back as early as the third millennia B.C. (*Jansen*, 1980). In Europe and later North America, massive numbers of smaller dams were built from medieval to early modern times, providing energy to mining, milling, and other energy intensive applications (*Walter and Merritts*, 2008). Hydro-electric power was among the first sources of electric energy and of paramount importance for the increasing electrification and industrialization at the beginning of the 20th century. Dams provided not only energy, but allowed storing and transferring water in time, space, and between different uses in a controlled way, increasing the utility of available water resources for human users (*Loucks et al.*, 2000). Numbers and magnitude of dam construction saw an unprecedented rise in in the second half of the 20th century. While there is uncertainty with regard to total numbers, *Vörösmarty et al.* (2003a) propose that there are globally more than 45000 dams with a dam height above 15 m, most of which erected in the post-1950 period. Numbers increase for smaller dams and *Lehner et al.* (2011) estimated the global number of small impoundments to reach nearly 17 million. As per now, up to 46 % of the world's major river systems are dammed (*Lehner et al.*, 2011). For the future, projections indicate an ongoing boom in dam construction with 3700 major dams planned or under construction, increasing the fraction of major dammed rivers by another 21 % (*Zarfl et al.*, 2014) . There are multiple reasons for this ongoing boom. Access to energy is considered a key factor for human and socio-economic development. In 2013, up to 1.3 billion of the world's population remain without reliable access to energy, which is presumably a major hindrance to economic development (*Agency*, 2015). Already now, hydro-power covers 20 % of total global energy production. Hydro-power is considered a renewable source of energy (*Rosenberg et al.*, 1997) that can help to tackle the worlds energy crisis while reducing greenhouse gas emissions and the dependence of countries from importing primary energy resources (*Chow et al.*, 2003). Due to the storage capacity of dams and the relative predictability of the hydrologic cycle, hydro-power

is considered the sole source of renewable energy to cover base as well as peak energy demands. Pumped storage plants have the potential to balance loads due to short-term fluctuations iinduced by renewable energy sources (*Kaygusuz*, 2009). Additionally, growing human populations and increasing levels of human development result in increasing water demands. Reservoirs might be used to mitigate impacts of global climatic changes that will change spatio-temporal patterns of water resources availability (*Ansar et al.*, 2014).

Despite their benefits, dams can create negative environmental externalities (*Rosenberg et al.*, 1997; *Brismar*, 2002; *Biswas*, 2004; *Richter et al.*, 2010; *Ansar et al.*, 2014) that are commonly underestimated in single large dam developments (*Ansar et al.*, 2014) as well as in the development of multi-dam scheme in large river networks (*Grill et al.*, 2015). As rivers are connected systems, these impacts extend beyond the direct vicinity of a dam and reservoir to wide spatio-temporal scales (*Rosenberg et al.*, 1997; *Grill et al.*, 2015). Locally, the construction of a reservoir requires resettling and expropriating residents and destroying ecosystems within the impoundment (*Brismar*, 2002). The impoundment itself might create additional geophysical hazards (*Liu et al.*, 2004). Evaporation and percolation from reservoirs can lead to the loss of a considerable amount of water (*Sivapragasam et al.*, 2008; *Elsawwaf et al.*, 2010).

Per definition, dams disconnect the flux of water, change the downstream hydrograph, and alter physical and chemical parameters of the impounded and then released water. In a free-flowing river, excess energy is available for the transport of sediment. Hydrodynamic forces drop as rivers enter a reservoir, which decreases the capacity to transport sediment in the reservoir (*Kondolf*, 1997). Sediment particles that were originally entrained in the flow settle out within the reservoir impoundment. The interruption of sediment transfers through reservoirs has impacts upstream, within, and downstream of reservoirs. Deltas form at the upstream end of reservoirs, where the majority of sediment is deposited. Delta formation emphasizes dam backwater effects, creates upstream flood risk, and damages upstream water infrastructures (*Morris and Fan*, 1998). Within reservoirs, sedimentation continuously reduces the impoundment volume up to the complete siltation. The loss in storage space reduces the ability of a dam to attain its original objectives like buffering flood peaks or providing water supply. The accumulation of sediment increases both maintenance costs for hydroelectric equipment and costs for decommissioning (*Palmieri et al.*, 2001). Removal of sediments from many large reservoirs after decommissioning might be unfeasible, making reservoir sites unavailable for future generations (*Palmieri et al.*, 2001, 2003; *Annandale*, 2013; *Wisser et al.*, 2013). Economic losses due to reduced storage volume are often neglected, but can

reach up to 30 % of annual costs (*Schleiss et al.*, 2010). Sediments stored behind dams increase the static load on the dam and increase the risk of dam failure (*Evans et al.*, 2000). Downstream, the discontinuity in water and sediment fluxes created by reservoirs changes fluvial hydromorphologic and ecologic processes with potentially major long-term and large scale impacts on river ecosystems and inhabitants of the river corridor. In a natural state, the downstream hydro-morphology can be seen as a transient state, driven by a balance between driving hydro-dynamic forces (*Vaughan et al.*, 2009; *Vogel*, 2011), and the dissipation of energy for the transport of sediment and the creation of bed-forms (*Kondolf*, 1997). River hydro-morphology is the physical template on which ecosystems within the channel and the fluvial corridor develop, and hence the foundation for fluvial biotic and abiotic processes (*Ligon et al.*, 1995). Dams change two key domains of sediment transport and have, therefore, a strong impact on the downstream hydro-morphology (*Grant et al.*, 2003; *Schmidt and Wilcock*, 2008). First, dams release water according to certain operating rules, which are commonly different from the original hydrograph, hence altering the magnitude and frequency of flows. Thereby, dams change the energy available for sediment transport. Second, the amount and composition of sediment downstream of the dam is commonly altered in comparison to pre-dam conditions. This is because dams do not trap sediment indiscriminate by its size, but larger particles settle more readily in an impoundment than smaller particles. The change in driving forces and sediment availability impacts downstream hydro-morphology and human livelihoods from local to regional scales. Impacts depend on interactions between biotic and abiotic processes, and the geologic legacy of the downstream river (*Grant et al.*, 2003). The decrease in downstream sediment supply creates erosion potential downstream of dams and leads to degradation of the downstream channels (*Kondolf*, 1997; *Brandt*, 2000; *Grant et al.*, 2003; *Schmidt and Wilcock*, 2008). The reduction in very high scouring flows can, at the same time, encourage vegetation encroachment which further emphasizes flood-plain river dis-connectivity. Hydrologic and hydromorphologic changes downstream of dams often occur in conjunction with other changes, such as increasing water abstraction, sediment mining, or land use changes, which might emphasize negative hydromorphologic impacts of dams (*Dudgeon*, 2000). By changing river hydro-morphology dams impact not only the natural functioning of rivers and riparian corridors, but also ecosystem services provided by the river system to human users (*Gilvear et al.*, 2013). Fluvial ecosystem services, i.e., " benefits people obtain from ecosystems" (*Millennium Ecosystem Assessment*, 2005), fall into four broad domains: provisioning services (provide food, water, and other primary resources), regulating services (control of climate, floods, disease,

wastes, and water quality), cultural services (recreational, aesthetic, and spiritual benefits); and supporting services (soil formation, photosynthesis, and nutrient cycling) . There is broad, global evidence for how dams, by changing river hydro-morphology, create negative externalities by reducing the ability of rivers to provide ecosystem services to human users. Often, some reservoir-induced processes impact multiple domains of ecosystem service delivery (see also *Ward and Stanford* (1995) and (*Bravard*, 1999) for comprehensive reviews). Scouring and incision downstream of dams destabilizes bridges, locks and other infrastructures (*Kondolf*, 1997; *Bizzi et al.*, 2015a). Scouring also changes or destroys local fish-habitats and spawning grounds (*Kondolf*, 2000; *Larinier*, 2001). On larger scales, often in combination with dam-controlled peakflow reduction and sediment mining, incision disconnects floodplains and channels. This separates water users from fluvial water resources, e.g., for irrigation. Lower water tables and less frequent overbank flows also decrease delivery of nutrients to flood-plain agriculture, dewater productive flood-plain wetlands, drain groundwater resources (*Rinaldi et al.*, 2005; *Lu et al.*, 2007), reduce the access of fish to flood-plain spawning grounds, and increase flood risks by reducing flood-plain storage during hydrologic extreme events (*Archer*, 1989; *Sholtes and Doyle*, 2011; *Wyżga et al.*, 2015). On regional and global scales, sediment trapping reduces the flux from erosional zones to river deltas, inducing delta subsidence and coastal erosion. These processes decrease delta resilience to pressures like sea level rise and coastal erosion (*Vörösmarty et al.*, 2003b; *Syvitski*, 2009; *Yang et al.*, 2011; *Rubin et al.*, 2015).

As per now, up to 472 million people live close to rivers downstream of major dams and are potentially impacted by upstream reservoirs (*Richter et al.*, 2010). At the same time, because of the indisputable direct benefits of dams for addressing global water and energy challenges, dam construction is progressing rapidly (*Zarfl et al.*, 2014). This development now focuses on emerging economies, where fluvial ecosystem services and water resources often support the livelihoods of a majority of the population. In the Mekong River, for example, it has been estimated that a vast majority of the basin's economically active population depends directly (63 %), or indirectly (28 %), on fluvial water resources and fluvial ecosystem services for their livelihoods (*MRC*, 2010). In such environments, balancing dam development with ecosystem services is crucial to maximize access to energy and water resources, maintain human benefits derived from the river's "natural infrastructures" (*Hoff*, 2011), and to preserve ecosystems. In many contexts, excessive development of water infrastructures can reduce the ability of coupled human-environmental systems to cope with immanent pressures, e.g., sea-level rise or climatic changes (*Palmer et al.*, 2008;

Palmer, 2010). Therefore, it has been proposed that future developments of water systems should adopt an integrated (i.e., spanning multiple sectors and spatio-temporal scales) (*Hering et al.*, 2010), basin-scale (*Palmer*, 2010) perspective on water resources management (WRM) (*UNESCO*, 2014).

Dams are a cornerstone of water resources management. Yet, because of their impacts on fluvial ecosystems, the question remains how their benefits can be balanced with potential negative environmental impacts. Towards this aim, *Richter et al.* (2010) proposed a hierarchical, three stage procedure to minimize negative dam effects. *Richter et al.* (2010) propose to first to adopt network-scale planning perspective to identify and avoid most detrimental dam sites. Second, to operate and design dams such that negative effects of selected dam sites are minimized further and, third, to monitor the downstream river system with an appropriate spatio-temporal resolution for early detection and mitigation of negative downstream effects (adaptive management). Conceptually, these three steps closely link to dam-induced sediment trapping and hydromorphologic alterations. First, regarding network-scale planning, impacts of single dams will vary widely, because of the high spatial variability in network hydrology and sediment supply (*Andrews*, 1991). Reservoirs built within an existing cascade of reservoirs might trap less sediment and have less impact on network sediment transfers in absolute and marginal numbers than a reservoir construction in a pristine part of a river network (*Ferrari*, 2008; *Fan et al.*, 2015). As a result, otherwise identical dams might result in different downstream effects, based on their location, the spatio-temporal pattern of runoff-generation, sediment supply, and resulting sediment transfers; and the legacy of previous dam constructions in a river network (*Andrews*, 1991). Second, dams design should include technical equipment (*Morris and Fan*, 1998; *Kondolf et al.*, 2014) to pass-through sediment to the downstream river network. This also includes developing appropriate operating rules for sediment pass-through for individual reservoirs (*Yin et al.*, 2014; *Bizzi et al.*, 2015a), and entire sediment cascades (*Wild and Loucks*, 2014). Additionally, reservoir sediment pass-through can be increased by mechanical sediment removal by dredging, sluicing, and hydro-suction and the subsequent reintroduction of sediment downstream of a dam (*Palmieri et al.*, 2003; *Kondolf et al.*, 2014). Last, network-scale adaptive planning and monitoring of the multiple domains of fluvial ecosystems (i.e., hydrology, ecology, morphology) is hardly feasible on the scale of entire large river systems. Dam impacts can be highly variable throughout the downstream river network. For aquatic ecology, it was recently shown that hot-spots of dam-induced change can be identified through numerical modelling (*Kennedy et al.*, 2016; *Poff and Schmidt*, 2016), which could then be prioritized for monitoring and mitigation. Given the underlying role of

hydro-morphology in many river processes, a-priori identification of future hotspots of morphologic change could advance network-scale monitoring and adaptive management of rivers downstream of dams. To conclude, designing reservoir developments with low impact on river sediment and hydro-morphology would require to formulate a network (basin) scale, optimal decision making problem trading off sediment trapping and economic objectives (*Jager et al.*, 2015). This is because many different configurations of hydro-power sites, technical designs, and operation strategies exist that, because of the network complexity in fluvial processes, can result in similar benefits at very variable levels of negative environmental externalities. The resulting, low-impact strategies for dam development can then be coupled with targeted monitoring and mitigation.

Yet, the challenge remains how to concretize these steps for reducing feedbacks between dam developments on hydro-morphology. This is despite the recent advances in integrated modelling of water resources systems and integrated water resources management (IWRM). Following the three steps outlined by *Richter et al.* (2010) would require above all formulating a multi-objective, spatial decision making problem at the scale of large, or even multiple river basins (*Jager et al.*, 2015). Multi-objective analyses (MA) of spatial problems are now widely applied in environmental decision making. Common examples include, for example, planning operations in forestry (*Mendoza and Martins*, 2006), prioritizing conservation action (*Williams et al.*, 2005), but also reservoir sizing (*Khaliquzzaman and Chander*, 1997; *Mousavi and Ramamurthy*, 2000; *Patskoski and Sankarasubramanian*, 2015), or reservoir siting and sizing (*Lall and Miller*, 1988) to balance multiple conflicting objectives. Advantages of such MA approaches are manifold, allowing to quantify trade-offs, to make trade-offs and conflicts transparent, to facilitate negotiations between stakeholders, and to find trade-offs which minimize environmental impact and maximize economic benefits (*Zheng et al.*, 2009). Regarding ecological objectives, there is a growing body of literature describing the application of numerical MA modelling, system analysis, and optimization techniques for dam planning, mainly with the objective to minimize barriers to fish-migration. Such approaches were applied both to strategic planning of dam removal (e.g., *Paulsen and Wernstedt* (1995); *Kuby et al.* (2005); *Zheng et al.* (2009)) or new dam development (*Ziv et al.*, 2012) (for a comprehensive review see *Jager et al.* (2015)). With regard to reservoir operation, MA approaches are now widely applied to single reservoirs or reservoir cascades regarding a wide range of objectives. Objectives commonly include hydro-power generation, flood protection, and water supply (*Castelletti et al.*, 2008a, 2012). Increasingly, additional objectives such as provision of cooling water, recreation, environmental flow

quantity (*Giuliani et al.*, 2014), quality (*Castelletti et al.*, 2014), or flow alteration (*Bizzi et al.*, 2012) are considered. For both optimal planning and operation numerical effective numerical models are required to represent complex, non-linear processes over a large scales and for a high number of potential scenarios (*Castelletti et al.*, 2008a,b).

Currently, low-impact dam planning and integration into IWRM remains fragmentary with regard to hydro-morphology. Most examples of network dam planning (*Paulsen and Wernstedt*, 1995; *Kuby et al.*, 2005; *Zheng et al.*, 2009; *Ziv et al.*, 2012) focus on fish migration without considering sediment transport or river hydro-morphology. *Opperman et al.* (2015) proposed to use a using a topologic indicator (length of disconnected river network) to balance hydro-power and river ecosystems. With regard to dam management, there are only few examples where sediment pass-through (*Wild and Loucks*, 2014; *Yin et al.*, 2014) or reduction of downstream hydromorphologic alteration (*Bizzi et al.*, 2015a) is explicitly considered as operational objective. It can be argued that the lacking consideration of hydro-morphology is because data are missing or processes are too complex to be fully appreciated or modelled on relevant scales. Complexity is a common problem in IWRM (*Pahl-Wostl*, 2007; *Alcamo et al.*, 2008), other disciplines, such as hydrology, seem to move towards integrating new modelling techniques and new global data-sets into IWRM at much faster pace (*Palmer*, 2010). Therefore, it is the scope of the following sections to explore hindrances and future potential for large scale sediment transport and hydro-morphologic modelling, which could open the potential for a more widespread integration of hydro-morphology into IWRM.

1.2 Complexity in connected sediment transfers

Since Walling's (1983) seminal paper, *The Sediment Delivery Problem* has been approached from the single grain to continental scales, with many different techniques, and in diverse geographic settings. *Walling* (1983) referred to "the sediment delivery problem" as the limited understanding of how sediment is delivered from the landscape to river channels and then transferred through the fluvial network. The aim of this section is to introduce relevant processes controlling the sediment delivery from a watershed, both on the landscape and fluvial network-scale, and pointing out the complexity within these processes. Second, this section introduces novel approaches for sediment transport modelling also at the scale of larger river basins. This is a pre-requisite for incorporating sediment transport and hydro-morphology into integrated water resources management and planning.

Sediment fluxes within and from a watershed are controlled by the sup-

ply of sediment to the fluvial network, both from landscape and in-channel sources, and by the rates with which sediment is transported throughout the fluvial network. Outside of the river channels, i.e., on the hillslopes, sediment particles are produced by weathering and erosion and delivered to river channels either through continuous, diffusive processes or by more singular events such as rock-falls or landslides. Key controls behind weathering and delivery processes are both a-biotic (tectonics, lithology, and climate) but also biotic (vegetation) or anthropic (human disturbance) factors (*Sklar et al.*, 2016). The combination of these factors controls how much sediment is delivered to a river channel. The multi-variate drivers behind sediment delivery result in a large variety in observed rates of sediment flux from the landscape to the channel. Sediment delivery rates vary widely over all scales: between continents and climatic zones (*Meybeck*, 2003; *Syvitski et al.*, 2003), within major drainage systems (*Andrews*, 1991), between adjacent catchments (*Andrews and Antweiler*, 2012; *Mueller and Pitlick*, 2013; *Mueller et al.*, 2016), within single, small catchments (*Riebe et al.*, 2015), and even on a single hill-slope (*Sklar et al.*, 2016). Also, the driving factors behind the variability in sediment yield are highly scale dependent. On large scales, differences in tectonics and basin relief are key factors behind sediment yield (*Syvitski et al.*, 2003). Within basins, differences in climate (*Andrews*, 1991) and lithology become more relevant (*Andrews and Antweiler*, 2012; *Mueller and Pitlick*, 2013; *Mueller et al.*, 2016). Within a catchment, sediment supply from low altitude slopes might differ from the supply of slopes at higher altitudes because of feedbacks between local climate, vegetation, and erosion (*Riebe et al.*, 2015), an effect that can be even emphasized on the single hillslope scale (*Sklar et al.*, 2016). Floodplains can disconnect rivers from hillslopes making the geomorphic connectivity between channels and hill-slopes another key control on sediment delivery to river networks (*Lane et al.*, 2008). The multitude of these drivers and their spatial variability make developing unifying models for landscape sediment supply to river networks a difficult task (*Trimble*, 2012; *Sklar et al.*, 2016). Additionally, also fluvial processes, such as bank erosion can constitute a substantial source of sediment supply to a fluvial network (*Darby et al.*, 2013; *Czuba and Foufoula-Georgiou*, 2015).

As a consequence, both the amount and the characteristics (i.e., grain size) of sediment delivered to a river channel are highly variable. The properties of sediment delivered to a river, both from local sources, and from upstream, is then a key control on fluvial transport processes. Sediment entering a river channel is subject to hydro-dynamic forces exerted by the flow of water in the channel. If the hydrodynamic forces exceed certain threshold conditions, sediment on the channel bed is mobilized and transported

downstream. The threshold of motion is not a single measure, but depends strongly on a variety of factors, e.g., the grain size of individual grains (*Engelund and Hansen*, 1967), the presence of other grain sizes (i.e., the local grain size distribution, *Wilcock* (1998); *Wilcock and Crowe* (2003)), or channel morphologic parameters, such as gradient (*Suszka*, 1991; *Lamb et al.*, 2008). Processes involved in the transport of sediment are highly variable and operate at different rates, ranging from event-based transport of cobble and gravel as bed-load to the continuous transport of silt and clay particles as suspended load, or the intermediate transport of sand as either bed or suspended load. Therefore, sediment transport processes operate at variable rates between the specific sources and sinks for each of the different grain sizes present in a river network (*Bracken et al.*, 2015). Transport processes do also operate in multiple dimensions, both longitudinal (i.e., from upstream to downstream) but also lateral, i.e., between river channels and floodplains. Together with the variability in hillslope sources, a complex pattern of sediment supply and transport emerges on the river network-scale (*Bracken et al.*, 2015; *Parsons et al.*, 2015). This variability in network sediment transfers is of major interest for IWRM. Channel morphology might be controlled by the transport of larger grain sizes (*Kondolf et al.*, 2014). Also river deltas are often dominated by the coarsest fraction supplied from the upstream river network (*Nittrouer and Viparelli*, 2014). Finer grain sizes drive nutrient-bound sediment transfers. Different grain sizes can be supplied from different parts of a river system at different rates, and rates of fluvial transfer vary spatially and between different grain size classes. As a consequence, human disturbance, such as the construction of a reservoir at a specific location, impacts different fluvial processes at different points in the downstream network with a specific magnitude and timing.

Recently, connectivity has been introduced as conceptual umbrella to address the spatio-temporal variability in network sediment transfers (*Hooke*, 2003; *Heckmann and Schwanghart*, 2013; *Bracken et al.*, 2015; *Heckmann et al.*, 2015; *Parsons et al.*, 2015). The concept of connectivity has been proposed to gain a unified description of processes connecting sediment sources and sinks over various spatio-temporal scales and process domains (sediment detachment and delivery to the channel, sediment entrainment, intermediate or final storage). Because of the different rates of supply of different sources, and different rates of transport for various grain sizes, functional sediment connectivity scales differently for sediment supplied from each source (*Hooke*, 2003; *Bracken et al.*, 2015; *Parsons et al.*, 2015). The term *functional* or *process-based* connectivity (*Parsons et al.*, 2015) is key to understand that such approaches go beyond considering topological connections, e.g., if two points are topologically connected in a river network. In-

stead, *functional* connectivity moves towards understanding which processes connect different points in a river at which rate. Concepts of *process-based* connectivity (further on in this thesis, "*process-based* connectivity" will be referred to just as "connectivity") could help in future to trace pathways of sediment movement in river systems and to address Walling's sediment delivery problem (*Fryirs*, 2013). This ability can then open new avenues for integrating sediment transfer processes into IWRM. At the same time, conceptualizing sediment transfers as connectors in river systems indicates the necessity to evaluate sediment connectivity, and human impacts on connectivity, not on isolated small scales, but on the scale of entire river networks.

1.3 State of the art in network sediment models

Despite these developments, there is still a lack in numerical tools to represent all relevant domains of sediment connectivity in integrated multi-objective water resources management. Common hydrologic models (e.g., SWAT) allow for modelling transport of suspended sediment (*Betrie et al.*, 2011; *Ranzi et al.*, 2012). On large scales, applications of such distributed models implies considerable computational efforts, which is further potentiated for sensitivity analysis or automated parameter estimation (*Yalew et al.*, 2013). Estimation of sediment inputs is commonly based on empirical soil loss equations (USLE, RUSLE) that are subject to major uncertainty. Especially, when such approaches are applied beyond the range of small-scale agricultural applications, for which they were originally developed (*Trimble and Crosson*, 2000). Bed-load and hence bed-forming sediment fractions are commonly not considered. Some hydraulic models operate on the network-scale (e.g., Mike11, HEC-Ras) and include the transport of different sediment fractions. In comparison to hydrologic models, hydraulic models do require even more detailed input data (e.g., cross sections, grain size distributions) and impose even higher computational costs. The high efforts for running and setting up these models limits their application to small catchments or single river sections (*Merritt et al.*, 2003).

Some more conceptual approaches for modelling bed-load have been proposed. *Wilkinson et al.* (2006) proposed a bed-load transport model for the catchment of a major (17.000 km^2) sandy river in Australia. *Benda and Dunne* (1997a,b) developed a conceptual framework to study network-scale timing of bed-load pulses traveling through a river basin. Both approaches focused on describing the bulk movement of sediment in the network only. By aggregating all sediment fractions into a single bulk measures, such approaches do not allow to explicitly track pathways of sediment of different characteristics through a river network. Multi-grain size models (often based on *Wilcock and Crowe* (2003) sediment transport formula) were used on

larger scales, that is longer river sections (*Ferguson et al.*, 2015) or network (*Mueller et al.*, 2016) scales. In these approaches, specific transport rates can be derived for each grain size fractions at any point in the river network. Yet, in these works mixed-grain size transport models are mainly applied for estimating the thresholds of incipient motion in a sediment mixture and not to track individual grain sizes through a river network. *Czuba and Foufoula-Georgiou* (2014) presented a framework based on empirical sediment transport formula for tracking of sediment parcels through a smaller, sandy river network. This framework allowed for explicating spatio-temporal patterns of sediment transport (*Czuba and Foufoula-Georgiou*, 2014, 2015) and the role of network structure for the dispersion of sediment pulses (*Gran and Czuba*, 2015). It was a great advance that this framework considered specific transport time scales for each sediment parcel and the probability to find sediment parcels from a specific source in a downstream reach at a given time. Reaches with a probability to find many parcels at the same time coincided with hot-spots of morpho-dynamic change. Based on their case study, where relatively homogeneous sand-sized sediment prevails, *Czuba and Foufoula-Georgiou* (2014) did not consider the transport of multiple grain sizes. The framework was based on potential transport capacities but did not derive sediment mass balances for each reach. Therefore, the framework could not be used to derive actual transport rates, or information on where sediment from a certain source was deposited. This information would be relevant, instead, to understand where and with which rates an upstream intervention would manifest in downstream change.

To conclude, sediment connectivity is a promising approach to analyze the connected functioning of river systems and to incorporate sediment transport into water resources management. A number of novel approaches has been proposed to explore various domains of network sediment connectivity without the prohibitive computational costs and data demand of physically based sediment transport models. Despite these advances, there is so far no approach to describe network connectivity in terms of all domains of sediment transport on the scale of large river networks.

1.4 Purpose of this thesis

The previous sections identified the link between sediment transfers and water resources management, and challenges for the integration between the two disciplines. With regard to the previously identified challenges, this research builds onto the current state-of-the art in sediment connectivity modelling, remote sensing, and water resources management and economics to explore the following main question of

a) How do sediment transfers act as connectors in large river networks, and are there large scale emerging patterns and similarities between basins?

b) Are the data that are commonly available for most rivers (e.g., some gauge records, topography from remote-sensing data, regional maps of relevant properties such as lithology) sufficient to progress the understanding of these processes and validate notions of connected sediment transfers?

c) How does the natural pattern of connectivity link to the impact of human disturbance on river systems?

d) what are optimal trade-offs between economic interests in hydro-power development and maintaining sediment connectivity?

To answer these question, this thesis has four objectives:

1. Development of a numerical model for network sediment connectivity. Such a model should cover relevant scales and domains of sediment connectivity as outlined in the preceding sections. In terms of scale, a sediment connectivity model should operate on the scale of entire river basin. In terms of process domains, it should cover the domains of mass flux, grain size, and timing of sediment transfers. It is explicitly not the objective to develop a network-scale hydro-dynamic model. Rather, this thesis aims to draw on developments in the field of system analysis and systems theory to overcome limitations of common sediment transport models regarding data-demand and computational cost, while providing a novel vision on network sediment connectivity.

2. Explore how such a connectivity model can progress our capacity to quantify sediment transfers and the connected functioning of network sediment transfers. This includes also to show how such a model can be used to test hypotheses on how sediment transfers are connectors in large river networks. Hypothesis could include different mathematical formulation of transport processes, or assumptions on how sources of sediment are distributed throughout a river network.

3. Development of different approaches for effective and veracious model initialization. This includes studying the impact of uncertain parameters due to data-scarcity on model results.

4. Application of a network connectivity model for identifying optimal trade-offs between sediment connectivity and hydro-power development in large river systems. So far, dam portfolios are rarely subject to thorough trade-off analyses on network-scales. Neither with regard to

economic performance, nor sediment connectivity. Such trade-off analysis could help making strategic decisions that balance a desired level of hydro-power with cheap energy and low environmental impacts.

The thesis is structured as follows.

1. Chapter 2 introduces the geographic background of the two case-studies included in this thesis. Chapter 2 also provides evidence for how hydro-morphology links IWRM based on one of the case studies.
2. Chapter 3 details the development of a network-scale sediment connectivity model (Objective 1) and the information that can be derived from it (Objective 2).
3. Chapter 4 details further on Objective 2 by putting model results in the context of the current scientific debate on network sediment connectivity.
4. Chapter 5 introduces the second case study, and proposes how inverse modelling of sediment connectivity can help the endemic scarcity of sediment data (Objective 3).
5. Chapter 6 explores how network connectivity modelling can be used to find optimal trade-offs between sediment connectivity and economics of multi-dam hydro-power portfolios (Objective 4).
6. Chapter 7 takes up results of previous chapters, discusses in how far objectives where attained, points out limitations of the proposed approach, and the future potential to advance the integration of network sediment connectivity and water resources management.

CHAPTER 2

Regional background

2.1 Hydro-power and dam developments in South East Asia

THE proposed methodology is developed based on two case studies in South-East Asia, the Da River Basin (50.000 km^2) in the Red River drainage system, and the Se Kong, Se San, Sre Pok System (3S) basin (80.000 km^2) in the Mekong drainage system. Both rivers are located in the South-East Asian mainland. For political, economic, and demographic reasons, this region is currently a focal point of hydro-power development (*Stone*, 2011). This section briefly introduces the ongoing broader discourse on hydro-power development in the region.

Nine of the world's 40 major rivers originate in South or South-East Asia (Indus, Godavari, Ganges, Brahmaputra, Irrawaddy, Salween, Mekong, Red and Yangtze River) (*Tandon and Sinha*, 2008). Most of these rivers originate within or close to the Himalayan orogene, resulting in a high relief and discharge regimes driven by strong monsoonal precipitation (*Wohl*, 2008). This combination of hydrologic and relief factors results in large potential for hydro-power installation. Amongst all continents, Asia harbours the largest total potential for installing hydro-power capacity (2037 GW) and hydro-power generation 7681 TWh/yr (53 % of the global generation potential of 14 576 TWh/yr) (*Agency*, 2015). Two Asian Nations, China and India, are

amongst the top 10 global hydro-power producers (China 1st place, India 6th place). Still, 80 %, of the hydro-power potential remains undeveloped (*Agency*, 2012a). At the same time, Asian economies grow dynamically with a projected growth rates of 6.2 % over the 2016-2020 period. Emerging economies in South-East Asia such as Vietnam, Laos, Myanmar, and Cambodia (*OECD*, 2016) lead this economic boom (*Bank*, 2016). As a result, the primary energy consumption is projected to rise sharply in South-East Asia, from 2709 TWh/yr (2010) to 12444 TWh/yr (2040) (*Agency*, 2015). Increasing economic integration and construction of regional high-voltage lines (*Agency*, 2015) makes hydro-power also a valued commodity and boosts ambitions of, e.g., Laos, to become the "Battery of South East Asia". Also Burma has claimed similar ambitions (*Simpson*, 2007). The economic dynamics make South-East Asia a focal point in hydro-power development, in terms of total numbers of planned facilities, installed capacity, and impoundment volume (*Zarfl et al.*, 2014) (Figure 2.1).

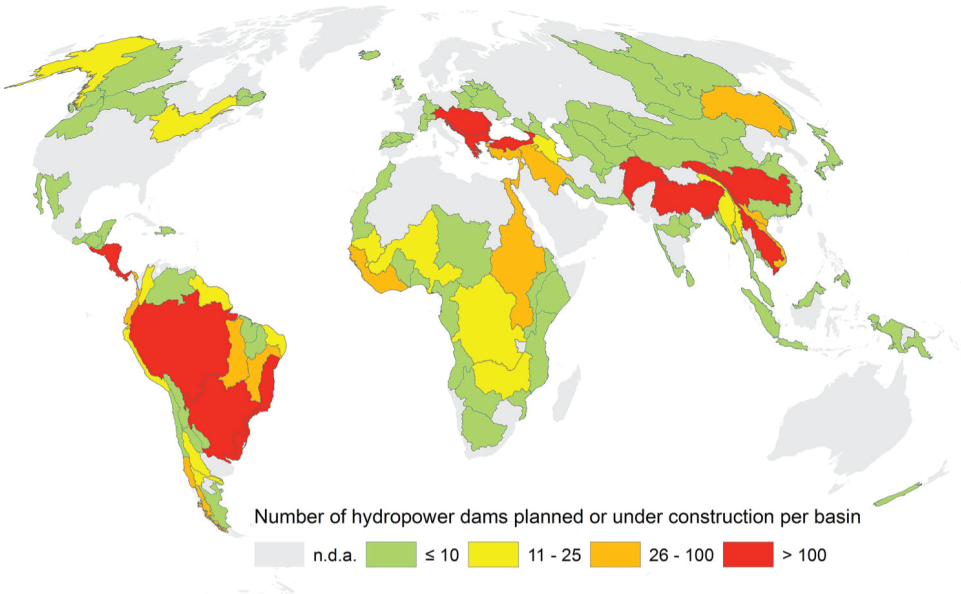

Figure 2.1: *Global planned large dams by numbers (Zarfl et al., 2014).*

At the same time, South-East Asian rivers are hotspots of freshwater biodiversity and human dependence on eco-system services. For example, all 10 of the above mentioned South East Asian river systems harbour at least 150 fish species, many of which are endemic (*Abell et al.*, 2008). Water resource in South East Asia are already under severe pressure in terms of catchment disturbance and pressure on fluvial eco-systems, resulting in a comparatively high vulnerability of human water users (Figure 2.2).

Such figures raise concerns regarding eco-system integrity and human

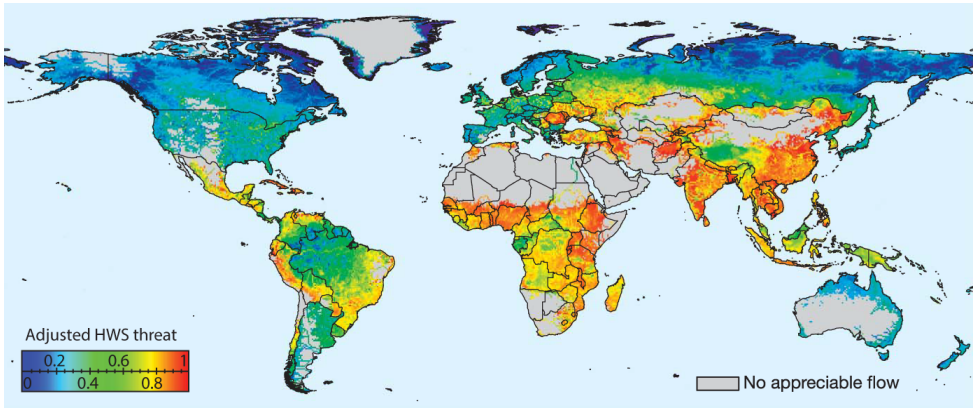

Figure 2.2: *Global distribution of Human Water Security (HWS) threat, adjusted to countries ability to scope with potential negative externalities with technical means. HWS includes factors goes beyond water scarcity and includes factors such as catchment disturbance, pollution, water system development, and biotic factors (Vörösmarty et al., 2010).*

livelihoods along South-East Asian rivers (*Stone*, 2011), resonating with concerns about the impact of large hydro-power projects on local communities (*Kareiva*, 2012). This is emphasized by the notion that more developed countries in the region (especially China, Vietnam, and Thailand) export environmental and social externalities to less developed neighbours, while importing economic benefits in form of cheap energy (*Simpson*, 2007). At the same time there is the concern that impacts from large hydro-power developments are not balanced with opportunities from other sources of renewable energy, or with addressing the region's notoriously inefficiency in energy use (*Imhof*, 2005). Defining such lower-impact development strategies for South East Asian Rivers requires tools to estimate impacts of hydro-power developments and to identify the carrying capacity of entire, transboundary river systems.

The combination of high hydro-power potential, increasing energy demands, poorly monitored and potentially highly vulnerable fluvial ecosystems makes South-East Asian rivers a relevant testing ground for integrating river hydro-morphology into IWRM. Specifically, this thesis will focus on two river systems originating from the longitudinal range gorge region (LRGR) in the Tibetian Himalaya and China's south-east Yunnan province (*He et al.*, 2007; *Zhai et al.*, 2010). 4 major, transboundary rivers originate from the LRGR (Yuanjiang/Red River, Lancang/Mekong River, Nujiang/Salween River, and the Irrawaddy River, Figure 2.3). Eco-system integrity in all of these rivers is currently compromised by an ongoing boom in reservoir developments (*He et al.*, 2007; *Zhai et al.*, 2010; *Grumbine et al.*,

2012; *Hennig*, 2016).

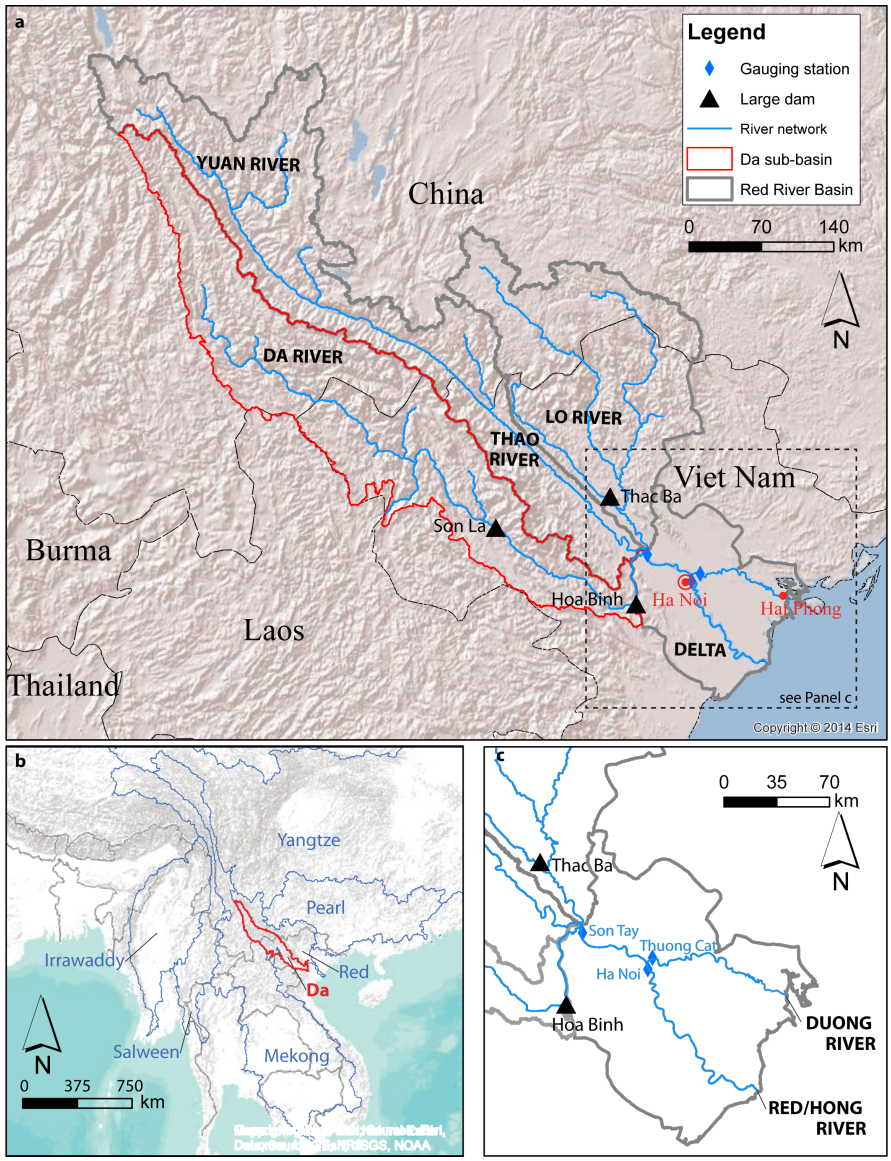

Figure 2.3: *a) overview over the Red River Basin. b) location of the Red River Basin on the SE-Asian mainland, and the context of other major rivers originating from the LRGR. Basin boundaries from www.hydrosheds.org. c) overview of the Red River Delta, see a) for location.*

2.2 Hydromorphologic alterations in the Da and Red River Basin impact Water Resources Management

The Da River Basin covers 50,570 km^2 between (100° 22' 30.587" E, 24° 51' 10.576" N, and 105° 50' 13.241" E, 20° 35' 44.263" N) (*Schmitt et al.*, 2016). The Da River Basin is shared between China, Vietnam, and, to a small fraction, Laos. The Da River originates from the Chinese Yunnan Mountain Range covering elevations from 3143 to 18 m (*Schmitt et al.*, 2016). It drains eastward through Vietnam until it reaches the Delta of the larger Red (Hong) River drainage system, where it merges with Lo and Thao River (the Thao River is also referred to as Red River or Yuan River) in the city of Son Tay (Figure 2.3 a, c) and drains eastward towards the Gulf of Tonkin. After the confluence, the river is referred to as Hong River (Son Hong). The total drainage area of the three rivers comprised within Red River system is around 160,000 km^2. This is small compared to other large river in South/South-East Asia, like the Mekong (800,000 km^2), or Irrawaddy (430,000 km^2) (*Wohl*, 2008; *Milliman and Farnsworth*, 2013). Despite its small drainage area, the Red River features an unusually high sediment load of 110 - 160 million tons per year, a similar magnitude to the Mekong or Irrawaddy River (*Milliman and Meade*, 1983; *Milliman and Farnsworth*, 2013). Based on *Milliman and Farnsworth* (2013) the Red River's sediment yield (690 t/km^2/yr) is exceeded only by three other major rivers worldwide (Huanghe, Fly, and Brahmaputra). Based on data provided in (*Le et al.*, 2007) 45 % of total sediment load originate from the Da River, 40 % from the Thao, and 15 % from the Lo River. Since the last glaciation, the high sediment supply from the Red River Basin to the Gulf of Tonkin formed the Red River Delta in the Gulf of Tonkin.

The Red River Delta covers an area of approximately 15,000 km^2, entirely in Vietnam (Figure 2.3 c). Within the Red River Delta, the flow of the Red River is distributed through a total of 7 distributaries. The Red River Delta includes the capital of Vietnam, Ha Noi (6 million inhabitants) as well as other important urban centres. such as the port city of Haiphong (Figure 2.3 a). In comparison to the sparsely populated upland river basins, the Red River basin is very densely populated (15 - 18 Million, population density around 1100 p/km^2, *Pilarczyk and Nuoi* (2005)). The Red River Delta is of national importance as a key production area for rice in Vietnam. Farming is mainly done by small scale farmers that rely on little mechanised production and a century old systems of gravity-fed irrigation channels (*Minot and Goletti*, 1998). Discharge from the headwater basins of Da, Thao and Lo River is distributed in the delta through a dense network of canals, and natural distributaries. The most important distributary is the Duong river, diverging

from the Hong River in Ha Noi (Figure 2.3 c). The Red River Delta was historically plagued by large floods that led to the construction of an intricate system of dikes and flood control structures (*Pilarczyk and Nuoi*, 2005).

The combination of energy-hungry urban centres, irrigation-dependent agriculture, and the high flood risks led to the development of several upstream dams. The first dams where Thac Ba Dam (Lo River), the larger Hoa Binh dam, and the recently completed Son La Dam (both Da River). Hoa Binh, which was commissioned in 1988, is located just before the Da River enters the Red River Delta (Figure 2.3 a,c). No reservoirs exist on the Thao River in Vietnam, but a cascade of smaller projects is under development in the Chinese part (*Zhai et al.*, 2010). Reservoirs in the Red River Basin mitigated major floods and are a keystone of Vietnam energy strategy. Hoa Binh's annual production contributed up to 15 % to Vietnam's energy demand, until the even larger So La Dam was built upstream (Figure 2.3 a).

At the same time, Hoa Binh Dam changed sediment fluxes in the Red River Basin, with hydro-morphologic consequences for the downstream Red River Delta. There is evidence that this change in sediment fluxes directly impact water users in the Red River Delta. It is informative to briefly assess the available historic data to demonstrate the possible impacts of dams on river hydro-morphology in major river systems, and the created negative externalities.

Historically, the majority of sediment delivered to the Red River Delta originated from the Da River basin. Available data over the 1960-2010 period (derived from the Institute of Integrated Water Resources Planning, IWRP, Ha Noi) indicate that the average pre-Hoa-Binh sediment flux into the Red River Delta (at Son Tay station, Figure 2.3 c) was around 110 Million tons/year (Figure 2.4 a, green marker on right y-axis). After the closure of Hoa Binh Dam (1985), these figures changed dramatically (Figure 2.4, b and c, green markers on right y-axis), the average sediment flux over the 1985 – 2000 period was reduced to around 60 million tons/year. The post-2000 period saw another reduction in the sediment flux to 35 million tons/year. Hence, to around 25 % of the pre-Hoa-Binh sediment flux. The change in sediment flux is also related to a change in discharge magnitude and frequency, with large flows above 20000 m^3/s disappearing after the closure of Hoa Binh (Figure 2.4 compare location of circle markers in a and c). However, also in the pre-Hoa-Binh period, these flows were too rare to contribute significantly to the cumulative sediment transport (see Figure 2.4 a for $Q >$ 20,000 m^3/s).

It is also informative to derive and analyse sediment rating curves in the 3 periods. (*Asselman*, 2000) proposed that deriving a sediment rating curve in the form

$$SS = a * Q^b \tag{2.1}$$

where SS is the suspended sediment concentration, Q is the water discharge can yield information on drivers behind sediment transport processes. Specifically, *Asselman* (2000) proposed that the coefficient (a) is an indicator for the capacity of the river to transport sediment and the exponent (b) relates to the sediment supply. For Son Tay station, the value of coefficient a initially increases from 3.56 (1960-1984) to 3.69 (1985-1999), before strongly decreasing to 1.75 (2000-2010). Exponent b decreased from 0.64 (1960-1984) to 0.59 (1985-1999), before slightly increasing to 0.60 (2000-2010) (Figure 2.4 d-f). In the interpretative approach of *Asselman* (2000), these trends indicate that transport capacity decreased slightly after the closure of Hoa Binh and remained constant, afterwards. The supply, instead, slightly increased immediately after the closure of Hoa Binh, but dropped strongly in the post 2000 period. As Hoa Binh is expected to trap more than 80 % (Le et al., 2007) of the incoming sediment, it seems likely that the initial stability in sediment supply can be related to incision processes, that mobilized some sediment from river bed or banks, but that these stores where exhausted 15 years after the closure of Hoa Binh Dam. This interpretation is supported by evidence from several domains.

First, Son Tay is the most upstream station in the Delta (Ha Noi and Thuong Cat stations are located more downstream , Figure 2.3, c). For these two stations, sediment rating curves experience much less change than for Son Tay (results not shown). This indicates that sediment is remobilized not only between Hoa Binh Dam and Son Tay station (Figure 2.3, c), but also downstream of Son Tay station, i.e., in the Red River Delta. The sediment balance in the delta, which is derived for the three station in the Red River Delta, supports this hypothesis. The only sediment input is Son Tay station, while the sediment output is defined by the sediment flux via the distributaries Hong (Ha Noi gauging station) and Duong River (Thuong Cat gauging station). A higher sediment output via Thuong Cat and Ha Noi stations in comparison to the input at Son Tay station indicates that sediment is mobilized in the Red River River Delta via incision or bank erosion. Results are shown in Figure 2.5 (x-axis: sediment input, y-axis sediment output). Two trends are evident. First, in the pre-Hoa-Binh period (pre 1988), sediment inputs were between 60 (1963) and 170 (1974) million tons per year. The annual sediment balances are equally distributed around the vertical equilibrium line at which sediment inputs equal sediment outputs. Post Hoa-Binh, sediment inputs are strongly decreased (in accordance with Figure 2.4). Additionally, the sediment balance is positive for nearly all years (points are above the equilibrium line). This indicates that a considerable amount of

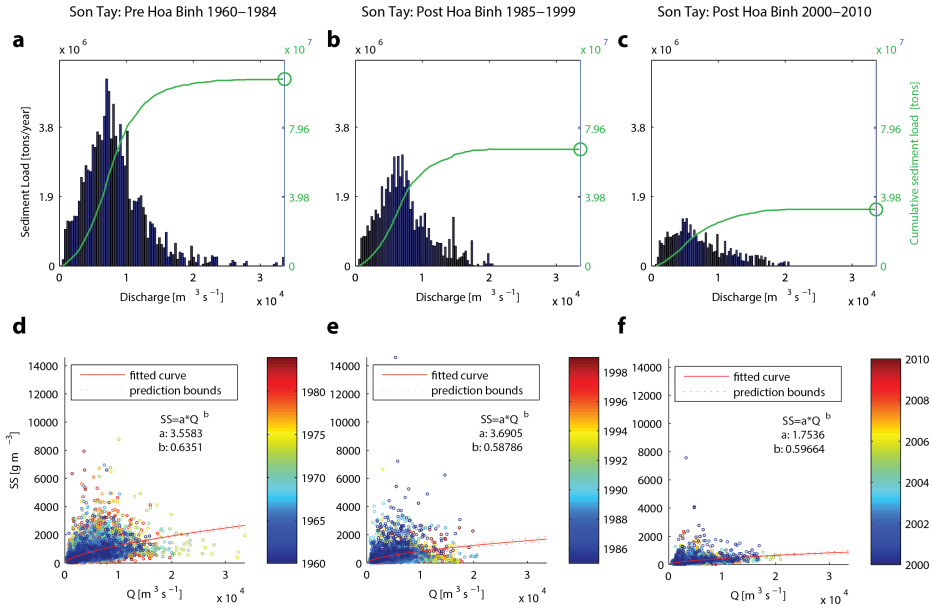

Figure 2.4: *Changes in sediment transport in Son Tay station (see Figure 2.3 c for location) over three periods froms 1960-2010. a-c: Magnitude and frequency of sediment transport events. Discharges (x-axes) were binned and the mean sediment transport in each bin was calculated. Cumulative curves (green, see right y-axes for values) show the cumulative value of discharge bins, and the mean annual transport (green circles) in each period. Sediment rating curves (d-f) were derived from daily measures of discharge and suspended sediment. Panels a and d, b and e, and c and f are for the same time period.*

sediment is mobilized over the Son Tay – Ha Noi/Thuong Cat reach (e.g., in 2000 input was 50 million tons, and the output was 110 million tons).

Such a mobilization of sediment in the upper delta should result in a massive change in river morphology in the impacted reaches. Massive incision was indeed observed at Son Tai (Red River) and Thuong Cat (Duong River distributary) stations (Figure 2.6). This spatial pattern suggests that incision occurred downstream of Son Tay in the Hong River but that incision downstream occurred preferentially along the Duong River towards Thuong Cat station. This preferential morphologic change at the diversion has direct consequences on the water resources system in the lower Red River Delta.

The morphologic change in the Duong River leads to an ever increasing flux of water towards the Duong (Figure 2.7 a), which changes the spatial distribution of availabile water resources. Between 1960 and 2000, the discharge diverted towards the Duong rarely exceeded 30 % of the total discharge (mainly during high monsoonal discharges). In general, the diversion toward the Duong was higher during the monsoon season (Figure 2.7 a, red sections of time series). Since 1998 the diversion rate towards the Duong increased, reaching a plateau of 0.5 between 2000 and 2004. After 2004, the diversion rate towards the Duong increased further, reaching a maximum of 0.65 in 2009. Not only the spatial but also the temporal pattern of the diversion shifted. Before 2004/2005, the diversion towards the Duong was highest during the Monsoon season (Figure 2.7 a, red sections of time series). After 2005, highest diversion rates occured during the dry season (Figure 2.7 a, blue sections of time series). This correlates to that the thalweg elevation in the Duong fell, for the first time, below the thalweg elevation in the Red River in 2005 (Figure 2.6). A visualization of change in channel morphology is presented in Figure 2.7 b, blue arrows indicate the flow rate in the diversion channels. There is some evidence that the hydraulic gradient along the Duong river is steeper (Duong River translates into “River of Rapids”). The changing flow diversion can be aligned with a conceptual hydraulic model of the bifurcation, assuming that the hydraulic gradient along the Duong is steeper than along the Hong River. The conceptual model predicts, that the flow towards the Duong River increases with increasing incision in the Duong. Compared to pre-incision conditions, the fraction of discharge flowing towards the Duong increased during lower flow conditions (Figure 2.8). Because lower flows typically occur in the dry winter season, the changing flow diversion changes the seasonality of flow distribution in the delta.

The changing magnitude and seasonality of flow diversion is directly impacting water resources management in the Red River Delta. A certain water level in Ha Noi (around 2 masl) is required to ensure sufficient feeding of

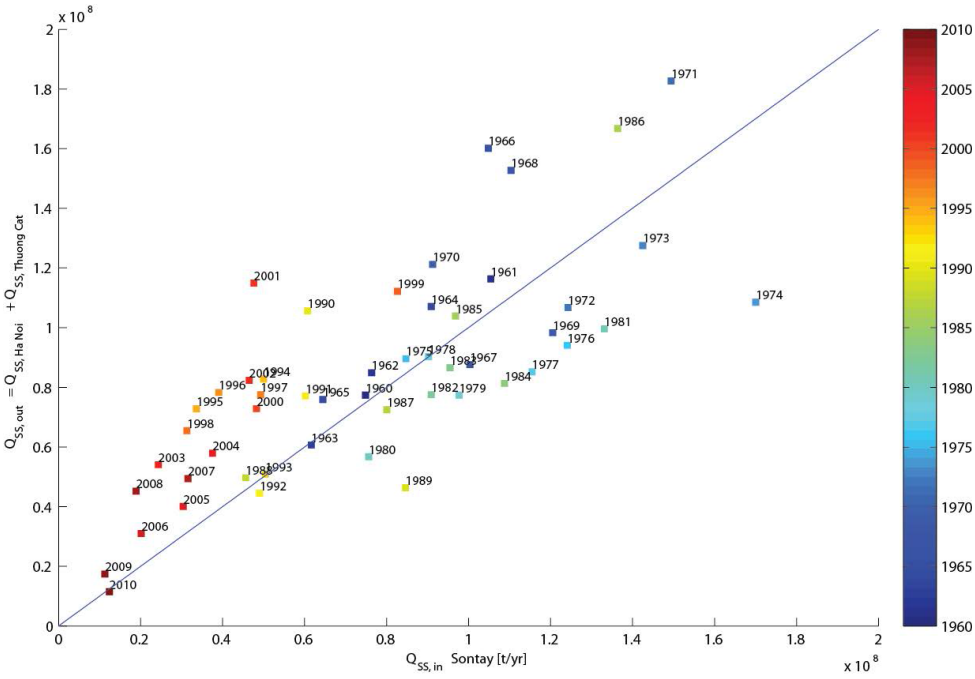

Figure 2.5: *Sediment balance in the Red River Delta in the 1960 - 2010 period.*

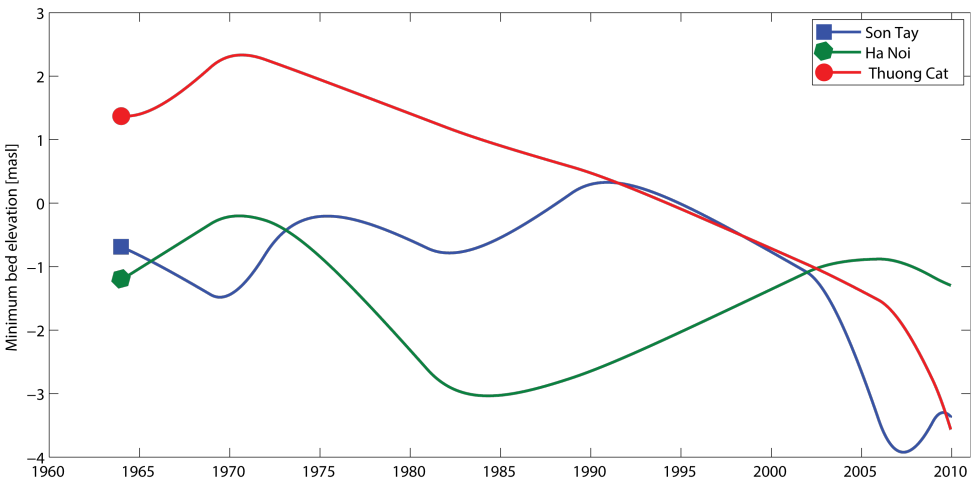

Figure 2.6: *Thalweg elevation in Son Tay, Ha Noi, and Thuong Cat station.*

gravity driven irrigation canals. Obviously, meeting this requirement is more critical in the dry season, and especially in January/February, when flow is lowest and the dry-season rice crop is planted (*Mussgnug et al.*, 2006). The water releases from upstream reservoirs indicate a strongly increasing water demand (Figure 2.7 c), i.e., the water input into the Delta at Son in 2010 was more than 300 % above the long time average. The strong change in releases correlates in time with onset of the observed change in flow diversion. Hence, insuring a sufficient water level in the Hong, where most of the irrigation sluice gates are located (Figure 2.7 d), requires an ever increasing amount of water, as the flow is preferentially routed towards the Duong River. Despite increasing water releases, irrigation districts along the main Duong and Hong river suffer from a strong water deficit (Figure 2.7 d). To conclude, evidence indicates that the construction of Hoa Binh Reservoir had a sustained impact on the sediment balance in the Red river Delta. The reduction in sediment input manifested in incision along the main river channels. Yet, the main morphologic impact is not created by the magnitude of incision, but by their spatial distribution. Incision in the Duong-Hong distributary system acted like a switch changing the spatio-temporal flow patterns within the delta. Hence, the disconnection of the Da catchment from the Delta through the construction of Hoa Binh had a direct impact on river hydro-morphology. This makes the Red River System a cautionary tale for how reservoir construction can induce changes in morphology, hydraulics, and hydrology in a river system that then directly feed-backs onto human water users. Additional feed-backs are possible, but not well documented. For example, there is anecdotic evidence, that farmers are increasingly shifting to pumped irrigation. The hereby created additional energy demand would create a nexus between reservoir constructions, hydromorphologic change, and energy demand, with part of the energy provided by reservoirs being consumed by the newly arising, incision-induced need for downstream pumped irrigation.

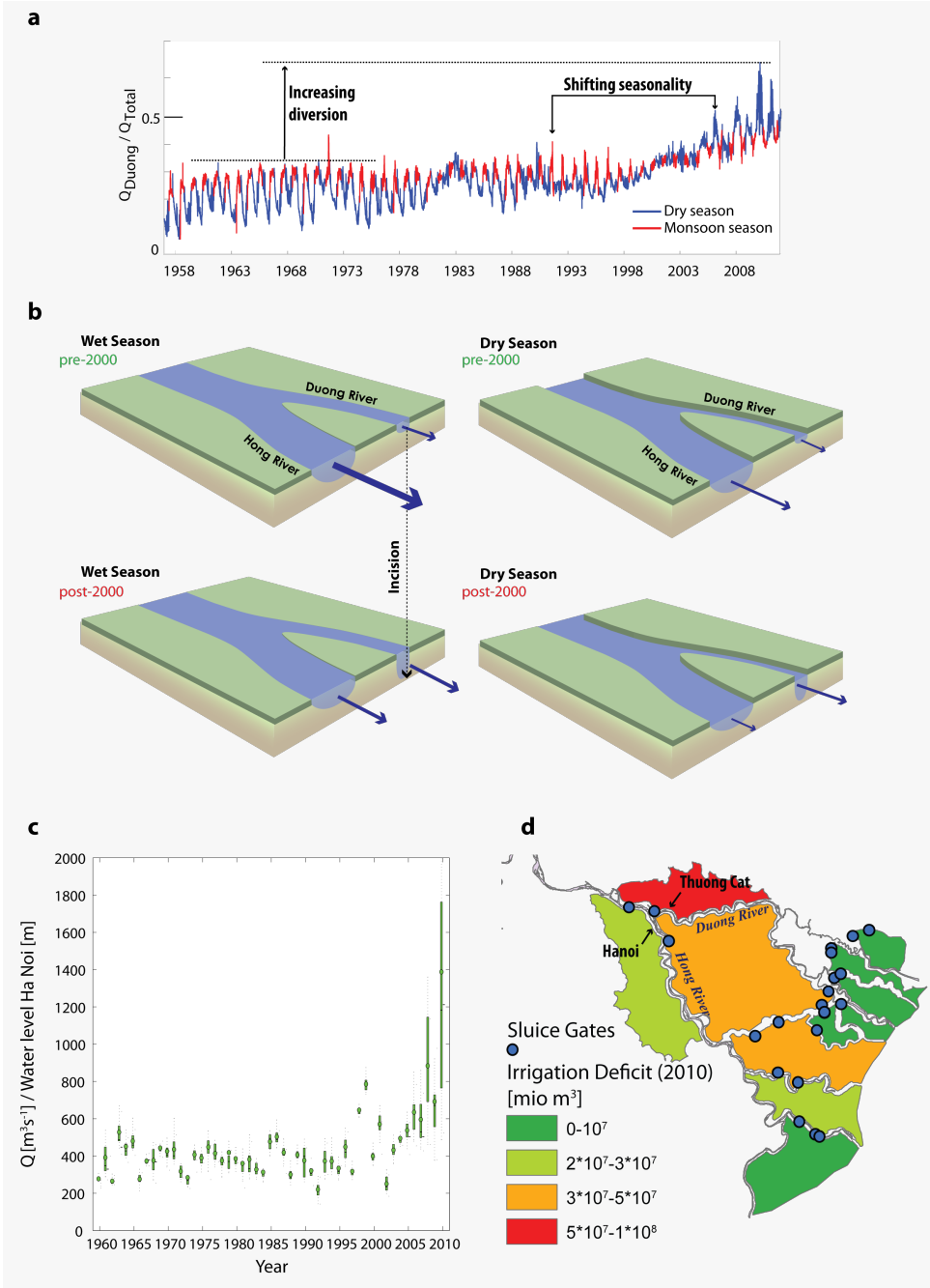

Figure 2.7: *a) Changing distribution and seasonality of discharge in the Red River / Duong River diversion. b) Conceptualization of preferential erosion along the Duong River. c) Changing water release into the Red River delta in January (at Son Tay station). d) Increasing water scarcity in irrigation districts in the Red River Delta.*

c

Variable	Water Level [masl]	Thalweg Hong [masl]	Thalweg Duong [masl]	Gradient Hong [m/m]	Gradient Duong [m/m]	Width Hong [m]	Width Duong [m]	Velocity Hong [m/s]	Velocity Duong [m/s]	Conv. Capacity Hong [m^3/s]	Conv. Capacity Duong [m^3/s]	Diversion Duong (% of total)
	h	z_H	z_D	I_H	I_D	W_H	W_D	v_H	v_D	Q_H	Q_D	
Pre-Incision												
High flow	20	-1	2,5	1,E-04	2,E-04	500	200	2,28	2,86	2,4E+04	1,0E+04	**29,45%**
Mean flow	10	-1	2,5	1,E-04	2,E-04	500	200	1,48	1,63	8,2E+03	2,4E+03	**23,00%**
Low Flow	5	-1	2,5	1,E-04	2,E-04	500	200	0,99	0,78	3,0E+03	3,9E+02	**11,62%**
Post-Incision												
High flow	20	-1	***-4***	1,E-04	2,E-04	500	200	2,28	3,53	2,4E+04	1,7E+04	**41,41%**
Mean flow	10	-1	***-4***	1,E-04	2,E-04	500	200	1,48	2,46	8,2E+03	6,9E+03	**45,82%**
Low Flow	5	-1	***-4***	1,E-04	2,E-04	500	200	0,99	1,84	3,0E+03	3,3E+03	**52,65%**

Figure 2.8: *A simplified hydraulic model for the Duong/Hong diversion, before (a) and after (b) the preferential incision along the thalweg of the Duong, and a simplified mode of conveyance capacity (c). Aim of the model is to check conveyance capacity and diversion ratio for arbitrary water levels (20, 10, 5 m). The calculation is performed before and after the incision (i.e., using the maximum and minimum thalweg elevation at Thuong Cat station and the average thalweg elevation in Ha Noi station (see Figure 2.3 and Figure 2.6). A steeper gradient is assumed for the Duong River. It is assumed that the water level is identical in both rivers at the diversion. Velocity is calculated in each river based on the Strickler equation (using kst=30 $m/s^{1/3}$), the active channel width was derived from Google Earth. Based on channel cross-sections and velocity, the conveyance capacity in each river is calculated for each of the three water levels. Total conveyance in the Duong increases after incision. In contrast to pre-incision conditions, the diversion to the Duong is higher for low flows than for high flows (colour code in c), which is in line with observations (Figure 2.7 a).*

CHAPTER 3

Tracking multiple sediment cascades at the river network-scale identifies controls and emerging patterns of sediment connectivity

SEDIMENT connectivity in fluvial networks results from the transfer of sediment between multiple sources and sinks. Connectivity scales differently between all sources and sinks as a function of distance, source grain size and sediment supply, network topology and topography, and hydrologic forcing. In this paper, we address the challenge of quantifying sediment connectivity and its controls at the network-scale. We expand the concept of a single, catchment-scale sediment cascade towards representing sediment transport from each source as a suite of individual cascading processes. We implement this approach in the herein presented **CA**tchment **S**ediment **C**onnectivity**A**nd **DE**livery (CASCADE) modelling framework. In CASCADE, each sediment cascade establishes connectivity between a specific source and its multiple sinks. From a source perspective, the fate of sediment is controlled by its detachment and downstream transport capacity, resulting in a specific trajectory of transfer and deposition.

From a sink perspective, the assemblage of incoming cascades

defines provenance, sorting, and magnitude of sediment deliveries. At the network-scale, this information reveals emerging patterns of connectivity and the location of bottlenecks, where dis-connectivity occurs.

In this paper, we apply CASCADE to quantitatively analyze the sediment connectivity of a major river system in SE Asia.

The approach provides a screening model that can support analyses of large, poorly monitored river systems. We test the sensitivity of CASCADE to various parameters and identify the distribution of energy between the multiple, simultaneously active sediment cascades as key control behind network sediment connectivity at the network scale. To conclude, CASCADE enables a quantitative, spatially explicit analysis of network connectivity with potential applications in both river science and management.

This chapter is developed based on: Schmitt, R.J.P., Bizzi, S., Castelletti, A., 2016. Tracking multiple sediment cascades at the river network scale identifies controls and emerging patterns of sediment connectivity. Water Resour. Res. 3941–3965. doi:10.1002/2015WR018097

3.1 Introduction

Connectivity in fluvial systems embodies magnitude and timing of transport processes ranging from the routing of discharge (*Rinaldo et al.*, 2006), to the travel of aquatic species, pathogens (*Gatto et al.*, 2013), or sediment (*Czuba and Foufoula-Georgiou*, 2014). Sediment connectivity is a determinant of river geomorphic processes (*Hooke*, 2003) and concerns fluvial ecosystem integrity, access to water resources (*Trush et al.*, 2000), delivery of nutrients or pollutants (*Walling*, 1983), natural hazard risks (*Bechtol and Laurian*, 2005), and, ultimately, human livelihoods in fluvial systems (*Habersack et al.*, 2014).

Sediment connectivity in river networks describes the delivery from sediment sources to sinks in the domains of magnitude, transport time, and delivered grain size (*Bracken et al.*, 2015). The concept encapsulates multiple spatio-temporal scales with a potential nexus between reach-scale entrainment, transport, and deposition processes, network topology (*Bracken et al.*, 2015), and network-scale patterns of sediment redistribution (*Brierley et al.*, 2006). Numerical models could greatly advance the study of connectivity because of the multiple involved process domains and spatio-temporal scales, which limit empiric studies of connectivity typically to small, well studied catchments (e.g., *Fryirs et al.* (2007a)).

Different numerical approaches to study network-scale sediment transfers, channel adjustments, and connectivity have been introduced. Stream-power based approaches on the single river (*Bizzi et al.*, 2015b) and net-

work (*Parker et al.*, 2015) scale predict deposition or erosion dominated reaches with high accuracy based on current hydro-morphologic forcing. Nevertheless, they do not consider sediment transfers as additional driver for channel adjustment. *Benda and Dunne* (1997a) used distributed sediment mass-balances to study how the spatial distribution and stochastic activation of sediment sources resulted in spatio-temporal patterns of flux along a sediment cascade. *Wilkinson et al.* (2006) applied a similar approach to identify depositional reaches at the network-scale. Both approaches pointed out potential sediment sinks, but could not explicitly identify and quantify sediment source-sink relationships or sediment provenance. This limitation was due to the aggregation of sediment transport from all sources into a single bulk measure. *Czuba and Foufoula-Georgiou* (2014), in contrast, implemented common sediment transport formulas in a graph-theoretic framework. The approach allowed the movement of individual sediment parcels to be traced through a river network, identifying both temporal trajectories of sediment parcels and resulting network-scale dynamics (*Czuba and Foufoula-Georgiou*, 2015). Nevertheless, this dynamic connectivity approach did not explicitly quantify sediment source-sink relations, because sediment parcels were not subject to local transport capacity limitations and deposition.

All of the above studies provide insight into specific aspects of network sediment connectivity. Nevertheless, to date, no approach explicitly appraises multiple sediment source-sink transfers, which would be a requirement for integrated assessments of sediment connectivity (*Bracken et al.*, 2015). In this paper, we combine previous approaches into a novel network-scale modelling approach to quantify sediment connectivity. The key novelty of the approach is that the transport of each sediment input is conceptualized as an individual cascading process. In the CASCADE (**CA**tchment **S**ediment **C**onnectivity **A**nd **DE**livery) modelling framework, each sediment source is assessed as the beginning of a new sediment cascade. In this way, CASCADE allows analyses of connectivity both from a source or a sink perspective. CASCADE quantifies how the sediment that is supplied from a source is delivered to all downstream sinks. From a sink perspective, CASCADE traces back all sediment inputs to their sources and determines the total local sediment flux, the flux of each grain size, the spatial distribution of sources, and the connection times between sources and sinks. From this information, statistical properties of connectivity can be derived. This process-related information opens up opportunities for reach- and network-scale studies of sediment connectivity from both a research and a management perspective.

In this paper, we focus on the theoretical framing and the formulation of the CASCADE modelling framework. We show for the Da River basin in SE

Asia (China, Vietnam, Laos; drainage area: 50570 km^2) how the CASCADE modelling framework can be initially parameterized based on remote sensing data that are available for most river systems world-wide. We present the novel kind of connectivity information that results from CASCADE. We use CASCADE to demonstrate how cascade-specific rates of sediment entrainment, transport, and deposition scale into spatio-temporal connectivity patterns at both local and network-scales. We analyze these patterns to clarify how different factors, above all the distribution of energy between different sediment cascades, and the spatial distribution and properties of sediment sources result in different patterns and statistical properties of network connectivity.

3.2 The CASCADE approach

The CASCADE framework represents the sediment transport from all sediment sources through the river network as individual cascading transport processes. An individual transport rate is assigned to each cascading process as a function of local (i.e., specific to a river reach) hydro-dynamics, morphology and transported grain size. Transport capacities are derived from these parameters through network-scale implementation of standard sediment transport formulas. A graph-based routing scheme was implemented based on recent advances in describing landscape (e.g., *Cheung et al.* (2015); *Heckmann et al.* (2015)) and fluvial (*Czuba and Foufoula-Georgiou*, 2015) sediment connectivity, resulting in a spatially explicit map of transport rates for each sediment cascade. The basic approach is clarified in Fig. 3.1: the river network (Fig. 3.1 A) is transferred into a directed acyclic graph (river graph), which represents the network topology as a set of nodes and edges (Fig. 3.1 B). For example, for the network shown in Fig. 3.1, the original set of five reaches is transferred into sets of five edges (see numbers in Fig. 3.1 B) and six nodes. Multiple sediment sources are active in the river network (Fig. 3.1 C, roman numbers). Each sediment source has a specific grain size (visualized by the dot size) and sediment supply. The sediment from each source is transported along an individual sediment cascade. Therefore, the river graph is expanded to represent attributes, e.g., grain size or sediment flux, of each cascade separately (Fig. 3.1 D). Each cascade is assigned a specific transport capacity in each reach downstream of its source. Transport capacities are calculated using standard sediment transport formulas based on the grain size of the source, and the local hydraulic forcing in the downstream reaches (Fig. 3.1 E, linewidth represents transport capacity). For example, in reach 5 (Fig. 3.1 E) cascade III has a lower transport capacity than cascade V, because cascade V transports a smaller grain size. Sediment cascades can be interrupted if their grain size cannot be entrained

in a downstream reach (Fig. 3.1 E, source II). The calculated transport capacity does not yet consider the presence of multiple sediment cascades in the same river reach. The more cascades that are present in a river reach, the less energy is available for each cascade. This competition for the available energy (Fig. 3.1 F) reduces the transport capacity for each cascade (compare line-widths between Fig. 3.1 E and F). The functioning of each cascade is determined based on sediment supply and the local competition corrected transport capacity (Fig. 3.1). It should be noted that no new sediment is taken up along a sediment cascade downstream of its source. Otherwise, a single cascade would encompass multiple sets of source-sink relationships and no unique connectivity information could be derived. Sediment is deposited if the input into a reach exceeds the local transport capacity (Fig. 3.1 G). A sediment cascade is interrupted as soon as the entire input is deposited (Fig. 3.1 G, sediment cascade I is interrupted in reach 3). Sinks are defined as reaches where a cascade deposits sediment (Fig. 3.1 F, for cascade III there are two sinks: reach 3 and 5). As a consequence, a reach can act as a sink for multiple cascades (e.g., in Fig. 3.1 G, Reach 5 acts as sink for cascades III, IV, and V). The assemblage of cascades connected to a reach defines sediment provenance (i.e., the location of sources), connection time to each source, and the sorting and magnitude of the total sediment delivery to a reach.

3.2.1 Graph notation

This subsection introduces key concepts of the multi-cascade sediment routing and the related notation. The river network is represented as a directed acyclic graph (DAG) $G = \{N, E\}$. G comprises a set of N indexed nodes and E is a spanning set of edges (each edge represents a river reach). The cardinality of E is $\mathtt{e}$ and the cardinality of N is $\mathtt{n}$ (e.g., in Fig. 3.1 B, $\mathtt{e} = 5$ and $\mathtt{n} = 6$). $n \in N$ is a node in N, $e \in E$ is an edge in E.

A set A_e of attributes is associated to each edge representing the properties of the associated river reach. The set A_e can be split in four subsets $A_e(1) \cdots A_e(4)$ of cardinality $\mathtt{a}_e(1) \cdots \mathtt{a}_e(4)$, each representing a dif-

Figure 3.1 ***(following page)*:** *Key concepts and steps behind the CASCADE modelling framework. A and B: original river network and graph representation. C: identifying source locations and grain sizes. D: graph expansion. E: transport capacity scaling, line width indicates transport capacity. F: competition reduces the original transport capacity (compare linewidth in E and F). G: cascade specific, edge-to-edge sediment routing discriminates cascade sediment fluxes. H: edges receive fluxes from multiple cascades, defining sediment flux, provenance, and sorting; and thereby connectivity of an edge .*

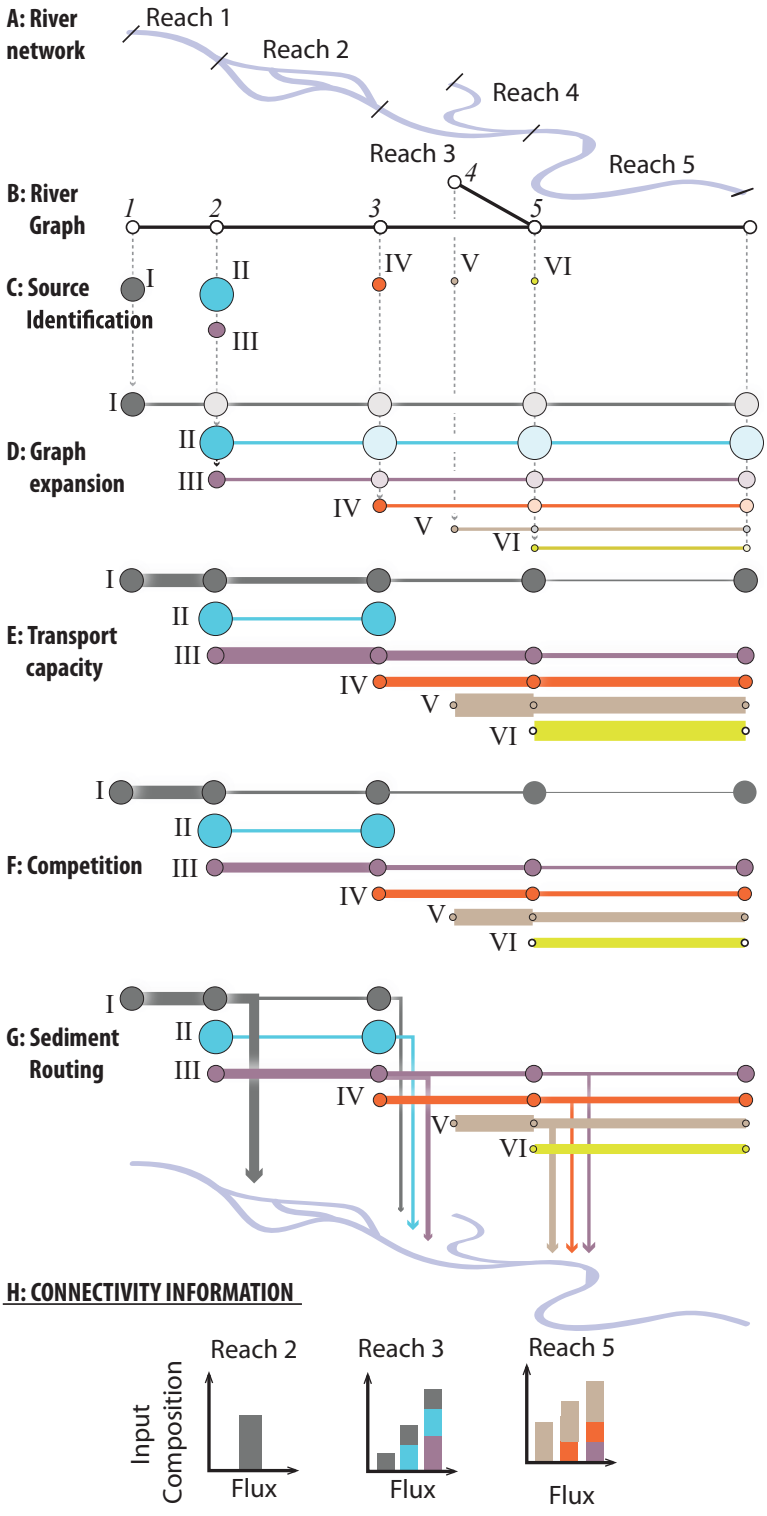
A: River network
Reach 1
Reach 2
Reach 3
Reach 4
Reach 5
B: River Graph
1
2
3
4
5
C: Source Identification
I
II
III
IV
V
VI
D: Graph expansion
E: Transport capacity
F: Competition
G: Sediment Routing
H: CONNECTIVITY INFORMATION
Input Composition
Flux
Reach 2
Reach 3
Reach 5

ferent domain . The first domain is the local geomorphic state (*Czuba and Foufoula-Georgiou*, 2014), which is defined by width, gradient, length, and drainage area of a reach (W_{Ace}, I_e, l_e, A_{De}). The second domain is the hydraulic state, a probability distribution function of water flow depth and flow velocity ($f(h_e)$, $f(v_e)$). The third domain describes the grain sizes delivered from upstream sources. The fourth domain defines the sediment transport state in a reach. This includes, e.g., Q_{S_e} (sediment transport capacity), Θ_e (sediment flux), t_{S_e} (sediment retention time), and any other measure of local sediment transport. The transport state is derived from the geomorphic, hydraulic, and grain size states using empiric sediment transport formulations.

Let now Γ be the set of sediment cascades. The cardinality g of Γ is equal to the number of all active sediment sources S in the river network. If $\varsigma \in S$ is a specific sediment source, than γ_ς is the associated sediment cascade that transports grain size d_ς. Next, the sediment pathways are defined. A pathway $\kappa \subseteq E$ is the set of edges along which a sediment source ς is topologically connected to the terminal node at the basin outlet (Ω). Finding all cascades that pass through an edge e defines $\Gamma_e \in \Gamma$: the set of cascades that are connected to edge e. Then, $S_e \in S$ are all sources connected to e. The cardinality $\mathtt{g}_e$ of Γ_e equals the cardinality $\mathtt{s}_e$ of the set S_e. For example, in Figure 3.1 D, $\Gamma_3 = \{I, II, III, IV\}$ is the set of cascade originating from the sources $S_e = \{I, II, III, IV\}$ and passing through edge 3 ($\mathtt{g}_3 = 4$).

The concept of multiple cascades that transport different grain sizes d_ς, and that therefore operate at different rates, requires expanding the sediment transport state in each edge. In Figure 3.1 D, for example, there are three sediment cascades in edge 2 ($\Gamma_2 = I, II, III$). Each cascade has a different transport capacity in edge 2 as a function of the source grain size (Fig. 3.1 E) and sediment flux (Fig. 3.1 G). Therefore, the cardinality of $A_e(4)$ is expanded into $\mathtt{a}_\mathtt{e}(4)' = \mathtt{a}_e(4) \cdot \mathtt{g}_e$ and, correspondingly, also the full cardinality of A_e is expanded into $\mathtt{a}'_e$. Hence, the attribute set A_e is expanded to include the original attribute subsets $A_e(1), A_e(2), A_e(3)$ and the the multiple set of $A_e(4)'$. Hence, for edge 2 in Fig. 3.1, $\mathtt{g}_2 = 3$ and $\mathtt{a}_\mathtt{2}(4)' = 3$.

3.3 Formulation of the CASCADE modelling framework

This section explicitly describes the formulation of the CASCADE modelling framework at the network-scale. The model requires a fully parameterized fluvial graph as input. The parameterization of the graph is case-study dependent and therefore is introduced later for a real case study. This section focuses instead on the implemented generic framework for sediment routing.

3.3.1 Transport capacity scaling

Sediment is mobilized in a reach and transported downstream if the local flow energy exceeds the threshold for sediment entrainment. The magnitude and frequency of flow events determines, therefore, how much sediment of a given grain size can be transported over a given time-span (e.g., over a year) in a reach. Processes involved in the transport of different grain size classes differ significantly. For example, fine silt and clay are mostly transported in suspension (wash load, suspended load), gravel and cobble fractions are transported on the river bed (bed-load), while sand fractions can be transported either in suspension or on the bed, depending on the hydraulic conditions. Empirical formulations that relate sediment transport rates to local hydraulic conditions are therefore applicable to a specific grain size range, only. Therefore, CASCADE uses two different sediment transport formulas to scale the sediment multigraph into a representation of local transport capacity (*Czuba and Foufoula-Georgiou*, 2014), one for sand (*Engelund and Hansen*, 1967), and one for gravel (*Wong and Parker*, 2006). The dimensionless transport capacity ${q_{S*e}}^{\varsigma}$ for grain size d_{ς} in edge e is defined as:

$${q_{S*e}}^{\varsigma} = \begin{cases} \frac{0.05}{C_{f_e}^{\varsigma}} \cdot {\tau_{*e}}^{\varsigma 5/2}, \text{if } d_{\varsigma} < 2 \times 10^{-3}\ m \\ \alpha \cdot (\tau_{*e}^{\varsigma} - \tau_{*ce})^{\beta}, \text{ else} \end{cases} \tag{3.1}$$

In these equations, α and β are the only constants and directly derived from *Wong and Parker* (2006) ($\alpha = 3.97$, $\beta = 1.5$). $C_{f_e}^{\varsigma}$ is the local friction factor,

$${C_{f_e}}^{\varsigma} = \frac{2 \cdot g \cdot I_e \cdot h_e}{{v_e}^2}, \tag{3.2}$$

the dimensionless shear stress ${\tau*_e}^{\varsigma}$ is derived from

$${\tau*_e}^{\varsigma} = \frac{I_e \cdot h_e}{R \cdot d_{\varsigma}}. \tag{3.3}$$

The dimensionless transport capacity is transferred into a dimensionful value through

$${q_{S*e}}^{\varsigma} = \frac{q_{S_e^{\varsigma}}}{\sqrt{R \cdot g \cdot {d_{\varsigma}}^3}}. \tag{3.4}$$

The final result from solving Eq. 3.4 is the volumetric sediment transport ${q_{Se}}^{\varsigma}\ [m^2 d^{-1}]$ for d_{ς} per unit channel width .

${q_{Se}}^{\varsigma}$ is an instantaneous value under given hydraulic conditions. Deriving the actual transport capacity of an edge requires information on the magnitude and frequency of flows. Therefore, CASCADE requires a hydrograph

$\boldsymbol{Q_e}$, a vector of n_{tote} flow observations for each edge. $\boldsymbol{Q_e}$ is divided into p percentiles and the mean discharge value $Q_e(p)$ in each of the p percentiles is derived. We define the percentiles as $-4\sigma ... + 4\sigma$ of a standard normal distribution (0.1% , 2.3% , 15.9%, 50%, 84.1%, 97.7%, 99.9%) .

CASCADE includes a hydrodynamic solver (Appendix 3.A). The solver calculates mean flow velocity and flow depth, $v_e(p)$ and $h_e(p)$, for each $Q_e(p)$ (hence p sets of $v_e(p)$, $h_e(p)$ for each edge). CASCADES calculates the mean transport capacity for d_ς in each discharge percentile by inserting d_ς, $v_e(p)$, and $h_e(p)$ into Eq. 3.1 - 3.4. The total transport capacity for d_ς in the $p-th$ percentile follows from ${q_{Se}}^\varsigma(p)$ and the number of observations within the $p-th$ percentile, $n_e(p)$

$$ {q_{S,tot}}_e^\varsigma(p) = {q_{Se}}^\varsigma(p) \cdot n_e(p). \tag{3.5} $$

The mean annual transport capacity of γ_ς in edge e is

$$ {q_{S,annual}}_e^\varsigma = \frac{\sum_{k=1}^{p} {q_{S,tot}}_e^\varsigma(k)}{n_{tote}} \cdot 365. \tag{3.6} $$

Where n_{tote} is the total number of observations available for edge e. ${q_{S,annual}}_e^\varsigma$ is converted from [m^2 yr^{-1}] to mass ([kg yr^{-1}]) by

$$ {Q_{Se}}^\varsigma = {q_{S,annual}}_e^\varsigma \cdot W_{ACe} \cdot \rho_S, \tag{3.7} $$

where ρ_S = 2600 kg m^{-3} is the sediment density.

In theory, CASCADE can calculate a specific sediment transport capacity for each of the n_{tote} discharge observations in all edges. Nevertheless, the computational demand of this approach is substantial, even for small river systems. Calculating ${Q_{Se}}^\varsigma$ in a river system with 100 edges, in which each edge contains an average of $g_e = 10$ different cascades and 10 years of daily discharge observations are available (n_{tot} =3650) would require calculation of 3.65E6 pairs of v_e and h_e, and then ${Q_{Se}}^\varsigma$. Using the discharge percentiles instead of the full hydrographs reduces the computational demand significantly. Dissecting the hydrographs using the σ intervals rather than constant intervals considers the potential impact of rare, but high magnitude events on sediment transport (e.g., *Wolman and Miller* (1960))

3.3.2 Competition

The sediment transport formulas that are implemented in CASCADE (Eq. 3.1-3.4, and Eq. 3.5 - 3.7) derive the transport capacity for a single grain size, only. They do not consider that the transport capacity for d_ς in edge e will be reduced if multiple grain sizes are present that compete for the locally available energy (e.g., *Wu et al.* (2003); *Hsu and Holly* (1992); *Sutherland* (1987)). Hence, $Q_{S_e^\varsigma}$ only represents the transport capacity for d_ς in

e if there is only a single source connected to e. A competition factor is introduced to derive a competition corrected transport capacity ($Q_{S_e^\varsigma}'$) that considers the redistribution of energy between cascades. Empirical formulations that describe the simultaneous movement of multiple sediment fractions (e.g., *Wilcock* (1998); *Wilcock and Crowe* (2003)) could be included in CASCADE in future. For this study we used some high level formulations of the competition factor, instead. This approach allowed to study the impact of some high-level assumptions regarding the simultaneous transport of multiple grain sizes on network sediment connectivity.

We developed three different scenarios for competition. For all three scenarios we derive $Q_{S_e^\varsigma}'$ by multiplying $Q_{S_e^\varsigma}$ with an edge and source specific competition factor, F_e^ς, which we obtained from a dynamic competition function. The three scenarios vary in the calculation of both, $Q_{S_e^\varsigma}$ and F_e^ς. For scenario 1 and 2, a characteristic transport capacity is assigned to each edge *a-priori*. The characteristic transport capacity is defined as transport capacity for the local median grain size $Q_{S_e}(d_{50e})$. d_{50e} is estimated as median grain size of all upstream sources. $Q_{S_e}(d_{50e})$ is calculated from Eq. 3.1-3.4 and Eq. 3.5-3.7 in all edges. $Q_{S_e}(d_{50e})$ is then divided between the g_e sediment cascades.
For scenarios 1 and 2 holds:

$$Q_{S_e^\varsigma}' = F_e^\varsigma \cdot Q_{S_e}(d_{50e}). \tag{3.8}$$

Scenario 1 postulates that sediment cascades with locally high transport capacity compete more effectively for transport capacity (local selective transport). Competition between sediment cascades is expressed as

$$F_e^\varsigma = \frac{Q_{S_e^\varsigma}}{\sum_{k\in\Gamma_e} Q_{S_e^k}} \tag{3.9}$$

according to (*Wu et al.*, 2003). The competition factor in this base-case compares the transport capacity of an individual cascade with the summed transport capacities for all other sediment cascades in edge e. Cascades with a locally higher transport capacity are assigned a higher share of $Q_{S_e}(d_{50e})$. This implies that $Q_{S_e^\varsigma}'$ depends on local hydro-morphologic conditions and on the local grain size distribution. Finer grain sizes are transported preferentially, in this case (*Sutherland*, 1987).

Scenario 2 postulates that cascades with high initial sediment supply (Q_{S,in_ς}) rather than high local transport capacity compete more effectively for a share of $Q_{S_e}(d_{50e})$. Thus,

$$F_e = \frac{Q_{S,in_\varsigma}}{\sum_{k\in\Gamma_e} Q_{S,in_k}}. \tag{3.10}$$

This follows the notion that the redistribution of transport capacity is strongly driven by sediment supply (*Hsu and Holly*, 1992). Sediment fractions with higher supply, instead of finer grain sizes are transported preferentially.

Scenario 3 postulates, instead, that the local transport capacity of a cascade is a direct function of sediment supply.

$$Q_{S_e^{\varsigma\prime}} = F_e^{\varsigma} \cdot Q_{S,in_{\varsigma}}, \tag{3.11}$$

while F_e^{ς} depends on the local grain size distribution as in scenario 1 (Eq. 3.9). This scenario follows the notion that the local bed-load transport capacity of an edge presents an adaptation to its sediment supply (*Dietrich et al.*, 1989). If cascades with the same supply are present in edge e, cascades with finer grain size will be more competitive. Without competition ($F_e^{\varsigma} = 1$ for all Γ_e) all sediment cascades can pass through the river network without deposition, except if the grain size fraction transported along a cascade cannot be entrained in an edge (i.e., $Q_{S_e^{\varsigma}} = 0$ in Eq. 3.9).

3.3.3 A routing scheme for multiple sediment fractions

CASCADE implements a node-to-node sediment mass balance to describe the functioning of the sediment cascades and the resulting sediment flux Θ between all pairs of sources and downstream edges. The sediment routing along a cascade is performed sequentially path-by-path. Hence, the sediment input into a cascade is routed along the entire cascade, (i.e., until the basin outlet or until the cascade is interrupted) before the routing of the next cascades begins. The calculation order can be defined as upstream-downstream (sediment cascades from more upstream sources are routed first), downstream-upstream (sediment cascades from more downstream sources are routed first), or random. The sediment flux in a cascade remains constant after the routing of that cascade is finished. Hence, we assume that sediment sources supply sediment continuously. CASCADE recalculates the competition factors in all edges after the routing of a sediment cascade is completed. The sediment flux along a cascade γ_{ς} in edge e is derived from a local mass balance

$$\Theta_{e^{\varsigma}} = \begin{cases} \Theta_{in,e}^{\varsigma}, \text{ if } \Theta_{in,e}^{\varsigma} < Q_{S_e{}^{\varsigma\prime}} \text{ (condition 1)} \\ Q_{S_e{}^{\varsigma\prime}}, \text{ else (condition 2).} \end{cases} \tag{3.12}$$

Hence, all sediment is routed downstream if the flux from the next upstream edge ($\Theta_{in,e^{\varsigma}}$) is smaller than the competition corrected transport capacity $Q_{S_e{}^{\varsigma\prime}}$ in edge e (condition 1). If $\Theta_{in,e}^{\varsigma}$ exceeds $Q_{S_e{}^{\varsigma\prime}}$, then only $Q_{S_e{}^{\varsigma\prime}}$ is routed downstream and the sediment cascade experiences deposition in

edge e (condition 2). Sediment cascades can be dis-connected (${\Theta_e}^{\varsigma} = 0$) based on two mechanisms: (1) because the local transport capacity is not sufficient to entrain d_{ς} in edge e, (2) because all or most of the sediment supply was deposited between the source ς and e. Hence,

$$ {\Theta_e}^{\varsigma} = 0, \text{ if } \begin{cases} {Q_{Se}}^{\varsigma\prime} = 0 \text{ (1)} \\ {\Theta_e}^{\varsigma} < 0.05 \cdot Q_{S,in_{\varsigma}} \text{ (2).} \end{cases} \tag{3.13} $$

${\Theta_e}^{\varsigma}$ also defines the residence time of γ_{ς} in e

$$ {t_e}^{\varsigma} = \frac{l_e}{{v_{Se}}^{\varsigma}}, \tag{3.14} $$

where ${v_{Se}}^{\varsigma}$ is the sediment travel velocity of d_{ς} in edge e, and l_e is the length of that edge. ${v_{Se}}^{\varsigma}$ is defined as flux per a characteristic area, A_e. A_e is a function of active channel width, W_{ACe}, and the part of the water column, ${\theta_e}^{\varsigma}$, in which d_{ς} is transported. ${\theta_e}^{\varsigma}$ is calculated as $2.1 \cdot d_{\varsigma}$ (***Church et al.***, 2012). ${v_{Se}}^{\varsigma}$ becomes

$$ v_{S_e}^{\varsigma} = \frac{{\Theta_e}^{\varsigma}}{A_e} = \frac{{\Theta_e}^{\varsigma}}{{\theta_e}^{\varsigma} \cdot W_{ACe}}. \tag{3.15} $$

The sediment retention times for cascade γ_{ς} can be used to calculate the connection time along any set of connected edges that participate in $\kappa_{\varsigma}^{\Omega}$. E.g., let ε be a set of connected edges along the pathway $\kappa_{\varsigma}^{\Omega}$. The total connection time for γ_{ς} along the ε is then

$$ T_{\varepsilon}^{\varsigma} = \sum_{k \in \varepsilon} {t_k}^{\varsigma}. \tag{3.16} $$

From equations Eq. 3.14 - 3.16 it is evident that connection times in CASCADE are a direct function of sediment fluxes, sediment supply, competition, and the hydromorphological drivers in the river network along the edges ε. Fluxes and connection times are cascade specific. Hence, connectivity scales differently along the edges ε, if ε participates in multiple cascades.

Last, the total flux of sediment in an edge is defined as the sum of sediment flux along all cascades Θ_e in that edge:

$$ \Theta_e = \sum_{k \in \Gamma_e} {\Theta_e}^{k}. \tag{3.17} $$

3.4 Implementing CASCADE at the river network-scale

This section introduces a possible approach for parameterizing CASCADE for a large river network in SE Asia. This section first introduces the case study and describes (1) the derivation of fluvial graph and geomorphic states, (2) estimation of edge hydrographs, and (3) parameterization of sediment sources and grain sizes.

3.4.1 Case Study

CASCADE was implemented for the Da River system which is shared between Vietnam, China, and Laos (100° 22′ 30.587″ E, 24° 51′ 10.576″ N, and 105° 25′ 13.241″ E, 20° 35′ 44.263 ″ N) (Fig. 3.2). The basin of the Da River covers an area of 50570 km^2 and an elevation range from 3143 to 18 m asl. The Da River basin provides the major sediment input into the Red River Basin (*Le et al.*, 2007), which ranks 9th in the world in terms of sediment output (*Milliman and Meade*, 1983). There is only very limited evidence for grain sizes or transport rates in the Da River. *Vinh et al.* (2014) cites a median grain size of 0.35 mm in the bed material of (supposingly) the lower Da River. *Bogachenko et al.* (1984) reports a median grain size of around 1 mm for drilling cores derived from the river bed during the construction of Hoa Binh Dam (at the outlet of the basin, see Figure 3.2), with gravel fractions up to 40 mm present.

For a better estimate of grain sizes in the Da River we resorted to "citizen science" in the sense of using geo-referenced pictures of bank and bed sediment material in the Da River basin that were uploaded to Google Earth by users. From these pictures (Figure 3.3) the following conclusions can be derived. Low order tributaries in the Da River basin are pre-dominantly gravel and cobble rivers (Figure 3.3 a-c), but sand and fine gravel is present in some smaller tributaries (Figure 3.3 b). For higher order rivers, i.e., along the main stem of the Da-River, sand dominates the bank material but gravel can be found even in very downstream reaches (Figure 3.3 d,e,g). To conclude, it seems reasonable to assume that the Da-River, though dominated by sand in higher order reaches, is essentially a mixed sand and gravel river. It should be noted that the distribution of pictures is not homogeneous throughout the basin, related to people's access to the river, proximity to tourist attractions, and limited access to Google-owned web-services from China.

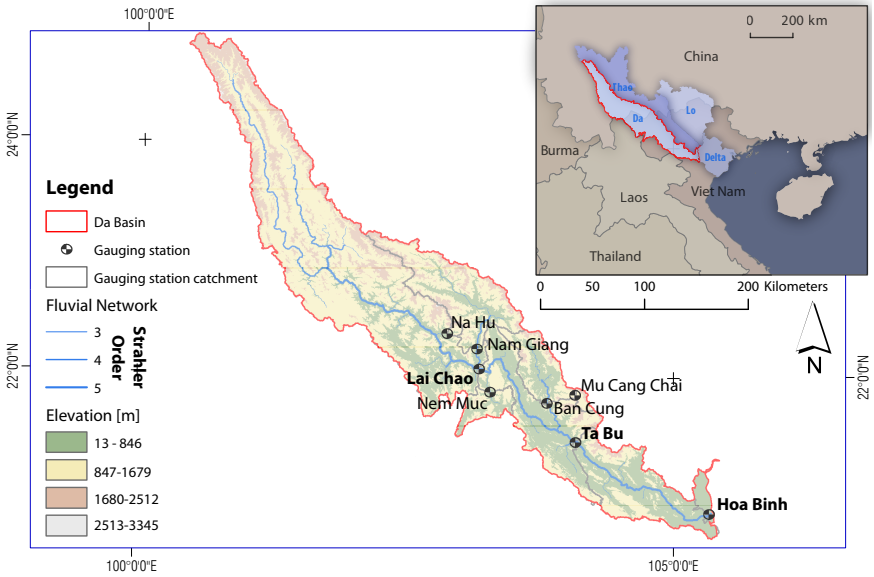

Figure 3.2: *Overview over the Da River Basin and the available gauging stations. Bold names indicate gauging stations for which total suspended sediment measurements are available. The small map indicates the location of the Da-River Basin within the Red River drainage system*

3.4.2 Deriving a fluvial multigraph

Delineating the river network and measuring reach geomorphic states.

We derived the river network from a DEM with 30 m resolution (ASTER GDEM) using the standard procedure of DEM filling and flow routing outlined in *Tarboton et al.* (1991). The river network was extracted using a

Figure 3.3 *(following page)*: *Geo-referenced pictures of bed sediment and morphology in the Da River basin, uploaded by various users and derived via Google Earth. a-c: Tributaries , and d-g: Main stem of the Da River. Small map for spatial reference. a: 3rd order tributary of the Na River, A_D = 180 km^2 (the Na river is the major left tributary of the Da). Gravel river with visible bars and point bars). b: Bridge over the Na River. Gravel dominated bars with some sandy deposits, A_D = 3700 km^2. c) 3rd order mountain river, dominated by boulders, finer bed material (fine gravel/cobble?) visible on the bed, A_D = 98 km^2. d: Mainstem of the Da upstream the Da-Na confluence, sand facies dominate banks under incised terraces, A_D = 21800 km^2. e: Mainstem of the Da, at the Da-Na confluence. Highly confined river with large gravel / cobble deposits and some sand facies, A_D = 25600 km^2. f: Sandy banks along the mainstem of the Da, A_D = 37500 km^2. g: Sand/gravel bar on the Da River, downstream of Son La Reservoir A_D = 42500 km^2. References: all pictures can be derived via* `http://www.panoramio.com/photo/`*, adding the photo-IDs to after the URL. Photo-IDs are, a: 66887780, b: 86817239, c: 55091946, d: 42578531, e: 57837156, f: 29985166, g: 51032245.*


a
b
c
d
e
f
g
b
a
c
e
d
f
g
N
0 100 200
km

drainage area threshold of 125 km^2. The resulting river network has a total length of 7433 km length with Strahler Orders ranging from 1 to 5. There are 5 major lateral tributary systems (with $A_D > 2500$ km^2). The network was first dissected at all confluences. All resulting reaches were split after a maximum of 5000 m, hence all reaches had a length 5000 m or shorter. This resulted in a total of 2123 reaches of which 949 had the full length of 5000 m (mean length 3511 m). CASCADE transferred the river network into a graph representation of 2123 edges and 2124 nodes. The geomorphic state was determined for all edges. Gradient was calculated from the length of an edge and the elevation difference between the start and end node. The drainage area was measured at the start and end nodes of an edge and the mean of both values was assigned to the edge. CASCADE calculated the active channel width, W_{AC} using an empiric scaling law that was derived for the basin under study in a previous study

$$W_{AC} = A_{D\,AD-W}^{m} * I_{AD-W}^{n} \tag{3.18}$$

with (m_{AD-W}=0.476, n_{AD-W}=-0.07675) (*Schmitt et al.*, 2014).

Deriving reach hydraulics

This step derives a reach-level hydrograph, dissecting each hydrograph into p flow percentiles, and calculating hydraulic conditions in each flow percentile. The local hydrograph was derived by down-scaling observed hydrographs with a scaling-law based on A_D. Eight long term discharge records (mean record length 47 yrs, daily resolution) were available. Gauging stations covered a range from very small upland (A_D=147 km^2) to major lowland rivers (A_D=50570 km^2). For location and details of all available discharge records refer to Fig. 3.2 and Tab. 3.1. The catchment of each flow gauging stations marks one of eight sub-basins. For the down-scaling we applied an edge-specific scaling factor J_e,

$$\boldsymbol{Q_e} = J_e \cdot \boldsymbol{Q_{SB}}, \tag{3.19}$$

where $\boldsymbol{Q_e}$ is the hydrograph assigned to edge e, and $\boldsymbol{Q_{SB}}$ is the observed hydrograph at the next downstream gauging station. We calculated J_e from

$$J_e = \frac{Q_{1.5_e}}{Q_{1.5_{SB}}}, \tag{3.20}$$

where $Q_{1.5_e}$ is the 1.5 year discharge in edge e and $Q_{1.5_{SB_e}}$ is the 1.5 year discharge in the next downstream gauging station. $Q_{1.5_e}$ was estimated using a scaling law derived from the same 8 gauging stations, which reached a high R^2 (0.94) (*Schmitt et al.*, 2014). Hence, J_e can be transformed into

$$J_e = \frac{a * A_D^b}{Q_{1.5SB_e}} \tag{3.21}$$

with a=1.321 and b=0.82. $\boldsymbol{Q_e}$ is therefore a non-linearly down-scaled version of an observed hydrograph. CASCADE split the reach hydrographs for each of the 2123 edges into $p = 9$ percentile values. Then, CASCADE calculated the mean discharge in each percentile and the 1.5 year discharge for each of the 2123 edges. CASCADE used the hydraulic solver (see Appendix 3.A) to calculate $v_e(p)$ and $h_e(p)$ for all $Q_e(p)$, as well as $v_e(Q_{1.5})$ and $h_e(Q_{1.5})$.

Table 3.1: *Overview over the available hydrologic observations*

Station Name		Ban Cung	Hoa Binh	Lai Chau	Mu Cang Chai	Na Hu	Nam Giang	Nam Muc	Ta Bu
Period		1962-2011	1956-2011	1957-2011	1980-2008	1968-2011	1965-2011	1960-2011	1961-2011
Ad	$[km^2]$	2577	50570	27151	270	147	5783	3119	6344
Mean Q	$[m^3\ I^{-1}]$	172,11	1517,79	1138,52	5,77	13,59	272,93	85,05	1517,79
Mean Q	$[mm\ d^{-1}]$	5,77	2,59	3,62	1,85	7,99	4,08	2,36	20,67

network-scale characterization of sediment sources

Identifying sediment sources and the supplied grain size is a key step for building the CASCADE modelling framework. Such information is not available for the river network under study, neither will it be for most river networks. Therefore, grain sizes in CASCADE can be initialized on the network-scale using an analytic approach. This approach assumes that each edge is the source of one single grain size d_ς, and that d_ς is a direct function of bankfull hydraulics, $v_e(Q_{1.5})$ and $h_e(Q_{1.5})$. This procedure is based on the assumptions that (a) the maximum bed shear stress occurs under bankfull hydraulic conditions and, (b) that the 1.5 year discharge is a good approximation of the bankfull discharge (*Knighton*, 1984). The maximum shear stress defines the equilibrium grain size that can persist in edge e, while smaller grain sizes are entrained (*Andrews*, 1983). We then assumed that the grain size of sediment produced in e is proportional to the equilibrium grain size. This results in $S = 1 \cdots 2123$ sediment sources that deliver sediment along $\Gamma = 1 \cdots 2123$ sediment cascades. The detailed calculation procedure for deriving d_ς is presented in Appendix 3.B

Estimating grain sizes and locating sediment sources at the network-scale is a major challenge in setting up CASCADE. The application of a single grain size throughout the basin has been successfully applied to model sediment transport in smaller catchments (*Czuba and Foufoula-Georgiou*, 2015, 2014; *Wilkinson et al.*, 2006). Nevertheless, we assumed that using a single grain size can hardly result in relevant results given the wide range of hydromorphologic conditions in the river network under study. For example, assigning a single sandy grain size to all reaches would result in a major overestimation of sediment outputs from steep upstream reaches and an underestimation of sediment transport in higher-order, downstream reaches. We tackle this problem by transforming the available hydrologic and topographic information into a consistent estimate of grain sizes. The resulting spatial distribution, probability distributions, and correlations between grain size d_ς and hydraulic parameters h_e, v_e, and $\tau_{*c_e}^\varsigma$ in the basin under study are reasonable and we discuss and present results in detail in Appendix 3.C. All sources are characterized by a specific supply Q_{S,in_ς}. Herein, we initialized sediment sources with

$$Q_{S,in_\varsigma} = {Q_{S}}_e^{\varsigma\prime}. \tag{3.22}$$

Hence, the sediment supply of d_ς is equal to the competition corrected transport capacity for d_ς in the edge where ς is located. This implies that sediment inputs are only detachment but not supply limited. Nevertheless, the rate of detachment will be strongly reduced for sources that are located in an edge with many active cascades and strong competition. Finally, CAS-

CADE applies a shortest path algorithm (*Dijkstra*, 1959) to determine the pathway $\kappa_{\varsigma}^{\Omega}$ for all sources.

3.4.3 Sediment routing and competition

CASCADES loops trough all $\varsigma \in S$ and calculates the transport capacity for all edges $e \in \kappa_{\varsigma}^{\Omega}$ using Eq. 3.1 - 3.7. At this stage, the sediment pathway for d_{ς} can be interrupted if d_{ς} cannot be entrained in a downstream edge (Eq. 3.13 (1)). After this step, each edge was traversed by an average of 26.7 sediment cascades. Competition between these cascades for the locally available energy was considered through the dynamic competition factor. We performed three separate runs of CASCADE, considering a different competition scenario in each run.

3.4.4 Scenario and sensitivity analysis

The main aim of this chapter is to introduce the CASCADE modelling framework and to provide evidence for how the derived information can provide novel insights into network sediment connectivity. We also test the sensitivity of cascade to some key assumptions. A full analysis of the distributed, network-scale sensitivity of CASCADE is beyond the scope of this chapter.

Therefore, we focus on the impact of competition scenarios, because competition interlinks empirical sediment transport calculations to more conceptual aspects of sediment connectivity and of the CASCADE modelling framework. There is no empirical information on sediment connectivity available for validating results in the network under study. Accordingly, we resort to a comparative analysis of the three scenarios, and match them to empirical observations and generic concepts of network-scale sediment connectivity. In a similar comparative approach, we evaluate the impact of grain size initialization on network connectivity. CASCADE in its current implementation considers only bed-load (i.e., sand or coarser fractions), while for the basin under study only observations of total suspended solids (TSS) are available (*Vinh et al.*, 2014; *Le et al.*, 2007). Therefore, we calculate the ratio between observed TSS and modelled bed-load, and compare results to available, global and regional observations (*Turowski et al.*, 2010; *Bravard et al.*, 2014). Additionally, a single estimate of median grain size in the main stem of the Da River was available from *Vinh et al.* (2014).

3.5 Results

Here, we present the outcomes of the CASCADE modelling framework for the Da River system. The analyses clarify how CASCADE allows assess-

ments of all domains of connectivity at the reach scale, as well as at larger (multi-reach or network) scales. Results on both scales are analysed with a focus on the impact of competition upom sediment connectivity. The execution of the CASCADE model for the Da River system is also shown in Movie S1 in the supplementary information.

3.5.1 Reach-scale connectivity

The reach scale analysis focuses on a single reach on the main stem of the Da River (Fig. 6.2). The reach is located at the confluence of a major sandy tributary with the main stream, see also Fig. 3.9 (tributary 3), and identical with Lai Chau (LC) gauging station (Fig. 3.2). We derive the connection times between all connected sediment sources and the reach under study. Connection times are used to group incoming sediment cascades into bins. The bins are defined between the 5 to 95 percentile of connection times in steps of 5 %. The 5 % (p_5), 50 % (p_{50}), and 95 % (p_{95}) percentiles are analyzed in more detail. The number of established connections increases with the percentile and p_{100} represents full connectivity, hence all upstream sources that can connect to the reach under study are connected. We identify which cascades connect to the reach under study within which bin of connection time, where their respective sources are located, and which fraction of the total input within that bin they provide. The analysis focuses on scenario 1 and 3, the end members between a local and a supply controlled perspective on sediment competition (for results of scenario 2 see Appendix 3.D).

Scenario 1 results in a heterogeneous spatial pattern of sources for small connection times (p_5, p_{50} in Fig. 6.2 A). The reach under study connects equally to main stem and to the major tributary within p_5. Preferential connectivity occurs to some reaches in lateral, mountainous drainage systems for p_5. These reaches present sediment sources with a locally small grain size which connect efficiently to the downstream network. Hence, the grain sizes delivered within p_5 from these remote sources are relatively fine. The median delivered grain size increases with increasing connection time when cascades which transport large grain sizes also connect to the reach under study (Fig. 6.2 B).

For scenario 3, the reach under study connects only to reaches along the main stem for small connection times (Fig. 6.2 C, p_5). Reaches in the major lateral tributaries and more upstream in the main stem connect within p_{50}. Smaller lateral tributaries are connected only above p_{50}. Preferential connectivity is limited to few reaches. The grain size delivered within p_5 is homogeneous, reflecting the grain size of sources located in the main stem. Delivered grain sizes fine for longer connection times as more upstream reaches connect to the reach under study (Fig. 6.2 D). The median grain size of delivered sed-

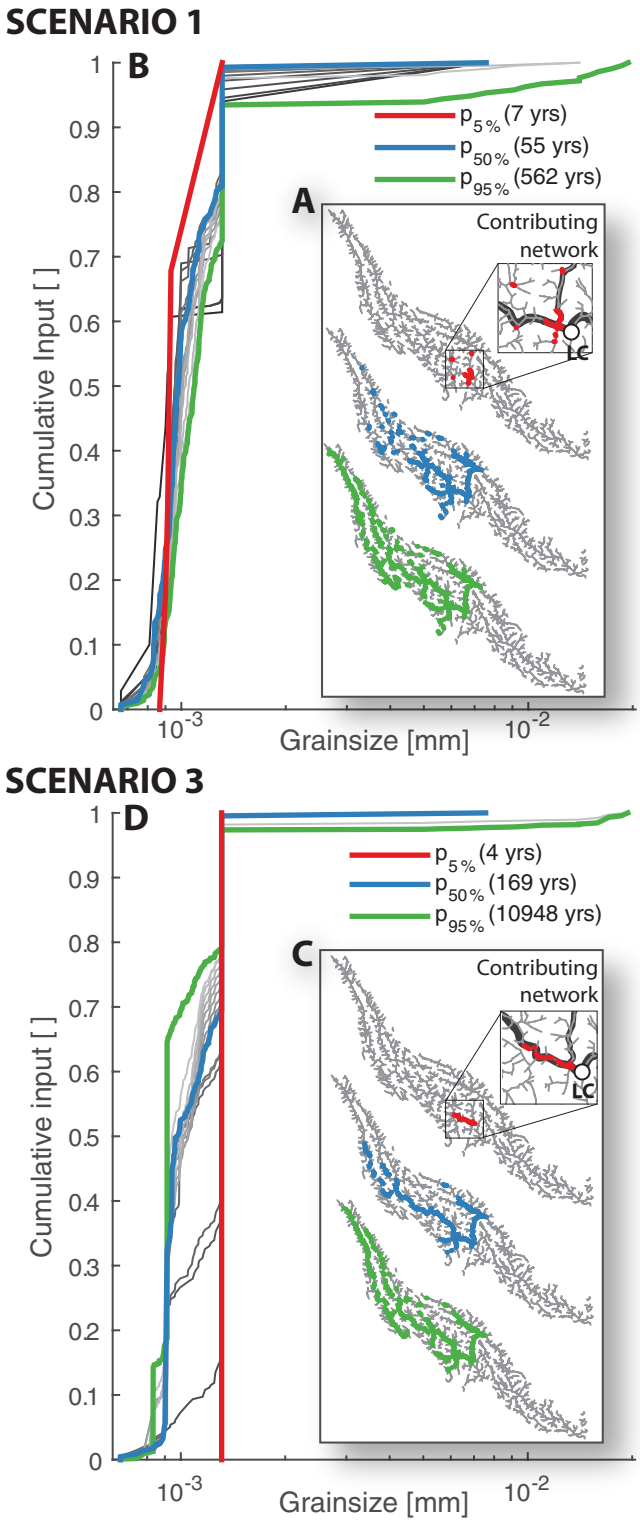

Figure 3.4: *Reach connectivity for scenario 1 (Panels A, B) and 3 (Panels (C, D) in terms of sediment delivery and source areas for different percentiles of connection time. The reach under study is identical with Lai Chau (LC) gauging station. Cut-outs in Panels A and C clarify the spatial distribution of sources for very short (5 % percentile) connection times.*

iment under full connectivity (p_{95}) differs between the two scenarios even though nearly the same upstream sources are connected. This is because fluxes from each source are different between scenarios, which impacts upon the sediment composition in the reach under study.

3.5.2 Basin scale sediment redistribution

The previous analysis indicated a significant impact of competition on reach connectivity. Here we enlarge the analysis to the entire main stem of the Da River and study the deposition trajectories from all sources located along the main stem. Each trajectory is defined by the sediment conveyance ratio along a sediment cascade. The sediment conveyance ratio describes which percentage of the sediment supply from source ς is delivered to downstream edge e. Hence, the inverse of the sediment conveyance ratio describes which percentage of the sediment supply from ς is deposited along the pathway κ_{ς}^{e} (Fig. 6.3 A & B). We also analyze the sediment conveyance ratio on the network-scale between all ς and the basin outlet node Ω. This analysis identifies preferential connections on the network-scale and the sediment recruitment areas in which sediment sources are located that deliver sediment to the basin outlet. (Fig. 6.3 B & D).

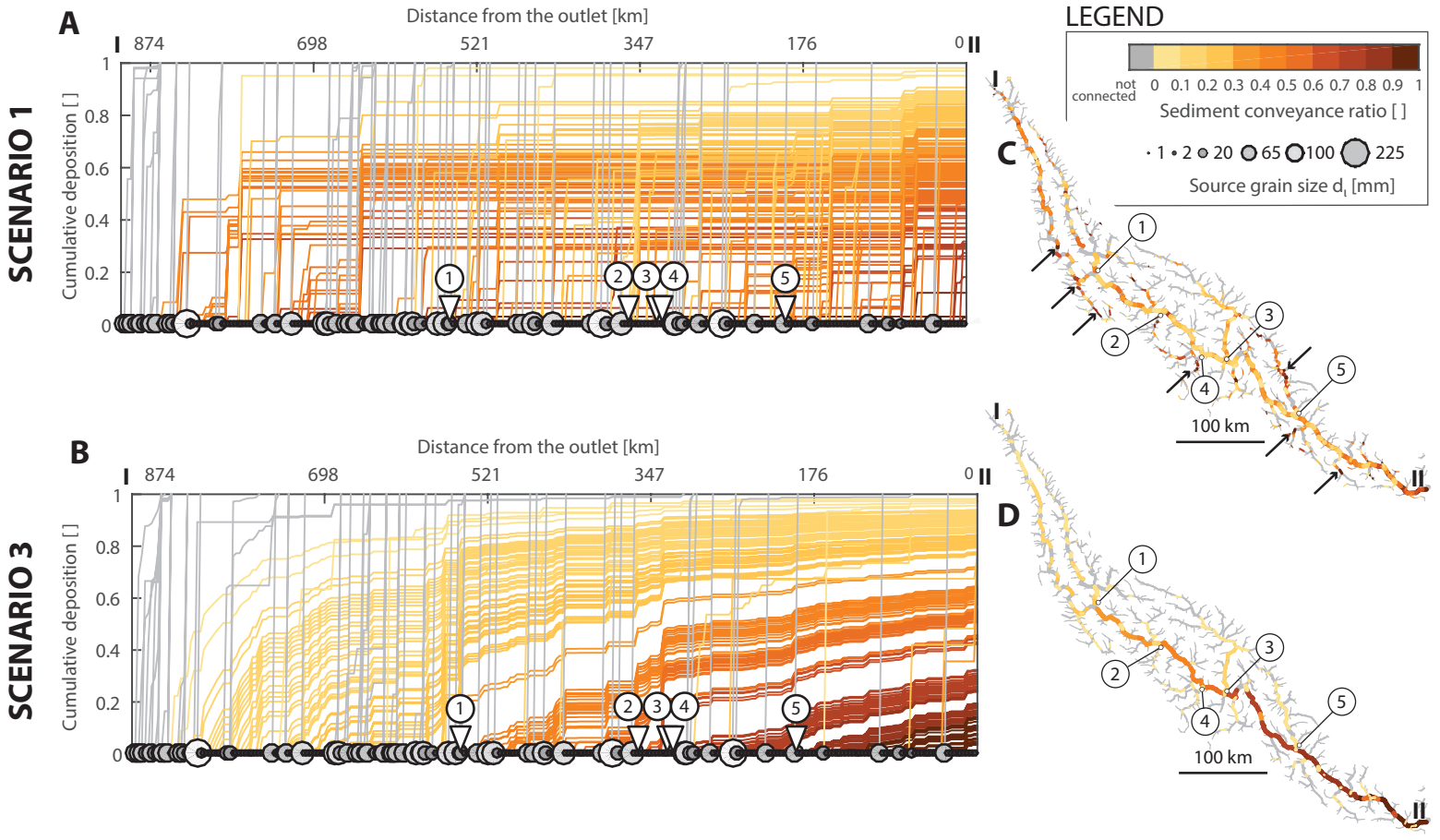

Figure 3.5: *Network connectivity for scenario 1 (Panels A, C) and 3 (Panels (B, D). Panels A and B show deposition trajectories, repectively the sediment conveyance ratio, along the main stem of the Da River. Dots indicate the source grain size d_ς of each cascade (identical between scenarios). Numbers and triangles indicate the location of major tributaries ($A_D > 2500km^2$, see also Fig. 3.9). The sediment conveyance ratio is also mapped on the network-scale throughout the river basin (panels C and D). Arrows in panel C indicate some hotspots of sediment recruitment.*

Scenario 1 results in an unstructured pattern of deposition along the main stem. Longitudinal organization, e.g., due to tributaries, is absent (Fig. 6.3 A). There is no upstream-downstream gradient in the sediment conveyance ratio, i.e., no correlation between the distance of a source to the outlet and its connectivity to the outlet. Scenario 3 results, instead, in a continuous deposition and a clear upstream-downstream gradient in the sediment conveyance ratio along the river. Sediment delivery is longitudinally structured by tributaries into distinct bands (Fig. 6.3 B). Deposition is emphasized for cascades that begin close to a confluence and that still have a high sediment conveyance ratio at the confluence. Cascades from sources between confluences 1 and 2 are, for example, subject to much stronger deposition at confluence 2 then cascades from sources upstream of confluence 1. This is because the latter already deposited the majority of initial sediment inputs further upstream. Hence, a higher sediment flux increases the sensitivity to competition, e.g., at tributaries, under scenario 3. At the network-scale, scenario 1 results in spatially discrete hot-spots of recruitment (Fig. 6.3, C, see arrows). Sediment cascades from these hot-spots compete effectively and reach the basin outlet without major deposition (conveyance ratio close to 1.). For scenario 3, hot-spots of recruitment are nearly absent (Fig. 6.3, D). There is a clear upstream - downstream gradient in sediment delivery. This gradient is a function of network hierarchy, with tributaries delivering less sediment to the basin outlet than the main stem. Results for scenario 2 are reported in Appendix 3.D.

3.5.3 Patterns of sediment dis-connectivity

Finally, we analyzed where dis-connectivity occurs. Dis-connectivity refers to sediment cascades that are disconnected from the basin outlet, either because the entire sediment supply from a source is deposited, or because the supplied grain size cannot be entrained in a downstream reach. The analysis of dis-connectivity includes (a) identifying the spatial distribution of sources that do not connect to the basin outlet and, (b) locating edges where the respective sediment cascades are interrupted. These edges can be considered potential in-channel sediment stores which could convert into sources. Though not considered in this chapter, the frequency of such an activation would link to hydro-climatic conditions that result in extreme flow events, and the local morphologic conditions that would define a maximum value for in-channel sediment accommodation. First we identify disconnected sources using sediment trajectories and network-scale patterns of sediment redistribution (Fig. 6.3). At the network-scale, the spatial distribution of disconnected reaches is nearly identical for all scenarios. Analyzing longitudinal pattern of dis-connectivity along the Da River indicates that dis-

connectivity is mainly related to large local grain sizes which are most abundant in the upper (km 900 to km 850) and the upper middle reaches (km 520 to km 700) of the Da-River. This becomes evident comparing the sediment trajectories of scenario 1 and 3 (Fig. 6.3, left panels). Large grain sizes (i.e., gravel-cobble size) are deposited within few reaches, because of locally insufficient energy to transport them further downstream. The transport of finer sediment fractions through reaches where large sediment fractions are deposited is unimpaired for either scenario. CASCADE locates the specific edges where a sediment cascades is interrupted. This information reveals bottlenecks for sediment connectivity. In these bottlenecks a high number of cascades is interrupted (Fig. 3.6 shows edges in which at least five cascades are interrupted). CASCADE also identifies the mechanisms for disconnectivity. Hence, if a cascade is interrupted because of a local hydro-morphologic control (EQ. 3.13, case 1), or because of competition (EQ. 3.13, case 2). We use scenario 3 for this analysis as the mechanisms for disconnectivity can be distinguished more clearly. Under scenario 3, all cascades could connect to a defined end-point without competition. That end-point is either the basin outlet, or an edge where a cascade's grain size cannot be entrained, and which can be identified *a-priori* using Eq. 3.13. In turn, cascades that are interrupted before their end-point are interrupted because of competition.

We find that local morphologic controls create bottlenecks (Fig. 3.6, red squares) where multiple cascades from smaller tributary convey larger grain sizes that cannot be entrained in the main river channel. Competition creates instead bottlenecks at the major confluences, with the number of disconnected cascades being proportional to the size of the confluence (Fig. 3.6, blue circles). This indicates that competition is an additional switching mechanism that controls which sources connect to the downstream river network.

3.5.4 Validation and sensitivity analysis

Comparing CASCADE sediment flux to observations

As a preliminary validation we compare modeled bed-load fluxes derived from Eq. 3.17 to available observations. Total suspended solids (TSS) observations are available for 3 gauging stations in the river network (Fig. 3.2). In average, predicted bed-load flux at these station was 2.2 ± 0.75 % of observed TSS (Fig. 3.7). These values are within the values of bed-load/TSS ratios (2-40 %) observed for major sandy rivers worldwide (*Turowski et al.*, 2010). Values are also within the range of estimates for the Mekong River, reflecting a river in a relatively similar geologic and climatic setting (1-3 %) (*Bravard et al.*, 2014). On the network-scale, scenario 2 resulted in the high-

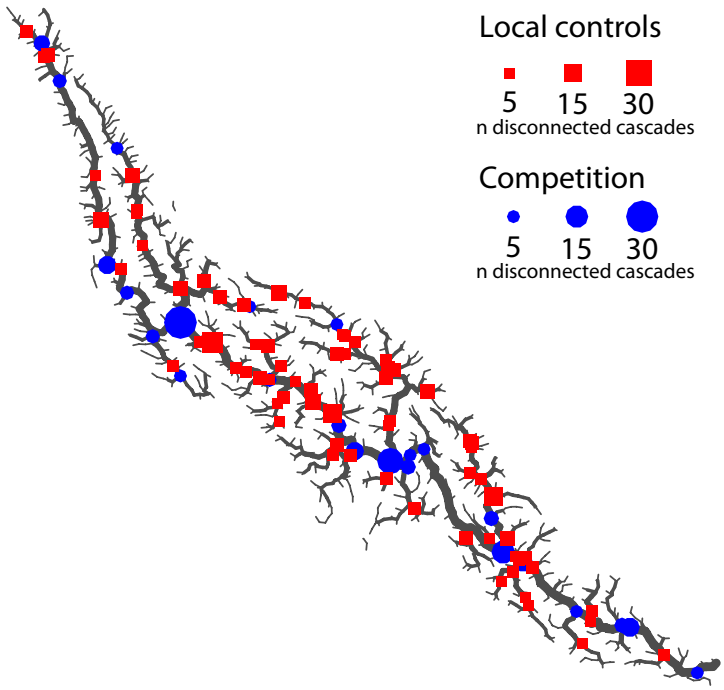

Figure 3.6: *Hotspots of disconnectivity for scenario 3. Red squares and blue dots indicate edges where multiple cascades are interrupted either due to local hydromorphologic controls or competition. The marker size indicates the number of interrupted cascades.*

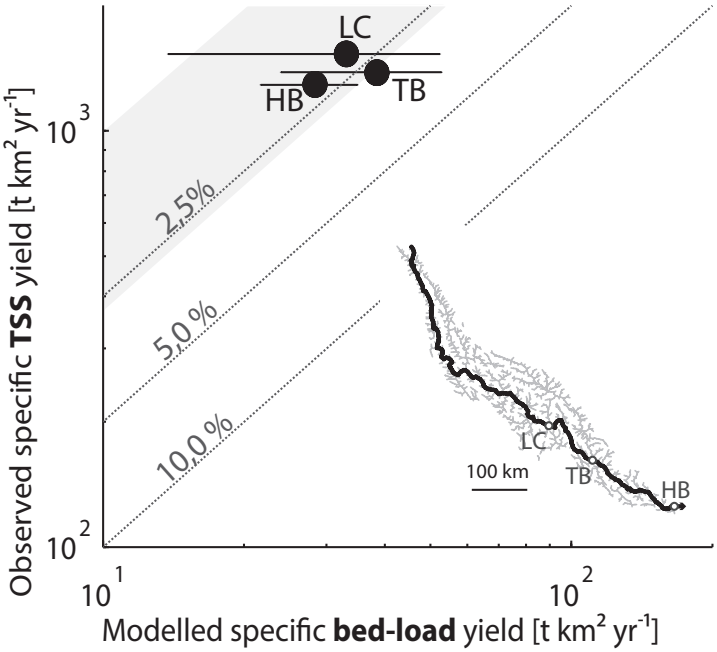

Figure 3.7: *Comparing CASCADE results to available sediment transport calculations. Letters indicate the name of sediment gauging stations (see Fig. 3.2). Dots represent the mean modeled value for each gauging station. Horizontal error bars give represent the range of values predicted at a station for the 3 scenarios. Diagonal lines indicate bed-load/TSS ratios. The shaded area indicates the TSS/bed-load ratios reported for the Mekong (1 - 3%, Bravard et al. (2014)).*

est sediment fluxes. Mean Θ_e for all 2123 edges was 2.1×10^9 kg yr^{-1} for scenario 1, 4.0×10^9 kg yr^{-1} for scenario 2, and 9.2×10^8 kg yr^{-1} for scenario 3. The difference in mean sediment fluxes was only significant between scenario 2 and 3 (p=0.0015, t-test with sample size 2123). The predicted median grain size diameter in the main river stem (Strahler Order > 5) was 1.3 mm, and hence around four times the value reported by *Vinh et al.* (2014) (0.35 mm). These results indicate that the assumptions behind CASCADE are a reasonable approximation to sediment transport processes, at least in the major river channels where some data are available.

Towards a networks scale sensitivity analysis

In this section we provide some insights into CASCADE sensitivity. We focus for now on the grain size of sources (d_ς) and use scenario 3 for the analysis. We selected d_ς for the sensitivity analysis for three reasons. First, d_ς is a direct function of local hydro-morphologic properties because of the proposed method for estimating d_ς. Analysing model sensitivity to d_ς there-

fore allows evaluating of model sensitivity to measurement errors in hydraulic and morphometric parameters, e.g., in gradient. Measurement errors in gradient relate, in turn, to low input data resolution, or the used reach length (e.g., shorter reaches might capture a higher degree of local variability in gradient and result in steeper gradient values). Second, d_ς directly impacts the sediment supply from sources (Eq. 3.22). Third, sediment inputs determine the competitiveness of a sediment cascade under scenario 3. Therefore, this analysis captures multiple aspects of model and parameter uncertainty. Fourth, the calculation of d_ς assumes that there is an equilibrium between bed shear stress and the grain size of a source. This assumption might not hold in many cases. For example, where mass-movements supply above-equilibrium grain sizes, or hillslope processes supply below-equilibrium grain sizes to the channel. We perturbed the grain size d_ς of each source by multiplying the original d_ς with a perturbance factor Φ_ς that represents deviation of the actual d_ς from the local equilibrium grain size because of the above mentioned factors. We created four versions of Φ_ς. v1 ranged from 1 – 10 (0 – 1000 % perturbance), hence d_ς was increased for all sources. v2 ranged from 0.1 – 10 (-90 – 1000 % perturbance), d_ς was increased and decreased for an equal number of sources. v3 ranged from 0.1 – 1 (-90 – 0 % perturbance), hence d_ς was decreased for all sources. v4 also ranged from 0.1 – 1, but d_ς was only decreased for 50 % of the sources. For each version we analyzed the sediment trajectories along the main stem of the Da River. Results are shown in Fig. 3.8. Panels A, C, E, G visualize the probability distribution and the spatial pattern of Φ_ς for v1 – v4. Panels B, D, F, H show the sediment trajectories along the main stem of the Da River (analogue to the information shown in Fig. 6.3)

The results of this analysis indicate how disturbing the model initialization may affect the previously discussed large-scale patterns of sediment connectivity derived from CASCADE. A major network-scale increase in grain sizes (v1, Fig. 3.8 A, B) leads to the disappearance of the clear upstream-downstream deposition pattern and a strong initial deposition along most cascades. Nevertheless, there are few cascades that are disconnected from the basin outlet (grey lines in Fig. 3.8 B). The low number of disconnected cascades can be related to a general decrease in the competitiveness of cascades because all cascades transport larger grain sizes. Under v2, with randomly increased and decreased source grain sizes, there are clearly more disconnected cascades (Fig. 3.8 D). This is because cascades with increased d_ς are in competition with cascades with decreased d_ς. Cascades reaching the basin outlet develop a continuous downstream deposition pattern. Sediment trajectories form a clear structure of different bands that are separated at tributary confluences. Nevertheless, the bands are more

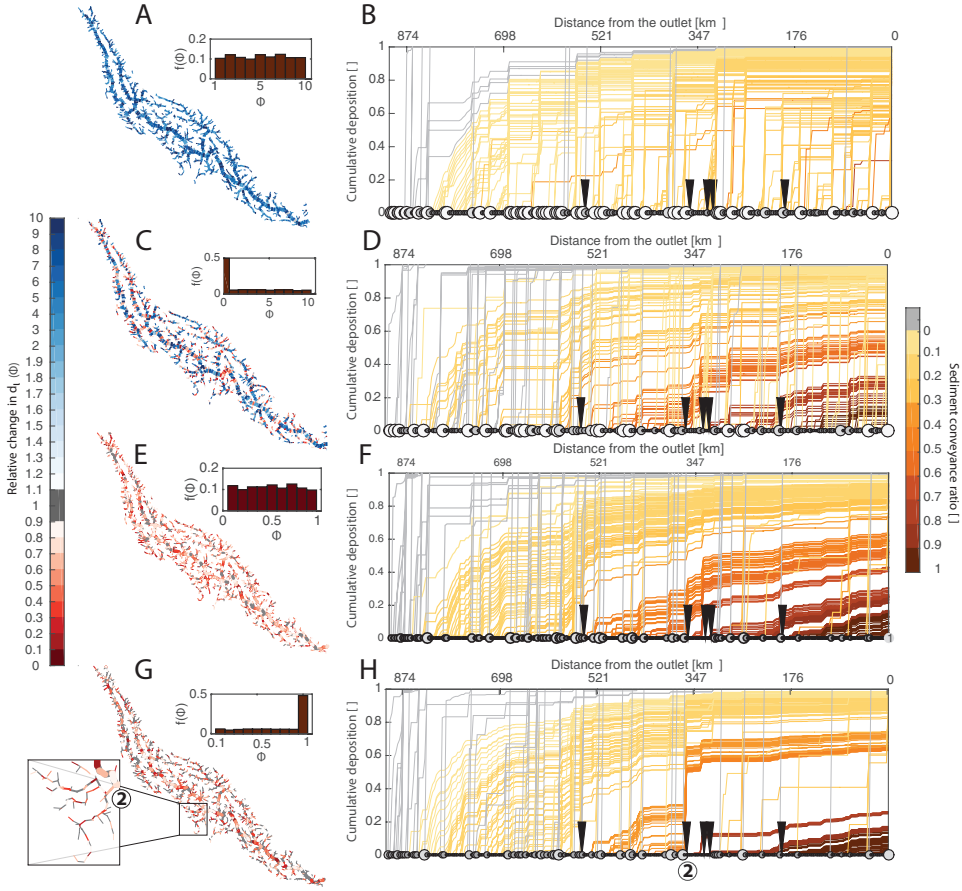

Figure 3.8: *Analyzing the sensitivity of deposition trajectories to source grain size d_ς. The right colorbar indicates the disturbance factor of grain size in comparison to the original values (Φ). The spatial distribution of Φ is displayed on panels A, C, E, G; small histograms show the probability distribution of Φ. Panels B, D, F, H visualize the resulting sediment trajectories. Black triangles mark tributary confluences, the point size on the x-axis indicate source grain d_ς*

sparse in comparison to the original result (Fig. 6.3 B), because some sources within the bands are disconnected or experience strong deposition. This is evident in comparison to v3 (Fig. 3.8 F), for which bands are more compact. Otherwise, the observed pattern for v3 is very similar to the pattern for the original scenario 3 (Fig. 6.3 B). All cascades receive a higher sediment input, but are accordingly more competitive. Decreasing d_ς randomly for only some cascades (v4) provides further clarification for the functioning of the CASCADE approach (Fig. 3.8 G, H). Using the current parameterization, sediment sources in steep, mountainous reaches will provide larger grain sizes. This limits the input from these sources and makes them less competitive. For example, tributary 2 contains the fewest sources with sandy grain size among the five major tributaries (Fig. 3.9). This indicates that tributary 2 is the steepest of the five major tributaries. Nevertheless, tributary 2 already had a clear impact on sediment trajectories along the main channel for the original scenario 3 (Fig. 6.3 B). Applying $\Phi(v4)$ strongly decreased d_ς for some sources in tributary 2 (Fig. 3.8, cutout in G). Decreasing d_ς then increased the sediment output from this tributary by an order of magnitude (from 4.1 $\times 10^4$ tons/year to 5.4 $\times 10^5$ tons/year). Sediment cascades which begin upstream of the confluence of tributary 2 now experience a much more emphasized deposition at the confluence (Fig. 3.8 H, km 360). Yet, the d_ς of sediment cascades from tributary 2 are still too large to be transported far downstream along the main stem. Therefore, the high deposition at tributary 2 reduces the competition for more downstream cascades, making them deliver sediment to the basin outlet more effectively (compare Fig. 3.8 F and H, downstream of km 360).

To conclude, this section provides first some evidence for the consistency of the CASCADE with regard to its reaction to changing grain sizes (e.g., larger grain sizes increase initial deposition, higher tributary inputs increase competition along the main channel). Second, there is some evidence that the presented model results are valid for a wide range of parameterizations. The general pattern of sediment trajectories under scenario 3 collapses only if the grain size in the main stem is massively increased, changing the main stem from a sand (68 % of sources deliver a $d_\varsigma < 2$ mm in the original parameterization) to a gravel dominated river (5 % of sources deliver a $d_\varsigma < 2$ mm for $\Phi(v1)$).

3.6 Discussion

The CASCADE modelling framework quantifies network sediment connectivity by explicitly tracing sediment cascades from sources to all connected sinks. We applied CASCADE to a large river network and present the connectivity information that can be derived using very limited input data. We

provide some indication for how CASCADE enables analyzes of complex sediment transport processes and connectivity on the network-scale. This novel connectivity information clarifies the internal functioning of the CASCADE model, allows assessment of its limitations, and its sensitivity to internal and external boundary conditions. Finally, we discuss how this new information could support river science and management. Nearly all analyses presented in this chapter rely on multiple domains of sediment connectivity (location of sources, source-specific flux, and delivered grain sizes). The ability of CASCADE to provide this information enabled us to reproduce often observed phenomena such as preferential connectivity that can hardly be reproduced with common sediment modelling approaches.

For example, field evidence points out the role of local hydromorphologic controls that act as grain size depending switches that either facilitate or disrupt sediment connectivity (*Fryirs et al.*, 2007b,a). CASCADE can readily locate such switches by identifying where a specific sediment cascade is disconnected from the downstream river network. Additionally, our results extend analysis of sediment switches. Not only local morphologic controls but also the continuous deposition along a sediment cascade can result in dis-connectivity for specific cascades at specific location. Yet, these switches are potentially variable in space. For example, if some cascades are disconnected by the construction of a reservoir, more downstream sources can become better connected to the remainder of the river network because competition is reduced. Hence, CASCADE points out permanent, physical disconnections but also partial or transient disconnections that can be connected under the right environmental circumstances, or as reaction to human interventions (*Jain and Tandon*, 2010)

Sediment trajectories provide source specific information on the fate of sediment but allow also reproducing large scale patterns of sediment connectivity. These spatial patterns can be compared to some well established concepts of network connectivity. Sediment trajectories obtained using a supply driven competition factor (scenario 3) closely match the observation of *Arnaud-Fassetta* (2004), who observed that the contribution of an upstream source to a downstream sink decreases with increasing distance between both. Yet, observations with this regard are equivocal. Results of *Clift et al.* (2004a) for the Mekong indicate that preferential connectivity, similar to the pattern observed under scenario 1, can be relevant even in very large river systems. CASCADE also allows quantification of the impact of local confluence effects on network-scale sediment connectivity. With regard to confluence effects, scenario 3 results in connectivity patterns that are in close accordance with empirical observations. For example, *Rice et al.* (2006); *Benda et al.* (2004a,b) document how tributaries effect main channel

morphology and sediment connectivity. The magnitude of these confluence effects strongly related to the fraction of main channel transport versus tributary inputs. Such a pattern is reproduced mainly under scenario 3. The sensitivity analysis provided evidence that CASCADE captures this correlation between main-channel connectivity and tributary inputs. The sensitivity analysis also indicates that these observed patterns strongly relate to the transported grain sizes, and that such clear network-scale pattern for scenario 3 mainly emerge for sand-bed rivers. Based on the results and the available information, we cannot state that any of the three scenarios is *per-se* more appropriate. Scenario selection should instead be based on comparing CASCADE results to, even sparse or broad, empirical observations for the river system under study. Yet, we propose that Scenario 3 can be a good starting point for model initialization, as it was able to reproduce some key traits of connectivity for the network under study. Analyzing the sensitivity indicate that these general observations are relatively insensitive to initial conditions.

Obviously, the presented modelling framework is not conceived as a process based hydro-dynamic sediment transport model for detailed studies of coupled sediment transport and river morphologic processes. So far, CASCADE does not consider a morphologic adaptation of the river network to sediment inputs, e.g., in terms of slope. The fluvial network presents a static template along which various bed-load fractions are routed and their interaction can be studied. The proposed initialization of grain sizes based on remote sensing data is a highly simplified attempt to address the widespread lack of sedimentologic data with a quantitative, spatially continuous, and globally applicable approach. network-scale source initialization will also improve with time-series of high-resolution fluvial data-sets on network or regional scales (*Bizzi et al.*, 2015a). Such data-sets will progress automated identification of, e.g., relevant sites of bank erosion or in-channel stores of sediment that can act as additional sources. In the future, there are relevant links between the automated, object-based structural mapping of fluvial forms (*Demarchi et al.*, 2016) and connectivity modelling. Information on local sediment connectivity can provide a stronger link between structural mapping of fluvial forms and fluvial processes. In turn, a detailed structural mapping can greatly support model initialization and validation of a connectivity model, e.g., with regard to identifying active channel margins, floodplains or in-channel landforms (*Fryirs et al.*, 2016) that can serve as sediment sources or sinks during overbank flow events. .

There are multiple aspects of network-scale sediment transport processes that should be included into future versions of CASCADE. Attrition of larger grains (*Parker*, 1991) could increase the connectivity of upstream gravel and cobble sources, while demobilization on floodplains could create additional

sinks for smaller grain size fractions. Through its multigraph structure, CASCADE can be easily expanded to consider additional connected transfer processes. Enlarging the scope from the network to the landscape scale could be achieved by adding additional sediment cascades that explicitly represent hillslope processes (e.g., *Heckmann and Schwanghart* (2013)) or the transfer from active sediment stores (*Tunnicliffe et al.*, 2012; *Tunnicliffe and Church*, 2011) . Additionally, cascades can be added to represent not only the routing of bed-load, but also of finer, suspended load fractions.

CASCADE should, above all, be considered as a flexible, exploratory tool to project the impact of local controls, conceptualizations, and empiric observations (which are, e.g., the basis of most sediment transport formulations) onto all scales and domains of sediment connectivity for a real river system (cf. *Bracken et al.* (2015); *Brierley et al.* (2006)). CASCADE will also support transferring new available fluvial data-sets into physically-based indicators for the connected functioning of fluvial systems. Second, it is increasingly evident that the long acknowledged complexity in sediment and, specifically, bed-load transport processes (*Walling*, 1983) is still missing from most numerical, or conceptual sediment management approaches (*Fryirs*, 2013). At the same time, information on sediment sources and stores is largely absent even in better studied river basins (e.g., *Walling* (2008)). CASCADE adds a relevant component with this regard in comparison to previous approaches,which is relevant for both knowledge discovery and river management. *Reid and Brierley* (2015) point out that the local sensitivity of river to change is a function of both local morphologic controls and uptream sediment inputs. The ability of CASCADE to identify the sediment sources for a specific reach can help to identify most vulnerable or resilient reaches, and the timescales over which upstream changes will impact downstream reaches. With this regard, CASCADE supports deriving spatially explicit indicators for fluvial resilience that embalm both the response time and the magnitude of downstream change to an upstream disturbance. Current models for management oriented, basin scale sediment assessments are computationally effective but rely often on scarce empirical observations (*Kondolf et al.*, 2014; *Wild and Loucks*, 2014). In comparison, CASCADE greatly increases the fidelity with which sediment transport processes can be reproduced on the network-scale. A single CASCADE run can only provide a first order estimate of network-scale sediment transport processes without more detailed input data. Nevertheless, CASCADE is an effective, process-related screening model to analyse a high number of different scenarios or parameterizations. Soon, CASCADE will be made accessible as a publicly available. CASCADE covers the most relevant process domains of connectivity (*Bracken et al.*, 2015), namely detachment, transport, and deposition

of each grain size fraction. CASCADE also provides new capabilities with regard to visualization, interpretation, and quantification of multi-scale sediment source-sink relations. With this regard, CASCADE can considerably increase our ability to analyse connected sediment transfers on the river network or basin scales, a prerequisite to foresee and communicate human impacts on sediment connectivity and related ecosystem functions and services (*Fryirs*, 2013).

3.7 Conclusion

The CASCADE (**CA**tchment **S**ediment **C**onnectivity **A**nd **DE**livery) modelling framework is a novel approach to quantify sediment deliveries between all sediment sources and sinks in large fluvial networks. The major novelty is that CASCADE describes the transport of sediment from each specific source as an individual cascading process. In this chapter, we demonstrate how the resulting information can be used to study most relevant domains of sediment connectivity over multiple spatio-temporal scales. We exemplify the application of CASCADE and the analysis of the resulting connectivity information for a major basin in SE Asia. Specifically, we used CASCADE to study the connectivity of a single reach to the contributing river network, to analyze the fate of sediment from manifold sources, to identify network patterns of connectivity, and to identify bottlenecks for sediment connectivity. In this chapter, the parameterization of CASCADE relied heavily on medium-resolution remote sensing data. Yet, this application demonstrated an implementation strategy that makes CASCADE applicable as an effective screening model for the very large, poorly monitored river network under study. Nevertheless, CASCADE can be readily adapted to assimilate additional information and to include further relevant processes. This encourages us to propose CASCADE as a powerful computational tool to derive multi-scale indicators for river network connectivity with applications in both river science and management.

3.8 Notation

A_D	Drainage Area $[km^2]$.
A_e	Set of edge attributes.
A_e	Set of edge attributes.
a	Cardinality of A_e.
a	Parameter $A_D - Q_{1.5}$ relation $[-]$.
b	Parameter $A_D - Q_{1.5}$ relation $[-]$.
C_f	Friction factor $[-]$.
d	Grain size $[m]$.
E	Full set of edges in G.
e	Specific edge in E.
e	Cardinality of E
F	Competition Factor $[-]$.
FR	Froude number $[-]$.
G	River Graph.
g	Gravitational acceleration $[kg\ m\ s^{-2}]$.
g	Cardinality of Γ.
h	Flow stage $[m]$.
I	Energy slope $[-]$.
J	Hydrograph scaling factor.
l	Edge length$[m]$.
m_{AD-W}	Parameter $A_D - W_{AC}$ relation $[-]$.
N	Full set of nodes in G.
n	Cardinality of N.
n	specific node in N.
n_{AD-W}	Parameter $A_D - W_{AC}$ relation $[-]$.
n_p	Number of observation within the $p-th$ discharge percentile $[-]$.
n_{Str}	Manning-Strickler friction factor $[s\ m^{1/3}]$.
n_{tot}	Total number of discharge observations for a reach $[-]$.
p	Discharge percentile $[-]$.
$\boldsymbol{Q}$	Discharge time series $[m^3\ s^{-1}]$.
$Q_{1.5}$	1.5 year return period discharge $[m^3\ s^{-1}]$.
Q_S	Transport capacity $[kg\ yr^{-1}]$.
$Q_S{}'$	Competition corrected transport capacity $[kg\ yr^{-1}]$.
$Q_{S,in}$	Sediment input $[kg\ yr^{-1}]$.
q_{S*}	Dim. less transport capacity $[-]$.
q_S	Transport capacity per unit channel width $[m^2\ d^-1]$.
R	Relative sediment density $[-]$.
R_h	Hydraulic radius $[m]$.
Re_p	Particle Reynolds Number $[-]$.
S	Full set of sources.
T	Connection time $[yr]$.

t	Residence time $[yr]$.
v	Flow velocity $[m\ s^{-1}]$.
W_{AC}	Active channel width $[m]$.
α	Parameter, Wong-Parker Sediment transport formula $[-]$.
β	Parameter, Wong-Parker Sediment transport formula $[-]$.
Γ	Full set of sediment cascades.
γ	specific sediment cascade in Γ.
ϵ	Sub-set of edges along a pathway κ.
Θ	Sediment flux $[kg\ yr^{-1}]$.
θ	Characteristic transport depth $[m]$.
κ	cascade pathway.
ν	Kinematic viscosity $[m^2\ s^{-1}]$.
ρ_S	Sediment density $[kg\ m^{-3}]$.
ς	Specific source in S.
$\tau*$	Dim. less shear stress $[-]$.
τ_{*c}	Dim. less critical shear stress $[-]$.
Ω	Identifier of basin outlet node.

Appendix

3.A The hydrodynamic solver

The derivation of hydraulic conditions in an edge for a given flow is based on the Manning-Strickler formula for uniform, open-channel flow (*Strickler*, 1923). Flow velocity is calculated as

$$v_e = \frac{1}{n_{Str}} \cdot {R_{he}}^{2/3} \cdot {I_e}^{0.5}, \tag{3.23}$$

where n_{Str} is the Manning-Strickler friction coefficient. Here we use $\frac{1}{n_{Str}}$= 35 as typical value of natural streams (*Chow*, 1959). R_{he} is the hydraulic radius defined as

$$R_{he} = \frac{h_e \cdot W_{ACe}}{2h_e + W_{ACe}}. \tag{3.24}$$

We assume that river channels are rectangular in all reaches and for all flow stages. We rewrite v_e as flow per channel cross-sectional area

$$v_e = \frac{Q_e}{W_{ACe} \cdot h_e}, \tag{3.25}$$

hence

$$Q_e = \frac{1}{n_{Str}} (\frac{h_e \cdot W_{ACe}}{2h_e + W_{ACe}})^{2/3} \cdot I_e^{0.5} \cdot W_{ACe} \cdot h_e. \tag{3.26}$$

There is no explicit solution for Eq. 3.26 but Q_e is a function of h_e only. Therefore we transfer Eq. 3.26 into

$$Q_{calc_e} = \frac{1}{n_{Str}} (\frac{h_e \cdot W_{Ace}}{2h_e + W_{Ace}})^{2/3} \cdot I_e^{0.5} \cdot W_{Ace} \cdot h_{este}. \tag{3.27}$$

Q_{calc_e} is the value of Q_e calculated by using an estimated value of h_e (h_{este}).We apply a non-linear minimization algorithm to identify h_e such that

$$h_e = \min_{h_{este}} |Q_e - Q_{calc_e}|. \tag{3.28}$$

From Eq. 3.25 it is evident that the estimation of h_e allows to calculate v_e. The selection of an initial estimate of h_e in Eq. 3.28 is relevant for the solving procedure. We used a hydraulic geometry relation

$$h_{este} = {Q_e}^{0.289} \cdot {I_e}^{-0.035} \tag{3.29}$$

for that purpose (*Huang et al.*, 2002).

3.B Deriving source grain size estimates

We assumed that only the largest fractions of the grain size mixture in a reach (e.g., $d > d_{90}$) are not entrained under bankfull flow conditions. We approximate the size of this fraction through

$$d_{90_\varsigma} = \frac{I_e \cdot h_{eQ_{1.5}}}{R \cdot {\tau_{*ce}}^\varsigma} \tag{3.30}$$

Shields (1936), where ${\tau_{*ce}}^\varsigma$ is the critical shields parameter for the entrainment of d_ς in e. The transport rate of d_{90_ς} would accordingly be negligible according to 3.30 even for bankfull flow conditions. Therefore, we convert d_{90_ς} into the source grain sizes

$$d_\varsigma = \frac{d_{90\varsigma}}{2.1}, \tag{3.31}$$

similar to the conversion from a d_{90} to a d_{50}(*Bray*, 1987).

${\tau_{*ce}}^\varsigma$ is crucial parameter in Eq. 3.30. ${\tau_{*ce}}^\varsigma$ is not constant but a function of the grain Reynolds Number (see, e.g., *Parker et al.* (2003); *Buffington and Montgomery* (1997)) which is defined as:

$$Re_{p_\varsigma} = \frac{\sqrt{R \cdot g \cdot d_{90_\varsigma}}}{\nu}. \tag{3.32}$$

Brownlie (1982) proposes to calculate

$${\tau_{*c\varsigma}} = 0.22 {Re_{p_\varsigma}}^{-0.6} + 0.06 \cdot 10^{-7.7 \cdot {Re_{p_\varsigma}}^{-0.6}}. \tag{3.33}$$

Besides, $\tau_{*c\varsigma}$ increases strongly with increasing slope as the proportion between discharge stage and local grain size decreases (e.g., *Lamb et al.* (2008)). Neglecting this effect yields very large d_{90_ς} from Eq. 3.30. *Suszka*

(1991) proposed that Eq. 3.33 holds only where $h_i/d_{90i} > 10$. For streams where this condition is exceeded we implemented therefore the formulation proposed by *Suszka* (1991). The final calculation routine was

$$\tau_{*ce}{}^{\varsigma} = \begin{cases} 0.22{Re_{p_\varsigma}}^{-0.6} + 0.06 \cdot 10^{-7.7 \cdot {Re_{p_\varsigma}}^{-0.6}}, \\ \text{if } h_e/d_{90\varsigma} > 10, \\ 0.0851 \cdot (\dfrac{h_e}{d_{90\varsigma}})^{-0.0261} \\ \text{, else.} \end{cases} \tag{3.34}$$

From Eq. 3.32 - 3.34 it is evident that there is no analytic solution for the calculation of $d_{90\varsigma}$. This is because the calculation of $d_{90\varsigma}$ (Eq. 3.30) is a function of the critical Shields parameter $\tau_{*c\varsigma}$, which is in turn a function of $d_{90\varsigma}$ (Eq. 3.32 - 3.34).

We approach this problem by first assuming fully turbulent flow conditions and $\tau_{*c\varsigma}$ takes a constant value of 0.047 (*Wong and Parker*, 2006). This value is used to solve Eq. 3.30 and to derive a first estimate of $d_{90\varsigma}$ denoted as ${d_{90\varsigma}}^*$. Equations 3.32 - 3.34 are subsequently solved using ${d_{90\varsigma}}^*$. The resulting $\tau_{*c\varsigma}({d_{90\varsigma}}^*)$ is then used to calculate d_ς.

Obviously, the proposed method is subject to a number of assumptions and sources of uncertainty. Assumptions are specifically:

- We assume steady flow throughout the basin and for all flows stages replacing the energy slope with the slope measured from the DEM. Channel geometry is rectangular for all channels.
- We use a constant friction factor derived from literature. The friction-factor in CASCADE is independent of grain size and does not consider for the presence of bed-forms (e.g., bed dunes) or vegetation.
- The estimation of local grain sizes from the critical shear stress is a rough approximation of the complex inter-dependencies of incipient sediment motion and, e.g., grain size mixture properties, small scale sedimentologic properties or local morphology (e.g., *Lamb et al.* (2008); *Wilcock* (1993); *Kirchner et al.* (1990)).

3.C Network-scale distribution of hydraulic parameters and grain sizes

Figure 3.9 displays the key hydraulic characteristics for the river basin that were derived using the hydraulic solver. All variables are shown for bankfull ($Q_{1.5e}$) flow conditions. As additional indicator for local hydraulic conditions we calculated the Froude Number $FR_e = v_e/\sqrt{gh_e}$.

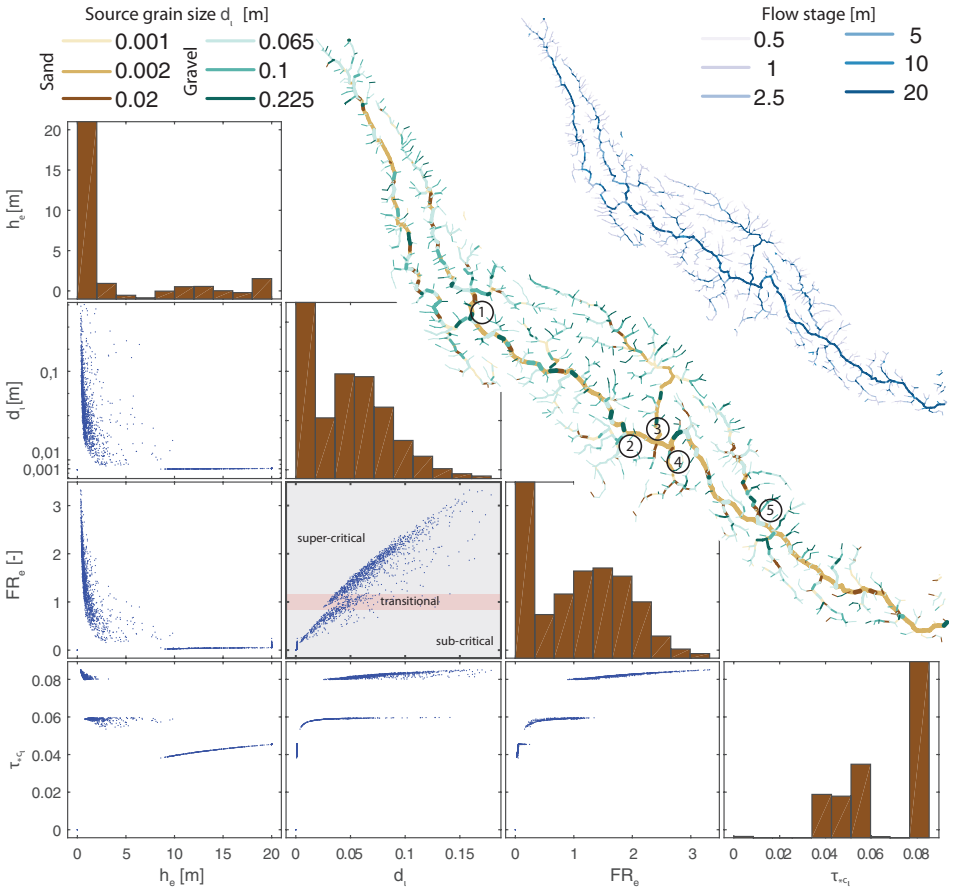

Figure 3.9: *Correlation and frequency distribution for key hydraulic parameters (scatter plots) and the spatial pattern of derived characteristic grain sizes and flow stages (top panels). Numbers indicate main tributaries ($Ad > 2500\ km^2$). Histograms in the diagonal of the scatter matrix indicate the frequency distribution of the respective variables. The Froude Number, $Fr = v/\sqrt{g * h}$, was calculated to epitomize local hydraulic conditions. All hydraulic parameters and the flow stage plot represent hydraulic conditions at 1.5 year discharge.*

The probability distribution of flow stages, h_e, is strongly left skewed with a probability maximum of 0-2 m. These observations occur in small reaches. These reaches cover a wide range of slope conditions, as FR for these reaches spans both the sub- and supercritical range. Supercritical flow conditions occur nearly exclusively within this group of reaches. As a result of the wide range of hydraulic conditions, these small reaches feature d_ς from sand to cobble size. It is also for these reaches that the correction of τ_{*c} (Eq. 3.34) takes effect. τ_{*c} is increased for the majority of these reaches (see distribution of τ_{*c}). This increase takes effect only for d_ς in the gravel or cobble range (see scatter of τ_{*c} vs. d_ς) and hence we can deduce that the majority of reaches with low h_e feature a gravel or cobble bed composition.

There is a major group of reaches with medium-high h_e (5 - 20 m) that exhibit a homogeneous hydraulic behavior (very low FR_e). This relates to the peak in grain size distribution for small grain sizes ($d_\varsigma < 0.02$ m). This group contains the major sandy reaches ($d_\varsigma < 0.001$ m) and the conditions at the water-sediment boundary range from hydraulically smooth (medium τ_{*c}), to transitional (low τ_{*c}) (see scatter of τ_{*c} vs. d_ς).

In general, there is a strong correlation between hydraulic parameters (FR_e, τ_{*c}) and d_ς. Nevertheless, the procedure clearly distinguishes between sub- and super-critical flow conditions. Large grain sizes ($d_\varsigma > 0.05$ m) are predicted to occur only under super-critical and small grain sizes ($d_\varsigma < 0.02$ m) only under sub-critical flow conditions with some overlap under transitional hydraulic regimes (see scatter d_ς vs. Fr_e).

The spatial distribution of hydraulic parameters is reasonable (Fig. 3.9, top right panels). Here, we display flow stage h_e and grain size d_ς. Both are key parameters in the hydraulic calculations. As expected, h_e increases with increasing A_d. The spatial distribution of d_ς is more heterogeneous. Main channel sources exhibit a sandy d_ς but with an increasing number of sources supplying coarser material in the upper parts of the basin and the major tributaries. Sources in smaller tributaries and headwaters feature a d_ς in the gravel/cobble range. Noticeably, sources in tributary 3 supply predominantly sandy sediment.

3.D Connectivity under scenario 2

This section reports findings for scenario 2 (not presented in the main chapter). Fig. A1 illustrates the results for connectivity analysis for the single reach under study (compare section 3.5.1). Observations are similar to scenario 3. Connectivity is mainly established along the main river for small connection times but the source areas are less connected than under scenario 3. We observe little preferential connectivity and upstream reaches connect only for longer connection times. Grain sizes are fining with increasing con-

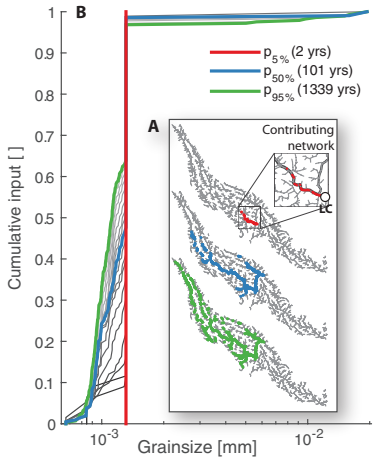

Figure 3.10: *Reach connectivity for scenario 2 (Panels A, B). Source areas (Panel A) and fraction of input belonging to a certain grain size class (Panels B) for different percentiles of connection time.*

nection times.

Figure A2 presents the sediment redistribution along the main stem and on the network-scale (compare section 3.5.2). Scenario 2 results in an intermediate situation between scenario 1 and 3. Most sediment cascades experience strong initial deposition, and tributaries have little influence on sediment redistribution along the main stem. Still, there is a clear upstream-downstream gradient in sediment delivery both along the main stream and on the network-scale.

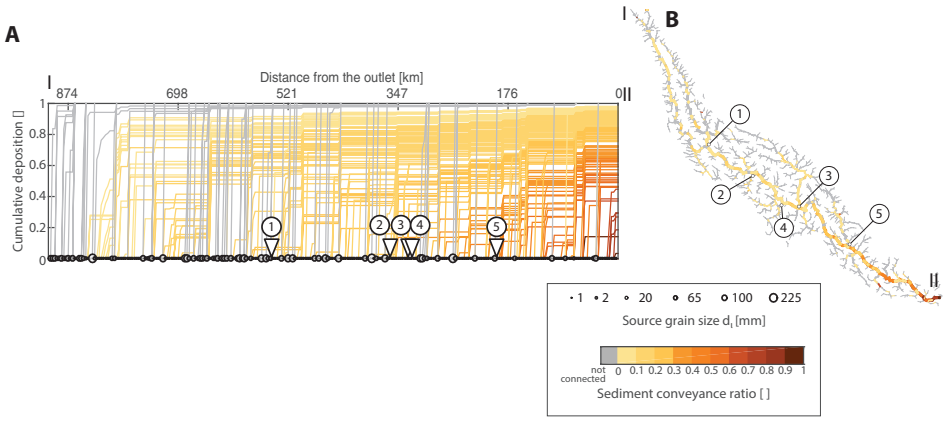

Figure 3.11: *Network connectivity for scenario 2. Panels A shows deposition trajectories along the main stem of the Da River. Dots indicate the source grain size d_ς transported along each cascade. Numbers and triangles indicate the location of major tributaries ($A_D > 2500km^2$, see Fig. 3.9). The sediment conveyance ratio is mapped throughout the river basin (Panel B).*

CHAPTER 4

Connectivity based river classification

NOVEL modeling approaches such as CASCADE (see chapter 3) allow to track sediment from individual sediment sources throughout entire river networks and to assess the resulting patterns of sediment connectivity at multiple scales. This opens new potentials for river management, e.g., to analyze local river processes within the overarching spatial pattern of network sediment connectivity. This information can help understanding drivers of reach morpho-dynamics, as well as identifying the role of single reaches for network sediment distribution. Yet, the resulting network information is high dimensional, spatially distributed, and therefore difficult to interpret, especially on the scale of large river networks. In this chapter, we demonstrate the analysis of such a distributed, multi-dimensional connectivity data-set derived from the CASCADE model. We apply a classification algorithm to reduce the complexity of the data-set into a low number of connectivity classes. Members of each class have similar connectivity to their respective sediment sources. We find that a low number of classes epitomize reaches that are characterized by a similar connectivity to upstream sources. Through a subsequent geo-spatial analysis, we assign each of the classes a specific function for network sediment routing (production, storage, conveyance). Hence, members of each class are driven by similar processes, and could react similar to upstream disturbance, making the proposed classifica-

tion also of interest for river management. We also interpret end-members of connectivity classes which present typical "connectivity styles". Based on the results we propose that sediment connectivity should be analyzed over multiple scales, and process domains, especially as new numerical models will make information on network-sediment connectivity more common in river systems and enable comparative connectivity analyses between different river systems.

This chapter is developed based on: Schmitt, R.J.P., Bizzi, S., Castelletti, A.,2015. Process based classification of sediment connectivity at the river basin scale. In: Novel Approaches to Assess and Rehabilitate Modified Rivers. Proceedings of the REFORM International Conference on River and Stream Restoration, Wageningen, NL.

4.1 Introduction

Sediment connectivity is a central driver behind fluvial processes as detailed in the previous chapters, and relevant literature (e.g., *Bracken et al.* (2015) and *Parsons et al.* (2015)). Understanding how sediment transfers operate at the basin scale is imperative for river basin management in order to understand how river channels and fluvial processes will react to past and future disturbances or restoration (*Ligon et al.*, 1995). Classification of rivers according to their sediment connectivity has been proposed for river management, e.g., to determine effects of dams on downstream rivers (*Brandt*, 2000; *Grant et al.*, 2003), and science, e.g., to clarify the role of river processes in landscape sediment cascades (*Bracken et al.*, 2015). Concretely, *Grant et al.* (2003), proposed to classify and predict the downstream response of a river to dam construction from analyzing the change in sediment load due to reservoir sediment trapping, and the shift in hydraulic forcing due to reservoir operation. *Bracken et al.* (2015), proposed to classify sediment connectivity on the landscape scale (i.e., not necessarily considering only rivers or fluvial sediment transfers) by mapping the degree to which sediment detachment and conveyance are driven by hydrologic processes (in contrast to e.g., eolian sediment transport, or mass movements). It is inherent to these classifications, that they should be applied on the network scale. This is because connected sediment transfers can span entire, large river networks (see also chapter 3). Nevertheless, field-data that span such scales are rarely present (for few examples see, e.g., *Attal and Lavé* (2006); *Mueller et al.* (2016)). With this regard, numerical models could bridge the gap between an increasing number of conceptual approaches, the demand of river basin managers for large scale connectivity information, and the widespread lack of data. Currently, the ability to model the full complexity of fluvial sediment transfers on relevant spatio-temporal scales is limited. Only recently,

numerical frameworks have been proposed to derive information on various domains of sediment connectivity on network scales (*Czuba and Foufoula-Georgiou*, 2014; *Schmitt et al.*, 2016). In the previous chapter, we introduced such a modeling framework (CASCADE) for assessing various domains of bed-load connectivity in large river basins. While the resulting information is potentially of high operational value at the reach scale, its assessment is complicated by its multi-dimensional and multi-scale properties.

Epitomizing the connectivity of a fluvial network by fewer reduced complexity indicators would be very useful to analyze sediment transfers in single river systems, but even more for comparative analyses between multiple river systems. Towards this aim, we present in this chapter how the data-set resulting from CASCADE can be analyzed on network scales. Therefore, we first reduce the complexity of the network connectivity data-set by transferring it into lower-dimensional indicators of connectivity via a data-driven classification. Then, we demonstrate how this reduced complexity data-set can inform on network-scale patterns of sediment connectivity, and identify certain "connectivity styles". A “connectivity style” identifies groups of reaches in which reach-scale morpho-dynamics are driven by a similar sediment connectivity, and that share a common role for network sediment routing.

4.2 Methods

We present the derivation of connectivity indicators based on the connectivity data-set derived in the previous chapter for the Da River in SE Asia. Connectivity information for the Da River was derived by applying the CASCADE framework (see previous chapter). In CASCADE, a river network is represented as a spanning tree, in which each reach (i.e., a finite section of the river network) is represented as edge e in that spanning tree. To derive network indicators of sediment connectivity, we start from the notion of *Grant et al.* (2003) and *Bracken et al.* (2015), which both defined a two-dimensional dimensional connectivity space. Herein, we propose a three-dimensional connectivity space. The three considered dimensions are a) sediment flux [kg/yr], b) incoming grain size [m], and c) connection time to sources [yr] for each reach/edge in the river network. We define connectivity in the upstream direction, i.e., we analyze how an edge connects to upstream sources, instead of how a source connects to downstream edges. This follows the approach by *Grant et al.* (2003), while *Bracken et al.* (2015) defined connectivity in the downstream direction (i.e., from the perspective of a sources). As discussed in chapter 3, each edge is potentially connected to many sources. Yet, an edge can be characterized only by a single value in each dimension of the connectivity space. Therefore, mapping an edge into

the connectivity space requires, in a first step, to aggregate the values of all connections of an edge, in all three dimensions. As described in the previous chapter, CASCADE derives

- The sediment flux ${\Theta_{S,e}}^{\varsigma}$ from an upstream source, ς to a downstream edge e.
- The travel time T_{ϵ}^{ς} of sediment from source ς through the set of edges ϵ between ς and e. Hence, we define ${T_{S,e}}^{\varsigma} = T_{\epsilon}^{\varsigma}$ as connection time between source ς and e.
- The grain size d_{ς} delivered to edge e.

Additionally, Γ_e defines all sediment cascades that connect e to its upstream sources. As indicators we define:

- Total sediment flux in e, which is the sum of sediment transport along all sediment cascades that connect to edge e

$$\Theta_{S,e} = \sum_{k \in \Gamma_e} {\Theta_{S,e}}^{k} \tag{4.1}$$

- Flux-weighted connection time

$$T_{S,e} = \frac{\sum_{k \in \Gamma_e} {\Theta_{S,e}}^{k} * {T_{S,e}}^{k}}{\sum_{k \in \Gamma_e} {\Theta_{S,e}}^{k}} \tag{4.2}$$

- Flux-weighted incoming grain size

$$d_{S,e} = \frac{\sum_{k \in \Gamma_e} {\Theta_{S,e}}^{k} * d_k}{\sum_{k \in \Gamma_e} {\Theta_{S,e}}^{k}} \tag{4.3}$$

For $d_{S,e}$ and $T_{S,e}$,we use flux-weighted average (instead of, e.g., a geometric mean) in order to consider that, for example, the grain size from a high-flux sediment cascade will dominate the sediment composition of a downstream edge, in comparison to the grain size delivered by a low-flux sediment cascade. This is based on the hypothesis, that the flux of an individual grain size into an edge is an indicator for the frequency with which a grain size can be found in the bed material (analogue to deriving a field-based sampling of river bed material).

The result is a connectivity matrix, C_{MX3} ,where M is the number of edges ($M = 2123$ for the Da River case study). C can be mapped into the connectivity space. We then applied a *k-means* clustering to identify edges with common characteristics within the 3-dimensional connectivity space.

The *k-means* clustering requires an expert based definition of the number of classes. Hence, there is a certain degree of subjectivity in that approach. The results of the clustering, i.e., the assignment of each edge to a certain cluster can be visualized on the river network.

4.3 Results

Figure 4.1 shows some of the complexity in the original data-set for the Da River (Figure 4.1 a for location). CASCADE identifies the flux between any source-edge pair connected by a sediment cascade. This results in a total of 56472 connections (Figure 4.1 b, curved lines), each line conveys information on the flux, travel time, and grain size delivered along each connection (the grey color code in Figure 4.1 b shows only the sediment flux [kg/yr]). The cutout in Figure 4.1 b illustrates that each edge receives sediment contributions from multiple upstream sources. At the same time, each edge contains itself a sediment source that that contributes to multiple downstream edges. Aggregating all sediment fluxes passing through an edge allows defining the total sediment flux in that edge (see color code of the river network in Figure 4.1 b).

The information that is available on the edge-scale is presented in Figure 4.2 for two different edges. Edge 1 (see Figure 4.1 b, for location) is located at the basin outlet. Edge 2 (see Figure 4.1 b, for location) is the terminal edge in a mountainous tributary basin. Each edge has a specific signature of the different connectivity attributes. First, the x-axis represents the connection time of the edge to upstream sediment sources. We classified connections to sources according to their connection time. The frequency with which connections fall into a certain bin of connection time are shown on the primary, left y-axis. For each bin, we also plot the mean grain size of delivered sediment (grey secondary y-axis, round markers). Last, Figure 4.2 shows how much of the sediment sources in each connection time bin contribute to the total sediment budget of an edge (red secondary y-axis, red-lines).

For edge 1 (Figure 4.2 b), a downstream, sandy reach connectivity to upstream sources is more homogeneous. Around 50 % of sources connect below 100 years (see sum the first two bins of connection time). The grain size within these bins is around 1.3 mm. Around 70 % (7E8 of a total of 10E8) of the total sediment budget is delivered within 100 years (see red line) . For longer connection times, i.e., 100 to 250 years, the grain size remains relatively constant. Sources connecting between 100 and 250 years contribute around 25 % to the sediment budget of edge 2. For connection times above 250 years, grain size decreases below 1 mm. This indicates that there are some remote sources of fine sediment. However, source with such a long connection time contribute only around 5 % to the sediment budget

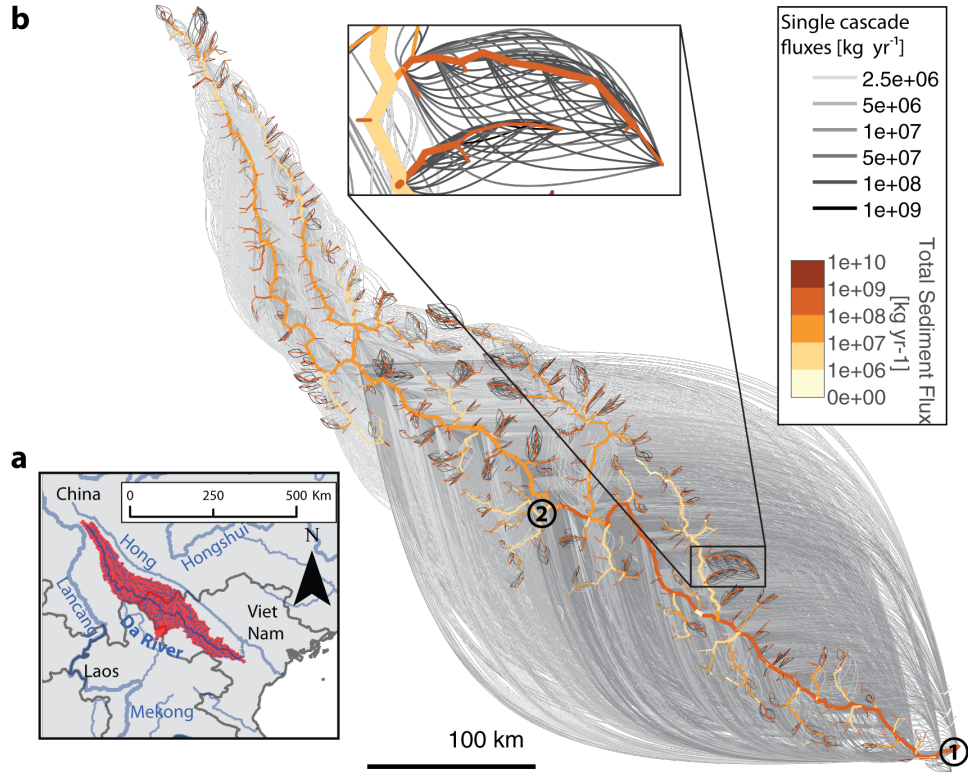

Figure 4.1: *Connectivity in the Da River (a) was derived using the CASCADE model. Some properties of that data-base are shown in (b). Grey, curved lines indicate the flux along individual sediment cascades, the color code of the network indicates the resulting bulk flux in each edge. The cutout illustrates more in detail that each edge contains a sediment source that contributes sediment to multiple downstream edges. Edges can, in turn, receive sediment from some multiple sediment sources. Numbers 1 and 2 indicate locations of reaches for which connectivity is discussed more in detail (see Figure 4.2)*

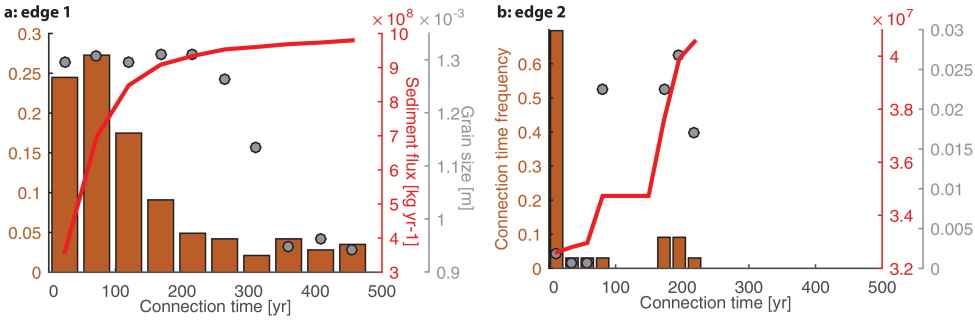

Figure 4.2: *Connectivity signatures (grain size, connection times, sediment flux) for two selected edges for a mountainous (a, edge 1), respectively a low land river (b, edge 2), see Figure 4.1 b for exact location.*

of edge 1.

Edge 2 (Figure 4.2 a) is the terminal edge in a major mountainous tributary. According to CASCADE, sediment from that tributary is a mixture of sand and gravel (also the main stem of the Da River at the confluence, which is located between picture locations d and e in Figure 3.3, is likely a mixed sand-gravel river). Sand constitutes the majority of the sediment budget (red line, right y-axis, around 3.3E7 kg/yr of a total sediment flux of 4E7 kg/yr) and frequency (brown bars, right y axis). This sources of sand connect to edge 1 below 25 years. Few sources of sand connect in between 25 and 75 years. There are some sources of gravel (0.02 m $< d <$ 0.025 m, see secondary right y-axis) that connect within 75 - 100 years. Then, there are some sources of gravel (0.015 m $< d <$ 0.0275 m) that contribute sediment with a connection time of around 200 years. Hence, the sediment budget in edge 1 is characterized by a bi-modal connectivity, with some fast sediment connections to sand sources, which make up the majority of the sediment budget, and a second group of more slowly connecting sources of gravel.

These two examples clarify the type of information that can be derived from the full, basin scale data set (Figure 4.1) on the scale of individual edges. To represent edges in the connectivity space requires some aggregation. For example, for reach 1, sediment flux would be represented by the cumulative sediment flux (4E7). Grain size and connection time would be represented by the respective, flux weighted mean.

We then aggregated this edge-scale information and mapped the results into a connectivity space (Figure 4.3 a). We also divided the connectivity space into four sectors in the connection time and sediment flux dimensions. End members in each sector would be edges with (i) high fluxes and short connection times, (ii) high fluxes and long connection times (iii) low fluxes and long connection times, and (iv) low fluxes and short connection times. There is a less clear correlation between the time/flux dimensions and grain size, but grain sizes in sector ii and iii are clearly lower than in sectors i and iv (see marker size in Figure Figure 4.3 a).

We used a k-means clustering to classify edges according to their connectivity. We set the number of classes to six, because this was sufficient to derive a good separation between classes. At the same time, six classes does not increase complexity too much, which would again hinder interpretation. Roughly, it can be stated that class 1 falls mainly into sector iv, class 2 into sector i, class 3 into sector i and ii, class 4 and 5 into sector iii, and class 6 into sector ii. Mapping these classes back to the river network indicates that each class has a characteristic location within the river network (Figure 4.3 b). Class 1-3, represent headwater edges, class 4 intermediate edges, and classes 5 and 6 edges in major tributaries or in the main stem (Figure 3

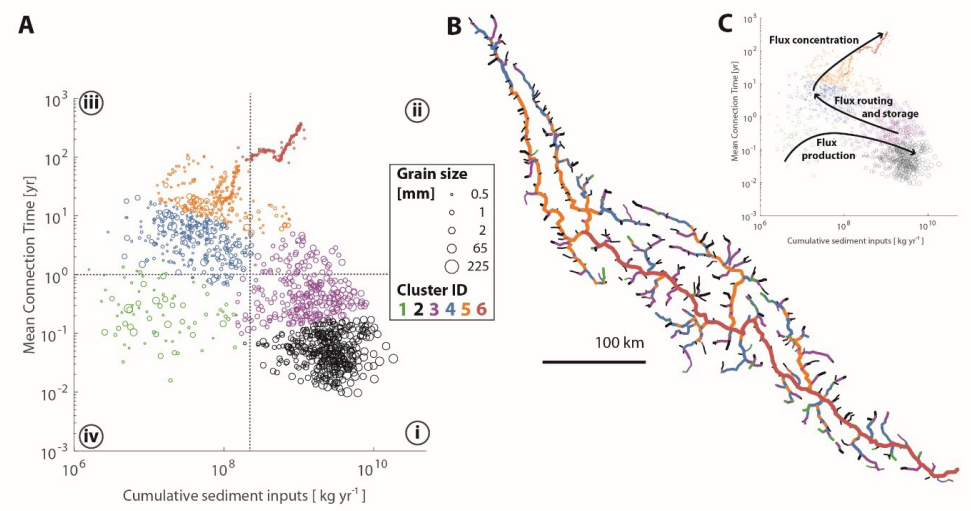

Figure 4.3: *Definition of connectivity classes based on model results. A) Connectivity properties of all edges are mapped into the connectivity space and divided into typical classes by unsupervised data-mining. B) geographic position of members of each class. C) functional interpretation based on results shown in A) and B).*

b). This clear spatial sequence of classes allows deriving a functional trajectory of sediment connectivity from up- to downstream (Figure 4.3 c). This trajectory provides a conceptual understanding of sediment connectivity in the river network, and allows understanding the dominant processes in each class. Classes 1-3 include edges where sediment is supplied to the river network at various rates (supply zone). Class 4 is more downstream and connection times increase. At the same time, fluxes decrease especially in comparison to classes 2 and 3. Hence, while sediment is routed downstream, the transition from class 2 and 3 to 4 marks also where excess sediment is stored in the river network. Apparently, edges of class 4 constitute a "transport filter" filter (c.f., *Meybeck and Vörösmarty* (2005) and *Attal and Lavé* (2006)) that decreases sediment flux especially for larger grain sizes. This is corroborated by smaller grain sizes in classes 5-6. Class 5 sees an increase in fluxes and also connection times. The increase in connection times indicates that increasing flux is not derived from local sources. Rather, the increase in flux it is due to network topology, i.e., that sediment transport increases after the confluence of rivers. Class 6, is then clearly distinguished from class 5 through an additional increase in flux and connection times. Class 6 contains only edges along main-stem, sandy rivers where the sediment budget is likely not dominated by local sediment inputs, but defined by conveyance of sediment from many upstream sources (transport zone).

Based on these findings, we assign a more generic interpretation to each

of four sectors in the connectivity space, which is shown Figure 4.4. Typical end members in each sector are:

i Connectivity determined by few sources with high supply and connectivity and short connection times. Sources supply large grain sizes. Fast connection times and large grain size of sources indicate that edges in in sector i are close to active sources of large grained sediment (Figure 4.4 a, i). Edges of type i are connected to these sources via some edges with high transport capacity. Example: mountainous headwater downstream of an active landslide, or in erodible lithology.

ii Connectivity determined by multiple sources with variable supply and connectivity, and long connection times. A fluvial transport filter (c.f. *Attal and Lavé* (2009)) allows only the passage of smaller grain size (Figure 4.4 a, ii), sources supplying larger grain sizes are disconnected. Edges of type ii are connected only to source of fine sediment for which transport capacity is high in the downstream network (Figure 4.4 ii). Example: large downstream rivers.

iii Connectivity determined by multiple sources with low supply or connectivity, and long connection times. A fluvial transport filter (c.f. *Attal and Lavé* (2009)) is active allowing only the passage of smaller grain size (Figure 4.4 a, iii), sources supplying larger grain sizes are disconnected, resulting in lower flow and smaller grain sizes than, e.g., in sector i. Example: intermediate sand-gravel rivers at the transition between sediment supply and transport zones.

iv Connectivity determined by few sources with low supply or connectivity, but short connection times. Upstream sources of large sediment could be supply limited (Figure 4.4 a, iv upper sketch), or a fluvial transport filter (c.f. *Attal and Lavé* (2009)) is active, allowing only the passage of smaller grain sizes that are not found among upstream sources (Figure 4.4 a, iv lower sketch). Example: mountainous rivers in resistant lithologies, or downstream of an external control of transport capacity (bed-rock control, mass-movement)

Figure 4.4 a shows how different connectivity styles are distributed in the connectivity space, and how different spatial configurations of supply and transport processes can result in different connectivity styles. Figure 4.4b shows how edges of different connectivity styles can then be spatially nested on the scale of a much larger river basin.

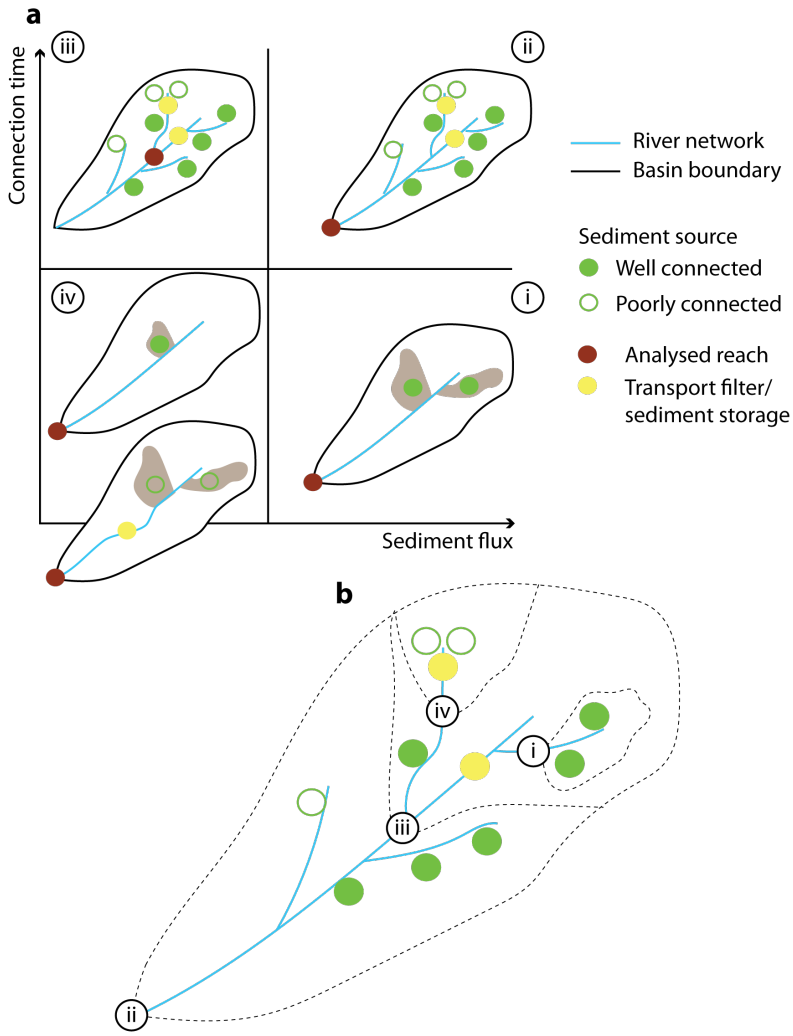

Figure 4.4: *a) Conceptualization of connectivity styles, i.e., typical end-members in the connectivity space (see Figure 4.3). Red dots show the spatial location of a hypothetical reach under study. b) potential hierarchy and nesting of different connectivity styles in the river network.*

4.4 Discussion and Conclusion

There is an increasing urge to introduce sediment connectivity into river management (*Fryirs*, 2013). This is because sediment connectivity allows putting observed local forms into a larger context of catchment scale processes, both in disturbed and undisturbed conditions (*Brierley and Fryirs*, 2005). As sediment connectivity controls fluvial morpho-dynamics, which are again a driver of other biotic and biotic functions of river, connectivity is a key control behind multiple eco-system services (*Ligon et al.*, 1995). Therefore, disturbed sediment connectivity can result in negative impacts on ecosystems and eco-system services. Towards integrating sediment connectivity in river management, it is key to derive indicators characterizing connectivity under the *status-quo*, or that allow to compare and rank impacts of management measures (both in terms of river development and restoration). Recently, some types of quantitative indicators of river hydromorphology have been proposed, e.g, by *Bizzi and Lerner* (2013); *Schmitt et al.* (2014) that can also be applied for large river networks. Yet these indicators were limited to local morphology and did not consider connectivity to the upstream river network. Therefore, these approaches cannot put observed forms in a larger, network scale perspective, or predict future morphologic alteration as reaction to an upstream disturbance. For future management applications, connectivity and local morphology indicators (*Bizzi and Lerner*, 2013; *Schmitt et al.*, 2014) from high-resolution remote sensing data can be combined. This would then allow to determine more in detail how local morphology is both a result and a control on sediment connectivity.

Some river management indicators that include sediment connectivity were proposed, for example, by *Grant et al.* (2003), to predict the reaction of a river edge to upstream disturbance. Yet, the application of these indicators was limited to few, well-studied river sections. This was because until recently, information on sediment fluxes was not available on network scales. *Bracken et al.* (2015), targeted a much wider range of process domains and spatio-temporal scales, but without pointing out a clear path for how the required data for such large-scale, multi-domain (i.e., considering landscape and river processes) assessments could be derived.

In this chapter, we propose that network connectivity modeling can help to derive functional classifications of river systems. The process of classification supports interpreting high-dimensional, spatially distributed results of network connectivity models. As pointed out in the previous chapter, CASCADE should for now be considered an initial screening tool. Hence, derived information should be analyzed under the premises of potentially large uncertainty. Another problem arises from the absence of information

on actual supply from sediment sources. For example, an edge could fall in sector iv (low supply, long connection times) for two reasons. First, upstream sources could supply little sediment (e.g., because of resistant lithology, or low precipitation). Second, it could also be that upstream sources supply a high amount of sediment, but that there is an additional upstream control on transport capacity which hinders the transport of that sediment to the downstream network. This problem can be partially addressed through a spatial analysis. E.g., edges of class 4 are downstream of edges of class 1, 2, and 3. Nevertheless, they transport less sediment than edges of type 2 and 3. This downstream decrease indicates that it is upstream transport capacity, rather than supply, which limits sediment transport in edges of class 4. Another limitation is that CASCADE in the presented initialization derives indicators for upstream sediment supply only from channel characteristics without consideration of hill-slope processes. For example, the presence of an upstream mass-movement supplying coarse sediment at high rates to edges in sector i could not be detected with the current initialization strategy. Yet, this limitation can be approached in better monitored basins, or with inverse modeling techniques, that are presented in the next chapter.

So far, the results presented in this chapter can be considered a proof-of-concept for how model-derived connectivity information support multi-scale, multi-dimension analysis of fluvial processes. Results align with common concepts in fluvial morphology, e.g., the "sediment conveyor'' belt of erosion, transport and deposition (*Kondolf*, 1994), or fluvial transport filters (*Meybeck and Vörösmarty*, 2005; *Attal and Lavé*, 2006). Yet, results show how novel, quantitative approaches can further concretize such concepts. It becomes evident for the network under study that the sediment conveyor belt is not following the supply-transport-deposition schema proposed by *Kondolf* (1994) but that transport and deposition zones are partially mixed and inversed for the network under study.

Several of the current limitations will hopefully be alleviated in smaller, better studied basins, or as soon as network connectivity models become more widely applied and high resolution input data become available on relevant scales (*Bizzi et al.*, 2015a). Nevertheless, we propose a hierarchy from the reach to the network scale. High-dimensional reach-scale connectivity signatures can be grouped into characteristic classes. On the next level of hierarchy, these classes are organized along the spatial template of the river network such that functional "connectivity styles" emerge. Edges belonging to a connectivity style have a well-defined position in the network, a specific functions for network sediment routing, and potentially similar driving forces behind local morpho-dynamics.

CHAPTER 5

Inverse connectivity modelling for reconstructing sediment provenance and sediment fluxes in unmonitored river tributaries

SEDIMENT provenance describes patterns and rates of sediment transfer between sources and sinks in fluvial networks. Governed by the spatial distribution of sources, supplied grain sizes, supply rates, and rates of fluvial transport, provenance controls the spatio-temporal variability in fluvial sediment flux and resulting forms and processes. CASCADE allows to model sediment provenance at network scales. At the same time, information on source characteristics is key to parameterize the cascade model. This information is missing for most river basins. Commonly, sediment provenance is estimated based on factors governing hill-slope detachment without considering subsequent fluvial transport processes. Yet, also network transport capacity might have adapted to sediment supply and grain size distribution and might record network sediment provenance. Therefore, we propose adopting a network perspective to quantify sediment provenance based on the spatial distribution of transport capacity within a river network derived by using CASCADE. The challenge is that the transport capacity is itself a

function of the sediment grain size distribution , and hence sediment provenance. We approach this problem by applying a distributed multi-grainsize sediment connectivity model in an inverse Monte-Carlo approach (MCA) to a major tributary basin of the Mekong. The model transfers many random initializations of sediment sources into distributed estimates of sediment grain size distribution and flux throughout the network. Yet, only few initializations are in accordance with observations at the confluence between the tributary and the Mekong.

Selected initializations reveal a clear pattern of sediment provenance, flux, and grain size distribution in the tributary network that coincides with lithologic maps and satellite imagery. Such a model-driven approach has high potential to validate uncertain sediment point measures, parametrize the CASCADE model, which then allows to disaggregate sediment point measures into spatially explicit provenance information in large, poorly monitored river networks.

This chapter is developed based on: Schmitt, R.J.P., Bizzi, S., Castelletti, A., Kondolf, G.M., (IN REVIEW). Inverse connectivity modeling for reconstructing sediment provenance and sediment fluxes in unmonitored river tributaries. Journal of Geophysical Research: Earth Surface.

5.1 Introduction

Transport processes connecting sediment sources to sinks in river networks are key controls of river morphology over a wide range of spatio-temporal scales (*Sklar et al.*, 2016; *Mueller and Pitlick*, 2013). Understanding transport processes and identifying sources of sediment is a prerequisite both for studying landscape dynamics, river morphology, and assessing the impact of human activities such as reservoir constructions on river morpho-dynamics (*Walling*, 1983; *Rice*, 1998; *Fryirs and Brierley*, 2001; *Merritt et al.*, 2003; *Rice et al.*, 2008; *Zaliapin et al.*, 2010; *Patil et al.*, 2012; *Mueller and Pitlick*, 2013; *Bracken et al.*, 2015). Features of sediment sources and their link to fluvial processes are poorly characterized in most river systems (*Merritt et al.*, 2003; *de Vente et al.*, 2006; *Sklar et al.*, 2016). This holds for different types of sediment sources, e.g., tributaries, fluvial processes (bank or bed erosion), and direct inputs from hillslopes. Over many scales, sediment supply from an apparent point-source is the aggregated signal of multiple processes. For example, the input of sediment from a single hillslope can be considered a point-source of sediment for the fluvial network, but results of multiple weathering and transport processes on the hillslope (*Sklar et al.*, 2016). Similarly, tributary sediment supply can be a key point-source of sediment along a river and control behind main-stem morpho-dynamics (*Rice*, 1998; *Benda et al.*, 2004a,b; *Rice et al.*, 2008). Sediment delivery from a

tributary is the aggregated signal of sediment source supply, transfers, and storage processes that act heterogeneously throughout the tributary network. These processes are often found to be highly variable and apparently similar tributaries in similar settings can have sediment loads that vary by orders of magnitude (*Warrick et al.*, 2015).

Finger-printing and remote sensing techniques have greatly improved the ability to identify sediment sources and construct network sediment budgets (*Ries and Marzolff*, 1997; *Pickup and Marks*, 2001; *Walling and Horowitz*, 2005) with applications mostly to suspended sediment. modelling approaches have, at least conceptually, advanced the study of spatial and temporal patterns of connected bed-load sediment transfers. *Benda and Dunne* (1997a,b) analyzed how stochastic sediment pulses and their routing through the river network affect sediment transport at the network-scale. *Czuba and Foufoula-Georgiou* (2014) developed a numerical model to study how network topology and the distribution of transport capacity in the network can translate into the sedimentary signal (total flux and grain size composition) at the basin outlet. A similar model was used by *Gran and Czuba* (2015) for studying network dynamics of sediment transfer and storage as a function of a homogeneous versus an observation-informed initialization of sediment sources. *Schmitt et al.* (2016) developed a model for tracking the movement of variable-sized grains through a river network and studied the emerging patterns of connectivity between sediment sources and sinks. All these approaches relied on a deterministic initialization of sediment sources (regarding sediment supply, grain sizes, or both), or analyzed a few scenarios of source characteristics. Such single deterministic initializations of a network sediment routing model is likely to be subject to a major uncertainty, both because of the huge uncertainty in input data (*Merritt et al.*, 2003) and because of the high sensitivity of sediment transport formulas to input grain sizes (*Pinto et al.*, 2006).

The purpose of this chapter is two-fold. First, we investigate how a signal of sediment source supply and grain size in a large tributary network is transformed by fluvial transport processes into a sediment signal at the tributary outlet. We argue that understanding this fluvial transformation process can identify network configurations of sediment provenance and network-internal sediment fluxes from an observed sediment signal at the tributary confluence. Towards developing that understanding, we apply a multi-grain size network connectivity model in an inverse Monte-Carlo Approach (MCA) to the lower Mekong River, a major tropical river in South East Asia, and its major tributary, the Se Kong, Se San, and Sre Pok (3S) river system.

Both, the Mekong River and the 3S tributary basin are subject to sub-

stantial development pressure with potentially severe environmental impacts. While there is some evidence that the 3S tributaries provide a substantial part of the Mekong's sediment budget (*Kummu et al.*, 2010; *Wild and Loucks*, 2014), there is no information on sediment provenance or transfers processes within the tributary system. Hence, second purpose of this chapter is deriving spatially explicit information on sediment provenance in the 3S, reconciling sediment provenance, with other sources of (map-derived) information, and quantify the relevance of the 3S for the sediment budget of the Mekong River. In broader terms, the proposed approach opens the opportunity to reconcile model derived and observational data to address the common data-scarcity regarding fluvial sediment transport.

5.2 Case Study

The Se Kong, Se San and Sre Pok (3S) basin (Figure 1) covers a total area of 82,500 km^2 (Se Kong 30,403 km^2, Se San 20,063 km^2, Sre Pok 32,034 km^2) draining the Vietnamese and Laotian highlands westward towards the Mekong River in Cambodia. The confluence between 3S and Mekong River is located upstream of the city of Stung Treng, 500 km upstream of the beginning of the Mekong Delta. The Mekong River constitutes a hot-spot of bio-diversity. Annual flood and sediment pulses support agriculture and fisheries in the delta and its flood-plains that are key economic factors in the economies of abutting countries. Bio-diversity and livelihoods are already under pressure from climatic changes and sea-level rise. These pressures are emphasized by a potential future reduction in sediment fluxes due to the construction of hydro-power cascades in the Upper Mekong (Lancang) (*Liu et al.*, 2013; *Fan et al.*, 2015), and in the Lower Mekong River Basin (LMRB) (*Kondolf et al.*, 2014). This reduction in sediment transport can be expected to impact fluvial eco-systems as well as to accelerate delta subsidence and coastal erosion (*Anthony et al.*, 2015; *Rubin et al.*, 2015).

The 3S basin has been cited as the most important source of sediment and especially sand in the Lower Mekong River Basin (*Bravard et al.*, 2014; *Kondolf et al.*, 2014; *Wild and Loucks*, 2014; *Piman et al.*, 2016). However, there are no measurements of sediment transport or grain size in the basin. Except for some qualitative estimates in *Bravard et al.* (2014) and *Kummu et al.* (2010), there is no information on sediment provenance or grain size distribution within the 3S. Such information could be of great relevance given the multiple hydro-power schemes that are currently planned in the 3S, threatening to disconnect the LMRB and the Mekong Delta from one of its most important remaining sources of sediment (*Wild and Loucks*, 2014; *Piman et al.*, 2016).

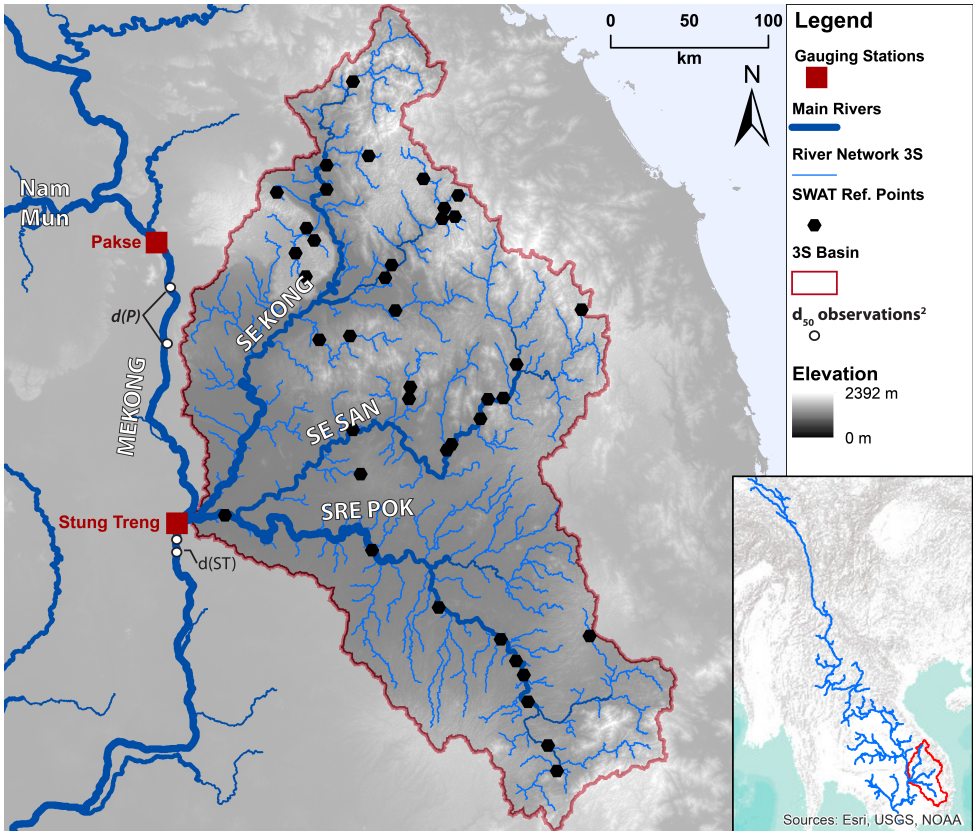

Figure 5.1: *Overview over the study area, available sediment gauge data (red squares) (Koehnken, 2012a,b), reference points of a hydrologic model (black hexagons) (Piman et al., 2013), and grain size samples (white circles) (Bravard et al., 2014).*

5.3 Available data

Data regarding the sediment transport in the Lower Mekong River are sparse, and both its total load and sediment grain size distribution are contested (*Lu et al.*, 2014). Sediment data in the 3S are nearly absent (*Wild and Loucks*, 2014). *Bravard et al.* (2014) qualitatively pointed out the role of the 3S as most relevant source of sand for the Lower Mekong. The sand supply from the 3S plays then a key role for river, delta, and coastal morphology (*Bravard et al.*, 2013).

For the lower Mekong, close to the 3S confluence, the following data are available. *Koehnken* (2012a) reanalyzed sediment measurements along the Mekong to derive new estimates of total sediment flux and estimated the fraction of sand in the total load. For Pakse (Figure 5.1, red square), where data are otherwise scarce (*Xue et al.*, 2011), *Koehnken* (2012a) reported a value of 73 MT/yr based on a reanalysis of available data and a campaign of sediment sampling (using depth integrated sampling) in the 2011 season. Sediment inputs from the 3S are approximately 25 Mt/yr (*Wild and Loucks*, 2014) resulting in a total load of 98 Mt/yr in Stung Treng, of which around 3-5 % was bedload (sand) (*Koehnken*, 2012b) (see Figure 5.1, red squares). In terms of grain size, (*Bravard et al.*, 2014) sampled grain sizes in sandy deposits in bed and bank material for numerous locations during 2 seasons. Two sample locations are downstream of Pakse and two downstream of Stung Treng (see Figure 5.1, white circles). For each location, a variable number of grain size samples was taken from sandy deposits at different elevations. Therefore, samples represent the grain size distribution of sand transported in the main Mekong during various flow stages. The grain size distribution of sand at each sample location is reported in terms of median grain size (d_{50}). 10 observations are available upstream of the 3S confluence (Pakse reach), and 6 observations are available downstream of the 3S confluence (Stung Treng reach). The mean values of median grain sizes in the Pakse reach are 0.132 mm and 0.182 mm in the Stung Treng reach, hence there is a coarsening of bed-material over the 3S confluence. These results are largely in line with single observations by (*Koehnken*, 2012b) in Pakse (0.08-0.125 mm) and Stung Treng (0.125-0.25 mm).

In order to build a network connectivity model for the 3S tributary, the following data are available. We used a void-filled, 90 m resolution Digital Elevation Model (DEM) (*CGIAR*, 2008) to extract the river network using standard procedures (*Schwanghart and Kuhn*, 2010) and applying a threshold for channel initialization of 75 km^2. The derived channel network had a total length of 8926 km and consisted of a total of 1422 reaches. We derived drainage area, A_D [km^2] and calculated the channel gradient, I [m/m], for all reaches from the DEM. We measured active channel width, W_{AC}

[m], for 200 randomly selected reaches using high resolution satellite imagery available in Google Earth. We derived a scaling law that relates W_{AC} to drainage area and slope (*Schmitt et al.*, 2014) for sampled reaches. We used this scaling law to calculate W_{AC} for all not-sampled reaches. Information on reach scale hydrology was derived as follows. *Piman et al.* (2013) developed a SWAT model of the 3S river basin and made modelled discharge time series publicly available (`http://www.mekongriver.info/3ss-flows`). Discharge time series are available for 41 reference locations throughout the basin (Figure 5.1, black hexagons) covering a 20 year period (1986-2006). To estimate discharge frequency and magnitude in all other reaches, we applied a technique that was prosed in *Schmitt et al.* (2016). First, we derived the discharge with a 1.5 yr return period ($Q_{1.5}$ [m^3/s] and drainage area (A_D) for all reference locations. We fitted a scaling law of the form $Q_{1.5} = a * {A_D}^b$ to the data and used this scaling law to interpolate $Q_{1.5}$ for all other reaches. We compared the interpolated $Q_{1.5}$ for each reach to the $Q_{1.5}$ at the next downstream reference station, and derived the ratio between both values. We then derived a hydrograph in each reach by multiplying the modelled 20 year hydrograph of the next downstream reference location with this reach-specific ratio (*Schmitt et al.*, 2016). Hence, we had information on slope, active channel width, $Q_{1.5}$, and a 20 year hydrograph available for each reach in the basin.

We derived a geologic map of the area (*Fromaget*, 1971) in digital form from `http://eusoils.jrc.ec.europa.eu/` (*Panagos et al.*, 2011) and georeferenced it to the study area. Some regional estimates indicate a sediment yield from the 3S in the range of 300 t/km^2 (*Kondolf et al.*, 2014) to 220-240 t/km ^{2} (*Kummu et al.*, 2010).

5.4 Methods

The available data stem from different data sources, cover different process domains (e.g., hydro-morphology, sedimentology, lithology), and spatial domains (i.e., point versus distributed data). This section describes how we processed available information towards deriving quantitative estimates of sediment provenance in the 3S. First, we developed a sediment mixing model at the Mekong-3S confluence. The model was used for broadly estimating sediment flux and grain size distribution from the 3S. Second, we derived estimates of erosion potential in the 3S from analyzing information on lithology and stream power in the 3S basin. Third, we parametrized a distributed network connectivity model (CASCADE, Schmitt et al., 2016) for the 3S. As major methodological contribution, we applied CASCADE in an inverse stochastic modelling approach. For defining and validating the inverse problem, we resorted to evidence from the mixing model and the analysis of

erosion potential.

5.4.1 Estimating 3S sediment flux and grain size distribution from observations at the Mekong-3S confluence

Based on the available data-sources on grain size (*Koehnken*, 2012b; *Bravard et al.*, 2014) and sediment flux (*Koehnken*, 2012a; *Wild and Loucks*, 2014) we built a mixing model describing the change in sediment flux and grain size distribution in the Mekong River over the Mekong-3S confluence. There is no major tributary between Pakse and Stung Treng except the 3S (Figure 5.1). Therefore, we assume that changes in sediment flux and grain size between the two stations can be attributed to the 3S confluence (*Wild and Loucks*, 2014), even though caution should be exercised calculating a variable of interest as a residual. This is because the residual term incorporates errors as well as the variable attributed to it (*Kondolf and Matthews*, 1991).

A key assumption is that the mixing process between sediment delivered to the Pakse reach via the Mekong (with a representative diameter $d(P)$ [m] and flux $\Theta(P)$ [kg/yr]) and the 3 S (with a representative diameter $d(3S)$ [m] and flux $\Theta(3S)$ [kg/yr]) determines the diameter of sand in Stung Treng $d(ST)$:

$$\frac{d(P) * \Theta(P) + d(3S) * \Theta(3S)}{\Theta(P) + \Theta(3S)} = d(ST). \tag{5.1}$$

Equation 5.1 derives grain size at Stung Treng as mean of $d(P)$ and $d(3S)$ weighted for the different flux from each input. This mixing model describes which sand fluxes (i.e., sand fluxes of a given magnitude and grain size distribution) from the 3S could explain the observed change in sediment load and grain size over the Pakse-Stung Treng reach.

Grain size observations cover sediment in the sand fraction, only (*Bravard et al.*, 2014; *Koehnken*, 2012b). Flux observations, in contrast, cover the total load, consisting of suspended load and bed-load (sand) (Koehnken, 2012a). Therefore, a conversion factor, F [-], is introduced to convert total load observations to sand load. Sand load is described as $\Theta * F$. Through this conversion, the mixing model becomes:

$$\frac{d(P) * \Theta(P) * F(P) + d(3S) * \Theta(3S) * F(3S)}{\Theta(P) * F(P) + \Theta(3S) * F(3S)} = d(ST). \tag{5.2}$$

F in the Mekong is around 3 % (*Koehnken*, 2012b) but the fraction of sand delivered from the 3S ($F(3S)$) is unknown. Accordingly, the above equations have two unknown variables: the grain size of sand in the 3S

($d(3S)$) and the fraction of sand in the sediment delivered from the 3S basin ($F(3S)$). Solving above equation for the $d(3S)$ yields

$$d(3S) = \frac{d(ST) * [\Theta(P) * F(P) + \Theta(3S) * F(3S)] - d(P) * \Theta(P) * F(P)}{\Theta(3S) * F(3S)}. \tag{5.3}$$

Different values of $d(3S)$ result from solving this equation for $F(3S)$. Additionally, there is uncertainty regarding the fraction of sand in the total load of the Mekong ($F(P)$, $F(3S)$) (*Bravard et al.*, 2014). Therefore, the mixing model was evaluated for a range of values for $F(P)$ and $F(3S)$, namely 0.01, 0.03 (as proposed by *Koehnken* (2012b)), and 0.1 (as approximate maximum value of the range of bed-load/suspended-load fractioning in very large rivers *Turowski et al.* (2010)). To conclude, the result of this mixing model is a range of values for magnitude and sediment grain size distribution delivered from the 3S. We later used this range to select only those initializations of the connectivity model that coincided with the this conceptual, observation-based mixing model.

5.4.2 Erosion potential in the 3S Basin

The sediment yield from river basins is controlled by lithology, climate, and topography (*Andrews and Antweiler*, 2012; *Mueller and Pitlick*, 2013; *Riebe et al.*, 2015; *Mueller et al.*, 2016; *Syvitski and Milliman*, 2007). We propose that analysing lithologic and climatologic/hydrologic drivers can yield some auxiliary information on where in the 3S basin more sediment can be mobilized and transferred. We base the analysis on a regional lithologic map (*Fromaget*, 1971). *Fromaget* (1971) identified four stratigraphic units. First, Igneous rocks of which Cenozoic basalt escarpments are most prominent (*Barr and MacDonald*, 1981). Second, metamorphic rocks in form of diverse granite, gneiss, mica, and some undifferentiated schists. Third, various sedimentary rock types, e.g., sand, mud and clay stones, of the Lower, Middle, and Upper Indosinian sequences of the Triassic period (*Lepvrier et al.*, 2008). Last, some Quaternary fluvial sediment deposits are present throughout the 3S. We propose, that this sequence (Igneous-Metamorphic-Sedimentary) defines a first order estimate of rock strength and erodibility (c.f., *Sklar and Dietrich* (2001)).

We assume that rock strength is a potential driver behind sediment supply to channels, while the transport of sediment through the river network and erosion through fluvial processes is driven by discharge and energy in river channels. To measures this component, we resort to unit stream power, ω [W/m^2]. A measure that is empirically well linked to both to sediment transport and direct erosion from bed and banks (*Bizzi et al.*, 2015a; *Parker et al.*,

2015). We calculate stream power for $Q_{1.5}$ for each reach in the network through:

$$\omega = \frac{\rho * g * Q_{1.5} * I}{W_{AC}}, \tag{5.4}$$

where ρ is the density of water (1000 kg/m^3) and g is the gravitational acceleration (9.81 m/s^2). Then, we analyze the spatial distribution of erodibility and stream power. This analysis cannot be directly translated in quantitative measures of sediment provenance. Yet, we argue that this qualitative information can be useful to interpret results of the sediment connectivity model.

5.4.3 Inverse modelling of 3S sediment transfers

In order to derive network-scale estimates of sediment provenance we applied the CASCADE sediment connectivity model (*Schmitt et al.*, 2016) in an inverse modelling approach to the 3S basin. The model is based on hydro-morphologic parameters (reach hydrographs, channel gradient, active channel width) that were available at the network-scale in the 3S (see section 3). However, building such a model requires information on sediment source locations and their characteristics (e.g., grain size and supply). In a previous application to a major sand-gravel river, CASCADE was initialized deterministically (*Schmitt et al.*, 2016) by assuming that each reach includes a single sediment source supplyin a grain size proportional to the equilibrium grain size at bank-full flow conditions in that reach. In this study, we applied instead a stochastic approach for the initialization of sources. This required a large number of model realizations, each based on a random parameterization of sediment sources. Each run resulted in a sediment flux $\Theta 3S$ and grain size distribution $d(3S)$ at the basin outlet. We accepted only those runs within the range of $\Theta(3S)$ and $d(3S)$ identified by the mixing model at the Mekong-3S confluence (see Equation 5.3). Non-uniqueness of solutions is a common challenge in inverse earth-system modelling (*Mosegaard and Tarantola*, 2002; *Sambridge and Mosegaard*, 2002). For our study, this implies that the mismatch between the model resolution (spatially fully distributed over the river network) versus resolution of data for selecting initialization (point data at the basin outlet) will likely result in multiple source initializations that produce results in accordance with observations. Nonetheless, we propose that combining the inverse modelling with the mixing model at the Mekong-3S confluence can constrain the plausible patterns of sediment transfer and provenance within the tributary network.

Modelling approach

We selected the CASCADE framework because it allows tracking sediment contributions from many sediment sources as separate cascading process through the river network (*Schmitt et al.*, 2016). CASCADE is a statistical model resulting in an instantaneous map of sediment source-sink relations. The numerical efficiency of CASCADE is a prerequisite for evaluating the multiple realizations required in the inverse modelling problem.

The model formulation is described in detail in *Schmitt et al.* (2016). Here, we briefly describe the approach (Figure 5.2 a) and identify changes in comparison to the prior application (Figure 5.2 b). In CASCADE, each source is the beginning of an individual sediment cascade. In Figure 5.2 a, two sediment sources $\varsigma = 1$ and $\varsigma = 2$ are delivering sediment to the network outlet Ω. The network is represented as a graph with $e = 1 \cdots 9$ edges. Each sediment source supplies a specific grain size d_ς (dot size Figure 5.2 a) to an individual sediment cascade, γ_1 and γ_2. Each edge along the cascades has a specific transport capacity, ${Q_{S,e}}^\varsigma$ [kg/yr], for d_1 and d_2 (Figure 5.2, width of grey lines). The calculation of transport capacity in an edge is as follows. CASCADE splits the hydrograph of an edge into discharge classes (as in a previous implementation, see *Schmitt et al.* (2016), we used 9 classes). A hydrodynamic solver derives flow velocity and flow depth in each edge based on solving the Strickler equation for open channel flow. Therefore, the hydro-dynamic solver uses the information on reach gradient and active channel width (*Schmitt et al.*, 2016). Based on that information, CASCADE derives the transport capacity in an edge for each discharge class using the Engelund-Hansen sediment transport formula (*Engelund and Hansen*, 1967). CASCADE calculates the total transport capacity according to the frequency of each discharge class over the 20 year period. CASCADE repeats this procedure for all edges along all sediment cascades. E.g., in Figure 2, there are two sediment sources (hence two separate sediment cascades) and 9 edges, of which three are shared between two sediment cascades. This requires to calculate 12 values of ${Q_{S,e}}^\varsigma$. For example, in edge 7, γ_1 and γ_2 are present and subject to the same hydraulic conditions, but the transport capacity of γ_1, ${Q_{S,7}}^1$, would be smaller than for γ_2, ${Q_{S,7}}^2$, because γ_1 represents the transport of a larger grain size. Engelund-Hansen is a total load formula, i.e., no grain size specific transport rate is derived for a sediment mixture. A fractional transport capacity for each sediment cascade is derived from the calculated total transport capacity based on the sediment grain size distribution in each reach and the source supply (see Scenario 3 in (*Schmitt et al.*, 2016)). Sediment flux (Θ) is a function of the local transport capacity, but also of the transport capacity in the upstream river network. For example, ${\Theta_{S,2}}^1$ is limited by the sediment flux from upstream edge 1, ${\Theta_{S,1}}^1$, which is

lower than the transport capacity in edge 2 (${Q_{S,2}}^1$, compare dotted versus shaded area). Sediment flux is reduced to match the local transport capacity in case sediment supply exceeds transport capacity. In reach 5 (see Figure 5.2 a), sediment inputs ${\Theta_{S,4}}^2$ exceed transport capacity ${Q_{S,5}}^2$ and a major part of ${\Theta_{S,4}}^2$ would be deposited. The limited transport capacity in edge 5 also limits the flux of sediment in γ_2 in the downstream network. How much sediment is delivered to the outlet from each source (see color and width of arrows at the basin outlet in Figure 5.2, a, is then a function of source supply and the spatial distribution of transport capacity in the river network.

Within this modelling framework, the initialization of source grain size and supply is key. In a previous work, source grain size was initialized proportionally to local hydraulic forcing and source supply was set to the local transport capacity for that grain size (*Schmitt et al.*, 2016). This mechanism limited sediment supply, as reaches with a high hydraulic forcing were assigned larger grain sizes. The inverse modelling approach assigns grain sizes randomly to sources. This means that a source located in a reach with high hydraulic forcing can be assigned a small grain size. In this case, setting source supply equal to transport capacity for that small grain size would result in very high rates of sediment supply. Therefore, we herein adopt a two-stage modelling approach. In the first stage, a random grain size is assigned to each source and transport capacities for all cascades are calculated (Figure 5.2, a). In the second stage, sediment supply of a source ς is set to the lowest transport capacity for d_ς in the river network. For example, supply of $\varsigma = 2$ (${Q_{S,4}}^2$) is reduced to match the transport capacity (${Q_{S,5}}^2$). This does not change the sediment flux to the outlet (compare arrow width and color at the basin outlet between Figure 5.2 a and b), but the source supply (compare source colors in Figure 5.2 a and b). We argue that this approach allows for a better estimate of sediment fluxes, assuming that the observed morphology (i.e., mainly gradient) and the resulting transport capacity can be considered an indicator for upstream source supply, and that the river network is in equilibrium regarding sediment inputs and outputs (cf. *Church* (2006) and *Mueller and Pitlick* (2013))

Defining network indicators for sediment connectivity

Setting the stage for an inverse modelling problem requires to define modeled indicators that can be compared to observations (*Refsgaard et al.*, 2007). Notably, CASCADE derives the specific flux for each grain size in each edge (Figure 5.2, area delineated by dotted lines). From this information, the total flux in each edge can be calculated as sum of fluxes along all sediment cascades in that edge. For example, the total flux in edge 7, $\Theta_{S,7}$, Figure 5.2 b, is the sum of ${\Theta_{S,7}}^1$ and ${\Theta_{S,7}}^2$. This holds also if the flux at the basin outlet is

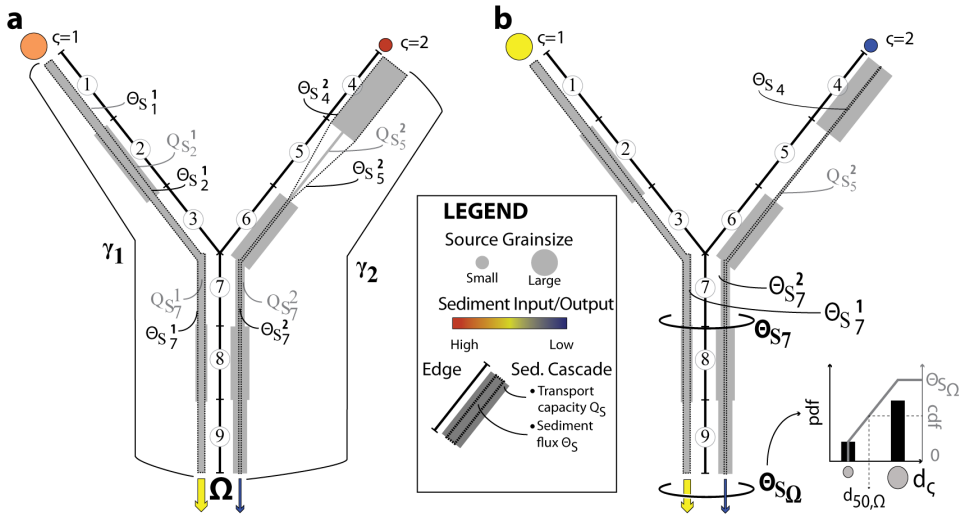

Figure 5.2: *Basic principles of the CASCADE model. a: original model setup. b: Modified model setup to represent detachment limited sources. Relevant variables are detailed in the text.*

calculated (e.g., $\Theta_{S,\Omega}$, Figure 5.2 b). In the 3S, $\Theta_{S,\Omega}$ defines the sediment supply from the 3S basin to the Mekong ($\Theta(3S) * F(3S)$) in Equation 5.3). We propose that the flux of a grain size in an edge is a proxy for its relative prevalence in the bed material (e.g., in $\Theta_{S,\Omega}$ more of sediment flux in Ω originates from $\varsigma = 1$ than from $\varsigma = 2$). Based on the fractional flux (see histogram Figure 5.2 b) the flux weighted median (*Cormen et al.*, 2001, p. 1994) of grain sizes is calculated to represent the median grain size, $d_{50,e}$, in every edge, and at the basin outlet Ω. $d_{50,\Omega}$ is then compared to the sediment grain size distribution ($d(3S)$) from the mixing model.

Inverse sediment transport modelling

CASCADE is implemented for the previously derived 3S river network composed of 1422 edges, with each edge representing one of the previously delineated river reaches. CASCADE does not consider attrition of grains i.e., there is no transfer from larger grains into sand fractions. As in a previous work (*Schmitt et al.*, 2016) , we assume that each edge contains a single sediment source (n_{source}=1422). CASCADE is run for 7500 random grain size initializations. It is not reasonable to assume that all sources will supply sand of the same grain size, given extent and diverse geological setting of the 3S. Yet, there is neither information on the frequency distribution of supplied grain sizes ($f(d_\varsigma)$), for example if they follow a normal or a lognormal distribution, nor regarding their spatial distribution in the network. Therefore, a Monte Carlo approach is applied to create a random vector $\mathbf{d_i}$ of source

grain sizes for each initialization i. This process is designed to not require any *a-priori* assumptions on the type of the distribution or its parameters. A Pearson random number generator generates a vector $\mathbf{d_i}$ of random numbers from a wide range of different probability distributions for each run. The length of $\mathbf{d_i}$ equaled the number of sources, i.e., 1422 for the 3S. $\boldsymbol{d_i}$ can then be scaled to a desired range of grain sizes. The entries of $\boldsymbol{d_i}$ are randomly assigned to the sediment sources. Hence, for each initialization i, both the source grain sizes $\boldsymbol{d_i}$ and the assignment of grain sizes to sediment sources (i.e., the spatial distribution) is randomized.

5.5 Results

5.5.1 Sediment flux and grain size distribution at the Mekong - 3S confluence

Figure 3 shows the results of the mixing model at the Mekong – 3S confluence (Equation 5.3). The middle line (with square symbols) in Figure 5.3 indicates the results of the mixing model for $F(P) = 0.03$, for values of $F(3S) = 5$ —100 % (Figure 5.3, bottom abscissa), while the upper and lower lines result from using values of $F(P) = 0.1$ (upper line with stars) and $F(P) = 0.01$ (lower line with crosses). Each value of $F(3S)$ can be translated into a value of total sand load from the 3S by the relation $F(3S) * \Theta(3S)$ (Figure 5.3, top abscissa) and using the proposed total load from the 3S of 25 MT/yr (*Wild and Loucks*, 2014). Coarsening is observed over the Pakse – Stung Treng reach (Figure 5.3, horizontal lines). While downstream fining could be explained by preferential deposition of coarser grains (*Paola et al.*, 1992) coarsening could be attributed to the storage of finer sediments on floodplains (*Walling et al.*, 1998). But, the Pakse - Stung Treng reach is dominated by confined bedrock channels with rare overbank flows (*Carling*, 2009) and potentially little floodplain storage. Therefore, we propose that the observed downstream coarsening is, instead, mainly due to delivery of sand from the 3S. The sand delivered from the 3S needs to have a coarser grain size than the sand inputs into the Pakse-Stung Treng reach at Pakse ($d(P)$). If less sand is supplied by the 3S, then its grain size ($d(3S)$) must be coarser to explain the coarsening (see Figure 5.3). The less sand that is transported in the Pakse reach, i.e., the smaller $F(P)$, the less sand supply is required from the 3S to yield the observed change in mainstem sediment size. This behavior is shown by the curves in Figure 5.3. The blue curve indicates results of Equation 5.3 for $F(P) = 0.03$. The observed coarsening could result from a low sand supply from the 3S. For example, a sand supply of only 5% of the total supply from the 3 S basin ($F(3S) = 0.05$, bottom abscissa, or 1.25 MT/yr, top abscissa) can result in the observed coarsening in

the Mekong, if the 3S basin supplies medium sand (0.35 mm). If, instead, all sediment supply from the 3S is sand ($F(3S) = 1$) than also finer sand (0.2 mm) could explain the observed coarsening in the Mekong. These results are meaningful from a perspective of sediment transport processes within the 3S. If the sand fraction in the 3S is dominantly fine sand, more sand can be transported, resulting in a higher fraction of sand delivered from the 3S basin. If the fraction of sand in the total load is different from the value of 0.3 proposed by (*Koehnken*, 2012b), the observed change in main stem sediment grain size distribution could still be explained if the sand fraction supplied by the 3S is finer or coarser, depending on the deviation from $F(P)$ (black lines in Figure 5.3). The impact of the different values of $F(P)$ on the expected grain size in the 3S decreases for increasing total supply from the 3S. The shaded area in Figure 5.3 indicates the potential range of the ratio between sand grain size and sand supply from the 3S. The potential sand grain size in the 3S spans the range from 0.2 to 0.47 mm.

5.5.2 Lithology and erosion potential in the 3S basin

Analysing the erosion potential in the 3S can derive some more information on the provenance of that fine sand. Stream power is highest in low-order tributaries of the Se Kong (Figure 5.4). When considering only the main rivers (Strahler Order $>= 3$) stream power is higher in the Se San (252 W/m) than in the Se Kong (206 W/m) and lowest in the Sre Pok (151 W/M). The analysis of lithology is based on the 3 relevant lithological classes (Ig: igneous rocks, Sch: schists, Sed: sedimentary rocks) identified by (*Fromaget*, 1971) (see Figure 5.4 for details). When using these broad classes, the Se Kong (Ig: 37 % Sch: 6 % Sed: 56 %) and Sre Pok (Ig: 36 % Sch: 6 % Sed: 59 %) are relatively similar, consisting mainly of sedimentary rock and a lower amount of igneous rock with schists being nearly absent. Lithology in the Se San is characterized by a higher fraction of schist and igneous rocks (Ig: 48 % Sch: 25 % Sed: 27 %). More in detail, lithology in the upper Se Kong catchment is dominated by coarse grained, quartz-rich sandstone formations of the upper Indonisian Sequence (*Buffetaut*, 2009, p47) (Figure 5.4 a). Stream power in the main stem of the Se Kong is relatively low in the upper parts. The first major tributary, the Se Kamane River, has very high stream power and drains a catchment dominated by schists (Figure 5.4 b). Below the Se Kamane confluence, mainstem stream power strongly decreases and a large deposit of Quaternary alluvium (the only such alluvial deposit in the Se Kong catchment) occurs (Figure 5.4 c). Further downstream, the Se Kong enters a large sedimentary basin dominated by Indosinian lithologies around the confluence of the three rivers (see Figure 5.4 for details). The Se San River originates from the Vietnamese Kontum Mas-

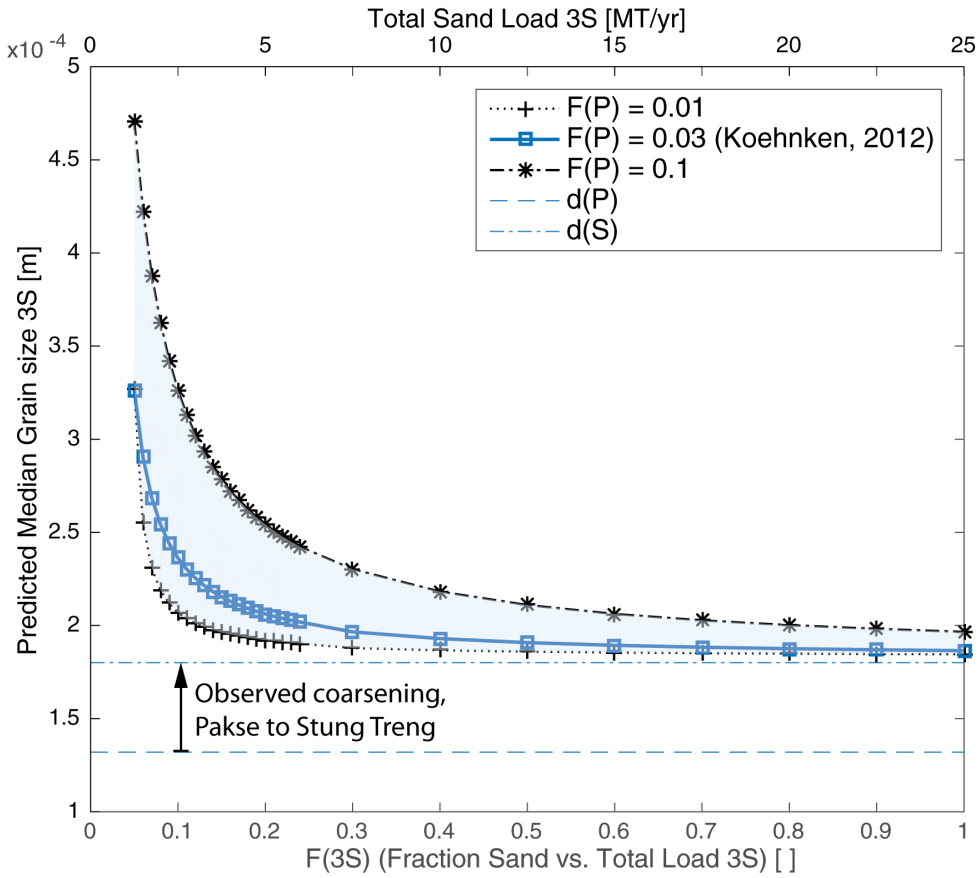

Figure 5.3: *Sand mixing model at the 3S confluence. Different lines indicate results for different values of F (Fraction of sand in total sediment load). Horizontal lines indicate the observed median sand grain sizes in the Pakse and Stung Treng reaches.*

sive (Figure 5.4 c). Its upper valley and the valleys of major tributaries are steep, with high stream power, and traverse mostly crystalline schists, with the course of the river itself closely following outcrops of schist (Figure 5.4 b,e). The lower part of the basin is dominated by sedimentary Indosinian rocks. The headwaters of the Sre Pok are underlain by a complex lithologic mosaic (Figure 5.4 f), sedimentary rocks of the Indosinian sequence (undifferentiated Indosinian and Middle Indosinian fine grained mud, marl and sandstones) are dominant and pockets of Quaternary sediment are present in the headwaters. Downstream, lithology is dominated by Indosinian rock types, with some outcrops of mud, clay, and sandstones of the lower indosinian sequence (*Fromaget*, 1971), and quaternary sediment. Locally, very high values in stream power occur in smaller tributaries in all sub-basins. Many of these reaches of high stream power occur on late Cenozoic basaltic escarpments (*Barr and MacDonald* (1981), Figure 5.4 g). Thus, there are distinct differences in lithologic setting and stream power distribution for the three tributaries. Differences are especially evident in the upper reaches of each river system, while in the lower reaches, as the three rivers approach their confluence, are more similar. It could be hypothesized that head-waters, where stream power is highest, can be relevant sediment source areas. In the headwaters, erodibility is in tendency lowest in the Se San (dominated by schists), followed by the Se Kong (dominated lower Indosinian sand-stones) and the Sre Pok (dominated by middle Indosinian clay and marlstones and Quaternary sediment). Combining this information with upstream stream power indicates that the erosion potential is likely to be highest in the Sre Pok (erodible lithology, high stream power). Ranking the Se Kong (more erodible lithology, low stream power) and Se San (less erodible lithology, very high stream power) is difficult with the available information.

5.5.3 Inverse modelling of sediment connectivity in the 3S

Network response to random grain size initializations

We created 7500 random grain size initializations. Based on the result of the mixing model, we scaled each realization such that is contained only grain sizes in the sand range (i.e., 0.0625E-3 to 2E-3 mm). We then ran CASCADE using a two-stage initialization for each initializations (15000 runs). The results for all theses initializations are difficult to analyse because of the large number of runs and multiple random properties (source grain sizes and their distribution in the network). However, some key findings emerge already from analysing the random inputs and outputs of the model for all initializations and the spatial distribution of network properties of sediment connectivity for few selected initializations. For each run, d_{50} and total sediment output from the 3S basin were evaluated (Figure 5.5). Each of the

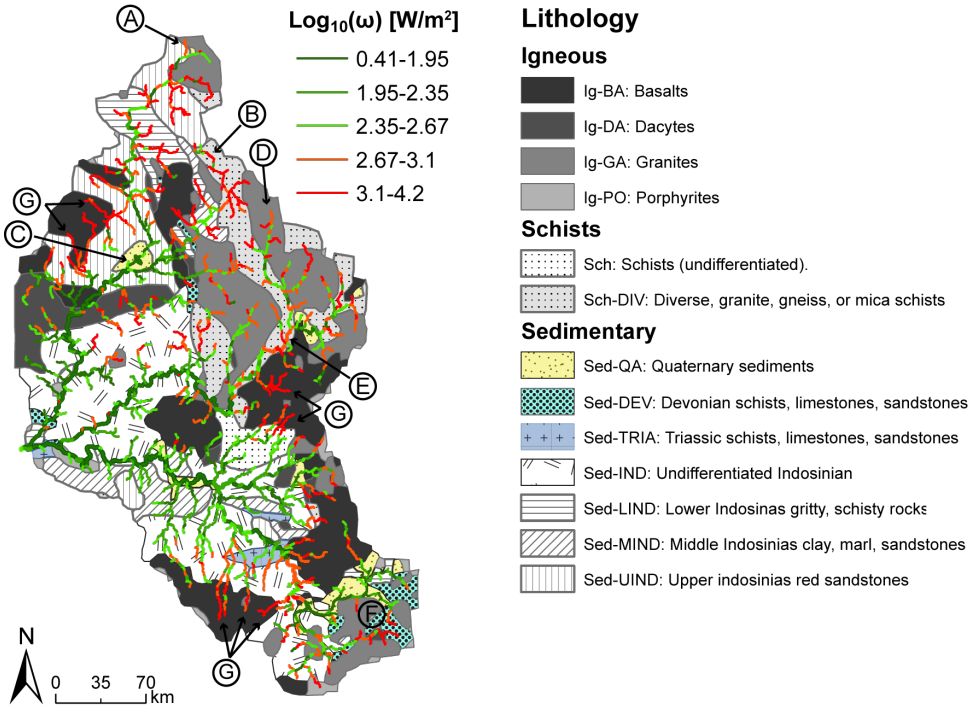

Figure 5.4: *Lithology according to Fromaget (1971) and stream power (ω) distribution of the 3S Basin. Letters refer to descriptions of relevant features in the text.*

initializations had two random components. First, the statistical distribution of sources grain sizes (Figure 5.5 a) for all sources in the network, and second the spatial distribution of source grain sizes, because grain sizes were assigned randomly to each source. Both, predicted d_{50} and flux at the basin outlet spanned more than one order of magnitude (Figure 5.5 b). For the d_{50}, this range is identical with the range of source grain sizes (i.e. covering the full range of sand from 0.064 to 2 mm). For flux, simulation results ranged from 4E9 to 2E11 kg/yr. There was a clear correlation between sediment grain size distribution (i.e., d_{50}) at the basin outlet and sediment flux. Hence realizations that resulted in a finer d_{50} also resulted in a higher sediment flux.

In order to clarify the relation between aggregate results of an initialization (i.e., d_{50} and flux at the outlet) and the grain size initialization from which it resulted is not unique, which is shown in Figure 5.5 and and b. A similar sediment grain size distribution can occur for a wide range of sediment fluxes and *vice-versa*. For example, realization 1371 (marked green in Figure 5.5 a, b) and 841 (marked red in Figure 5.5 a, b) resulted both in a d_{50} of 0.5 mm at the basin outlet but the sediment flux was very different (1.79E10 vs. 9.8E9 kg/yr). This result is in accordance with the statistical distribution of source grain sizes, which was considerably coarser for initialization 1371 than for initialization 841 (Figure 5.5 a). In initialization 841, the few sources that supply finer sediment (e.g., below 0.05 mm) are randomly distributed throughout the river network (Figure 5.5 c). Evidently, these sources provided the majority of the cumulative sediment flux at the basin outlet (Figure 5.5 c, small panel). The cumulative sediment flux indicates a strongly right-tailed distribution, hence the majority of sources contributed relatively little to the cumulative fluxes. The distribution of sediment fluxes contrasts the statistical distribution of source grain sizes, which was strongly left-tailed (see Figure 5.5 a, green line).

Hence, the routing through the river network results in strong fining from the median source grain size (around 1.5 mm) to the observed median grain size at the basin outlet (0.5 mm). Source grain sizes for initialization 841 were not only finer but also more homogeneous than for initialization 1371 (see distribution in Figure 5.5 a), resulting in a homogeneous spatial pattern of source grain sizes (Figure 5.5 d). For initialization 1371 there was little transformation between statistical distribution of source grain sizes and the cumulative sediment flux per grain size (compare the shape of distributions in Figure 5.5 a, red line, and Figure 5.5 d, small panel). The median grain sizes at the basin outlet was only slightly finer than the median source grain size. Hence, the network-sediment routing and hydraulic sorting, i.e., the preferential routing of finer grain sizes, exerted a much stronger control on larger than on finer grain sizes. Even though sources of large sediment

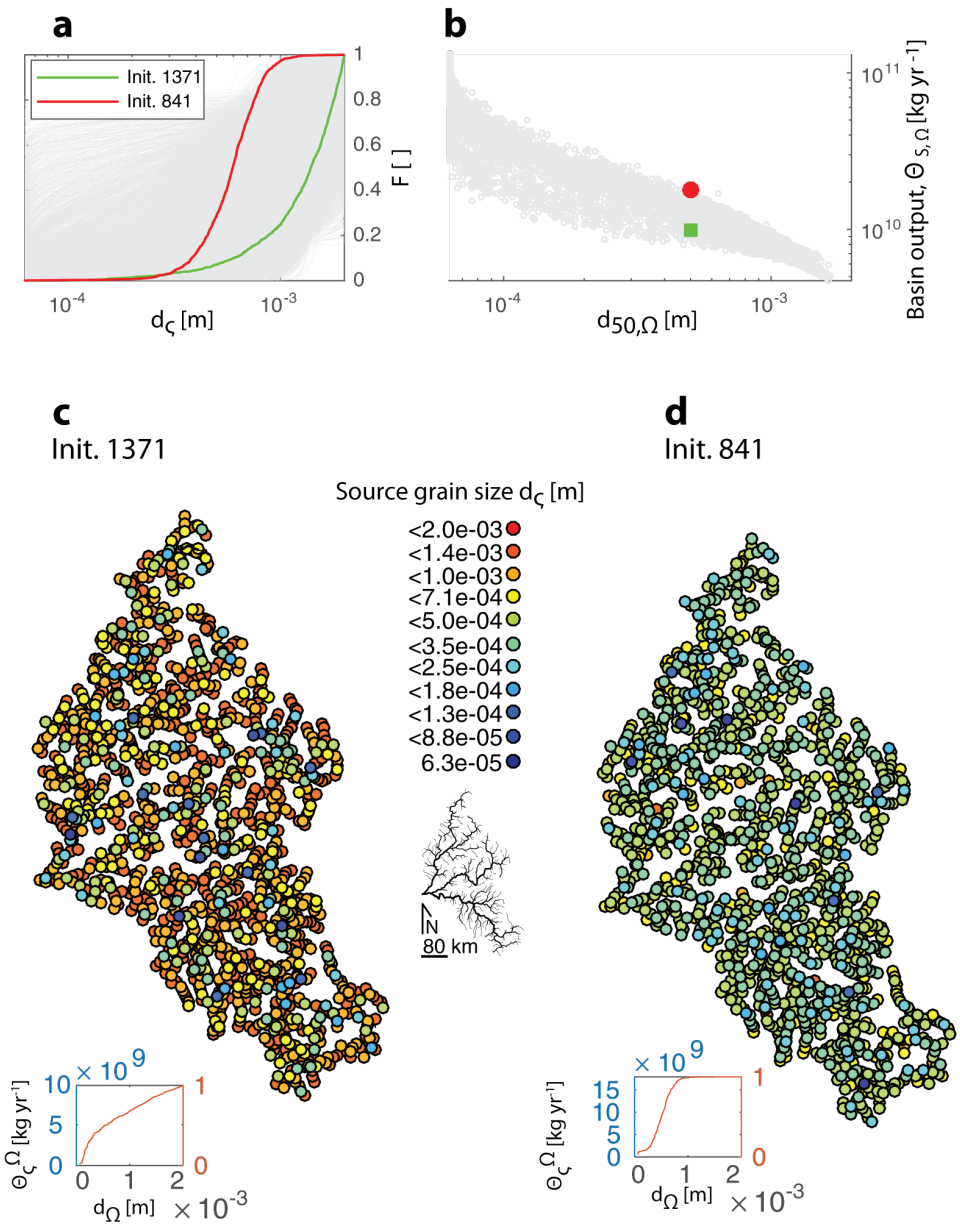

Figure 5.5: *Cumulative distribution function of all created grain size realizations (a) and the resulting sediment flux and median grain size (d_{50}) at the basin outlet (b). Two initializations (1371 and 841) were selected. c (Initialization 1371) and d (initialization 841) show the spatial distribution of source grain sizes, and the cumulative flux over all grain sizes at the basin outlet (small panels). Small network for scale and orientation.*

dominated by numbers, few sources of fine sediment drove the total sediment flux and, as a consequence, the sediment grain size distribution at the outlet. Sediment delivery from each sub-basin cumulatively controlled flux and sediment grain size distribution at the outlet of the 3S. This cumulative signal at the basin outlet potentially carries a specific signature of network properties (spatial distribution of sources, geo-morphologic properties, or hydraulic forcing) in each sub-basin.

Disaggregating the basin response into the signals from each of the sub-basin indicates how each sub-basin transforms the input signal of source grain sizes into an output signal of sediment flux and grain size distribution . The correlation between d_{50} and flux is shown in Figure 5.6 for each sub-basin, and the entire 3S. There is a high correlation between flux and the median grain size (d_{50}) at the sub-basin outlet size for each sub-basin. A linear regression between the log-normalized flux and d_{50} resulted in a R^2 of 0.8 for Se Kong and Se San sub-basins and for the entire 3S, and a R^2 of 0.77 for the Se Kong sub-basin. An analysis of variance (ANOVA) was applied to test if the 3 groups have significantly different total fluxes. An analysis of covariance (ANOCOVA) was applied to test if the slope of the regressions (see lines in Figure 5.6) were significantly different. The ANOVA indicates that sediment fluxes from the three sub-basins are significantly different ($p<0.01$). Amongst the sub-basins, flux is highest for the Sre Pok, and lowest for the Se Kong sub-basin. The regression slope is significantly ($p<0.01$) less negative (i.e., flatter) for the Se Kong compared to the other sub-basins. Hence, a unit increase in sediment grain size at the basin outlet relates to a lower decrease in sediment fluxes in the Se Kong than for the other sub-basins. To conclude, network properties of each sub-basin result in a specific transformation of random input signal into a (sub)-basin specific response in terms of overall magnitude and response strength.

Selection of model realizations

The range of sand flux and d_{50} at the outlet obtained from all model runs spans two orders of magnitude (4E9 - 2E11 kg/yr, 0.0065-2 mm). This wide range can be narrowed by exploiting the available observations on sediment flux and grain size distribution at the Mekong-3S confluence.

Results of only 65 of 7500 (0.8 %) initializations fall within the boundaries of the sediment-mixing model (Figure 5.7 a, blue shaded area is identical with shaded area in Figure 5.3). The median grain size of accepted realizations is in the range between 0.19 and 0.22 mm, flux is between 10.5 to 24.8 Mt/yr (Figure 5.7 a). Hence, the range in fluxes for accepted grain size realizations is much higher than the relatively narrow range for median grain sizes. In turn, only a small part of the envelope identified by the mix-

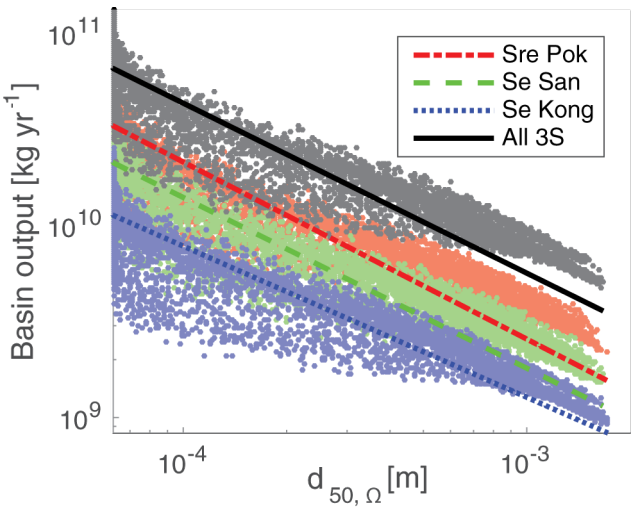

Figure 5.6: *Relationship between $d_{50,\Omega}$ and sediment flux for the 3S basin outlet, and the outlets of the three sub-basins.*

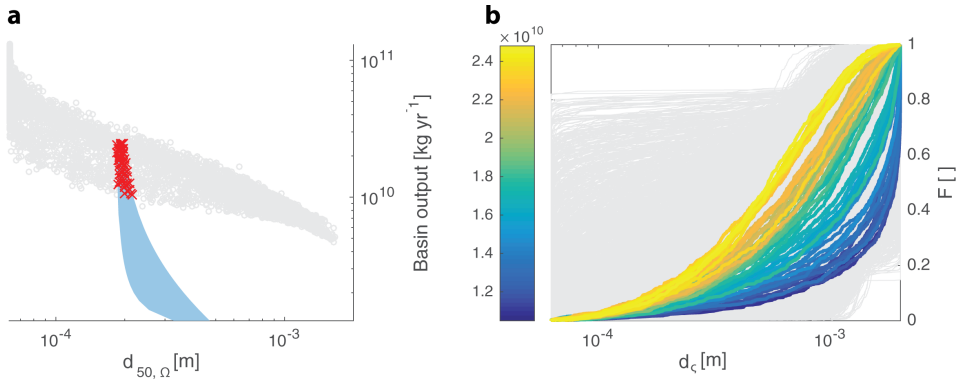

Figure 5.7: *Inverse modelling initialization (a). Only realizations that fall in the d_{50}/total flux range identified from the sediment mixing model (blue overlay, compare Fig. 4) were accepted (red crosses). Cdfs of accepted source grain size initializations (b). The colorbar gives the resulting flux from the 3S tributaries for accepted initializations.*

ing model is in accordance with the result of network connectivity model. Especially, possible solutions in which 3S supplies a small amount of large grained sand (i.e., > 0.22 mm) do not occur amongst the simulation results. This is because already the presence of some fine-grained sand sources suffices to cause a strong fining of the sediment grain size distribution at the basin outlet. This is also evident analyzing the probability distribution of source grain sizes for selected realizations (Figure 5.7 b). The average source grain size for accepted realizations is 1.14 mm, considerably coarser than the output d_{50} for the accepted realizations. The probability distribution of source grain sizes is directly correlated to the flux at the basin outlet (see colors in Figure 5.7 b, realizations containing larger grain sizes result in lower fluxes). The median source grain size in an initialization and the flux at the basin outlet correlate strongly (R^2=0.93). This high correlation shows again that the grain size of source supply is much more relevant to determine sediment flux and grain size distribution at the basin outlet than the spatial distribution of sources. Otherwise, the random assignment of grain sizes to the sources would result in a weaker correlation between source grain sizes and sediment grain size distribution at the basin outlet.

These statements are confirmed analyzing the spatial patterns of sediment source grain sizes, downstream fining patterns in bed-material, and the network pattern of grain size distributions throughout the network (Figure 5.8). First, Figure 5.8 a shows the average source grain sizes over all accepted realizations. There is no visible spatial pattern in mean source grain sizes for accepted realizations (Figure 5.8 a), and no link between the distance of a source from the outlet and the grain sizes assigned to it (Figure 5.8 c). Such a pattern could occur, for example, if only initializations in which large grains are assigned to steep headwaters result in realistic sediment fluxes. There is, instead, a clear spatial pattern for the flux weighted median grain size in each edge ($d_{50,e}$) (Figure 5.8 b, shown is the average over all accepted realizations). Downstream fining is evident for all reaches from the clear correlation between the distance of a reach from the basin outlet and $d_{50,e}$ (Figure 5.8 d). Because of the two-stage model initialization there is no deposition, and no preferential deposition of larger grains. The fining is instead caused by the network structure. The more downstream a reach is located, the higher is the probability that sources of finer sand are located upstream. Because the $d_{50,e}$ is weighted based on the flux for each grain size, some sources of fine sediment can lead to a strong fining downstream. The downstream fining trend is complemented by the spatial heterogeneity in $d_{50,e}$ between the sub-basins. The mean $d_{50,e}$ in the network of the Sre Pok is 0.79 mm, which is significantly ($p<0.01$) smaller than in the Se San (0.81 mm), and in the Se Kong (0. 83 mm).

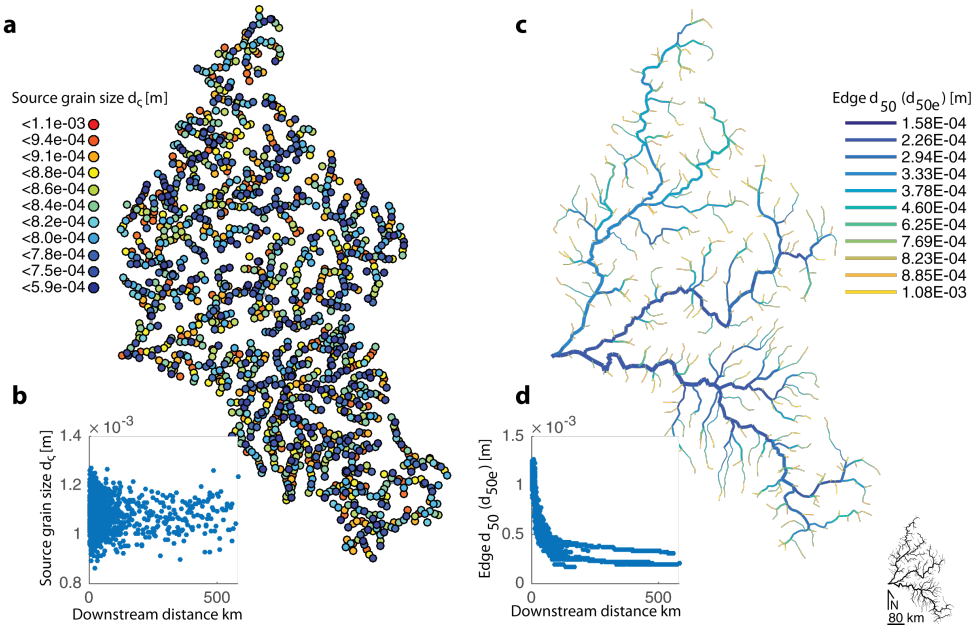

Figure 5.8: *Mean source grain size over accepted initializations (a). Grain sizes are randomly assigned to reaches. Hnece there is no downstream pattern in source gain size (b). Resulting median grain sizes in all reaches in the network (c), and resulting fining pattern (d). Small network for scale and orientation.*

Magnitude and uncertainty in network sediment fluxes

Mean sediment flux showed a clear spatial pattern. Sediment flux increases downstream with different rates for the three sub-basins (Figure 5.9 a). Notably, in the Se Kong, sand fluxes in the main stem are lower than in the main-stems of the Se San and Sre Pok Rivers. The variation of sediment fluxes over all accepted realizations is relatively low (Figure 5.9 b). Variation over realizations is measured as relative standard deviation, i.e., the standard deviation divided by the mean (Figure 5.9 b), in order to correct for the different magnitudes of sediment fluxes across the river network. The spatial distribution of the relative standard deviation is characterized by a clear downstream pattern. High order reaches have a lower relative standard deviation than low order reaches. This result is not an artifact of the normalization and a similar spatial pattern is visible for the interquartile range (IQR) of sediment flux (Figure 5.9 c). Variation in terms of IQR can be an order of magnitude higher for low order reaches and headwater than for high order reaches in large rivers. The median normalized standard deviation is only around 3 % of reach flux, and only for few reaches higher than 15 %. These findings show how uncertainty in sediment fluxes is a function of network topology. The more sources connect to a reach, the higher is the probabil-

ity that the flux from these sources balances over the various initializations. For reaches with few upstream sources, there is an increased probability that all sources are assigned either a very large or a small grain size in different initializations. This would result in a high difference in fluxes between initializations.

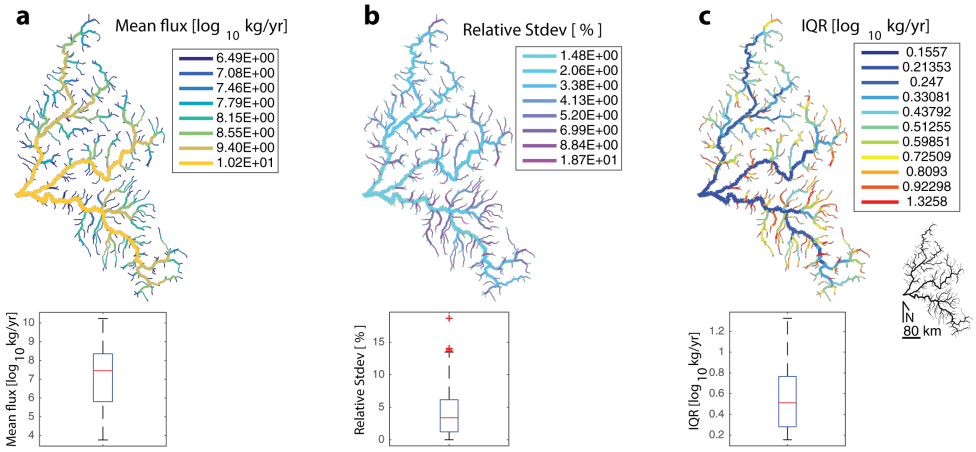

Figure 5.9: *Statistical properties of sediment flux in the river network: mean sediment flux (a), relative standard deviation (b), IQR (c). Boxplots show the statistical distribution of plotted properties. Small network for scale and orientation.*

Sediment provenance and total fluxes in the 3S basin

Despite the absence of spatial organization in source grain sizes (Figure 5.8 a,b) a clear pattern of sediment fluxes arises at the network-scale (Figure 5.9 a). Similarly, there is a clear pattern in sediment provenance. Provenance herein refers to the spatial distribution of delivery from sediment sources to the basin outlet. From Figue 5.10 it is evident that most of the sediment delivered to the 3S outlet originates from sources in smaller upstream tributaries, especially in the Se San and Sre Pok rivers. Also for the Se Kong, most sediment originates from more upstream sources, but the rate of supply is lower than for the two other rivers. The amount of sediment supplied from sources in the main stems of all rivers is negligible for all sub-basin. The sediment provenance at the outlet links strongly to the channel gradient at a sediment source. A power law of the form ${\Theta_\varsigma}^{\Omega} = a * {I_e}^b$ was used to link sediment delivery from a source to the basin outlet (see Figure 5.2, b) to the local channel gradient at the source (I_e). Considering the data of all three sub-basins together, the coefficient of correlation is low (R^2=0.25). The coefficient of correlation increases considerably when separating the Se Kong (R^2=0.47) from the Sre Pok and Se Kong sub-basins (R^2=0.63). The strength

of correlation expressed as exponent b of the power-law differs between sub-basins and is much higher for the Se San/Sre Pok ($b = 0.6$) than for the Se Kong ($b = 0.26$). A in the Se Kong supplies less sediment to the network and eventually to the outlet than a source in a reach with the same slope in the other sub-basins. In terms of mechanisms, that can be interpreted as lower erodibility in the Se Kong, i.e., a reach with a similar hydraulic forcing supplies less sediment.

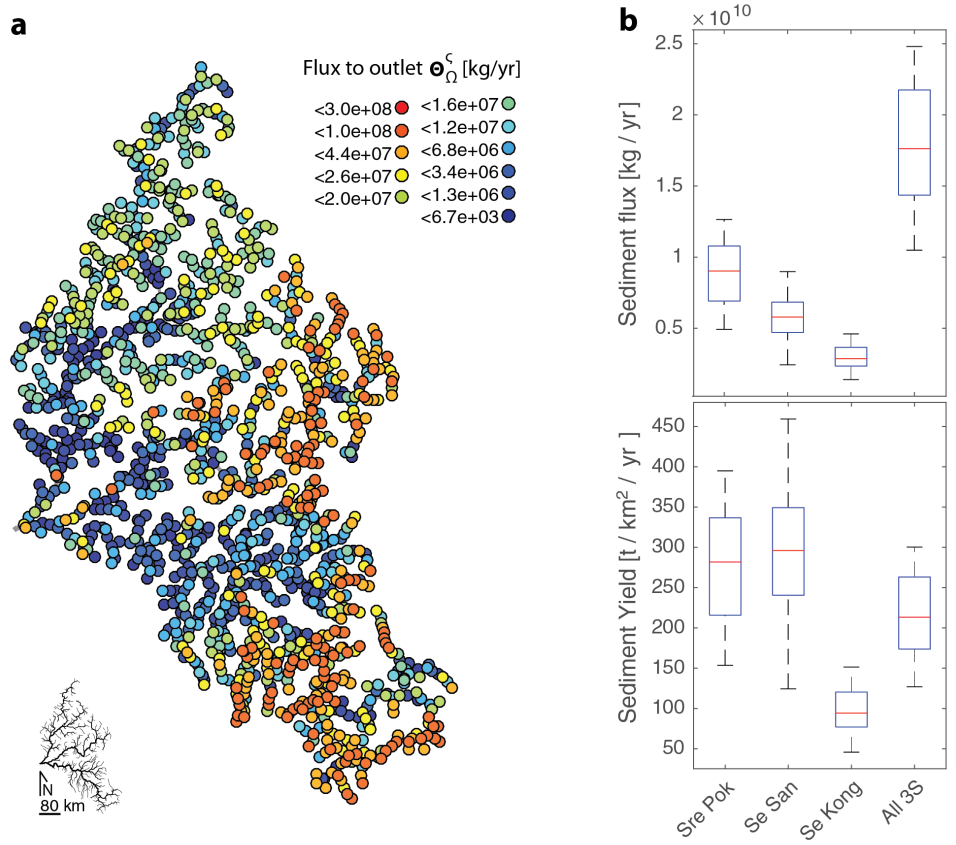

Figure 5.10: *a: Sediment provenance (i.e., delivery from each source to the basin outlet. Colors indicate the mean over all accepted initializations. b: Total sediment flux and yield for each sub-basin. Boxplots indicate the statistical distribution over all accepted initializations.*

Previous results indicate that sediment fluxes are not homogenously distributed within the 3S basin. This section concludes the findings on mean sand flux and yield for the 3 sub-basins and the range of values (expressed as plus-minus one standard deviation) over all accepted initializations) (see Figure 5.10 b). Mean sediment flux from the 3S of 1.8E10 $\pm$ 3.4E9 kg/yr. As expected from the spatial pattern of provenance, sub-basin wise flux is high-

est from the Sre Pok (1.1E10 ± 2.1E9 kg/yr). Flux from the Se San is 5.3E 9 ± 1.3E9kg/yr and 1.9E9 ± 5E8 kg/yr from the Se Kong. This translate into a yield of 218.61 ± 41.36 t/km2/yr for the 3S, 333.91 ± 66.156 t/km^2/yr for the Sre Pok, 271.85 ± 65.715 t/km^2/yr for the Se San, and 61.473 ± 16.356 t/km^2/yr for the Se Kong (sub-) basins. Results for 3S yield are between values proposed by (*Kondolf et al.*, 2014) (290 to 300 t /km^2) and lower (for the Se Kong) or similar to values proposed *Kummu et al.* (2010) (based on MRC data) (220 (Se San) -240 (Se Kong, Sre Pok) t/ km ^{2}). When comparing results to these data, it should be considered that CASCADE considers only sand fractions, i.e, no very fine washload that could constitute the remaining part of the sediment yield. In accordance with our findings, *Bravard et al.* (2014) indicated that the sand yield from the Se San is higher than the yield from the Se Kong. Though *Bravard et al.* (2014) do not mention the Sre Pok as relevant sand carrying river, it remains unclear if this is due the absence of data, or based on actual observations.

Though the information on lithology is sparse, modeled sediment provenance matches the reported differences in rock types between sub-basins. Concretely, it suggests that the indosinian sedimentary rocks in the Se Kong (mainly sand-stones) are less erodible than schists in the Se San or the undifferentiated Indosinian rocks and quaternary sediments in the Sre Pok (Figure 5.4). Transport capacity in the headwaters of the Se Kong is by an order of magnitude higher than in the Se San/Sre Pok (Figure 5.11). But, transport capacity in the Se Kong is in general lower than in the Se San and Sre Pok rivers (matching the observations of high stream power in the upper main stem of Se San, Sre Pok rivers, Figure 5.4 e) more downstream. high transport capacity upstream in the Se Kong is contrasted by two sections with very low transport capacity (Figure 5.11 a and b). Transport capacity in these sections is lower than in any section in the Se San / Sre Pok networks (e.g., Figure 5.11 c and d). These low transport capacity sections explain the lower sediment fluxes in the Se Kong river network and the lower delivery from the Se Kong to the outlet. This is because the 2-stage model initialization assigns supply in such a way to sources that transport capacity in downstream reaches is never exceeded. Geographically, reach B occur where the Se Kong river flows around major igneous outcrop, which increases river length and accordingly slope.

Obviously, a downstream reach cannot exert a direct control on any remote upstream source. We argue that if upstream source supply exceeded local sediment transport capacity for a prolonged period, local deposition and slope adaptation would occur, which would manifest as reaches with alluvial deposits, increased local slopes, and a higher transport capacity. Hence, a low local transport capacity is, while not directly controlling source sup-

ply, a good indicator for the sediment supply from upstream sources. Nevertheless, there are some potential shortfalls with this approach. First, a low local transport capacity could be the result of either a measurement error or an artefact of a recent human disturbance (e.g., a reservoir), which would reduce channel gradient. Second, also a bed-load slug could result in a transient reduction of local slope (*Fryirs et al.*, 2007b). In this case, a low local transport capacity could be an indicator of a high source supply that, at least temporarily, exceeds local transport capacity. All of these mechanisms should be detectable from high-resolution satellite images. Satellite images of sections with low transport capacity (Figure A1) indicate no human disturbance (Figure A2-A5). All of the reaches A-D show a straight channel planform. Especially reaches A and D are straight bed-rock reaches with very limited in channel sediment storage. Reaches B (upper Se Kong), Figure A2, and C (middle Se San), Figure A3, show some vegetated bars and point bars, but no sign of over-bank sediment storage. Low-flow channel morphology shows that no sediment deposits are visible in the lower Se Kong (Figure A8), which is instead dominated by in-channel bed-rock features (Figure A9). Sedimentary bed-forms are visible in the low-flow channel of the lower Sre-Pok (downstream the Se-San Sre-Pok confluence, Figure A10). This is despite a similar stream power in the two rivers (Figure 11, at km 0). Based on the results of the inverse modelling, we propose that observed in-channel sediment deposits in the lower Sre-Pok/Se San are the results of high active sediment supply and transport, instead of low transport capacity and deposition.

5.6 Discussion

Based on the different hydro-morphologic, climatic and lithologic conditions in each of the 3S sub-basins, we expected that sediment connectivity in each sub-basin differs, and that sediment provenance from the 3S is spatially heterogeneous. To better understand sediment provenance and the role of the 3S as sediment source for the Mekong, we asked if and how the range of plausible sediment provenance and sediment fluxes in the 3S can be quantified by analyzing the single, aggregated sediment signal at the network outlet at the mainstem confluence, and spatially distributed information on network hydro-morphology.

We presented a two-stage approach for how information on sediment provenance can be extracted for a river system from inferring rates of source supply and sediment transport from observable river hydro-morphology and calculated transport capacity. We propose, that a first estimate of provenance can be extracted based even on a single random or uniform initialization of sediment sources using that two-stage approach. This is based on the finding

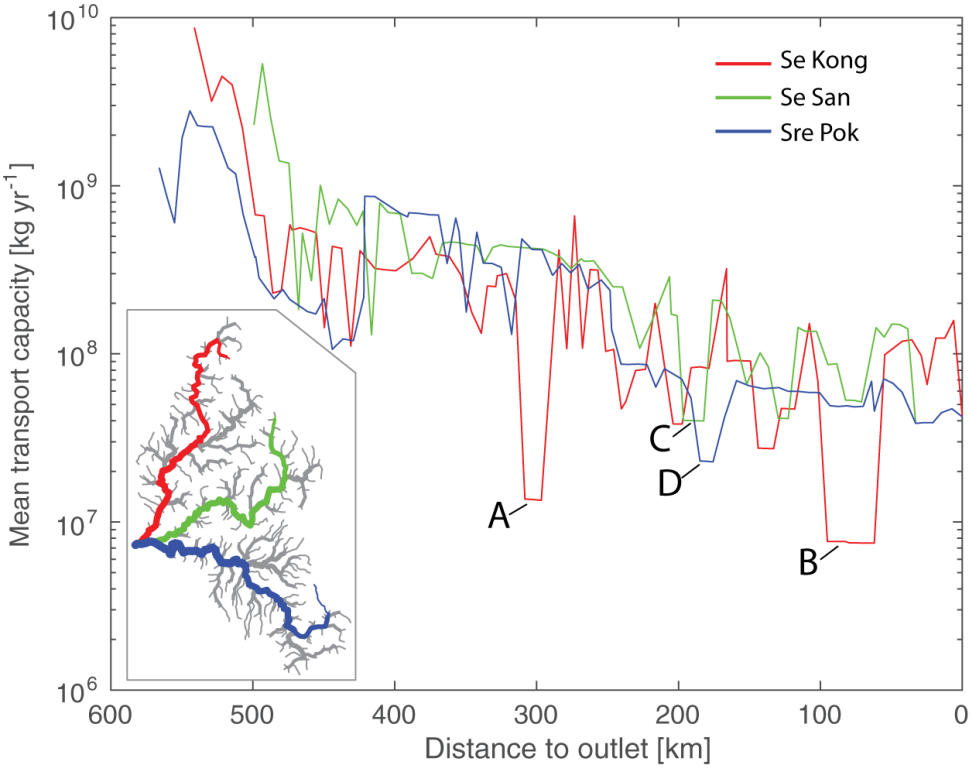

Figure 5.11: *Longitudinal profiles of transport capacity (mean over all accepted realizations) along the Se Kong, Se San, and Sre Pok Rivers. Letters are explained in the text. location on longitudinal profiles is shown in the small panel (linewidth indicates stream order.)*

that, for the 3S case-study, sediment fluxes between sub-basins are significantly different even for the full set of random initializations. Yet, the range of uncertainty regarding absolute sediment flux and grain size distribution is large. This is because transport capacity is no property of a river system that can be calculated *ad-hoc* from local hydro-morphologic parameters (like, e.g., stream power). Transport capacity is, instead, a function of both local hydro-morphology and the supplied grain sizes. Hence, transport capacity is partially controlled by properties of the upstream catchment, i.e., the grain size supplied from upstream sources, and the fluvial transport processes linking upstream sediment sources to the downstream river network. Our results demonstrate the wide range of sediment fluxes that a river network can accommodate in function of source characteristics.

Then, the inverse approach allowed us to reduce the full set of model initializations to few initializations that reproduced available field evidence at the basin outlet. In turn, model results allowed constraining the broad range of potential sediment outputs from the 3S tributary that were estimated from that limited field evidence, i.e., from residuals of the main stem sediment budget. The observed equifinality, i.e., that multiple initializations result in a similar match between model results and observations, could be greatly reduced if some additional measurements of sediment fluxes could be obtained throughout the network, hence formulating many nested inverse problems on the network scale. Additionally, properties such as sediment geo-chemical composition could help to further the ability to narrow the problem of equifinality. Additional data would also help uncovering inconsistencies between process representation in the model and real world processes, which cannot be identified purely from an inverse MCA approach (*Refsgaard et al.*, 2007). The assumption that no sediment is stored in the basin, is no prerequisite for the approach. Even where sediment is stored, e.g., on floodplains, a sediment budget of local sediment stores could be applied to estimate by how much upstream supply exceeds local transport capacity. An information that can then be used to determine upstream source supply. In general, inverse reasoning is common in geomorphology (*Linde et al.*, 2015). For example, *Church* (2006) noted the benefits of inverse approaches for determining transport processes from local morphologic forms, because fluvial forms are more readily observable than the processes that created them. With the presented approach we demonstrate how numerical modeling can transfer inverse reasoning to larger scales, reconcile various types of information, and create a quantitative assessment of sediment transport and sediment source properties on network scale. It should be noted, that the proposed approach infers the grain size that is delivered from each source to the outlet and not necessarily that is supplied at the source. This is

relevant especially with regard to the concept of attrition and abrasion. For example, an upstream source might supply gravel, which breaks down while traveling through the network, hence the source would act effectively as a source of sand. Therefore, despite the fact that sources in upstream reaches might supply gravel, the inverse approach implicitly accounts for processes that transfer these gravels finally to the sandy grain size fractions that are assigned to the sources in the random initializations.

The method allows, in contrast to general (e.g., *Syvitski and Milliman* (2007)), or basin specific (*Kondolf et al.*, 2014) interpolations of sediment yield, to evaluate the spatial heterogeneity in sediment provenance even with limited data. This ability is of great relevance for basin-scale planning or research, e.g., for forecasting the impact of human developments such as reservoir developments, on the river system. Based on our results, we propose that transport capacity in the river network reflects patterns of sediment source supply (c.f., *Young et al.* (2001); *Ferguson et al.* (2015)), while being more readily observable than hillslope processes (especially with the increasing availability of high resolution river remote sensing data on regional scales, e.g., *Bizzi et al.* (2015b)). The inverse modeling identifies steeper headwaters of each sub-basin (Figure 10) as most relevant source areas. In the model, a single source is assigned to each reach, representing all direct inputs into that reach from hill-slope and channel processes. The model prediction that sources with higher supply are located in the steeper headwaters coincides, first, with general field observations and model results (*Willgoose et al.*, 1991; *Montgomery and Buffington*, 1997; *Tucker and Bras*, 1998), showing that steeper channels are better connected to hill-slopes, potentially subject to more active incision (*Sklar et al.*, 2006), and hence likely to receive more sediment from hill-slope and channel processes. Second, the spatial pattern of supply is in line with basin-wide provenance studies, which suggest that around 40 % of the Mekong's sediment yield originates from the central highlands of Vietnam where the Se Kong, Se San, and Sre Pok headwaters are located (*Clift et al.*, 2004b).

Information on basin lithology and erosion potential alone were non-conclusive, but could then be matched to model results. Our results indicate that lithology in the Se Kong, which is dominated by coarse grained sandstones is less erodible than in the other sub-basins. For the 3S, lithology is a stronger driver behind sediment supply and provenance in the 3S than channel gradients (and hence sub-basin relief). On a global scales, *Syvitski and Milliman* (2007) propose that lithology might only play a minor role for controlling basin sediment supply in comparison to basin relief. Compared to the global data-set of *Syvitski and Milliman* (2007), the 3S basin is homogeneous in terms of relief, which makes other factors, such as lithol-

ogy, more important. This assumption is in line with studies of *Mueller and Pitlick* (2013) and *Andrews and Antweiler* (2012) indicating that sediment flux from drainage basins in a similar geographic setting was controlled by lithology rather than by relief. The transport capacity in lower parts of the sub-basins is, according to that interpretation, an adaptation to that variability in supply rates. One of the most obvious spatial patterns that we observe is the modelled downstream finning, and the downstream decrease variability in sediment fluxes between initializations. As detailed above, the model assigns a high supply to low-order reaches in the upper part of the catchment. Sediment grain size distribution and supply in higher order reaches is, instead, "inherited" *Menting et al.* (2015), i.e., dominated by fluvial transport from the upstream network. Results reproduce findings by *Sklar et al.* (2006) in the sense that a random spatial distribution of source grain sizes is transformed by fluvial transport processes into a clear pattern of bed-material grain size distribution . We propose that the spatial distribution of source grain sizes, i.e., which specific source is assigned which grain size, seems to be less as there is no clear spatial pattern in source grain sizes amongst accepted initializations. Instead we find that network distribution of hydromorphology, and especially channel gradient, and the statistical distribution of sources grain sizes controls sediment provenance.

With the available data it is not possible to circle out a single most appropriate grain size initialization. Nevertheless, the original, large set of source grain sizes, supply rates, and sediment fluxes is greatly reduced to a much smaller subset by few measures of sediment flux and grain size distribution. Bulk results of the model in terms of sediment yield are similar to expert based estimates (*Kondolf et al.*, 2014) but with the added benefit of clarifying the spatial pattern of sediment provenance. We hope that such inverse approaches can be of great benefit for modeling sediment transfers in large river basins, where detailed observations of processes and process rates may not exist and may be difficult and costly to obtain.

5.7 Conclusion

We parametrized the CASCADE model for network sediment connectivity for the 3S tributaries of the Mekong. We used the CASCADE model to describe the transport of sediment from 1422 sediment sources through the network resulting in information on sediment fluxes and bed material grain size distribution throughout the basin and at the basin outlet. Characteristics of sediment sources, i.e., source supply and grain size are a-priori un-known. We set up the model in a 2-stage approach, such that in a first run fractional transport capacities are determined throughout the network, and in a second run, sediment supply from sources is set such that there is a balance between

sediment supply and transport capacity, which is based on the observation that there is no major sediment accumulation in the basin. We ran the model for many random initializations of source grain sizes, studied the resulting patterns of transport capacity and source supply in the network, and compared model results to an observation-based mixing model at the tributary outlet, reaching the following conclusions:

1. Model results can be matched to observations indicating that the 3S tributaries supply around 10 to 25 Mtons/year (median 18 Mtons/year) of fine sand (around 0.2 mm) to the Mekong river.

2. Based on the observed patterns of transport capacity, it seems likely that the most relevant source areas of that sand are located in the Vietnamese and Laotian highlands, where the headwaters of the 3S are located.

3. Sediment provenance is heterogeneous between the 3 rivers, and sediment yield is highest from the Se San river and lowest from the Se Kong River. Total sediment load is highest from the Sre Pok river, which also has the largest drainage area. This information is inferred from the spatial distribution of transport capacity. This observation indicates that the lithology in the upper Se San and Sre Pok is more erodible than in the Se Kong Rivers which mostly matches map-derived lithologic information.

4. Last, our approach to extract sediment source supply and sediment grain size distribution from the spatial distribution of transport capacity can be applied to many settings and with different degrees of data-availability. Even without data to formulate an inverse problem, relative patterns of sediment provenance can be extracted. The inverse problem can be narrowed down the more data are available throughout the network. This approach has potential applications both for modeling human disturbance, but also to study natural patterns in sediment provenance and to understand their link to drivers such as basin lithology, climate, or tectonics.

Appendix

Figures A2-A5 show reaches with comparatively low transport capacities in the Se Kong, Se San, and Sre Pok rivers. These reaches are of interest in the proposed inverse modelling approach. The sediment supply from each source is set such that it equals the lowest transport capacity for sediment from that source in the downstream network. This implies, that there is no sediment accumulation in the river network. Reaches with low transport capacity are therefore and indicator for low sediment supply from upstream, hence that a low transport capacity is sufficient to route all incoming sediment downstream. This assumption could be falsified by the presence of accumulated sediment in reaches with low transport capacity. In this case, a low transport capacity could be the result of high upstream source supply. Figures A6-A10 show the confluence of the Se Kong river with the Sre Pok river (shortly downstream the Se-San Sre-Pok confluence). Inverse model results indicate that the majority of the sand load in the 3S originates from the upper catchment of the Se San and Sre Pok rivers. Analyzing satellite images at the confluence during low flow conditions indicate indeed a higher sediment load from the Sre Pok that manifests as clearly visible transport forms in the Sre Pok river after its confluence with the Se San. All images were derived from Google Earth, if possible selecting images during low flow, pre-monsoon conditions.

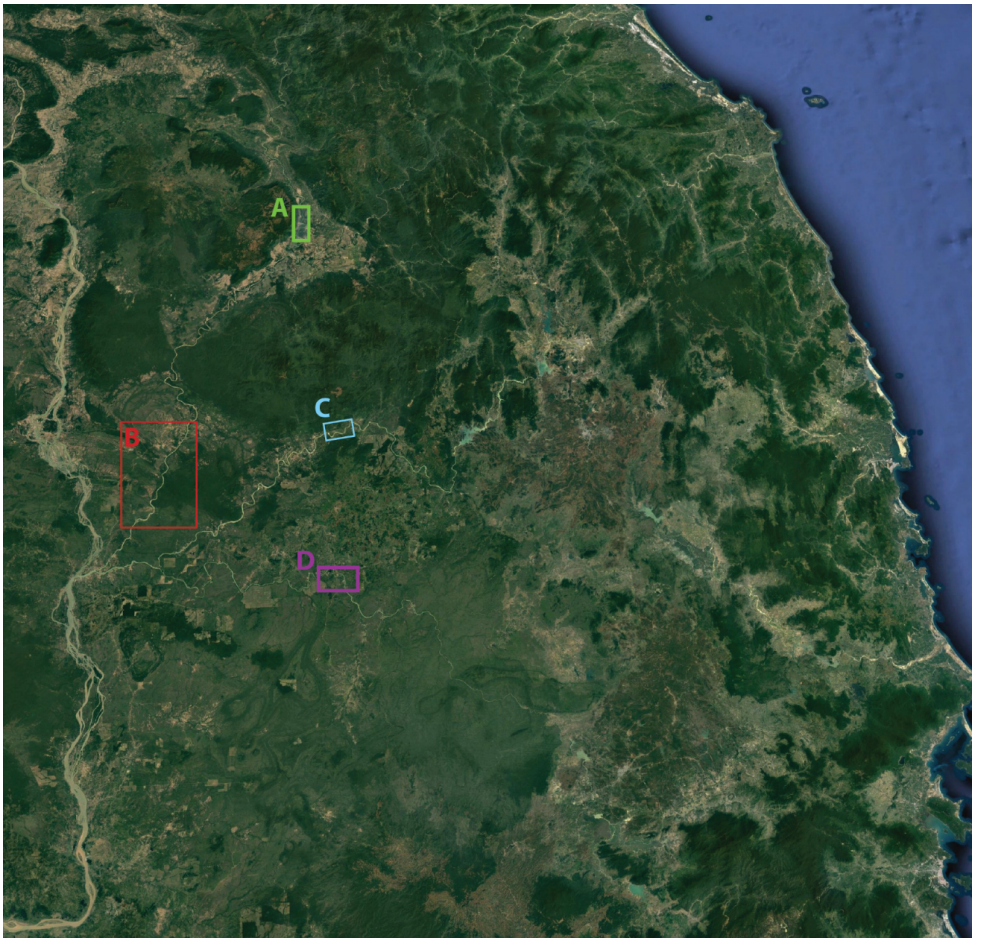

Figure A1: *Location of reaches with decreased transport capacity in the 3S. Letters refer to Figure 12 in the main chapter. Reaches A and B are located in the Se Kong River, reach C is located in the Se San River, and reach D is located in the Sre Pok River.*

Figure A2: *Upper Se Kong reach with decreased transport capacity. Several, vegetated bars are visible. There are no major sediment accumulations visible on the banks. Channel planform is predominantly straight.*

Figure A3: *Middle Se Kong reach with decreased transport capacity. Transport capacities in this reach are lowest amongst all reaches in the 3S system. Visible fault systems in the upper part of the figure indicate the bed-rock control on this reach. Planform is straight, with no in-channel sediment deposits visible.*

Figure A4: *Middle Se San reach with decreased transport capacity. Planform is predominantly straight, but sediment deposits are visible in the channel and at several point bars.*

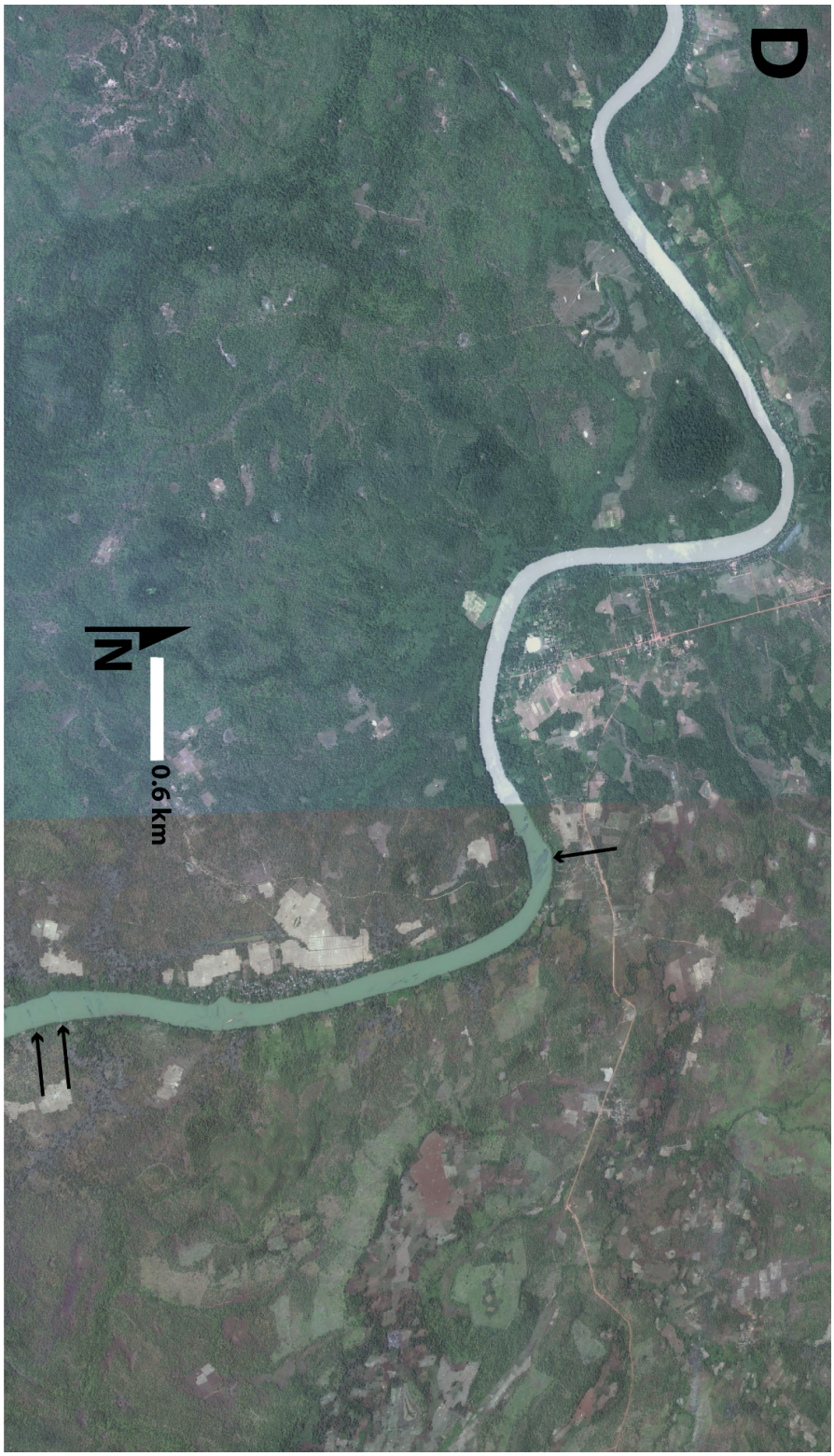

Figure A5: *Middle Sre Pok reach with decreased transport capacity. Planform is straight. No sediment deposits but multiple bed-rock steps (arrows) are visible.*

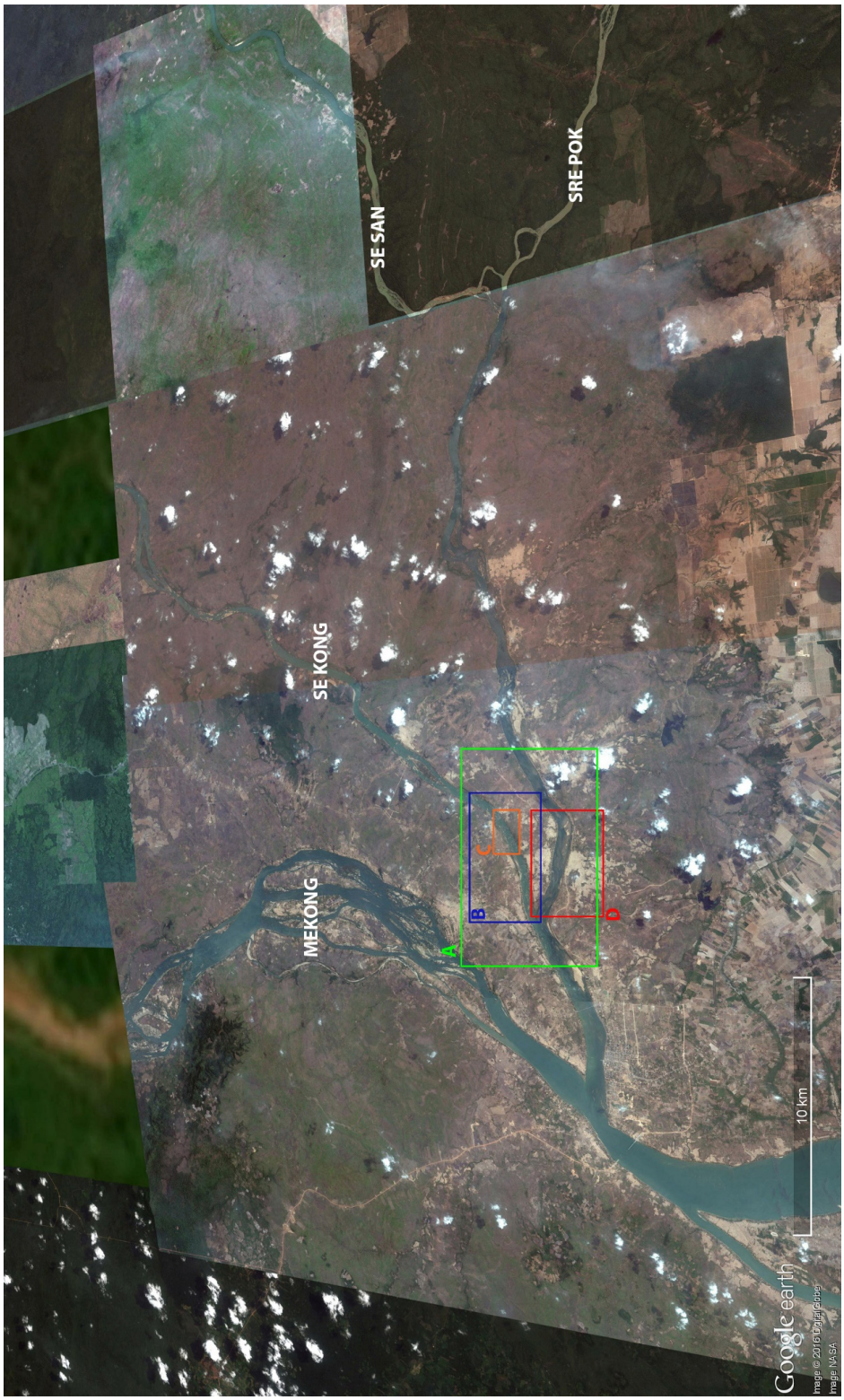

Figure A6: *Overview over satellite images at the Se Kong - Sre Pok/Se San confluence. A: Overview over the confluence. B: Se Kong at the confluence, C: Enlarged bedrock features in the terminal reaches of the Se Kong. D: Sre Pok at the confluence. All selected images were taken under low flow conditions in April-March 2013.*

Figure A7: *Se Kong-Sre Pok confluence during low flow conditions (20th March 2013). Different bed material of the two rivers is clearly visible. Bed rock steps and small bed-rock bars are abundant in the Se Kong River (Figure S8 and S9). Bed material in the Sre Pok is dominated by sedimentary bed-forms with a braiding pattern of the low for channel (Figure S10). These channel patterns continue downstream of the confluence.*

Figure A8: *In-channel bed-rock features in the Se Kong River (20th April 2013). Some in-channel sediment deposits are limited to the northern bank at the center of this image.*

Figure A9: *In-channel bed-rock features in the Se Kong River, enlarged (20th April 2013). This enlarged view clarifies that visible in channel features (see Figure S10) are rocky outcrops, i.e., non-sedimentary features.*

Figure A10: *Sedimentary bed-forms in the Sre Pok river (20th March 2013). Out-crops and bed-rock features are limited to few locations close to the confluence, and on the very right hand of that image.*

CHAPTER 6

Is big beautiful? Balancing power production, cost, and sediment connectivity in network hydro-power portfolios

SEDIMENT transport and related fluvial morpho-dynamics are drivers behind many eco-system services that support human livelihoods in the river corridor. Sediment trapping in dams raises concerns regarding the impact of rapidly advancing dam constructions in undeveloped river basins in emerging economies. While sediment transport connects entire river networks, dam planning is mostly performed on the scale of single projects. This local planning omits potential cumulative, network-scale impacts of dam cascades as well as the potential to maximize hydro-power production and reduce sediment trapping through concerted planning of dam portfolios.

In this chapter, we present how coupling an economic analysis of dam portfolios with an analysis of network sediment trapping can identify trade-offs and synergies between ecologic impacts and economic benefits of hydro-power dams. We perform that analysis for the 3S basin, where 42 major dam sites exist. These sites would allow developing many different portfolios of hydro-power dams. Each portfolio consists of a specific combination and hence spatial configuration of dams. In this chapter, we

presents the analysis of 17,000 dam portfolios in the 3S. An empirical life-cycle model is calibrated to unit costs of hydro-electricity for each portfolio. Sediment trapping for each portfolio is modelled by expanding CASCADE with a module for reservoir hydraulics and sediment trapping. Each portfolio is analysed in terms of economic indicators (total costs, unit production costs, and total production) and environmental impact in terms of sediment trapping and sediment deficit in downstream channels. Only a small number of dam portfolios is Pareto-optimal, i.e., minimizes sediment trapping while maximizing economic benefits. Different dam portfolios can attain similar level of hydro-power production at very different levels of cost and sediment trapping. For the river network under study, dam configurations exist that exploit up to 80 % of the hydro-power potential in the 3S while trapping only around 20 % of pre-dam sediment load. These configurations focus development on dam sites in the upper catchments of Se San and Se Kong Rivers. In comparison to added hydro-electric potential, developing large downstream dams invariably results an over-proportional sediment trapping. In terms of economics, we find that there is only weak economy of scale for very large hydro-electric dams, i.e., unit production costs do not decrease strongly for very large dams. Hence, for the 3S, dam portfolios that focus on medium size upstream dams result in low environmental impacts and are also economically advantageous for reducing unit production costs. We also show, how the current development strategy that is based on national economic interests only, results in over-proportional impacts on the river network compared to optimal dam portfolios.

This chapter is developed based on: Schmitt, R.J.P., Bizzi, S., Castelletti, A., Kondolf, G.M., (IN PREPARATION). Strategic hydro-power planning trades-off network sediment connectivity and hydro-power generation in the transboundary Se Kong, Sre Pok River Basin. Water Resources Research.

6.1 Introduction

Construction of reservoirs is globally progressing at high pace (*Lehner et al.*, 2011; *Zarfl et al.*, 2014). This boom, which is driven by an increasing demand for reliable and carbon-free energy, is emphasized in developing and emerging countries (*Zarfl et al.*, 2014). Especially in Asia, South America, and Africa where there is still a major untapped hydro-power potential (*Agency*, 2012a). The construction of reservoirs massively alters connectivity in river systems, hence rates and spatial patterns with which organisms, water, and sediment travel through river systems (*Ligon et al.*, 1995). Where multiple dams are planned on the network-scale, negative cumulative effects can occur that by far surpass the effect of a single reservoir (*World Commission on Dams*, 2000; *Kummu et al.*, 2010; *Ziv et al.*, 2012; *Kondolf et al.*,

2014). Additionally, it remains a disputed issue if many small projects or few mega-dams can balance better between economic interests and environmental impacts (*Ansar et al.*, 2014).

Concerted assessments of cumulative dam impacts and benefits on network or basin scales have been emphatically called for (see, e.g., (*World Commission on Dams*, 2000, pp. 61, 168)) in order to identify optimal tradeoffs between a societal interests in cheap and realibale energy, and minimal environmental impacts. Yet, such assessments were so far performed only for few case studies (*Jager et al.*, 2015). Astonishingly, this holds not only with regard to environmental impacts, but also for economic benefits. Few studies quantify risks and total and marginal benefits of dam projects (*Ansar et al.*, 2014), but none adopts a basin scale perspective on dam economics. Instead, dam sizing, siting (*Lall and Miller*, 1988), economic analysis (*Bank*, 2004b,a), and estimation of negative externalities (*Orr et al.*, 2012) focus mainly on individual reservoirs (*Jager and Smith*, 2008).

The impact of reservoir cascades on network sediment transport processes is a prime example for cumulative impacts of reservoirs (*Kondolf et al.*, 2014). Sediment ladden river flows that enter reservoir impoundments experience a change in hydro-dynamic conditions, which lead to the settling of sediment in the reservoir, and the downstream release of water with a much lower sediment concentration. This sediment trapping can significantly impact the expected economic benefits from reservoir developments (*Schleiss et al.*, 2010), e.g., through reduced storage volume, or damages to the hydroelectric equipment (*Palmieri et al.*, 2001, 2003; *Annandale*, 2013; *Wisser et al.*, 2013). Reservoir sediment trapping reduces total magnitude and changes the grain size composition of network sediment fluxes. Changed composition and magnitude of sediment fluxes, and the release of sediment starved water from reservoirs impacts network nutrient transfers, the integrity of river deltas (*Syvitski*, 2009), and channel morphodynamics (*Kondolf*, 1994; *Kondolf et al.*, 2014). Morphodynamic processes control the physical template of rivers, and dam induced changes in river morphodynamics impacts river ecosystems, fluvial infrastructures (*Kondolf*, 1997; *Bizzi et al.*, 2015a), hydrologic processes (*Archer*, 1989; *Sholtes and Doyle*, 2011; *Wyżga et al.*, 2015), and human livelihoods, alike.

Because of this intrinsic links to river eco-systems and eco-system services, we propose that sediment transfers can be a good indicator for many environmental impacts of dams. Assessing sediment trapping in reservoirs and potential downstream impacts on the network-scales is complicated by several factors. Sediment trapping in reservoirs depends on the characteristics of single reservoirs (i.e., impoundment volume and shape, technical measures for sediment management, flux and composition of incoming sed-

iment *Morris and Fan* (1998)), their relative location in a reservoir cascade (*Minear and Kondolf*, 2009), and the absolute location in the river network (*Andrews*, 1991). This is because sediment transfers are a spatially heterogeneous property of river networks (see also chapter 5).

A dam built within an existing cascade of dams might impact network sediment transfers less in absolute and marginal numbers than a dam construction in a pristine river. Hence, otherwise identical dams might result in different downstream effects, based on their location, the spatio-temporal pattern of sediment transfers, and the legacy of previous dam constructions in the river. To minimize reservoir sedimentation and dowsntream impacts, it is therefore crucial to consider a) the technical layout of single dams, b) the location of dams in a dam cascade, and c) the spatial heterogeneity in river networks.

Quantitative studies regarding the cumulative impact of reservoir cascades on network sediment transfers are rare. *Minear and Kondolf* (2009); *Kondolf et al.* (2014) used regional estimates of sediment yields in California and the Mekong River Basin (MRB) to study the cumulative trapping efficiency of existing and proposed dams. *Wild and Loucks* (2014) used sediment yield estimates proposed by *Kondolf et al.* (2014) to study future losses in reservoir storage and the possibility to increase network sediment passage by concerted reservoir management. These approaches focused mainly on the observed past, and concretely planned future. This means on the planned trajectory of hydro-power developments under the legacy of already implemented dams.

Because of the network complexity in fluvial processes, slightly different dam portfolios can result for similar economic benefits in very variable levels of negative environmental externalities (*Jager et al.*, 2015). Yet, even a small set of dam sites can results in a large number of dam portfolios. Evaluating the environmental and economic performance of these portfolios requires numerically effective modelling tools that represent dominant complexity in processes on dominant, i.e., network, scales. Selecting optimal portfolio from sets of dams for removal (*Paulsen and Wernstedt*, 1995; *Kuby et al.*, 2005; *Zheng et al.*, 2009) and construction sites (*Ziv et al.*, 2012) has been proposed. None of these approaches included a full economic appraisal of dam sites. Instead, indicators such as total electricity production are used, which undoubtely indicate some economic benefits, but cannot shed light on economics behind dam site selection which might be driven by construction and unit production costs.

In terms of dam environmental impacts, all mentioned approaches focused on fish-migration, only. In terms of sediment transport there exist only few models that are numerically sufficiently efficient and parsimonious

to work also for poorly monitored, large river basins, where dam developments are nowadays focused. Based on advances in network-scale sediment transport and connectivity modeling (*Czuba and Foufoula-Georgiou*, 2014), we recently introduced the CASCADE (CAtchment Sediment Connectivity And DElivery) framework. CASCADE models the transport of multiple sediment fractions on the scale of large river networks (*Schmitt et al.*, 2016). CASCADE derives grain size size specific transport rates using a statistical handling of time, and conceptualizing total sediment transport as superposition of many individual cascading processes between individual sources and sinks. As a result, CASCADE is computationally effective and covers domains of network sediment transfers that are dominant for the proposed network-scale planning task. CASCADE considers that different grain sizes are supplied and transported at different rates to different parts of the network. Accordingly, CASCADE can represent that a dam, or a cascade of dams, results in a specific change in magnitude and composition of sediment transport and downstream fluvial processes in function of its location in the river network. CASCADE is computationally sufficiently efficient to model a large number of dam portfolios, and to derive process-related, spatially-distributed indicators for many dam portfolios. The objective of this chapter is to introduce how network-scale portfolio analysis can be applied for selecting dam portfolios that maintain sediment connectivity while maximizing economic objectives. This analysis is developed for the 3S basin (see chapter 5). In comparison to previous versions of CASCADE, we add a spatially explicit component for the routing of multiple sediment grain sizes in reservoirs. This component allows to study the total reduction in sediment transport downstream of a reservoirs and beyond also how the trapped sediment is redistributed within the reservoir.

We approach the network dam siting on various levels. First, we analyze the recent historic trajectory of dam developments in the basin under study. This analysis points out how spatial patterns and magnitude of sediment connectivity in the basin under study changed in response to dam developments. Dam development in the basin was not the result of concerted strategic planning, but rather of different development trajectories in the multiple abutting countries. Second, we aim to show that a lack of strategic planning caries the risk to result in an over-proportional environmental impacts compared to economic benefits. To quantify this hypothesis, we assume that all dam sites that are developed or under development present the full set of feasible dam sites in the basin. Based on this full set of dam sites, we analyse many potential dam portfolios in the river network. This exhaustive analysis allows first to identify dam portfolios that maximize connectivity for a given level of hydro-power production. Second, the analysis clarifies the trade-

offs between connectivity and hydro-power for various levels of development. Third we compare the historical trajectory of dam developments with identified optimal dam portfolios. The objective of this analysis is showing how dam planning that focusses on single sites instead of a network strategic planning results in dam portfolios that do not create maximum economic benefits, but an inflict over proportional damage to fluvial ecosystems and eco-system services. Fourth, we also show how different environmental objectives can result in very different dam portfolios. We end with an analysis of dam portfolios based on economic indicators (construction costs vs. hydro-power production and unit production costs), only, and compare results of ecomically optimal scenarios with those that minimize impacts on the river system.

6.2 Reservoir developments in the LRMB and the 3S basin

This argument is developed for the major tributary systems of the Mekong River Basin (MRB). The MRB covers an area of 760000 km^2 shared between China, Laos, Cambodia, Thailand, Myanmar, and Vietnam (Figure 6.1, cutout). The MRB is home to approximately 65 million people and numerous endemic aquatic species (*MRC*, 2010). Driven by a strong increase in energy demand in the abutting countries, hydro-power development saw a recent rise in the last decades with first major projects being developed in the upper, Chinese part (referred to as Lancang) of the basin and a now ongoing development of hydro-power in the Lower Mekong River Basin (LMRB) (*Kondolf et al.*, 2014). Serious concerns have been raised that the increasing development of dams and reservoirs could have a potentially devastating effects on eco-systems and human livelihoods. Common concerns regarding MRB dams are the disturbance of fish migration routes, endangering biodiversity and a critical food supply for up to 80 % of the MRB's population (*Orr et al.*, 2012; *Ziv et al.*, 2012), and the disturbance of sediment flux from the Lancang and lateral tributaries in the LRMB (*Kondolf et al.*, 2014). The reduction in sediment load is projected to create an additional pressure on fluvial biomes, and to endanger the river morphologic integrity of the LRMB, especially in the Mekong Delta (*Rubin et al.*, 2015). This directly endangers the livelihoods of an estimated 25 Million people living in a 15 km corridor around the Mekong main stem (*MRC*, 2010). Especially the Mekong Delta is already suffering from strong coastal erosion and subsidence related to decreasing sediment fluxes (*Anthony et al.*, 2015) and sediment mining (*Bravard et al.*, 2013). The progressing construction of the Lancang hydro-power cascade alone is expected to trap around 50 % (*Kummu et al.*, 2010) of the Mekong's annual sediment load. There is also a strong interest to develop hydro-power in the lower LRMB, to match the cur-

rent and fuel future economic development, both through access to reliable cheap energy, and revenues from trans-boundary energy sales (*Grumbine and Xu*, 2011). In the LRMB, hydro-power potential is concentrated on the main stem of the Mekong, and few major tributaries. Amongst those, the three tributaries Se Kong, Se San, and Sre Pok (3S), that enter the Mekong upstream the city of Stung Tren, approximately 500 km from the Mekong river delta, are a hotspot of ongoing hydro-power development (Figure 6.1). The development of hydro-power in that basin is likely to have a major impact on the sediment dynamics in the entire LRMB. This is because the 3S remains the most important single sediment source for the LRMB and the Mekong Delta after the completion of some main stem LRMB dams and the Lancang hydro-power cascade (*Wild and Loucks*, 2014). Information on past and future dam development is available from the Mekong River Commission (MRC). The MRC database contains relevant technical information, such as location, storage volume, installed capacity, production and the date of commercial operation (COD) for major reservoir projects (see Table 6.1-6.4). Currently, the dam portfolio in the 3S includes 14 existing reservoirs in the 3S basin (Figure 1). Additional seven dams are under construction and 21 are planned. Hence, the final dam portfolio for the 3S includes 42 dams (Cambodia: 9, Laos: 19, Vietnam: 14) with an installed capacity of 6805 MW and an estimated annual production of 30463 GWh (Table 6.1-6.4). The MRC database also contains construction costs for each dam site. Costs for built projects are reported in as cost at the time of construction. For planned dams, costs are reported as today's cost. Tabulated costs include costs for grid connection and mitigation (e.g., resettlements), according to the MRC. As per now, development focused mainly on the Vietnamese Se San and Sre Pok rivers. A major current development is the Lower Se San / Sre Pok 2 Dam (commonly referred to as Lower Se San 2 Dam or LSS2). Planned hydro-power developments focus on the so far undeveloped Laotian Se Kong River and on the Cambodian parts of the 3S basin.

6.3 Methods

6.3.1 Numerical modelling of network sediment transport

Assessing dam impacts on network sediment transfers in the 3S is based on the application of the CASCADE modelling framework (*Schmitt et al.*, 2016) as presented in chapter 3 and 5.

CASCADE represents the river network as a directed graph, in which each river reach is represented as an edge e. Multiple sediment sources ς are located on that river graph. Each source ς is defined by its location, its grain size d_ς and a supply rate of sediment. Cascade tracks the sediment transport

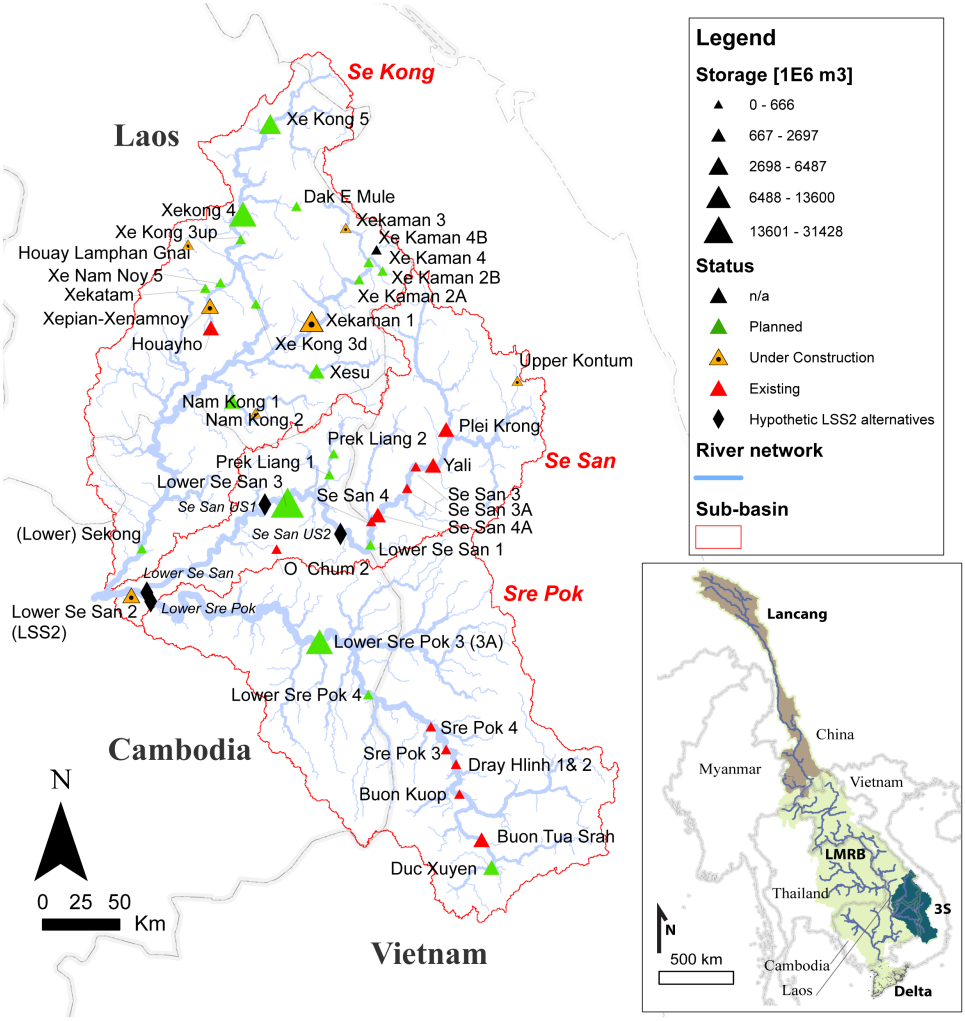

Figure 6.1: *Planned, existing and under construction hydro-power dams in the Se Kong, Se San, Sre Pok (3S) basin. The cutout shows the 3S basin in the context of the larger Mekong River Basin (MRB).*

Table 6.1: *3S Dam portfolio, derived from Mekong River Commission resources. [1]: L: Laos, V: Vietnam, C: Cambodia. [2]: Commercial operation date.*

Code [1]	Name	River	Latitude	Longitude	COD[2]
L006	Houayho	Houayho, Xekong	14,8931	106,6661	1999
L012	Xekaman 3	Houayho, Xekong	15,4361	107,3367	2015
L017	Xekaman 1	Xe Kaman	14,9633	107,1517	2017
L027	Xepian-Xenamnoy	Xepian/Xenamnoy	15,0258	106,6056	2019
L028	Xekatam	Xenamnoy	15,1354	106,5891	2020
L029	Xekong 4	Xekong	15,5139	106,7878	2022
L030	Nam Kong 1	Nam kong	14,5529	106,7299	2019
L031	Xe Kong 3up	Xekong	15,3841	106,7766	2022
L032	Xe Kong 3d	Xekong	15,1221	106,8211	2022
L033	Xe Kong 5	Xekong	15,975	106,9306	2019
L061	Xe Kaman 2A	Xe Kaman	15,2169	107,4389	2018
L062	Xe Kaman 2B	Xe Kaman	15,2753	107,45	2018
L063	Xe Kaman 4	Xe Kaman	15,2244	107,5261	2020
L064	Xe Kaman 4B	Xe Kaman	15,3472	107,5358	0
L065	Dak E Mule	Xe Kong	15,555	107,0711	2022
L097	Xe Nam Noy 5	Xe Kong	15,1639	106,6686	2013
L098	Houay Lamphan Gnai	Xe Kong	15,36	106,4983	2017
L099	Nam Kong 2	Xe Kong	14,4927	106,8532	2018
L100	Xesu	Xe Kong	14,7083	107,1764	2022
C001	O Chum 2	O Chum	13,7917	106,9667	1992
C002	Lower Se San 2	Se San	13,5533	106,2	2017
C009	Lower Se San 3	Se San	14,0316	107,0236	0
C010	Prek Liang 1	Prek Liang	14,2166	107,2507	0
C011	Prek Liang 2	Prek Liang	14,2833	107,2667	0
C012	Lower Sre Pok 3 (3A)	Sre Pok	13,3883	107,05	0
C013	Lower Sre Pok 4	Sre Pok	13,0383	107,45	0
C015	Sekong	Sekong	13,7939	106,2544	0
C016	Lower Se San 1	Se San	13,8139	107,4614	0
V001	Upper Kontum	Se San	14,7111	108,2375	2014
V002	Plei Krong	Se San	14,4083	107,8611	2009
V003	Yali	Se San	14,2228	107,7931	2002
V004	Se San 3	Se San	14,2167	107,7	2006
V005	Se San 3A	Se San	14,1061	107,655	2007
V006	Se San 4	Se San	13,9667	107,5	2010
V007	Se San 4A	Se San	13,9333	107,4664	2011
V008	Duc Xuyen	Sre Pok	12,1428	108,1006	0
V009	Buon Tua Srah	Sre Pok	12,2853	108,0478	2009
V010	Buon Kuop	Sre Pok	12,5244	107,9314	2009
V011	Dray Hlinh 2	Sre Pok	12,6769	107,9133	2007
V012	Sre Pok 3	Sre Pok	12,7542	107,8614	2010
V013	Sre Pok 4	Sre Pok	12,8731	107,7806	2010
V014	Dray Hlinh 1	Sre Pok	12,6769	107,9133	1990

Table 6.2: *3S Dam portfolio (continued).* [3]*: E: Existing, C: Under construction, P: Planned.* [4]*: P: (hydro-power), A: Agriculture, W: Municipal water supply, C: Flood control, N: Navigation, R: Recreation, F: Fisheries.* [5]*: Full supply level .*

Code	Name	Progress[3]	Purpose[4]	Drainage Area [km^2]	Mean Q [m^3/s]	FSL[5] [m]
L006	Houayho	E	P	192	9,5	880
L012	Xekaman 3	C	P	712	29,6	960
L017	Xekaman 1	C	P	3580	175	230
L027	Xepian-Xenamnoy	C	P	820	42,7	786,5
L028	Xekatam	P	P	38	12,3	911
L029	Xekong 4	P	PC	5400	205	290
L030	Nam Kong 1	P	P	1250	42	320
L031	Xe Kong 3up	P	PAR	5882	240,3	160
L032	Xe Kong 3d	P	PAR	9700	316,4	117
L033	Xe Kong 5	P	P	2518	137	487
L061	Xe Kaman 2A	P	P	1970	77,5	280
L062	Xe Kaman 2B	P	P	1740	68,4	370
L063	Xe Kaman 4	P	P	265	10,2	860
L064	Xe Kaman 4B		P	192	7,4	865
L065	Dak E Mule	P	P	127	16,1	780
L097	Xe Nam Noy 5	P	P	60	3,6	800
L098	Houay Lamphan Gnai	C	P	140	6,5	840
L099	Nam Kong 2	C	P	860	45	460
L100	Xesu	P	P	1273	77,2	180
C001	O Chum 2	E	P	45	2,2	254
C002	Lower Se San 2	C	PCF	49200	1306	75
C009	Lower Se San 3	P	PCF	15435	330	140
C010	Prek Liang 1	P	P	917	40,2	275
C011	Prek Liang 2	P	P	580	25,4	495
C012	Lower Sre Pok 3 (3A)	P	PCF	25311	713	120
C013	Lower Sre Pok 4	P	PC	13727	378	148
C015	Sekong	P	P	28008	1323	63
C016	Lower Se San 1	P	P	11114	385	141
V001	Upper Kontum	C	P	350	16,7	1170
V002	Plei Krong	E	PAF	3216	128	570
V003	Yali	E	PAFN	7455	262	515
V004	Se San 3	E	P	7788	274	304,5
V005	Se San 3A	E	P	8084	283	239
V006	Se San 4	E	PAF	9326	328,9	215
V007	Se San 4A	E	C	9368	330	155,2
V008	Duc Xuyen	P	PAF	1100	35,7	560
V009	Buon Tua Srah	E	PAF	2930	102	487,5
V010	Buon Kuop	E	PAF	7980	217	412
V011	Dray Hlinh 2	E	P	8880	241	302
V012	Sre Pok 3	E	PF	9410	250,6	272
V013	Sre Pok 4	E	P	9568	273	207
V014	Dray Hlinh 1	E	P	8880	241	302

Table 6.3: *3S Dam portfolio (continued).* [6]*: Low supply level.*

Code	Name	LSL[6] [m]	Live storage [1E6 m^3]	Gross storage [1E6 m^3]	Innundated area (at FSL) [km^2]
L006	Houayho	860	527	674,1	38,3
L012	Xekaman 3	925	108,5	141,5	5,2
L017	Xekaman 1	218	1683	4804	149,8
L027	Xepian-Xenamnoy	745	980	1092	53
L028	Xekatam	890,5	121	126	7,8
L029	Xekong 4	270	3100	10500	170,3
L030	Nam Kong 1	287	505	682,7	21,8
L031	Xe Kong 3up	155	95,1	0	20,8
L032	Xe Kong 3d	111	168,4	0	0
L033	Xe Kong 5	485	1700	3300	32,8
L061	Xe Kaman 2A	275	20,8	20,8	1,5
L062	Xe Kaman 2B	340	333	333	8,6
L063	Xe Kaman 4	840	332,3	0	14,4
L064	Xe Kaman 4B	850	0	0	0
L065	Dak E Mule	756	154	243,1	9,6
L097	Xe Nam Noy 5	780	8,8	9,8	0,6
L098	Houay Lamphan Gnai	800	122	480,5	6,8
L099	Nam Kong 2	437	30,6	166,2	4,2
L100	Xesu	160	26,1	2671	7,2
C001	O Chum 2	251,5	0,1	0	0
C002	Lower Se San 2	74	333,2	1792,5	334,4
C009	Lower Se San 3	118	14528	16900	726,9
C010	Prek Liang 1	260	19,3	0	1,73
C011	Prek Liang 2	480	19,5	0	2,09
C012	Lower Sre Pok 3 (3A)	112	3931	5863	721
C013	Lower Sre Pok 4	146	44	204	33
C015	Sekong	61,5	133,55	0	93,73
C016	Lower Se San 1	140	15,4	100,7	16,3
V001	Upper Kontum	1146	122,7	173,7	8,6
V002	Plei Krong	537	948	1048,7	53,3
V003	Yali	490	779	1037,1	64,5
V004	Se San 3	303,2	3,8	92	3,4
V005	Se San 3A	238,5	4	80,6	8,8
V006	Se San 4	210	264,2	893,3	58,4
V007	Se San 4A	150	7,5	13,1	1,8
V008	Duc Xuyen	551	413,4	1749,78	77,3
V009	Buon Tua Srah	467,5	522,6	787	37,1
V010	Buon Kuop	409	25,6	73,8	5,6
V011	Dray Hlinh 2	299	1,5	2,9	0
V012	Sre Pok 3	267	62,9	219	17,7
V013	Sre Pok 4	204	8,4	29,3	3,8
V014	Dray Hlinh 1	299	1,5	2,9	0

Table 6.4: *3S Dam portfolio (continued).*

Code	Name	Installed capacity [MW]	Production [GWh/yr]	Type
L006	Houayho	150	487	Reservoir
L012	Xekaman 3	250	982,8	Reservoir
L017	Xekaman 1	290	1096	Reservoir
L027	Xepian-Xenamnoy	410	1748	Reservoir
L028	Xekatam	68	380	Reservoir
L029	Xekong 4	380	1901	Reservoir
L030	Nam Kong 1	150	469	
L031	Xe Kong 3up	105	598,7	
L032	Xe Kong 3d	100	375,7	
L033	Xe Kong 5	330	1201	Reservoir
L061	Xe Kaman 2A	64	241,6	
L062	Xe Kaman 2B	100	380,5	
L063	Xe Kaman 4	54	375	
L064	Xe Kaman 4B	0	301	
L065	Dak E Mule	130	506	
L097	Xe Nam Noy 5	20	124	
L098	Houay Lamphan Gnai	84,8	264,4	
L099	Nam Kong 2	66	309,5	
L100	Xesu	30	286,2	
C001	O Chum 2	1	3	
C002	Lower Se San 2	400	1953,9	Run-of-River
C009	Lower Se San 3	260	1310,2	Run-of-River
C010	Prek Liang 1	72	324,3	Reservoir
C011	Prek Liang 2	56	259,6	Reservoir
C012	Lower Sre Pok 3 (3A)	300	1201,4	
C013	Lower Sre Pok 4	48	220,7	
C015	Sekong	190	557,5	Run-of-River
C016	Lower Se San 1	96	485	
V001	Upper Kontum	250	1056,4	Reservoir
V002	Plei Krong	100	417,2	Reservoir
V003	Yali	720	3658,6	Reservoir
V004	Se San 3	260	1224,6	Reservoir
V005	Se San 3A	96	479,3	Run-of-River
V006	Se San 4	360	1420,1	Reservoir
V007	Se San 4A	63	296,9	Run-of-River
V008	Duc Xuyen	58	181,3	Reservoir
V009	Buon Tua Srah	86	358,6	Reservoir
V010	Buon Kuop	280	1458,6	Reservoir
V011	Dray Hlinh 2	16	85	Run-of-River
V012	Sre Pok 3	220	1060,2	Reservoir
V013	Sre Pok 4	80	329,3	Reservoir
V014	Dray Hlinh 1	12	94	Run-of-River

from each sediment source ς to the basin outlet (denoted Ω) as an individual cascading process. This tracking is based on calculating the fractional transport rates for d_ς in all reaches between ς and Ω based on the local morphologic parameters (i.e., slope, active channel width), the statistics, i.e., magnitude and frequency of discharge, and the resulting reach hydraulics (i.e., flow depth and discharge). Fractional transport capacities are derived using these parameters in common total sediment transport formulas by *Engelund and Hansen* (1967) and distributing total transport capacities between multiple grain sizes based on an approach proposed in (*Schmitt et al.*, 2016). The sediment flux from each source through the downstream river network is described as an individual cascading process, γ_ς. This means, that the transport capacity for d_ς in an edge e, $Q_{S,e}{}^\varsigma$, is compared to the sediment input of d_ς from the upstream edge and part of the input is deposited in edge e if the input exceeds the transport capacity. This results in the fractional flux of d_ς in an edge e ($\Theta_{S,e}{}^\varsigma$). As a consequence of multiple cascades being present in each edge, the total flux in an edge $\Theta_{S,e}$ is defined as sum of fluxes for all grain size fractions present in e. The median grain size d_{50} transported in e is defined as the flux weighted average over all grain size fractions in e. After completing a model run, this information on fractional sediment flux and median grain sizes is available for all reaches in a river network. In terms of required data, hydro-morphologic information can nowadays be derived directly from global data-sets, or interpolated from high resolution satellite imagery, gauging station observations, or hydrologic model outcomes (e.g., *Schmitt et al.* (2014, 2016)). Deriving information on the sediment sources, i.e., location, grain size, and supply rates of sediment sources is instead a challenge as such information is absent for most river sources. In chapter 5, we applied an inverse Monte-Carlo approach to disaggregate available information on sediment flux and composition at the Mekong-3S confluence into spatially distributed estimates of source grain sizes and sediment supply, and hence also sediment fluxes, in the 3S basin. We identified 65 model initializations that revealed a clear spatial pattern of sand flux and grain size distribution in the 3S, with finer sand grain sizes and higher fluxes from the Sre Pok and Se San, and coarser grain sizes and lower fluxes in the Se Kong sub-basin. The results of this analysis are the basis for the herein presented analysis. In this chapter, we used the 65 source initializations for analyzing sediment fluxes under past and several alternative future hydro-power development. Dam portfolio anaylsis was instead performed using the flux-weighted mean over the all 65 initializations for clarity and computational reasons. We do not consider that sediment starved water might take up sediment downstream of dams which, on a short term, could balance sediment trapping. This is because a previous analysis of lithology and channel forms

indicate that there is only very limited sediment stored in the 3S that could be mobilized.

6.3.2 In-reservoir sediment routing

Regional analyses of reservoir sediment trapping (e.g., *Minear and Kondolf* (2009); *Kondolf et al.* (2014); *Wild and Loucks* (2014) commonly rely on empirical relationships, such as the Brown or Brune curves (*Brown*, 1943; *Brune*, 1953) to describe the trapping of sediment in reservoirs. Such approaches describe the total trapping efficiency of reservoirs as function of some reservoir characteristics. In this chapter, we created a reservoir trapping model that makes use of CASCADE, specifically its spatially explicit handling of sediment routing and the explicit routing of multiple grain sizes. Reservoirs are directly integrated in CASCADE by adding a component for in-reservoir sediment routing. This component calculates the transport capacity for each incoming grain size in all compartments of a reservoir. A compartment represents the average hydraulic conditions in an inundated river reach after the impounding. The transport capacity for each incoming grain size in each compartment k is determined using the Engelund Hansen transport formula (*Engelund and Hansen*, 1967). The volumetric transport capacity for a single grain size is defined as

$$q_{S,k}{}^{\varsigma} = \frac{\sqrt{R * g * d_{\varsigma}} * d_{\varsigma} * 0.05}{C_{F,k} * \tau_{*}{}^{\varsigma 2.5}} \tag{6.1}$$

where R is the relative density of sediment, g is the gravitational acceleration, d_{ς} is the grain size supplied by source ς, $C_{F,k}$ is the friction factor in compartment k and τ_* is the dimensionless shear stress. $C_{F,k}$ is defined as

$$C_{F,k} = \frac{2 * g * I_k * h_k}{{v_k}^2} \tag{6.2}$$

Where I_k is the energy slope and v_k is the flow velocity in compartment k. τ_* is defined as

$$\tau_{*}{}^{\varsigma} = \frac{\rho_W * g * h_k * I_k}{g * (\rho_S - \rho_W) * d_{\varsigma}}. \tag{6.3}$$

Where ρ_S and ρ_W are the densities of water and sediment (assumed to be 2600 and 1000 kg/m^3). $q_{S,k}{}^{\varsigma}$ [m^2 /s] is converted to $Q_{S,k}{}^{\varsigma}$ [kg/yr] by

$$Q_S, k^{\varsigma} = q_S, k^{\varsigma} * W_k * \rho_S * 3600 * 24 * 365. \tag{6.4}$$

Hence, in order to calculate the transport capacity for a grain size d_{ς} in a reservoir compartment k information on I_k, h_k, v_k, and W_k, that is, on energy

gradient, water level, velocity and width of that compartment is required. The derivation of these parameters, demonstrated for a reservoir with four inundated reaches, three on the main stem, and one in a tributary is shown in Figure 6.2. The geometry of a reservoir is mainly determined by its full supply level (FSL). First, all edges $1 \ldots k$ upstream of the dam and with a lower downstream elevation than the FSL are identified. The reservoirs compartments are identical with these inundated edges in terms of length and location. The energy slope in each compartment is derived according to

$$I_k = \frac{{v_k}^2}{2g} \tag{6.5}$$

The average flow velocity in k is given by

$$v_k = \frac{L_k}{/} \frac{V_k}{Q_k} \tag{6.6}$$

Where L_k is the length of k, and $\frac{V_k}{Q_k}$ defines the residence time of water in k (V_k: compartment volume, Q_k: water inflow). Q_k can change downstream, if tributaries enter the reservoir (see chapter 3, for the determination of the discharge in each compartment). L_k is the inundated length of k (Figure 6.2 A). V_k is determined assuming that compartments are rectangular with a uniform depth, and width such that

$$V_k = h_k * W_k * L_k. \tag{6.7}$$

Hence, each compartment is assigned the mean impoundment depth and the mean impoundment width of the original edge (Figure 6.2 B). Based on these parameters, the transport capacity in each reservoir compartment is calculated for each incoming grain size. All calculations are based on the mean annual inflow, and the tabulated FSL, hence assuming that reservoirs are kept full. This assumption is reasonable given that most reservoirs in the 3S are operated to maximize hydro-power production (see Table 6.2). Then, the original transport capacity in the river network is replaced by the newly calculated transport capacities that was calculated for each grain size in all inundated nodes . In most cases, this transport capacity for a sediment cascade γ_ς will be drastically lower than in the original river reach. Sediment routing in CASCADE is performed as follows:

$$\Theta_{S,e}{}^{\varsigma} = \begin{cases} \Theta_{S,e-1}{}^{\varsigma}, \text{ if } \Theta^{\varsigma}_{S,e-1} < Q_{S,e}{}^{\varsigma} \text{ (condition 1)} \\ Q_{S,e}{}^{\varsigma}, \text{ else (condition 2).} \end{cases} \tag{6.8}$$

Hence, if the local transport capacity for d_ς, $Q_{S,e}{}^{\varsigma}$, is lower than the input from the next upstream reach (case 1), only an amount of sediment equal to

local transport capacity can be transported downstream. This also implies, that the difference between local transport capacity and sediment input is locally deposited, hence that

$$\Delta_{S,e}{}^{\varsigma} = \Theta_{S,e-1} - \Theta_{S,e} \tag{6.9}$$

Where Δ is the deposition rate [kg/yr]. Over a given time period, the total deposition in any reservoir compartment

$$\Delta_{S,e} = \sum_{i=1}^{n} \Delta_{S,e}{}^{i} * \delta t \tag{6.10}$$

i.e., the deposition over all incoming sediment cascades multiplied by the time step δt. After each time step, the elevation of all reservoir compartments is updated (based on a sediment density of 2600 kg/m^3 and width and length of the compartment), and hydraulic parameters and transport capacities are recalculated (Figure 6.2 C). Hence transport capacities and trapping rates become a function of time. Like this, the model takes into account that siltation increases the reservoir bottom elevation, reduces the compartment volume and residence time of water, increases thereby the velocity, energy slope and transport capacity, and reduces finally the sediment trapping. Last, we assume that all reservoirs are equipped with bottom-outlets or similar devices, hence that sediment reaches the dam can be routed downstream. As there is no information on which dams in the 3S are equipped with bottom outlets, this presents a best-case scenario. It should also be noted that this assumption takes effect only if sediment can actually pass through the reservoir and reach the dams.

6.3.3 Economic and portfolio analysis

Some economic data are available for existing and planned dams from the Mekong River Commission's dam database. Yet, the only reported value is the construction costs of single dams (supposedly including grid connection and environmental mitigation). To include total costs and production costs into the portfolio analysis some additional considerations were required. For dams built in the past, we corrected costs at the time of construction to match today's costs. We assumed an inflation rate of $r_i = 5\%$. For a dam site D with construction year $T(D)$ this results in

$$c^{D}_{construction}(2016) = c^{D}_{construction}(T(D)) * (1 + r_i)^{2016-T(D)} \tag{6.11}$$

Not only the construction costs, but also the unit production costs, i.e., the costs per produced unit of energy are of interest. Production costs, c^{D}_{prod}, [$/GWh or $/KWh] of a hydro-electric project are defined as

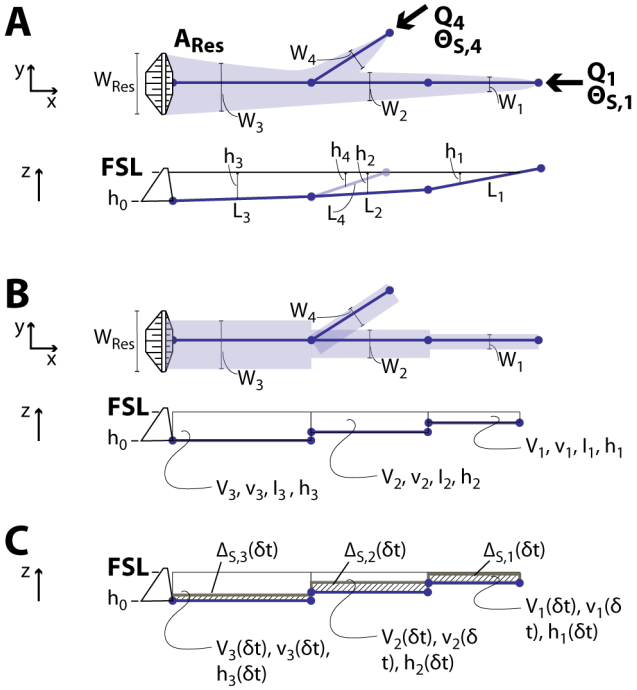

Figure 6.2: *Reservoir routing model. A: original plan-view and cross-sectional parameters for a reservoir with 4 inundated edges and two tributaries. B: Representation of reservoir dimensions as set of rectangular compartments. C: Siltation over a period δt requires updating the reservoir bottom, siltation reduces volume and changes hydraulic conditions in reservoir compartments.*

$$c^D_{prod} = \frac{c^D}{E^D}, \tag{6.12}$$

where c^D are the annual cost [$/yr] and E^D is the annual production (see Table 6.4) for dam site D [$/GWh or $/KWh]. Annual costs of the dam consist of capital costs (c^D_{cap}, [$ / yr]) and O & M (operation and maintenance) costs ($c^D_{O\&M}$, [$ / yr]) hence,

$$c^D = c^D_{cap} + c^D_{O\&M}, \tag{6.13}$$

Capital costs are defined as annuity of a dam project, calculated through multiplying the construction costs with the annuity factor a [-]

$$c^D_{cap} = c^D_{construction}(2016) * a, \tag{6.14}$$

with

$$a = \frac{r_{cap}}{1 - (1 + r_{cap})^{L^D}}, \tag{6.15}$$

(*Burneikis et al.*, 2001). r_{cap} is the interest rate [-]) and L^D is the lifespan of the project [yr]. Operation and maintenance costs are calculated as:

$$c^D_{O\&M} = c^D_{construction}(2016) * r_{O\&M} \tag{6.16}$$

where $r_{O\&M}$ is fixed factor for annual O & M. Equation 6.12 can be combined with Equations 6.14 and 6.16 to

$$c^D = c^D_{construction}(2016) * (a + r_{O\&M}), \tag{6.17}$$

Variables in the equations 6.17, namely a (and thereby r_{cap}, L^D in Equation 6.15), and $r_{O\&M}$, are unknown. Therefore, we derived these parameters by fitting the production cost model (Equation 6.12) to reported production costs that were available for eight Laotian hydro-power plants in the 3S (*Bank*, 2004b,a). To determine r_{cap}, L^D, and $r_{O\&M}$ we applied a non-linear least-square solver to minimize the sum of squared errors (SSE) between the results of the cost model and reported production values. It is reasonable to assume that the project lifetime will be between 50 and 100 years, capital costs between 5 - 10 % and O & M around 2 - 5 % of construction costs (*Agency*, 2012b).

The full portfolio P consists of all dam sites in the 3S database. Yet, the aim of this chapter is to focus not only on the full portfolio, but also on other portfolios, i.e., subsets $p \subset P$ of the full dam portfolio. As each portfolio p consists of a different subset of dam sites, this also implied that

each portfolio results in a different spatial configuration of dam sites in the river network.

p incurs the construction costs

$$c^{p}_{construction} = \sum_{m \in p} c^{m}_{construction}, \tag{6.18}$$

where $m \in p$ refers to a dam site D in portfolio p. For the annual costs of portfolio p, it is importnat that a and $r_{O\&M}$ are the same for all dams. Therefore, the annual production costs of a portfolio can also be determined as

$$c^{p}_{prod} = \frac{c^{p}_{construction} * (a + r_{O\&M})}{\sum_{m \in p} E^{m}}, \tag{6.19}$$

analogue to Equation 6.12.

6.4 Results

6.4.1 Hydro-power production and network changes in sediment connectivity

Figure 6.3 A shows modeled past and future changes in sediment flux from the 3S basin as function of increasing reservoir construction. Each marker in Figure 6.3 A stands for the construction of an additional reservoir over time (see color-code for commercial operation date, COD). CASCADE predicted a mean pre-Reservoir (i.e., pre-1990) sediment output from the 3S basin of 1.48E10 kg/yr (mean over all 65 source initializations identified in the previous chapter. The total transport is slightly lower than described in the previous chapter. This is because of a slightly different assignment of reaches to gauging stations).

The provenance, i.e. the delivery of sediment from each source to the basin outlet (in kg/yr) of sediment in this pre-1990 state is shown in Figure 6.3 B. The small panel indicates the respective statistical distribution of sediment delivery from each sub-basin over all source initializations. As discussed in chapter 5 most sediment originated from the Sre Pok basin, while the Se San and Se Kong basins delivered less sediment to the basin outlet, reflecting both the different basin size, but also their different lithologic setting. Most relevant sediment source areas were located in the upper parts of each sub-basins, notably in the Sre Pok and Se San rivers (Figure 6.2 B), while sources along the main stems of the three rivers and lowland tributaries contributed only a small fraction to the total sediment budget. Sources in the upstream Se San and Sre Pok contributed up to an order of magnitude more

to the total sediment budget than sources in the Se Kong, resulting in higher total sediment fluxes from these sub-basins.

Before 2000, only few reservoirs were commissioned in the 3S. First operating reservoirs were O Chum (Cambodia, Se San sub-basin, COD 1992) and Houayho (Laos, Se Kong sub-basin, COD 1999). Both reservoirs had a relatively small drainage area, and a limited impact on the network sediment balance. The first major reservoir, Yali, (Vietnam, Se San, COD 2002) added substantially to the hydro-power production (3658 GWh/yr), while disconnecting sediment transfers from the upper Se San sub-basin (Figure 6.3 C, map. Compare also boxplots in Figure 6.3 B and C) and trapping 15 % of the total load in comparison to the pre-1990 and reducing sediment flux to 1.26E10 kg/yr. Major developments in the 2002-2010 period focused on a cascade of reservoirs in the upper, Vietnamese Sre Pok sub-basin (Buon Tua Srah, Buon Kop, Sre Pok 3 and 4) and Se San sub-basin (Se San 4 and 4A, and 3 and 3A). The projects in the Sre Pok basin significantly reduced sediment flux. Especially Buon Tua Srah reservoir trapped sediment inputs from the Sre Pok headwaters, while the other dams potentially allowed for some sediment passage (Figure 6.3 D, map). The impact of Se San dams was likely limited, because their location downstream of Yali dam which already trapped most sediment from the Sre Pok headwaters (compare maps in Figure 6.3 C with D and E). Hence, by the current state of reservoir development sediment flux from the 3S is reduced by 52 % to 7.1E9 kg/yr. Yet, a major further reduction is immanent after the completion of Lower Se San 2 (LSS2) reservoir (Figure 6.3 A) which is downstream of the Se San – Sre Pok confluence in Cambodia (Figure 6.3 F). According to model results, LSS2 will nearly completely disconnect sediment sources in the Se San and Sre Pok rivers, allowing only for the pass trough of an insignificant amount of sediment from the upper Sre Pok (Figure 6.3 F, map and boxplots). The average post-LSS2 sediment flux is 1.4E9, hence a 90.6 % reduction in comparison to pre-1990. This compares to an increase in production capacity from 14538 to 16492 GWh/yr (13 %).

The Se Kong Basin, instead, will remain relatively undeveloped until 2025, when Xe Kong 4 (Figure 6.3 F) and 5 (Figure 6.3 G) and Xepian Reservoirs are constructed, each with a high production potential (Figure 6.3 A). The most downstream reservoir on the Se Kong river, (Lower) Se Kong reservoir allows for limited sediment passage. Nevertheless, these developments will strongly reduce sediment flux from the Se Kong (see boxplots in Figure 6.3 F). The reduction of total flux due to developments in the Se Kong is limited in comparison to major reservoirs on the Se San and Sre Pok rivers. This is because of the lower amount of sediment originating from the Se Kong basin. Hence, post-2025, nearly all sediment sources in the 3S are

disconnected from the Mekong, except for some sources in the lower and mid Se Kong, resulting in a total reduction in sediment delivery to 4E8 kg/yr or a reduction in 97.3 % in comparison to pre-1990. Notably, uncertainty in the impact of reservoirs is reduced for progressing reservoir construction (see error bars in Figure 6.3 A). Hence, the impact of various source initialization on model results is reduced. The reason is, that a longer cascade of reservoirs has a higher potential to trap sediment fractions independent of their size. In comparison, trapping efficiency of a single reservoir might vary strongly in function of the composition of incoming sediment, and hence between different grain size initializations. To conclude, sediment deliveries from the 3S to the Mekong will experience a reduction by nearly two orders of magnitude.

While many individual reservoirs had effects on sediment delivery, the impact of LSS2 reservoir, which is currently under construction, is dominating the overall impact of the 3S sediment cascade. Therefore, the future construction of a cascade of reservoirs further upstream in the Se San and Sre Pok basins has only a comparably small impact on sediment fluxes to the Mekong. Beyond the change in sediment delivery to the Mekong, reservoirs are also changing the sediment budget within the 3S river system and will potentially impacts the river morpho-dynamics and ecosystems. Changes are going to impact both total sediment flux but also the sediment composition within the 3S river systems (Figure 6.4). In total numbers, sediment flux is to be reduced by -0.35E10 (Sre Pok), -0.12E10 (Se San) and -0.11E10 (Se Kong) (average over all reaches in the respective sub-basins). Hence, the reduction in total flux is strongest in the Sre Pok sub-basin and relatively similar in the Se San and Se Kong sub-basins. In terms of relative reduction compared to pre-1990 conditions (Figure 6.4 B), the Sre Pok is most impacted (-87.5 %), but the Se Kong (-80 %) will experience a significantly stronger reduction than the Se San (-54 %). This is despite the observation that some tributaries in the Se Kong can locally mitigate the relative reduction in sediment flux (Figure 6.4 B, arrow b,c). The observation that relative reduction in the Se San is lower than in the Se Kong is because of the low number of impacted reaches in the Se San, as most main-stem reaches will be inundated, and the presence of some upstream reaches where the reduction in sediment flux is relatively weak (Figure 6.3 B, arrow a).

CASCADE predicts a reduction of grain size along the Se Kong and Sre Pok river. In the Se San, the average change in grain size is not significantly different from 0. Both Se Kong and Sre Pok see a reduction in median grain size (-0.11 and -0.06 mm). While this absolute reduction is small, it equals an average reduction of -34.0 % (Se Kong) and -21.5 % (Sre Pok). A major part of main stem rivers in the 3S will be inundated by reservoirs (see grey

marked reaches in Figure 6.4). The remaining free-flowing river sections downstream of dams are going to experience a strong reduction in sediment load and a change in delivered grain size. According to common geomorphic frameworks (e.g., *Grant et al.* (2003)) such a change downstream of dams is likely to result in erosion, manifesting as bank failures, river bed incision, and erosion of in-channel sediment features (banks, bars) However, such effects might be dampened downstream, as tributaries add additional sediment, or sediment is remobilized from channel sediment stores close to dams.

As we detailed in chapter 5, most rivers in the 3S are bedrock dominated. Nevertheless, in-channel sediment features, which are common especially in the lower Sre Pok (see chapter chap:InverseModelling) and might play an important role as habitats, are at high risk after the construction of the 3S reservoir cascades

6.4.2 Sediment trapping and storage loss in the 3S hydro-power cascade

Reservoirs in the 3S might be subject to important storage loss given the magnitude of sediment trapping (1.4E10 kg/yr, nearly 100 % of the total undisturbed sediment flux) after full construction of the 3S reservoir cascade. Nevertheless, as pointed out by Wild and Loucks (2014), this number must be set in perspective to the huge total impoundment volume of 5.63E+10 m3 (3.22E+10 m3 live storage) in the 3S. Assuming a sediment density of 2600 kg/ton and a porosity of reservoir deposits of 0.4, it would require several millennia to fill the existing reservoirs. Yet, different reservoirs will be impacted to various degrees by siltation in function of various factors. First, the spatial heterogeneity in sediment production will result in varying siltation rates. Second, in a reservoir cascades, upstream reservoirs might trap the majority of sediment and can therefore be more impacted than downstream reservoirs. Third, small reservoirs or run-of-river plants that have a low impoundment volume and low residence times might be able to pass through more sediment then larger reservoirs. Therefore, we analyzed the storage loss in all reservoirs over the period from their COD up to 2050

Figure 6.3 ***(following page)*****:** *Predicted historic and future impacts of reservoirs on sediment outputs from the 3S basin (A), error bars indicate uncertainty over the 58 different source initializations. Colored diamond markers indicate the median over all initializations, diamonds color indicates the commercial operation date (COD) of each hydropower plant. The resulting spatial pattern of residual sediment connectivity is shown for various past and future dates (B-G). Boxplots indicate the sediment provenance from the different sub-basins.*

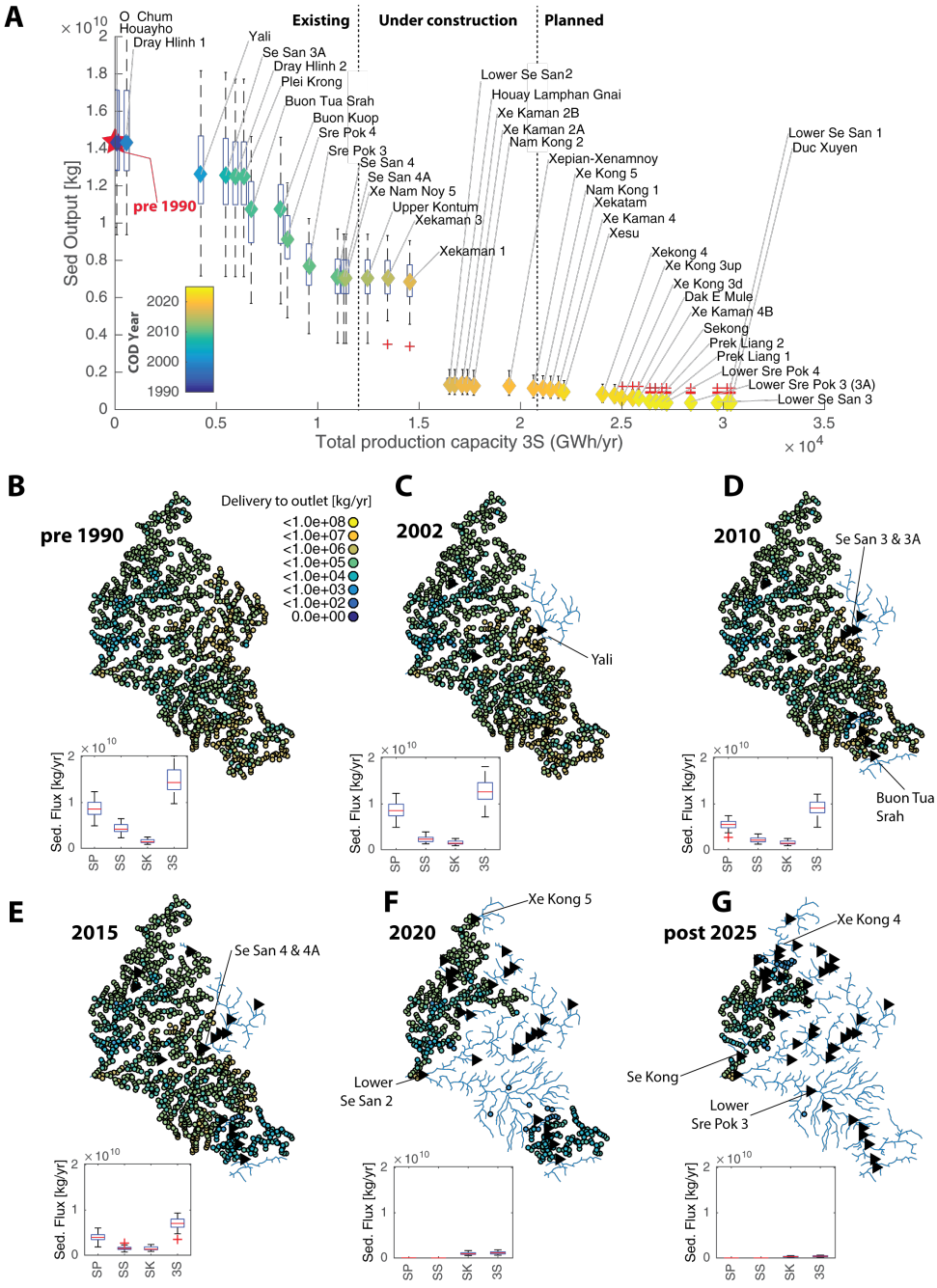
A
Existing
Under construction
Planned
O Chum
Houayho
Dray Hlinh 1
Yali
Se San 3A
Dray Hlinh 2
Plei Krong
Buon Tua Srah
Buon Kuop
Sre Pok 4
Sre Pok 3
Se San 4
Se San 4A
Xe Nam Noy 5
Upper Kontum
Xekaman 3
Xekaman 1
Lower Se San2
Houay Lamphan Gnai
Xe Kaman 2B
Xe Kaman 2A
Nam Kong 2
Xepian-Xenamnoy
Xe Kong 5
Nam Kong 1
Xekatam
Xe Kaman 4
Xesu
Xekong 4
Xe Kong 3up
Xe Kong 3d
Dak E Mule
Xe Kaman 4B
Sekong
Prek Liang 2
Prek Liang 1
Lower Sre Pok 4
Lower Sre Pok 3 (3A)
Lower Se San 3
Lower Se San 1
Duc Xuyen
pre 1990
COD Year
Sed Output [kg]
Total production capacity 3S (GWh/yr)
B
pre 1990
Delivery to outlet [kg/yr]
C
2002
Yali
D
2010
Se San 3 & 3A
Buon Tua Srah
E
2015
Se San 4 & 4A
F
2020
Xe Kong 5
Lower Se San 2
G
post 2025
Xe Kong 4
Se Kong
Lower Sre Pok 3
Sed. Flux [kg/yr]
SP
SS
SK
3S

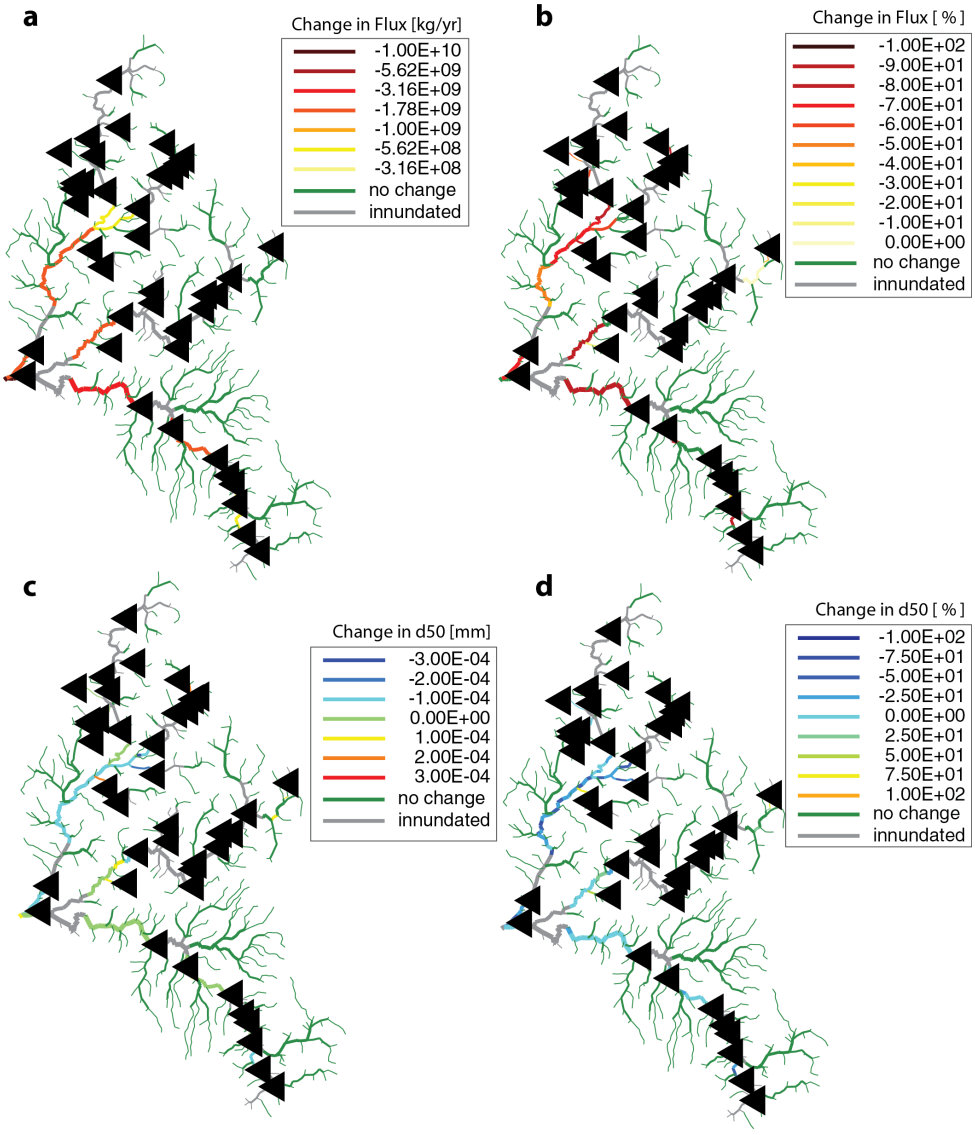

Figure 6.4: *Change in flux (A and B) and median grain size (C and D) in the 3S after the construction of the entire reservoir cascade.*

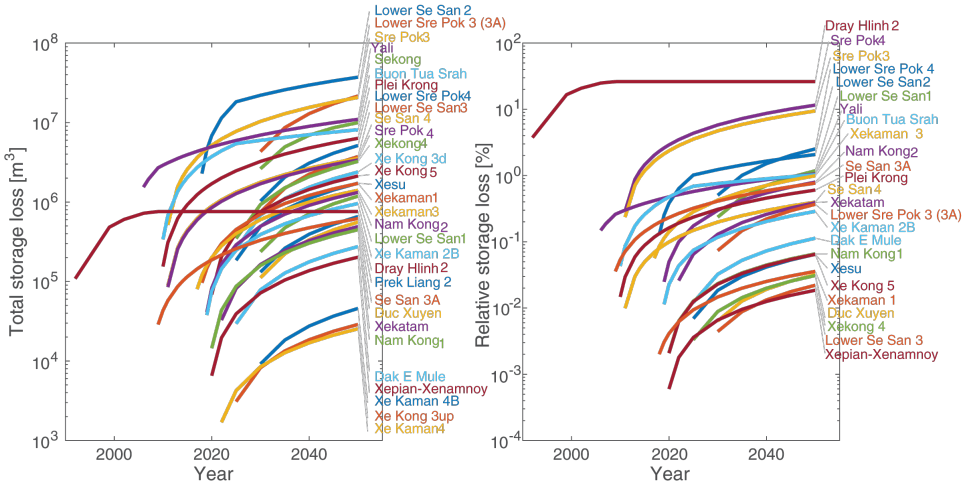

Figure 6.5: *Trajectories of storage loss in planned and existing hydro-power plants until 2050 in terms of total lost volume (left) and relative in comparison to the reservoirs' total volume (right)*

(Figure 6.5) both in absolute numbers (Figure 6.5 A), and in relation to the total water storage volume (Figure 6.5 B). Major downstream reservoirs, especially along the Sre Pok (such as LSS2, Sre Pok 3, and lower Sre Pok 3) will be subject to substantial siltation, most notably LSS2 (2E7 m3) (Figure 6.5 A), which is in line with the high pre-1990 sediment flux from the Sre Pok sub-basin. Yet, also some upstream storage reservoirs, for example Yali and Buon Tua Srah can be subject to high siltation. Despite their upstream location with a relatively small drainage area, both reservoirs are located downstream of importnat sediment source areas and trap all incoming sediment (see also Figure 6.2 C & D). In terms of relative loss of storage volume, Drai Hlinh, a run-of-river plant with relatively small storage volume, is most impacted. Of the major storage reservoirs, mainly reservoirs on the upper Sre Pok (Sre Pok 3 and 4) are most impacted loosing around 10 % of total storage volume until 2050. Siltation in the next most impacted reservoirs (Yali and Buon Tua Srah) is already one order of magnitude lower, and the average relative storage loss excluding Drai Hlinh, Sre Pok 3, and Sre Pok 4 until 2050 is only 0.5 %.

For most reservoirs, there is a decreasing siltation rate with time. For many reservoirs, this relates to the construction of upstream reservoirs. This is evident, for example, for Yali reservoir where sedimentation rates are predicted to have dropped after the completion of upstream Plei Krong reservoir. For Plei Krong, which is most upstream in the Se San Cascade, there is instead no change in trapping efficiency over time. Similarly, also trapping

rates in LSS 2 will decrease post 2025 when the entire Sre Pok and Se San cascades is completed. A reduction of trapping efficiency because of siltation and hence a reduced residency time is observed, for example, for Dray Linh 1 & 2, a run-of-the-river project. Siltation rates are reduced already before any upstream reservoir is completed, and remain constant after 2005, hence all incoming sediment is passed through downstream.

The spatially explicit tracking of sediment in the CASCADE model allows evaluating the spatial distribution of sediment in the reservoir impoundments. Figure 6.6 shows the change in bottom elevation for all reservoirs up to 2050. In general, siltation in most reservoirs is concentrated at the upstream end of reservoir impoundments. That indicates that sediment is deposited in an artificial delta soon as it enters the impoundment, while little sediment is routed more downstream in the impoundment towards the reservoirs. This effect is most emphasized for upstream storage reservoirs. In these reservoirs already most upstream compartments are relatively deep because of the steeper topography in headwaters. For example, Xesu reservoir traps most of the incoming sediment in the first two upstream compartments, resulting in a change in bottom level elevation of several meters (Figure 6.6 B1 and C1). A different pattern is observed for the (Lower) Se Kong reservoir. (Lower) Se Kong reservoirs allows for limited sediment pass-through (see Figure 6.3 G: upstream sources remain partially connected to the basin outlet). This is in line with the relatively shallow impoundment of this run-of-river plant (Figure 6.6 C2). Siltation predominantly occurs in some middle compartments of the reservoir where also some lateral tributaries enter into the reservoir (Figure 6.6 B2 and C2). For LSS2 reservoir, siltation not in the most upstream, but in more intermediate compartments (Figure 6.6 B3). This is in accordance with the bottom profile, where initial compartments are relatively shallow Figure 6.6 C3), allowing for the downstream routing of incoming sediment. In subsequent, deeper compartments available hydrodynamic forces are lower and resulting deposition is stronger.

In summary, direct impacts of reservoir siltation on storage volume in the 3S hydro-power cascades is low. Yet, some reservoirs will lose significant amounts of storage volume, and siltation in reservoirs might be considerably higher in case that upstream reservoirs are not constructed in future. Model results indicate that only few reservoirs are able to pass sediment through the impoundment downstream towards the dam, which will limit the selection of sediment management strategies.

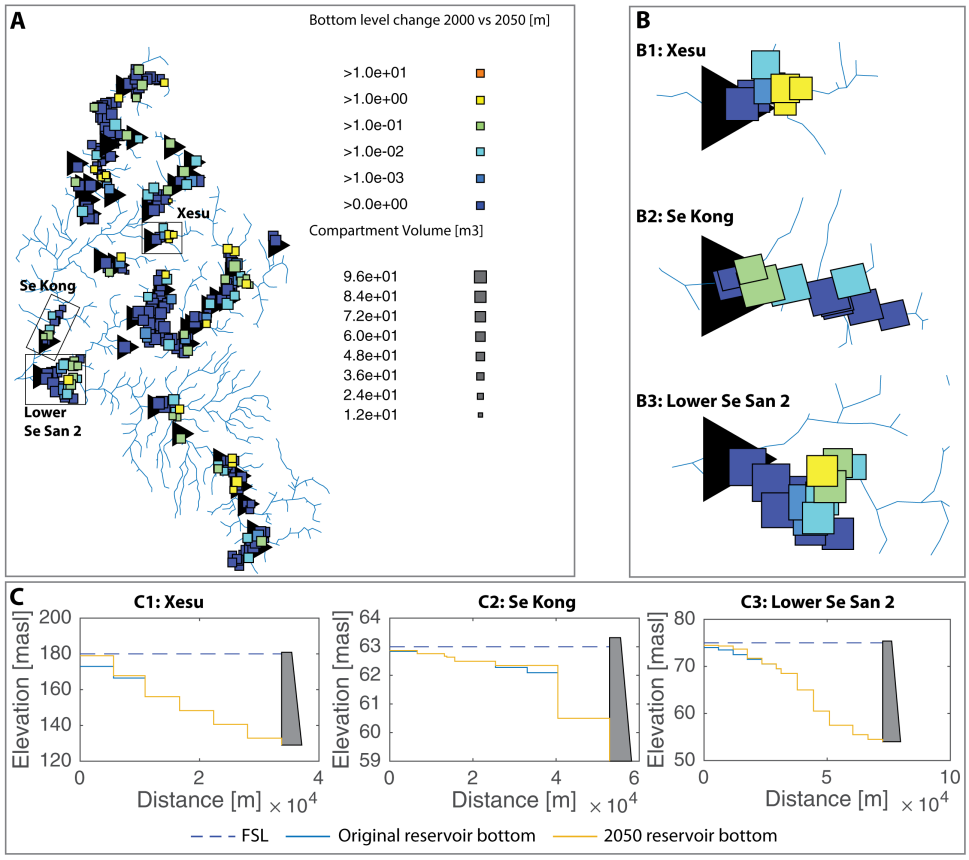

Figure 6.6: *A: Spatial distribution of reservoir siltation, marked reservoirs are discussed in detail in the text. Each square indicates a reservoir compartment in CASCADE. Marker color indicates the change in bottom level due to siltation. B Siltation patterns for Xesu, Sekong, and the Sre Pok branch of Lower Se San 2 reservoirs. C: Modelled 2050 Longitudinal section through these reservoirs.*

6.4.3 Reducing reservoir sediment trapping by strategic network-scale reservoir siting

Future sediment outputs from the 3S basin under the past and near future development trajectories have been discussed in previous sections. The objective of this section is first to identify if alternative development strategies with less impact on network sediment transport would have existed. This also includes identifying general conflicts between sediment flux and hydro-power production. Second objective is to clarify if re-siting and redesigning some of the key reservoirs would have increased the possibility for balancing hydro-power and sediment flux. Third objective is quantifying the remaining development alternatives given the already built reservoirs in the 3S basin. Towards this, we analyzed numerous portfolios of hydro-power development. Each portfolio consists of a random combination of sites from the full portfolio of all reservoir sites. Hence, each portfolio contains a subset of between 1 and 42 reservoirs. For any given size of this subset, the number of potential portfolios, C ,is given by

$$C(n_{Sites}, r) = \frac{n_{Sites}!}{(n_{Sites} - r)! * r!} \tag{6.20}$$

where r is the number of reservoir sites to be included in the generation of portfolios, and n_{sites} is the number of potential reservoir sites. As mentioned, r is variable between 1 (each portfolio contains only a single reservoir site) and the total number of reservoir sites in the portfolio (a portfolio $p = P$ that includes all reservoirs), hence the total number of portfolios is

$$C_{tot} = \sum i = 1 n_{sites} \frac{n_{sites}!}{(n_{sites} - i)! * i!}. \tag{6.21}$$

modelling all portfolios, i.e., $n_{sites} = 1 \ldots 42$ would require a huge computational effort (C_{tot}=4.4E12). To reduce this effort, we focus the analysis on the dam sites with the highest production capacity (high capacity sites). Dam sites that trap less than 1 % of the total sediment flux at the basin outlet (low impact sites) are included in all portfolios. This reduces n_{sites} to $1 \ldots 14$ and C_{tot} to 16638. Each of the portfolios is analyzed in terms of two objectives. J_1 is total hydro-power production (GWh/yr) and J_2 is sediment flux to the basin outlet (kg/yr) (Figure 6.7 left and bottom axes), respectively the fractional trapping efficiency in terms of pre-1990 sediment output (Figure 6.7 right axis) and fraction of hydro-power potential developed in comparison to the full portfolio (Figure 6.7 top axis). Figure 6.7 shows trade-offs between hydro-power production and sediment connectivity. We find that low impact sites (light blue circles) alone would have allowed for a development of 31 % of the total hydro-power production potential, while trapping only 6 %

sediment flux (Figure 6.5 A). For all other portfolios, there is a clear trade-off between hydro-power production and sediment flux. Pareto optimal (PO) portfolios are highlighted in Figure 6.7 A.

PO portfolios result in a minimal sediment trapping for a given production capacity. That also implies that increasing the production capacity from any of the PO portfolios requires increasing the sediment trapping. We find that the strength of the trade-off, i.e., the slope of the Pareto front is divided in two distinct regions. The trade-off between hydro-power and sediment flux is relatively weak up to 70 % of the full hydro-power capacity. Hence, the decrease in sediment flux is under-proportional to the increase in hydro-power capacity. Beyond 70 % of hydro-power capacity, an increase in capacity results in a strong decrease in sediment flux. The Pareto front is clearly separated in several groups (Figure 6.5 A) and we hypothesize that these groups are due to the addition of certain key-stone reservoir sites. Such key-stone reservoir sites are major reservoirs that are required to increase the production capacity while strongly impacting sediment flux. In order to identify this key-stone reservoir sites, we analyzed with which probability any of the high capacity reservoir sites is included within each group of PO portfolios (Figure 6.5 B). Group 1 includes all portfolios with a weak trade-off between production capacity and sediment flux. Group 1 includes various portfolios of reservoir sites in the upper Se Kong and Se San rivers, with the highest probability of inclusion for Yali and Se Kong 5 reservoirs, i.e., most upstream major reservoirs with a high production capacity. Groups 2 and 3 are characterized by an increasing probability for the other Se Kong and Se San reservoirs. Group 4 and 5 are similar with that regard, but include the construction of Sre Pok 4 reservoir. The gap in sediment flux between group 2 and 3, respectively groups 4 and 5 results from either including or omitting Lower Se Kong reservoir. There is a relatively large gap between groups 5 and 6, which relates to adding Lower Sre Pok 3 reservoir. Group 8 and 9 include construction of LSS2 reservoir. Hence, progressing along the Pareto front in direction of increasing energy production and decreasing sediment flux relates to a clear spatial pattern in reservoir development. We find a high production potential in Se San and Sre Pok rivers (70 %) with a comparatively small impact on sediment flux (see Figure 6.7 A, group 3). We interpret the clear breakpoint in the Pareto front as the maximum carrying capacity of the river network with regard to hydro-electric development. Beyond that point, sediment connectivity collapses, while relatively little production capacity is added. From a whole-basin perspective, reservoirs on the Sre Pok add comparably little production potential while trapping a major part of the 3S sediment output. Rational reservoir development in terms of maximizing energy production and minimizing impacts

on downstream sediment-related ecosystem services should prioritize development of the Se Kong and Se San over the Sre Pok basin. PO portfolios are very different from the historical and planned developments. Without network sediment fluxes being considered, and without a concerted strategical planning, the historical trajectory of reservoir developments is different (Figure 6.7 A, square markers) with a major gap between PO and actual developments. The historic development trajectory focused first on the upper, Vietnamese, Se San and Sre Pok sub-basins (Figure 6.1), while downstream dams in Cambodia including the most downstream dam on both rivers, LSS2 are currently under construction. Especially before the construction of LSS2 there was a major potential to increase the hydro-power production without further reducing sediment fluxes by focusing developments on the upper Se Kong and Se San (compare pre-LSS2 and group 5 in Figure 6.7 A). Yet, with the ongoing construction of LSS2, there is little potential to decrease the conflict between hydro-power production and sediment flux in the 3S.

Alternative designs for LSS2 have been proposed. For example, *Annandale* (2013), recommended replacing LSS2 with 4 smaller reservoirs, 3 in the Se San and 1 in the Sre Pok River (Lower Se San, Lower Sre Pok, and Se San US 1 & 2, see Figure 6.1). These alternative sites would cover around 90 % of the annual production of LSS 2. Therefore, we repeated the previous analysis, but replacing LSS2 reservoir with the alternative reservoir sites. We find that none of the proposed LSS alternative sites has a major trapping potential for sediment, which is in line with findings by *Annandale* (2013). Hence, all of the alternative reservoir sites are included as low impact sites in the analysis. PO portfolios with LSS2 alternatives in comparison to portfolios including LSS2 are shown in . Energy production for most portfolios is increased, because the LSS alternative reservoirs are added to all portfolios. For the fully build portfolio, energy production is slightly lower with the LSS2 alternatives than with LSS2. But, there is a major difference in the sediment trapping in comparison to original portfolios that included LSS2 (compare Figure 6.7 , Group 8,9). The trapping rate for the final, fully built portfolio is substantially (14.2 %) lower with the LSS2 alternatives than with LSS2. Yet, this difference is small compared to the predicted reduction in sediment flux after the construction of LSS2 (see Figure 6.3). This is because of the historical sequence of reservoir constructions. The emphasized effect of LSS2 is because it was constructed before more upstream reservoirs (e.g., Lower Sre Pok 3 and 4, Lower Se San 3). Hence, as the current design of LSS2 already traps most of sediment flux to the Mekong, the later construction of upstream reservoirs will have a limited effect on the total sediment flux from the 3S. If the LSS2 alternatives would have been constructed allowing for sediment passage, the trapping effect of upstream reservoirs

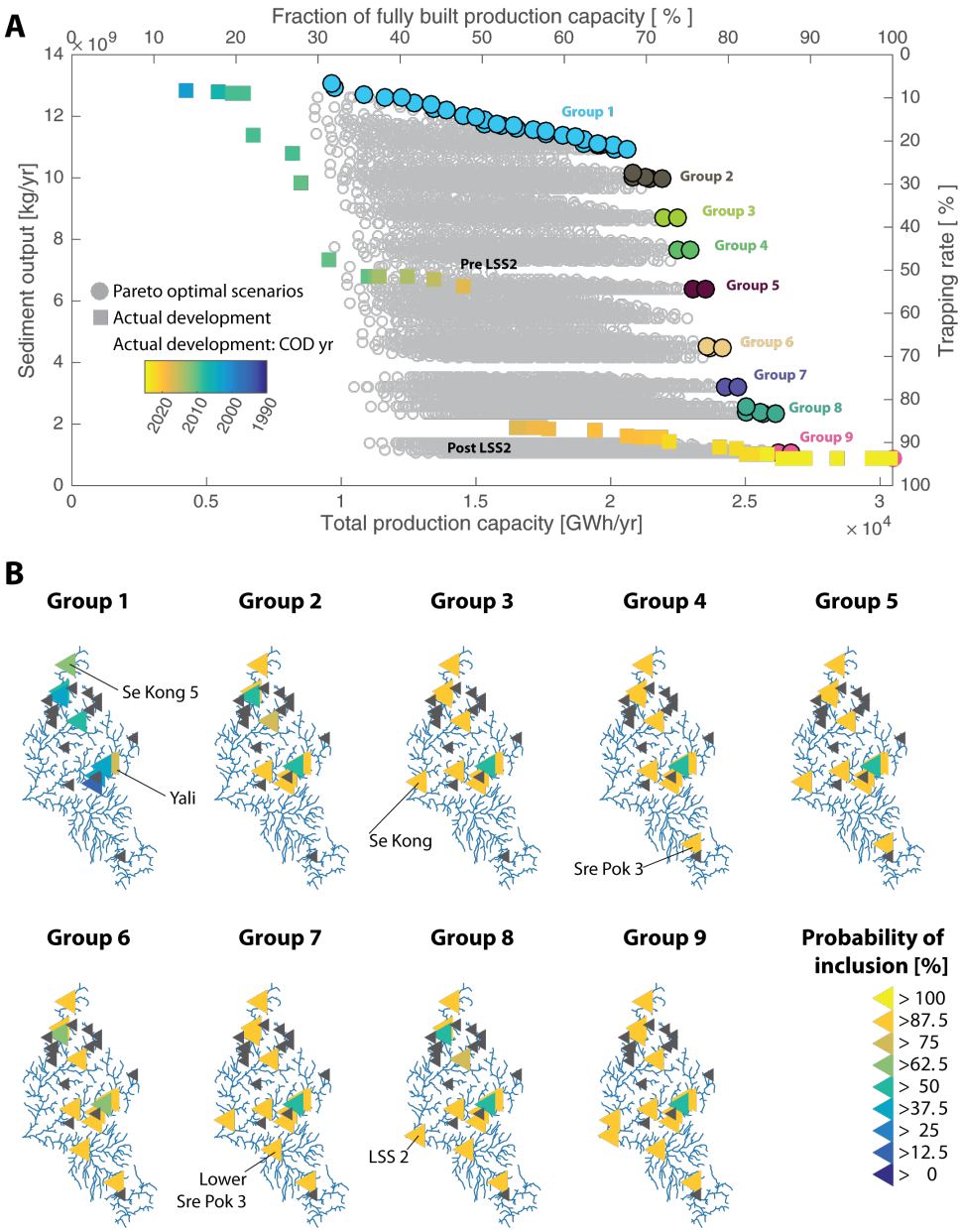

Figure 6.7: *Panel A: Hypothetic dam portfolios and resulting objective values in terms of total sediment output and relative trapping (y-axes) and energy production (x-axes). Circle filled markers indicate PO solutions, colors mark different groups of PO portfolios. Square filled markers indicate the historic development trajectory. Panel B: Reservoir portfolios for groups of PO portfolios. Black triangles are sites with low trap efficiency that are included in all portfolios. The color code of dams indicate with which probability a dam is included within each group of portfolios.*

would have had a higher impact on the sediment flux from the 3S. Hence, fully exploiting the pass-through capacities of LSS2 alternatives would have required to also adapt reservoir design of other upstream reservoirs in the Se San and Sre Pok sub-basins. With the construction of LSS2 reservoir well advanced, options for reducing sediment trapping in the 3S are limited. The last part of this analysis focusses therefore on reservoirs that are currently in the planning phase (Figure 6.8, yellow). Amongst the remaining reservoir locations, especially (Lower) Se Kong reservoir has the potential to trap a significant fraction of the remaining sediment flux, while it will only slightly reduce the energy production (see gap in yellow Pareto front in Figure 6.8).

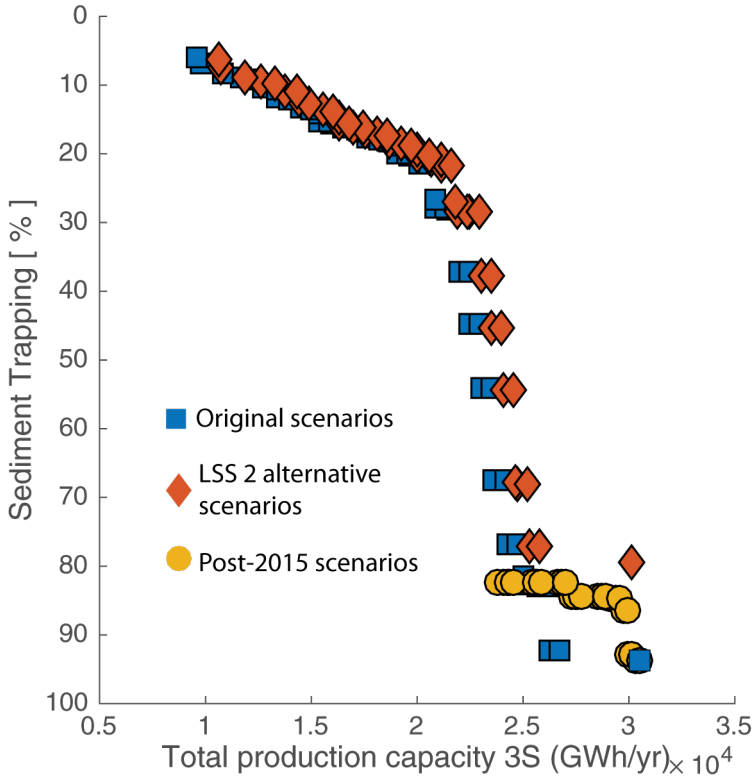

Figure 6.8: *PO Trade-offs between hydro-electric energy production and sediment trapping for the current development strategy (blue), and for the remaining undeveloped reservoir sites (yellow). Some potential existed to reduce sediment trapping by alternative siting of LSS2 reservoir (red).*

6.4.4 Trading off total sediment trapping and local channel integrity

The previous analysis showed how spatial heterogeneity in sediment fluxes impacts the strategic siting of reservoirs to minimize sediment trapping and

maximize total sediment flux to the Mekong. Yet, it omitted potential impacts of reservoir constructions on the rivers in the 3S system downstream of dams. As shown in Figure 6.4, reservoir developments are going to go in hand with potentially severe changes in the sediment fluxes and fluvial processes downstream of reservoirs. Therefore, we propose that reservoir portfolios should also be analyzed with the perspective of minimizing impacts on channel processes within the 3S system. A range of indicators and frameworks for assessing hydromorphologic impacts of reservoirs has been proposed (e.g., *Grant et al.* (2003); *Schmidt and Wilcock* (2008)). Mostly based on comparing changes in pre- and post-dam sediment load and transport capacity. Because there is no information on the change in transport capacity, which amongst other factors, will rely on the operation of reservoirs, we focus on the analysis of post-dam sediment load. We calculated the reduction in total sediment flux in a reach a measure of magnitude of future change, weighted by the length of impacted reaches. Such that the objective J_3 is defined as

$$J_3 = \sum_{i=1}^{n} \Theta_{S,i} - {\Theta_{S,i}}^{1990} * L_i. \tag{6.22}$$

Where $i = 1 \cdots n$ are all reaches downstream of reservoirs, ${\Theta_{S,i}}^{1990}$ the pre-1990 sediment flux, $\Theta_{S,i}$ is the sediment flux after the reservoir construction, and L_i is the length of an impacted reach. Interestingly, the river system has a similar hydro-power carrying capacity with regard to local morphologic impacts than it has with regard to total sediment output. 75 % of the hydropower potential in the 3S could have been developed while incurring only 25 % of the impact magnitude of full development (Figure 6.9). Additional developments then result in a strong increase in impact magnitude. Again, PO portfolio are marked and grouped. portfolios of Group 1 include with a high probability (>60 %) reservoirs in the upper Se Kong and Sre Pok (e.g., Se Kong 4 and 5, and Yali), which is similar to PO portfolios regarding sediment flux (Figure 6.7 , Group 1). Groups 2 to 4 show a major difference to previous results, as the construction of more downstream reservoirs would be strategic to reduce impact magnitude in the 3S river system. Such, construction of LSS2 is included already in the second group of portfolios, and also Se Kong reservoir is included in groups 2 to 4, as these downstream reservoirs increase the energy production, while only impacting a smaller fraction of the 3S river network. Two levels of conflict exist in reservoir planning in the 3S. First, there is an immanent trade-off between hydro-power production and both sediment fluxes from the 3S to the Mekong and within the 3S. Second, there is a potential trade-off between downstream (i.e., downstream of the Mekong 3S confluence) and upstream (i.e., upstream of the Mekong-

3S confluence within the 3S network) environmental objectives. In order to minimize downstream impacts, reservoir development should focus on major upstream reservoirs that balance a high power production with a limited trapping potential (e.g., Figure 6.7, groups 1-3). Reducing upstream impacts would instead favor the construction on downstream reservoirs, that reduce the length of impacted rivers within the 3S system.

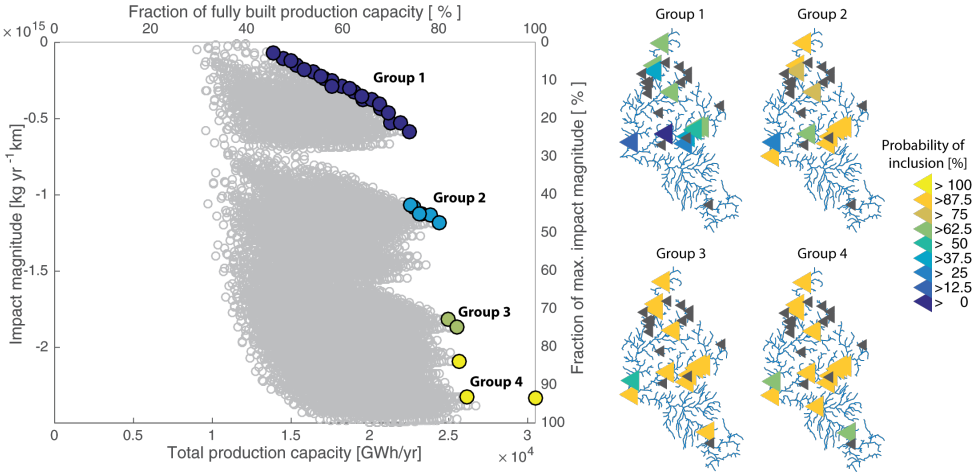

Figure 6.9: *Tradeoffs between energy production and impact magnitude, and the spatial configuration of reservoirs for groups of PO portfolios.*

6.4.5 Optimal trade-off between production, unit costs, and network sediment trapping in the 3S dam portfolios

The previous results showed trade-offs between hydro-power production, sediment connectivity, and river channel integrity. Results also indicated that the past and future trajectory of hydro-power planning in the 3S is far from the optimal trade-offs between ecosystem integrity and hydro-power production. In energy-hungry economies of South-East Asia, planning could be motivated by not only maximizing production but also reducing production costs. For example, large main-stem dams could have lower unit production costs per KWh than smaller upstream dams, favoring them for earlier development. Therefore, this chapter closes with an economic analysis of hydro-power portfolios. First, this section shows results of analysing production costs of single dam sites, and analyses dam portfolios purely based on economic indicators. Second, this section analyses trade-offs between hydro-power economics and eco-system integrity based for all portfolios. Finally, based on the results of this analysis an environmentally and econmically optimal dam portfolio is identified.

An economic model was built to link construction costs [$] to unit production costs [i.e., $ or ¢/ KWh], which must include both capital and operation and maintenance costs. The economic model (see Equations 6.12- 6.16) was calibrated to reported unit production costs for some Laotian plants. Results are shown in Figure 6.10. A best fit in terms of minimum SSE between reported and modelled unit production costs [¢/ KWh] was found for capital costs of 9.1 %/yr and O & M costs of 1,5 %/yr of construction costs (R^2=0.67). The model was found insensitive to the plant life time (assuming a lifetime between 50 and 100 yr as boundary condition), so a plant lifetime of 100 year was used. These results seem reasonable. The *Agency* (2012b) proposes O & M costs of 1 - 5 % of investment costs and capital costs of 10 % for economic appraisals of renewable energy projects. Hence, the parameters of the economic model seems to agree well with generic data and reports from the 3S. It should also be noted, that residuals between reported and modeled costs are well distributed (compare model results to the hypothetical line of perfect fit in Figure 6.10). As a consequence, the mean of modelled unit production costs for all eight dams (3.98 ¢/KWh) is not significantly different (T-test, p=0.44) from the reported production cost (4,06 ¢/KWh). Hence, the economic model accurately predicts the production costs based on the tabulated construction costs from the MRC.

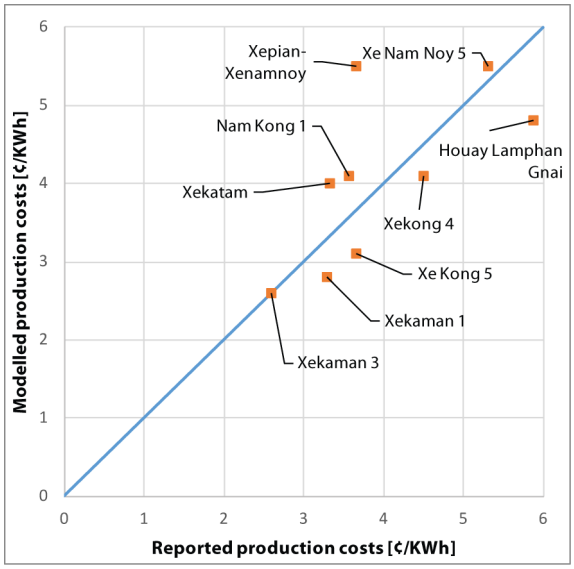

Figure 6.10: *Correlation between unit production costs reported by the Bank (2004a) and hydro-power unit production costs modelled from dam construction costs reported by the MRC for Laotian dams in the 3S. Diagonal line indicates a perfect fit between reported and modelled values.*

Based on the derived construction and production costs for the 3S dams

we performed the economic analysis of hydro-power portfolios. We perform this analysis in two steps, first in terms of economic indicators (for both single dams and dam portfolios) and then comparing economic and environmental performance of dam portfolios. For comparability, portfolios are the same as used in the previous sections. The construction and production costs are listed in Table 6.5.

Big dams are expensive in total numbers, as construction costs increase with higher production capacity(Figure 6.11 a). Most expensive project in the 3S is Lower Se San 3 dam with investment costs of 1.2 billion dollars. A power law of the form

$$c^D_{construction} = a * E^{D^b} \tag{6.23}$$

fitted to the data (Figure 6.11 a, red line, R^2=0.71), has an exponent $b = 0.77$. This means that there is some economy of scale: costs grow somewhat under-proportional for larger projects. Dams that are above the fit-line, are comparably expensive. It is interesting to note, that all the dams above the line (except for Xe Kong 4 and Houayho) are mainstem dams (see also Figure 6.1).

For unit production costs, there is a strong economy of scale. A power law of the form

$$c^D_{prod} = c * E^{D^d} \tag{6.24}$$

fits the data very well (Figure 6.11 b, green line,R^2=0.84, d = -0.49). Unit production costs decrease most strongly between small and medium dams (below around 1000 GWh annual production). For dams with higher capacity unit production costs remain around 4 to 5 ¢/ KWh.

We then analyzed potential trade-offs between portfolio hydro-power generation and portfolio costs, assuming that economic decisions should be driven by the aim of combining high energy production with low construction and unit production costs. The total portfolio value in the 3S is 12.8 billion dollars for an annual production of around 31,000 GWh (Figure 6.11 c). We find that there is a major potential for cost-reduction through strategic portfolio analysis. For example, 2E4 GWh can be reached for construction costs between 7 and 9 billion dollars. Hence, the cheapest 2E4 GWh portfolio is nearly 25 % less expensive than the most expensive one. The difference between the PO (Figure 6.11 c, red dots) and non-PO portfolios (PO with regard to construction costs vs. energy production) decreases with higher installed capacity. The difference between PO and non-PO scenarios is even more emphasized for unit production costs (Figure 6.11 d, green dots). In contrast to single dams (Figure 6.11 b), there is little economy of scale on the portfolio level. Unit production costs for the full portfolio are around

Table 6.5: *Economic indicators for single dam projects in the 3S basin*

Code	Name	Original Cost [Mio USD]	Cost per 2016 [Mio USD]	Annuity [Mio USD / yr]	Maintenance [Mio USD / yr]	Production cost [Mio USD/GWh]	[c/KWh]
L006	Houayho	166,0	447,0	40,51	6,52	0,10	9,66
L012	Xekaman 3	266,0	282,0	25,55	4,11	0,03	3,02
L017	Xekaman 1	343,6	343,6	31,14	5,01	0,03	3,30
L027	Xepian-Xenamnoy	607,1	607,1	55,02	8,85	0,04	3,65
L028	Xekatam	120,2	120,2	10,90	1,75	0,03	3,33
L029	Xekong 4	815,4	815,4	73,90	11,89	0,05	4,51
L030	Nam Kong 1	159,1	159,1	14,42	2,32	0,04	3,57
L031	Xe Kong 3up	168,3	168,3	15,25	2,45	0,03	2,96
L032	Xe Kong 3d	112,9	112,9	10,23	1,65	0,03	3,16
L033	Xe Kong 5	417,0	417,0	37,79	6,08	0,04	3,65
L061	Xe Kaman 2A	104,3	104,3	9,45	1,52	0,05	4,54
L062	Xe Kaman 2B	158,0	158,0	14,32	2,30	0,04	4,37
L063	Xe Kaman 4	145,0	145,0	13,14	2,11	0,04	4,07
L064	Xe Kaman 4B	115,7	115,7	10,49	1,69	0,04	4,04
L065	Dak E Mule	251,0	251,0	22,75	3,66	0,05	5,22
L097	Xe Nam Noy 5	52,6	62,6	5,68	0,91	0,05	5,32
L098	Houay Lamphan Gnai	147,7	147,7	13,39	2,15	0,06	5,88
L099	Nam Kong 2	124,5	124,5	11,28	1,82	0,04	4,23
L100	Xesu	121,4	121,4	11,00	1,77	0,04	4,46
C001	O Chum 2	3,6	14,6	1,32	0,21	0,51	51,12
C002	Lower Se San 2	790,3	790,3	71,62	11,52	0,04	4,26
C009	Lower Se San 3	1184,9	1184,9	107,38	17,28	0,10	9,51
C010	Prek Liang 1	163,9	163,9	14,85	2,39	0,05	5,32
C011	Prek Liang 2	120,7	120,7	10,94	1,76	0,05	4,89
C012	Lower Sre Pok 3 (3A)	973,7	973,7	88,24	14,20	0,09	8,53
C013	Lower Sre Pok 4	309,9	309,9	28,08	4,52	0,15	14,77
C015	Sekong	407,6	407,6	36,94	5,94	0,08	7,69
C016	Lower Se San 1	225,2	225,2	20,41	3,28	0,05	4,89
V001	Upper Kontum	287,3	322,8	29,25	4,71	0,03	3,21
V002	Plei Krong	178,8	268,8	24,36	3,92	0,07	6,78
V003	Yali	456,1	1031,2	93,46	15,04	0,03	2,97
V004	Se San 3	236,3	423,2	38,35	6,17	0,04	3,64
V005	Se San 3A	121,7	205,6	18,63	3,00	0,05	4,51
V006	Se San 4	349,8	496,1	44,96	7,23	0,04	3,68
V007	Se San 4A	79,1	105,9	9,60	1,54	0,04	3,75
V008	Duc Xuyen	82,6	82,6	7,49	1,20	0,05	4,79
V009	Buon Tua Srah	136,0	204,4	18,53	2,98	0,06	6,00
V010	Buon Kuop	300,0	451,0	40,87	6,58	0,03	3,25
V011	Dray Hlinh 2	13,5	22,8	2,07	0,33	0,03	2,82
V012	Sre Pok 3	266,9	378,6	34,31	5,52	0,04	3,76
V013	Sre Pok 4	92,5	131,1	11,88	1,91	0,04	4,19
V014	Dray Hlinh 1	3,1	14,0	1,27	0,20	0,02	1,57

4.4 ¢/KWh. Portfolios with lower annual production can result in considerable lower unit production costs than portfolios with higher production. The cheapest PO portfolio results in generation costs of 3.65 ¢/KWh, hence considerably (-32 %) cheaper than the portfolio with highest costs (5.3 /KWh), even though both have a similar annual production of around 2E4 GWh. The PO portfolio with the cheapest unit costs focusses hydro-power production in the upper Se San and Se Kong River (see cutout in Figure 6.11 d) The higher the total production (i.e., the more dams are built) the lower is the difference between least and most expensive portfolios.

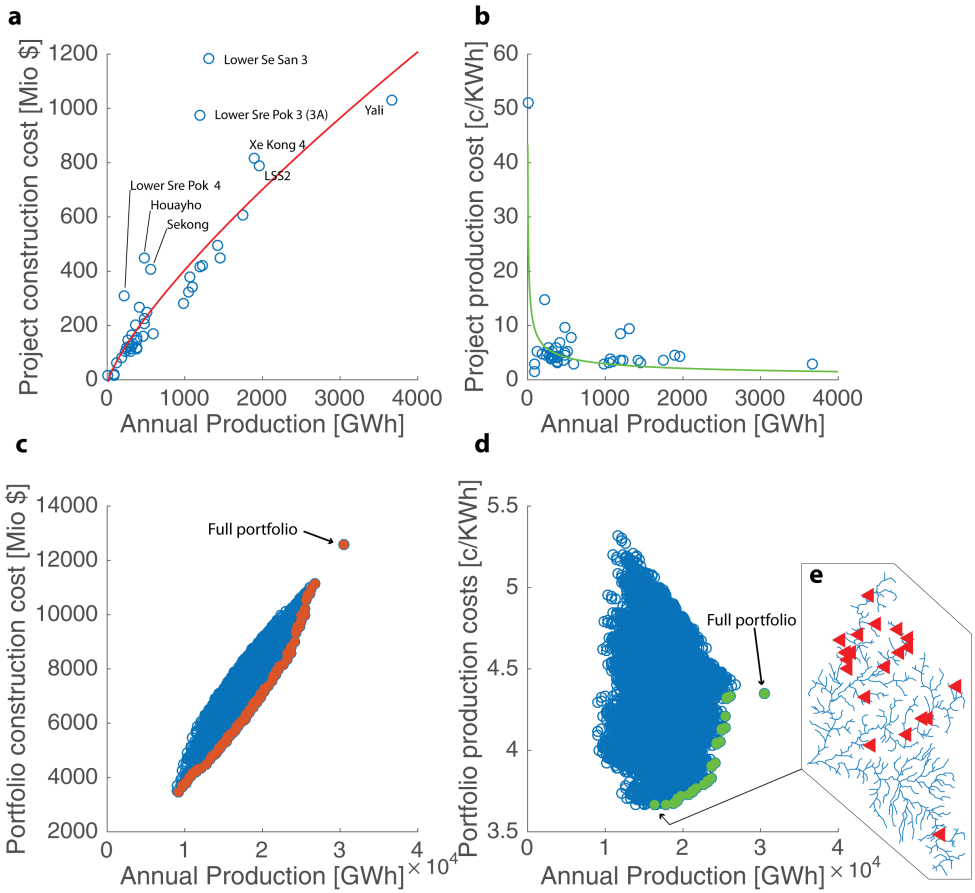

Figure 6.11: *a: Correlation between construction costs for single dam projects and annual hydro-power production. b: Correlation between single-dam annual hydro-power production and unit production costs. c: Portfolio construction costs. Red dots are PO regarding annual production and construction costs. d: Correlation between portfolio annual production and unit production costs. Green dots are PO regarding annual production and unit production costs. e: dam configuration for portfolio with cheapest unit production costs.*

There is a direct link between portfolio construction costs and sediment trapping. Figure 6.12 a, shows the tradeoff between sediment output, production capacity, and total portfolio costs (color scale). Portfolios with lower sediment output have in tendency higher portfolio costs. I.e., 2E4 GWh capacity can be installed for 9 billion dollars and a sediment output of around 1E9 kg/yr or for only 7 billion dollars and a sediment output that is one magnitude higher (11E9 kg/yr). This is because portfolios that are more expensive contain potentially more dam sites. This is validated by considering PO scenarios with regard to total production and sediment trapping (Figure 6.12 a, square filled markers), only. For PO scenarios it is clear that portfolios with higher sediment trapping and higher annual production result also in higher production costs, as these portfolios include more dams, (see Figure 6.7 a). Costs are highest, obviously, for the fully build scenario. Portfolios in group 1, that result in comparably low sediment trapping (Figure 6.7 a), have portfolio costs between 3.5 and 7 billion dollars.

Building more dams, which increases sediment trapping, is not necessarily the way to go, if the objective is reduction of unit production costs. It is evident from Figure 6.11 e that a dam portfolio with low unit production costs shares a spatial configuration similar to dam portfolios with high sediment output (compare configuration in Figure 6.11 e with Figure 6.7 b, Group 1). Both portfolios focus reservoir developments in the upper Se Kong and Sre Pok rivers and the major tributaries while not developing downstream mainstem dams. This is in accordance with findings that major downstream dams are not very competitive in terms of total production vs. production and construction cost (see Figure 6.11 a). Mapping unit production costs of dam portfolios into the trade-offs between total production and sediment output shows that portfolios with the most competitive unit costs (< 4 ¢/ KWh) are also those with the lowest sediment trapping and within the carrying capacity of the river network (if defining the carrying capacity as including all portfolios in group 1 6.7 a). Further hydro-power development (i.e., increasing the total production) does not result in an decrease, but an increase of unit costs.

Given that information, what would have been the optimal dam portfolio in the 3S? Obviously, if the objective is to maximize energy production, the fully built scenario is most attractive. To produce cheap energy, a dam portfolio in the upper Se Kong and Se San is best. To maintain channel integrity in the 3S and sediment transfers to the Lower Mekong the best scenario would be not to develop hydro-power in the 3S. Yet, we assume that a scenario that balances hydro-power production, cheap unit production costs, and low sediment trapping would be the most rational decision. We identify the best trade-off by calculating the distance of all PO portfolios

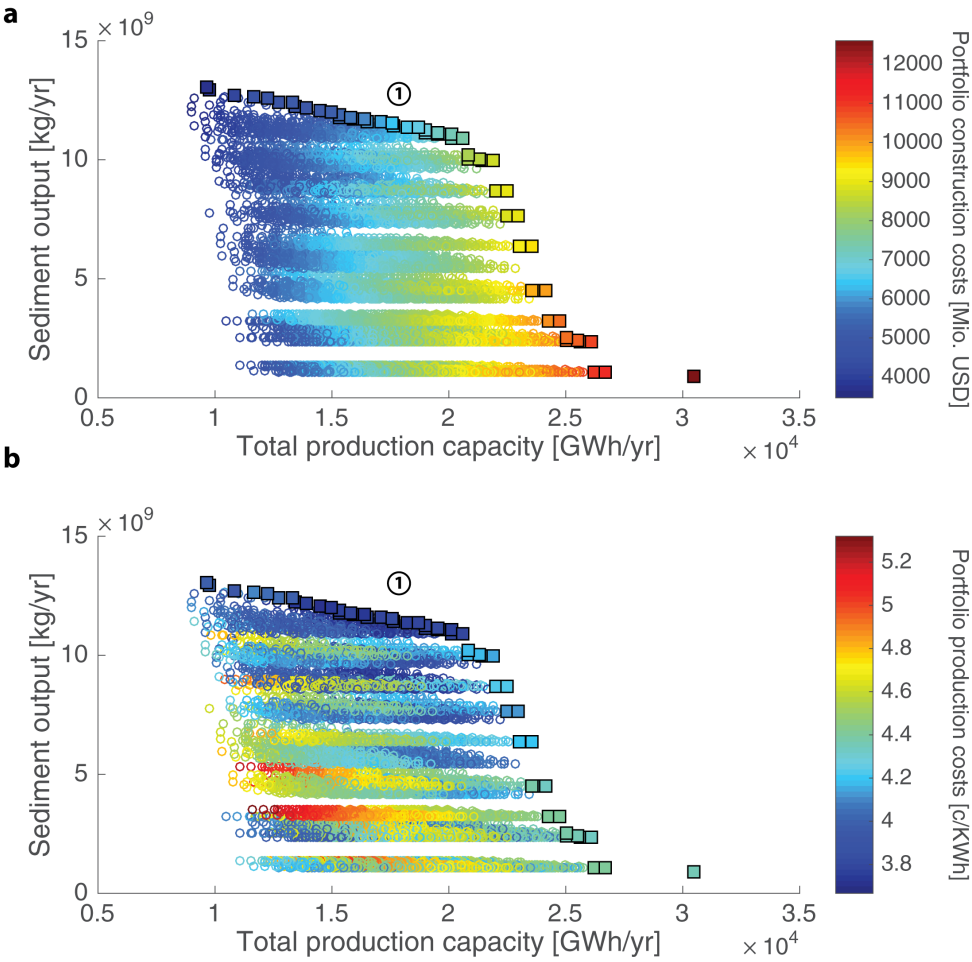

Figure 6.12: *a: Tradeoffs between sediment outputs, total production capacity, and portfolio construction costs. b:Tradeoffs between sediment outputs, total production capacity, and production costs. Portfolios that are PO regarding sediment output and production capacity are emphasized by square markers.*

from the Utopia point. The Utopia point refers to the point where all objectives would have been maximized. For the 3S, the Utopia point is located at 30463 GWh/yr annual production, 1.31E9 kg/yr sediment output and production costs of 3,67 ¢/KWh. We calculate the Euclidian distance between the normalize objective values of each PO scenario and the Utopia point as measure of their performance. The objective values for each PO portfolio are normalized by the respective value of the Utopia point in order to correct for the different scales of the objectives. Otherwise, the Euclidian distance would be dominated by the objective with the highest values (i.e., sediment output). Results are shown in Figure 6.13. Each dimension shows one of the 3 objectives. That means, that the x-y plane is equivalent to results shown in Figure 6.12. The y-z plane is equivalent to Figure 6.11 d. The x-z plane (unit production costs vs. sediment output) is equivalent to the colors in Figure 6.12 b. The black lozenge in Figure 6.13 shows the Utopia point. Filled points indicate PO portfolios, colored according to their normalized Euclidian distance from the Utopia point.

Table 6.6: *Dam sites included in an optimal dam portfolio. See also cutout in Figure 6.13.*

Se Kong		**Se San**	**Sre Pok**
Houayho	Xe Kaman 2A	O Chum 2	Buon Kuop
Xekaman 3	Xe Kaman 4	Lower Se San 1	
Xekaman 1	Xe Kaman 4B	Upper Kontum	
Xepian-Xenamnoy	Dak E Mule	Yali	
Xekatam	Xe Nam Noy 5	Se San 3	
Xekong 4	Houay Lamphan Gnai	Se San 3A	
Xe Kong 3up	Nam Kong 2	Se San 4	
Xe Kong 5		Se San 4A	

Interestingly PO portfolios (PO with regard to production costs, energy production, and sediment connectivity) have nearly always cheaper unit production costs compared to non PO portfolios. For example, compare the portfolios marked with i (non PO) and ii (PO) in Figure 6.13. Both portfolios result in a similar sediment output (around 5E9 kg/yr). Yet, the PO portfolio (ii) has lower unit production costs (4.3 vs. 5 ¢/ KWh). This is because of the connected structure of river sediment transfers. As soon as a downstream dam is built, a certain level of sediment trapping is fixed (i.e., in point i). Based on that premise, it is then rational to develop also all upstream dams to increasing total production and reducing unit production costs (i.e., move towards ii).

High production scenarios have the highest Euclidian distance from the Utopia point. A portfolio within group 1 (see Figure 6.12 a) has the lowest Euclidian distance to the Utopia point. The dam configuration in that port-

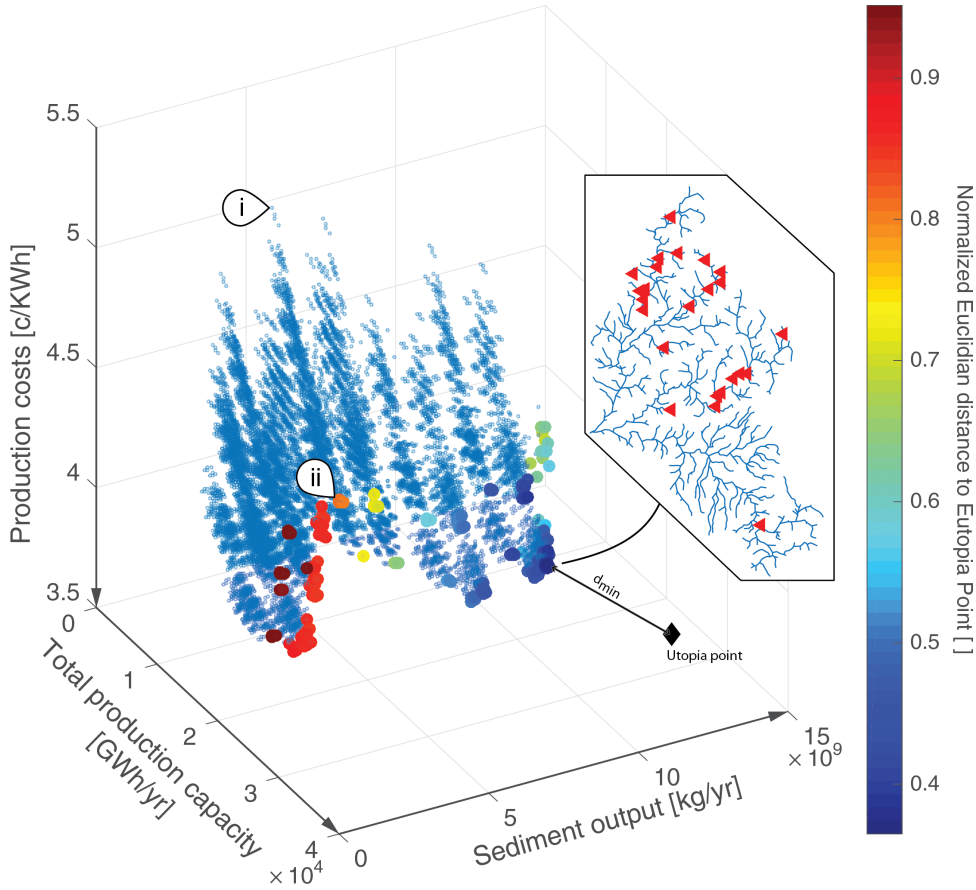

Figure 6.13: *Trade-offs between hydro-power production, unit costs, and sediment outputs in the 3S basin. Colored points are PO dam portfolios. The color scale indicates the distance of PO dam portfolios to the Utopia point (black lozenge). Arrows on axis indicate the desirable direction of objectives. The spatial configuration for the portfolio that is closest to the Utopia point is shown in the cutout. See Table 6.6 for tabulated dam names in that portfolio. Roman numbers are explained in the text.*

folio (cutout in Figure 6.13 b for spatial configuration and Table 6.6 for dam sites in that portfolio) includes all dams in the upper Se Kong (including the Se Kataman tributary) cascade, but not the SeKong Dam on the lower Se Kong. In the Se San, all dams are included except Lower Se San 3. In the Sre Pok, only Buon Kop dam is included. This dam portfolio has 20,598 GWh (around 70 % of the total) annual production capacity at 3,8 ¢ KWh unit production costs (3 % above cheapest scenario). Sediment output is reduced to 1.1E10 kg/yr, i.e., by around 30 % compared to the pre-dam state.

To conclude, an optimal portfolio of dams in the 3S would have allowed to balance a high sediment output, with total hydro-electric production at very competitive unit costs. The optimal dam portfolio does not include any of the major mainstem dams, that are now mostly under construction or planned for the near future (LSS2, or Lower Se San 3, for example). From a multi-objective environmental and economic perspective on the 3S dam portfolio, the development of these dams is not desirable, except if the full development of the 3S hydro-power potential, without considering unit costs or eco-system services, is the only objective.

6.5 Discussion

International organizations call increasingly for network assessment of benefits and impacts of hydro-power cascades and reassessments of very large hydro-electric dams (*World Commission on Dams*, 2000). Only recently, these calls have been transferred into conceptual considerations of how different spatial configurations of dams could results in very different trade-offs between ecosystem services and economic objectives (*Jager et al.*, 2015; *Opperman et al.*, 2015). How such concepts translate into real-world planning was so far poorly studied. It also remained unclear if selection of high-impact dam sites, especially in emerging economies, was a potentially rational decision to optimize short-term economic benefits regardless of ecologic impacts, or if large dams are not even desirable from an economic perspective (*Ansar et al.*, 2014).

With this regard, the 3S case study is a prime example for how enlarging hydro-power planning from single dams to the portfolio-scale can improve economic and ecologic performance. For the 3S, we found that past, ongoing, and future hydro-power developments have the potential to reduce the flux of sediment from the 3S to the Mekong delta by nearly 2 orders of magnitude. In accordance with previous works (e.g., *Wild and Loucks* (2014)) we find that the impact of the entire reservoir cascade is dominated by Lower Se San 2 (LSS2) dam. LSS2 will trap nearly all sediment from the Se San and Sre Pok rivers, where the most importnat sediment sources are located. The construction of LSS2 dam alone has the potential to increase the trapping

efficiency of the 3S hydro-power cascade by an additional 70 % to around 90 % of total trapping. This relates to an increase in hydro-electric energy production of only 13 %. Then, because of the trap efficiency of LSS2, future upstream dam developments in in the Se San and Sre Pok will have a very small impact on sediment delivery from the 3S to the Mekong River.

Assessing the cumulative impacts of dams within the 3S showed that the development of the full hydro-power cascade will have a major impact in terms of reduced sediment fluxes and changing grain sizes. This will likely translate in strong morphologic alterations within the 3S and deprive the Lower Mekong River of its most importnat source of sediment. In terms of network sediment trapping, we propose that negative environmental impacts in rivers downstream of dams will likely exceed the negative impacts of reservoir siltation. Because of the multitude of dams, only few of them will receive sufficient sediment to lose a importnat fraction of storage capacity over a 50 year horizon. There are increasing efforts to include sedimentation into a holistic, life-time economic assessment of dams (*Palmieri et al.*, 2003). Our results show that such approaches should move from a single dam to a network perspective on sediment trapping in order to yield relevant results for single dam sites, which resonates with findings by *Minear and Kondolf* (2009). In terms of technical contribution, we showed how a network connectivity model can be readily enlarged by a reservoir hydraulics component to evaluate spatial patterns of reservoir sedimentation.

The main motivation of this chapter was quantifying conflicts between economic and environmental aspects of hydro-power developments from both a network perspective on natural processes, and a portfolio perspective with regard to hydro-power economics. For natural processes there are some studies that show how different spatial configurations of dams can result in very different levels of impacts on fish migration (e.g., *Ziv et al.* (2012)). For hydro-power economics, there are so far very little studies that would analyse which dam-sites portfolios are optimal regarding economic benefits. A tradeoff analysis between the reduction in sediment flux and energy production showed that the conflict between both objectives is relatively small, as long as a certain carrying capacity of the river network is not exceeded. For the 3S, up to 70 % of the hydro-electric potential could have been developed while reducing sediment flux from the 3S by only around 20 %. Yet, attaining this weak level of conflict would have required careful planning, as only specific portfolios result in optimal trade-offs between hydro-power and sediment trapping. After that threshold, adding additional dams results in a very strong reduction in sediment fluxes. The currently ongoing hydro-power development in the 3S is reducing sediment flux over-proportionally in comparison to the installed capacity, showing the risks of non-coordinated

hydro-power developments. With regard to that carrying capacity, it is informative to observe that the carrying capacity is similar for sediment transport and fish migration in the Mekong (*Ziv et al.*, 2012). Yet, in function of the objective, optimal spatial configurations are very different. For fish migration, optimal dam portfolios would omit developing the Se Kong River, while this is where dam development should focus in order to maximize sediment transport. Hence, it seems likely that there are conflicts between economic and ecologic objectives, and on a second level also between different ecologic objectives. This is a first hint, how future network analysis will have to include many different objectives. With this regard, already only considering sediment transport processes uncovered a strong conflict between sediment delivery to the lower Mekong River versus maintaining fluvial ecosystem integrity within the 3S. For maintaining river processes intact, building large mainstem downstream dams is advantageous, while it has a major negative impact on total sediment flux. Another impact is that is not considered in this analysis is hydro-peaking. Hydro-peaking from reservoirs in the upper Se San is reported to cause major damage to downstream ecosystems, and impact downstream inhabitants in the river corridor (*Hirsch and Wyatt*, 2004). Reducing hydropeaking impacts might also favor more downstream dams, that reduce the length of impacted rivers.

With regard to such large dams we expected that it would be economic considerations that make them attractive to decision makers. Dams such as Lower Se San 3 or LSS2, with a construction value of around a billion dollar, are major infrastructure projects, especially in comparison to local buying power. Hence, it could be expected that such "Mega Dams" are constructed for economic considerations. The analysis presented in that chapter indicated instead that very large dams are not necessarily more economic than smaller dams (around 1000 GWh/yr), when it comes to unit production costs. On the portfolio level, a multi-objective economic analysis can result in major economic savings in terms of construction costs and even more in terms of production costs. In terms of production costs, building large dams is not rational, except if exploiting the full hydro-power potential is required. Instead, a combination of medium upstream dams is most economic. With the price of other renewables strongly dropping, it might be speculated that large dams could be outcompeted in near future.

Multiple studies pointed out the conflict between dams and ecosystem services (*Ziv et al.*, 2012; *Kondolf et al.*, 2014; *Wild and Loucks*, 2014) in the Mekong. Based on the economic and ecologic portfolio analysis, we find that portfolios with less, well placed dams tend to be cheaper and reduce the impact on sediment trapping by an order of magnitude. The analysis also quantified the relevance of most downstream dams as determinant for

network sediment trapping. For a given downstream dam, it is rational to develop the upstream dam cascade in order to optimize costs and production without additional impacts on sediment fluxes. The most relevant result of the trade-off analysis is that there is a synergy between cheap and low-impact hydro-power in the 3S. For both objectives, developing the upper Se San and Se Kong cascades would have been the strategy of choice. Reasonably, it can be argued that this might not be hold for all river networks. Yet, it shows how the spatial distribution of dam-sites, and the spatial distribution of fluvial processes can allow for low impact hydro-power development based on environmental and economic portfolio analysis.

For concrete decision support, additional research would need to be directed on several aspects. First, it is assumed that the representation of sediment transport processes which serves as indicator for dam impacts, is accurate. Yet, this assumption would need careful validation, because the spatial distribution of pre-disturbance sediment transport in the basin has a major impact on the results. Very recently, some network planning approaches have been published based on purely topologic indicators (i.e., length of river network disconnected by a dam portfolio) that can be derived very readily developed from global datasets (e.g., *Opperman et al.* (2015) based on *Lehner et al.* (2008) and *Zarfl et al.* (2014)). Instead, results from the 3S showed that the spatial distribution of river processes is a key determinant for the impact of dam portfolios. A comparative analysis between optimal dam portfolios identified using topological and process oriented indicators (e.g., derived from CASCADE) could clarify limitations and applicability of both approaches. This analysis also assumed that all dam sites are potentially ready to be developed. Yet, the absence of access roads or grid connections in the upper mountainous parts of the basin might favor dam developments in the lower basin and along mainstem rivers. We also did not consider any effects on local populations or on other ecosystem functions. Additionally, we analysed dam portfolios as if they would all belong to the same market. Instead, the 3S is shared between three nations and missing transmission lines and strong national interests add an additional level of complexity. We also assumed that hydro-power is the only benefit provided by dams, but other benefits such as water storage or flood protection might be importnat criteria for decision making.

To conclude, this chapter showed for a real-world case-study how adopting a network perspective has a major potential to maximize economic and ecologic performance of hydro-power portfolios. This research is just the beginning of such studies. Nevertheless, it might be timing given that dam development is moving more and more towards private investors that might have little interest in adopting a larger perspective on hydro-electric develop-

ments. Our results urge, instead, for planning and oversight of hydro-power development on the scale of river networks and considering multiple economic and ecologic objectives.

CHAPTER 7

Conclusion

THIS thesis addressed how to model sediment connectivity on the scale of large, data-scarce river basins and how to include resulting information into network scale dam planning. Sediment connectivity has recently become of strong interest in water resources planning and management. This is because, after half a century of large dam construction, it has become evident that sediment trapping in dams is an important mechanism behind negative externalities of dams, both on local and network scales. This raises concerns regarding the currently ongoing boom of hydro-power dam construction in poorly monitored, large river basins, and the potential impact on eco-systems, eco-system services, and finally human livelihoods. On the one hand, the current hydro-power development in so far little developed river basins opens up opportunities to design low-impact developments that balances economic objectives with eco-system integrity. On the other hand, large spatial scales, absence of data, conflicting objectives and the large number of potential development strategies hinder informed decision making and impose a great risk to damage fluvial ecosystems. This research had the ambition to present how these challenges might be addressed in the future through new model and data analysis approaches for network sediment transfers and river hydro-morphology.

This chapter synthesizes key findings and identifies deficiencies in the

proposed modelling approach, with a special focus on process representations. Based on this discussion, potentials and needs for future research are clarified. This includes also some outlook on how application of new sensors and data-analysis techniques will help to progress the understanding of network sediment transfers in future. Third, this chapter concludes the experience of multiple years of analyzing sediment and hydro-morphologic dataset in large rivers in emerging economies. Therefore, a section introduces thoughts on how to best analyze and exploit few available data in poorly monitored river basins. This chapter closes with some practical recommendations on how comprehensive numerical analysis supports developing low impact hydro-power in fluvial systems.

7.1 Key findings

Model development

First result of this research was the development of the CASCADE framework for network sediment connectivity. The rationale behind developing CASCADE was to develop a numerically effective, parsimonious modelling framework that opens opportunities for integrating sparse data and approaching large-scale planning tasks. CASCADE is built based on a simplified representation of hydrology, processes, and results in instantaneous spatial maps of basin sediment transfers. Nevertheless, the development of CASCADE had the ambition to not only simplify process representations and make sediment transport modelling computationally more effective, but also to add a new perspective on network sediment transfers. Therefore, we combined the explicit tracking of multiple sediment cascades with nework-scale sediment balances. CASCADE relies on the availability of some hydrographs and otherwise mainly on remotely sensed information that is globally available. This information is transformed into fractional (i.e., specific for a given grain size) transport rates for sediment supplied from many sediment sources. The transformation is based largely on common sediment transport formulas. The result is an information on transport capacity for each grain size in each reach of the river network. Based on a graph-based scheme and the derived transport capacities, the transport of sediment from each source is tracked throughout the river network, identifying where sediment of a certain grain size is potentially deposited, and quantifying the fractional sediment fluxes in the entire river network.

Case study specific findings

This research presented the application of CASCADE to two different case studies. Broadly, it can be stated that the Da River case study served as proof

of concept for the modelling framework, and for introducing data analysis for resulting information on sediment connectivity. The 3S case study was used to show how information of sediment connectivity can be used for river basin management, and how CASCADE can derive that information. Yet, while each case-study was analyzed with a specific objective, there are many points that can be substantiated for both case studies. Independently from the case study, the parameterization of sediment sources is crucial, because the properties (grain size, sediment supply) of sources have a direct impact on a) where which grain size is present in the network and b) with which rates it is subsequently transported. In each case study, parameterization of sediment sources was approached with a different technique. In the first case study (Da River), sediment sources were parametrized deterministically based on hydraulic equilibrium considerations. In the second case study (3S Rivers), parameterization of sediment sources was done based on an inverse stochastic approach. For both approaches, CASCADE predicted sediment transport rates that are in line with observations (keeping in mind that there were only very few observations), and, for the 3S case study, also within observed sediment composition (i.e., distribution of grain sizes in the bed material).

Model initialization

Uncertainty in network sediment transfers and grain size composition is high. For the 3S basin, the inverse modelling approach gave an indication of model sensitivity to source grain sizes. The results indicate that the network can accommodate sediment fluxes that span orders of magnitude in function of the grain size initializations. This is in line with more detailed studies on the sensitivity of sediment transport formulas (e.g., *Pinto et al.* (2006)). In general, it challenges the application of deterministic modelling approaches for larger river networks, except for when source grain sizes and supply rates are well defined throughout the network. This has practical consequences for how to approach sediment connectivity modelling in data-scarce environments. Without data provided in *Koehnken* (2012a,b) and *Bravard et al.* (2014) no formulation of a stochastic inverse modelling problem would have been feasible. Hence, there would have been no possibility to constrain the absolute sediment transport and composition from the 3S. Nevertheless, the results for the 3S indicate that the inverse approach can derive relevant results even where no sediment observations are available. The inverse approach identified patterns of sediment provenance based on the distribution of channel hydro-morphology throughout the river network of the 3S. Sediment flux from the three sub-basis was significantly different, independent from the source initialization. Hence, while the absolute

figures might be off by orders of magnitude, the relative spatial pattern of sediment provenance can likely be identified using even a single grain size for all sediment sources. This is also in line with findings for the Da River, where random disturbances of sediment source grain sizes led to a change in the quantity but not the overall spatial patterns of sediment provenance. A very strong alteration of source grain sizes, i.e., on the order of magnitudes, changed both magnitude and spatial pattern of provenance. Hence, we propose that CASCADE can be used even in very data-scarce environments for a first screening, as long as at least the general character of rivers and sediment sources (i.e., sand vs gravel dominated) is known. This information should be available now for most rivers from freely available, high resolution satellite imagery. Yet, many additional source of information can be assimilated in the framework, and every additional observation can greatly increase model accuracy as shown for the 3S case study.

Consideration of hillslope processes

CASCADE does not explicitly consider hillslope processes. For now, each implementation assumed that a balance between channel and hill-slope processes. For example, in the inverse modelling of the 3S basin, we assigned a sand supply rate such that supply from a source equaled the downstream transport capacity. But, there was no specification if sediment is derived from channel or hillslope sources. The results shows that the supply is well-correlated to reach slope and stream power in the reaches. Assuming that the majority of sediment is delivered from hillslope processes this implies that hillslope processes around steeper reaches are potentially more productive. This is in line with empirical observations (*Montgomery and Buffington*, 1997) and model results (*Willgoose et al.*, 1991; *Tucker and Bras*, 1998). These studies show that hillslopes are steeper and better connected to channels in higher gradient up-land rivers with potentially active incision (*Sklar et al.*, 2006). Mechanistically, it seems therefore reasonable to assume that steeper channels receive more sediment from both channel and hillslope erosion.

Quantifying multi-scale sediment connectivity

This research pointed out that local sediment transport must be analyzed from a network perspective. Even in the large river basins under study, processes of supply and transport from remote sources can have a major impact on the sediment balance of downstream reaches. For the Da River, some remote sources in otherwise gravel dominated headwaters can supply sand (which is also visible from the collected pictures of river channels) through the entire network to the basin outlet. In the 3S, this pattern is even more em-

phasized, as results indicate that a majority of sediment flux originates from headwaters and lower order river reaches. These results indicate that caution must be taken for local assessment of sediment transport in higher order river reaches without considering the nework-scale patterns of sediment connectivity. This conclusion resonates with calls, e.g., by *Brierley and Fryirs* (2005) to interpret local fluvial forms and processes nested within a hierarchy of nework-scale sediment transfers. This research provides quantitative evidence for how network sediment connectivity is a multi-scale, multi-domain property of fluvial systems. On smaller scales, it is a common-place in geomorphologic reasoning that observed fluvial forms and processes are the results of the magnitude, composition, and timing of sediment inputs (*Linde et al.*, 2015). Here, this work provides evidence, how these concepts can be pushed to larger scales through numerical modelling. The ability of CASCADE to track individual sediment cascades on nework-scales is central to derive network indicators of sediment connectivity. Results also concretize how these indicators can be used for studying specific processes for concrete river systems. For example, for identifying grain size specific "bottlenecks" (*Fryirs and Brierley*, 2001) for sediment transfers, studying the network sediment "conveyor belt" (*Kondolf*, 1994), or identifying fluvial "transport filters" (*Meybeck and Vörösmarty*, 2005; *Attal and Lavé*, 2006) in large river networks. This research puts forward evidence that all of these concepts are relevant, but adds a quantitative component that was so far limited to very few, well studied river basins.

Applying CASCADE for network scale hydro-power planning

Sediment connectivity is a concept of management relevance. This claim was brought forward recently e.g., by (*Bracken et al.*, 2015; *Parsons et al.*, 2015) and was substantiated most clearly for the 3S case study. Conceptualizing sediment transport in the 3S network as connected transfer of sediment between multiple sediment sources and the Mekong River allowed to quantify sediment provenance in the basin. The concept of a source specific connectivity in function of the source grain size was a prerequisite for the proposed inverse modelling exercise. The inverse modelling allowed then to reconcile information from different data sources. Sources covered different domains (e.g., hydrology, lithology, sedimentology) and various spatial scales (single observations, multi-point observations in space and/or time, spatially continuous maps). This information was synthesized into a nework-scale estimate of sediment flux and composition. It is noteworthy that this information could not have been derived from any of the individual data sources without the model derived knowledge on the connected functioning of the river system. This information was then used for a concrete

planning exercise.

This research set out to identify the impact of hydro-power dams on network sediment transfers and the opportunity to reduce these impacts using a model-driven, exhaustive analysis of hydro-power portfolios. This required linking fluvial connectivity, on the one hand, and reservoir hydraulics, reservoir engineering and design, and reservoir economics on the other hand. Making this link was greatly facilitated by the model structure of CASCADE that allowed to readily transfer concepts of fluvial connectivity to in-reservoir sediment routing. This research showed how a portfolio of hydro-power sites opens a wide decision space for identifying spatial configurations of dams that, for a desired level of hydro-electric production, minimize the impact on network sediment connectivity. At the same time, based on the research on 3S we put forward the idea that river networks might have a specific carrying capacity for hydro-power developments. Up to that carrying capacity, hydro-power can be developed with a limited impact on fluvial processes. Installing hydro-electric facilities beyond that capacity will result in an over-proportional impact. For the 3S, this research showed that this carrying capacity links strongly to the spatial pattern of sediment provenance, on the one hand, and the spatial distribution of dam sites, on the other hand. The historic and currently pursued development strategy in the 3S is driven not by strategic, transnational planning of reservoir portfolios on basin-scales, but by particular national or private economic interests. Here, the results show how such the absence of network portfolio planning results in over-proportional impacts on fluvial processes, both in the 3S, and then likely also in the downstream Lower Mekong River and Mekong River Delta, for a given level of hydro-power production. Last, our results indicate, that dam portfolios that minimize conflicts between connectivity and energy production would have had competitive unit production prices. Such portfolios have in common that they omit the construction of very large downstream dams. These "mega dams" have very high environmental impacts, but do not necessarily provide energy at lower unit production costs than lower-impact, upstream dams.

7.2 Limitations and future research

Despite the potential of CASCADE to analyze network sediment transfers, some key challenges remain. The computational efficiency of cascade, with a runtime of few seconds for the presented case studies, is at the cost of a statistical handling of time. Instead of modelling the full temporal sequence of sediment transfers, a time-averaged "snapshot" of connectivity is derived that represents a statistical measure over a prolonged period of time. This is a limitation for studying systems and research questions where fast tem-

poral dynamics (e.g., from land-sliding, see *Bennett et al.* (2014)), or time-variable effects such as hysteresis are of importance (e.g., *Walling* (1977); *Slaets et al.* (2016)). Here, some initial experiments indicated that this limitation might be addressed by parametrizing CASCADE with discharge time series that cover shorter, discrete periods, i.e., certain months, or certain seasons. The result of this discrete approach are static maps as well, but for a specific period of time. These maps can then be analyzed in their sequence to estimate changes in sediment connectivity over time. Similarly, care must be taken when applying CASCADE to evaluate impacts of climate change on sediment connectivity, in future. For such studies it should be taken into account that the time-scales of climate change might be much faster than the time-scales of network sediment connectivity. In CASCADE it is so far always assumed that connectivity is established between all sources and sinks. Yet, under rapid change, detachment rates at the sources might change much faster than the time-scales on which these sources connect to downstream sinks. Hence, sediment connectivity under rapid change and non-stationary conditions would be an overlay of pre- and post-disturbance conditions.

Network-scale balance of source supply and transport capacity

Assuming a network balance between sediment supply and transport capacity is key for the proposed inverse model initialization, in which supply of sediment sources is limited such that the downstream transport capacity is not exceeded. This assumption seemed to be justified for the 3S case study, given the absence of sediment accumulation in the river basin. Nevertheless, zones of sediment storage, where sediment is actively deposited, are a common feature in many river systems (*Fryirs and Brierley*, 2001; *Meybeck and Vörösmarty*, 2005). Hence, cases where sediment storage coincides with reaches with low local transport capacity are possible. In this case, setting the supply of sediment sources upstream of a sediment storage equal to the transport capacity of the related sediment cascades in that storage would result in an underestimation of source supply. This would also result in an underestimation of sediment fluxes in the river network upstream of the sediment storage. Such an underestimation of sediment flux upstream of a storage zone could impact certain management tasks. For example, lead to an underestimation of siltation risks in dams upstream of the sediment storage. Hence, in cases where a transport capacity limited reach coincides with an area of active sediment storage, CASCADE should be coupled to local sediment budgets to justify the application of the proposed inverse reasoning. Such a coincidence between a sediment storage and low capacity-limited reach should be identifiable based on remote sensing evidence in most settings. Then, the area of sediment storage, and an estimates of accretion rate,

and sediment density can be used to estimate by how much sediment inputs exceed local transport capacity (Trimble and Crosson, 2000). The estimate on how much upstream source supply exceeds local transport capacity can then be used to parametrize upstream sources.

Additional fluvial and hillslope processes

Issues of sediment storage and transport capacity limitations are directly linked to three other limits of the CASCADE framework. First is the lack of attrition. For example, in the Da River, many upstream sources of coarse sediment can never connect to the basin outlet, because hydrodynamic forces in the downstream network never exceed the threshold of motion for large grain sizes. Instead, the information on travel time along a sediment cascade could be used to reduce the grain size along a sediment cascade as it traverses the river network. Second, is the lack of morphologic adaptation, i.e., in cases where the local transport capacity is exceeded for prolonged times, deposition could lead to a change in slope, and an increase in transport capacity. Again, also for this task, additional research would be required to investigate efficient and consistent ways of introducing time in the CASCADE framework. Third, CASCADE should be extended for considering a more detailed evaluation of how sediment is exchanged between floodplains and river channels. For example, the hydro-dynamic solver of CASCADE could be readily coupled with a module for on-floodplain hydraulics. DEM extracted floodplain extents (Schmitt et al., 2014), an estimate of frequency for overbank flows, and the fractional transport capacity on the floodplains could then be calculated to estimate the exchange of sediment between channels and floodplains. It could also be informative to study the correlation between CASCADE results and hillslope processes in more detail. Towards this, either conceptual models of hillslope processes (e.g., *Sklar et al.* (2016)) or hillslope-channel connectivity (e.g., *Heckmann and Schwanghart* (2013); *Cavalli et al.* (2013)) could be compared to CASCADE, or even integrated in the modelling framework. Additionally, the CASCADE framework can be expanded without modification to consider multiple sources per reach, hence, sediment deliveries from hillslope processes could be explicitly added to the framework.

Representation of fractional transport rates

All the above limitations are always based on the assumption that the representation of fractional transport rates in CASCADE, i.e., the scenarios that are proposed in chapter 3, are appropriate for representing the different rates with which sediment of different grain size is transported under the same hydrodynamic forces. Some discussion of empirical and theoretical consid-

erations with this regard are given in the relevant chapter (chapter 3). Here, the developed "scenarios" for fractional transport will be discussed in relation to some of the most common, empirical fractional transport formulas of (*Wilcock and Crowe*, 2003) (for sand and gravel mixtures) and the review of fractional transport of sand transport in (*Molinas and Wu*, 2000). Throughout this research, mainly Scenario 1 and 3 was used. Scenario 1 assumes that a river reach has a certain local transport capacity defined by local hydro-morphology and the grain size supplied from upstream sources. This total transport capacity is converted to fractional transport capacities using a non-linear function based on common sediment transport formulas. Scenario 3, instead, sets transport capacity for a sediment cascade proportional to source supply, again corrected for the presence of other grain sizes using a non-linear function based on common sediment transport formulas. In general, Scenario 3 was applied widely for this work. Because local transport capacity is a function of supply, Scenario 3 results in a more homogeneous redistribution of sediment. In contrast Scenario 1, results in a more "stepwise" redistribution of sediment. I.e., where these "steps" occur, transport capacity is low (transport capacity limitation). In most other reaches, transport capacity is sufficient to transport the supplied sediment. This indicates that the river network, except for some limiting reaches, is mainly supply limited. Yet, at these limiting reaches large rates of deposition occur. Hence, by selecting scenario 3, we apply a first level of inverse reasoning, assuming that the network should be largely able to transport the sediment supply. As an alternative approach to maintain connectivity, *Gran and Czuba* (2015), set the transport capacity in a reach either to the transport capacity of the next upstream reach, or to an expert-defined minimum value if a minimum threshold for transport capacity was not met. It should be noted, that the need for such a correction, or the application of Scenario 3, is an adaptation to low DEM resolution. Higher-resolution topographic data will likely result in a much better ability to judge were transport capacity is actually low and where low transport capacity is an artifact of the available digital elevation data.

Comparing CASCADE scenarios to empirical fractional transport formulas, three main limitations become obvious, especially where sand-gravel mixtures are transported (i.e., especially in the Da River). First, in CASCADE fine fractions are transported at the cost of a lower transport capacity for larger fractions for all scenarios. Instead, empirical evidence suggest that the presence of large fractions might result in a hiding of fines behind larger grains and a lower transport capacity for fines (*Wilcock and Crowe*, 2003). Second, in fractional transport models, such as *Wilcock and Crowe* (2003), fractional transport capacities are a nonlinear function of bed-shear

stress, with the differences in fractional transport capacities decreasing for higher bed-shear stress. In CASCADE, fractional transport capacities are calculated as function of transport capacities for single grains. Hence, transport capacities for smaller grain sizes over-proportionally increase for higher bed-shear. These limitations are partially due to the CASCADE approach, which requires to calculate transport capacities *a-priori*. Fractional transport capacity models would, instead, require to continuously update transport capacities in all reaches, because transport capacity would be a direct function of sediment composition. Sediment composition would then change as more cascades connect within the network. A two- or multi-stage approach could be applied to derive a first estimate of grain size composition and then to calculate a final value for transport capacity. Last, CASCADE always assumes that the bed material composition is defined by the mass-fraction of each grain sizes. Yet, in real rivers coarse material is concentrated on the bed-surface, such that it is more prone for being transported. Hence, differences in transport capacity is equilibrated, and hiding effects for finer grains (see above) are additionally equilibrated by the vertical sorting of sediment. Vertical sorting then reduces the fraction of fine grains that is actually present on the bed, and that can be transported. This effects can then lead to equal mobility and equal transport rates for different grain size fractions (*Parker and Toro-Escobar*, 2002). In sand-bed rivers, effects due to heterogeneous grain size distributions are likely less emphasized. For sand-bed rivers, Scenario 3 is similar to the " TCF" (Transport Capacity Fraction) approaches in *Molinas and Wu* (2000), if it can be assumed reasonable that the total transport capacity in a reach is defined by the sediment supply. As mentioned before, CASCADE seems to represent sediment transport at the outlets of the basins under study well. But for both river systems are major sandy rivers at their outlet. Hence, CASCADE should be tested for smaller rivers with mixed sand gravel beds, and if possible a transition between sand and gravel. Such a transition would be a good testing ground for whether cascade could predict where sand begins to dominate over gravel transport (*Venditti et al.*, 2015).

7.3 Planning with connected sediment transfers in data-scarce environments

Implementing the Da/Red River and the 3S case studies required reviewing many sources of scientific literature, as well as numerous reports and other kinds of "grey" literature. This literature review included many other river systems, especially in South East Asia. The results of this work can be informative also for other river basins. In general, as pointed out by many scholars, data on sediment transport are extremely scarce, and where they exist,

hard to obtain. Much scientific research and planning oriented assessments are based on decade-old data-sets. While the validity of these data-sets can often be hardly validated, today, they are re-cited until today (as pointed out by *Le et al.* (2007) for the Red River).

Global datasets

For example, in 1983 Milliman and Meade (*Milliman and Meade*, 1983) compiled sediment data for the world's 20 rivers with the highest sediment flux. The data-sources for this study are mostly disclosed, but date back to the late 1960ies and most of them are not accessible anymore, today. Nevertheless, this work is still widely cited in sediment related studies. A meta-analysis of citations using the online service Web of Science reveals that Milliman and Meade's 1983 work was still cited by 173 papers in 2015 and 2016 [1] - more than 10 % of its total citations (1648). Recent citations span all fields of research, from protection of shorebirds (Melville et al., 2016), regional sediment management (Wu et al., 2015; Zhao et al., 2015), to continental and global scales studies in high-level journals (Galy et al., 2015; Nie et al., 2015). This analysis is informative because it shows, on the one hand, the relevance of sediment transport estimates in many different disciplines of science and environmental management. The reliance of research on this decade old data show, on the other hand, the limited alternatives regarding more recent or more case specific data. For the case studies in this work, these global data were barely in the right order magnitude compared to newer analysis of sediment data (for the Red River see the analysis in chapter 2, for the Mekong, refer to *Koehnken* (2012a,b)).

Global empirical models of sediment provenance

It is interesting to observe how data-scarce the case studies in this research were in a global context, and how the global absence of sediment transport data can be addressed. Much of this research on Asian rivers was motivated by an apparent data-scarcity, which hindered the application of many common, hydrodynamic models for network sediment transport. Nevertheless, the two studied river systems are definitely not amongst the most data-scarce environments. For the lower Mekong, at least 67 sediment sampling stations with up to 80 years of records (in total 2026 data-years) exist, though the data of most stations are not publicly available (see `http://portal.mrcmekong.org/`). In Africa, where not most (*Zarfl et al.*, 2014), but some of the largest and most controversial hydroelectric schemes are planned (*Showers*, 2011; *Green et al.*, 2015), a total of 377

[1] `http://apps.webofknowledge.com/CitationReport.do?action=home&SID=3FXMxLzbcRnV8HG7TUT&product=WOS&cr_pqid=5&qid=5&search_mode=CitationReport`

sediment gauges with 1714 years of record exist (*Vanmaercke et al.*, 2014). Hence, there are less data-years of gauge records available on the African continent than for the Lower Mekong River Basin. Given the large temporal variability in sediment transfers and increasing instationarity due to human activities *Walling and Fang* (2003), short term sediment measurements will become increasingly inaccurate in the future. Even where resources are available for monitoring or measuring, e.g., as preparation for a dam project, a single measuring campaign could not replace historic time series, because sediment transport processes typically display large variations in both time and space (*Lenzi et al.*, 2003). Often empirical models (e.g., QBART, *Syvitski and Milliman* (2007)) are applied when planning for poorly or un-monitored river basins. This might be because such models provide a rapid way of transferring factors that link intuitively to sediment generation in a basin (relief, land use, climate, human activities) to sediment yields. It should be considered that e.g. the QBART model even during model calibration derivated by up to an order of magnitude from the data used for calibration (*Syvitski and Milliman*, 2007). This uncertainty is likely strongly emphasized when applying such an empirical model to different, ungauged catchments. A major limitation of all empirical models and global sediment load data-bases is that they focus only on suspended sediment and neglect the role of bed load. Bed load transport is instead often estimated from global observations of bed-load/suspended-load ratios (e.g., *Turowski et al.* (2010)) or it is argued that bed-load is of limited management relevance, because it constitutes typically less than 10 % of total load (*Walling and Fang*, 2003) . In contrast, bed-load is, much more than suspended load, a driver behind many geomorphic processes in both rivers and deltas (*Bravard et al.*, 2014; *Kondolf et al.*, 2014). For example, sand constitutes around 20 % of the sediment load of the Mississippi, but constitutes 70 % of the Mississippi delta (*Nittrouer and Viparelli*, 2014). For reservoir siltation, bed-load is also of relevance, because it is much more difficult to pass it through an impoundment, than finer, suspended fractions.

New data and models for sediment transport in large rivers

Some aspects of this research will hopefully help addressing that data-scarcity with regard to bed-load in large rivers. Especially, the inverse modelling approach has a major potential with that regard. As pointed out above, the inverse modelling can be applied to identify relative sediment provenance even without data for a proper formulation of the inverse problem. E.g., even just applying a single grain size for all sources is sufficient to extract the information on network sediment transfers from measured river hydro-morphology. River hydro-morphology can, in turn be extracted readily on

global scales, now, and major progress is immanent in the future. DEMs of 90 m resolution are available for nearly 80 % of the world (*CGIAR*, 2008) and are replaced by higher resolution DEMs in many places. For discharge, global data-sets of observations have been collected (*Fekete et al.*, 1998) and are freely available. For rivers that are not covered, global hydrologic models (*Döll et al.*, 2003) could help deriving discharge estimates. In future, inverse exploratory modelling with CASCADE has the potential to accommodate and cross-check data derived from very different sources. Such fluvial data-sources could range from citizen scientist (*Kennedy et al.*, 2016), to unmanned aerial vehicles (*Carbonneau*, 2005), and new remote sensing platforms (*Gilvear and Bryant*, 2016). All sources with different coverage in both space and time. Numerical models can then help to crosscheck data derived from these different sources and put them into a network perspective.

The computational efficiency of CASCADE was and will be a prerequisite for combining these data of variable spatial coverage, quality, and spatio-temporal resolution into a consistent, qualitative description of fluvial processes. Computational efficiency is key to address uncertainty, with regard to many processes (e.g., the above mentioned floodplain storage). Computational methods that require many runs, such as Monte Carlo Analyses, will be crucial for that task. Also, evaluating the impact of network portfolios of hydro-power plants is only possible with a computationally effective screening models, no matter if applied in an exhaustive search (as in this research), or in future optimization based approaches.

7.4 Low impact planning of hydro-power cascades

This research started out to study the link between water resources management, such as reservoir constructions, sediment transfers, and then eventually on eco-system services, in large rivers. Indeed, this study showed that the many possible portfolios of hydro-power dams resulting from a set of dam locations, can result in vastly different environmental impacts and economic benefits. Based on the findings for the 3S, some key points and future potentials should be made for planning for so far not or little developed basins.

First, this research hopefully substantiates that network-scale modelling allows for screening single reservoir locations as well as reservoir cascades, regarding sedimentation risks in the reservoir and the impact on downstream fluvial systems, at early planning stages. As per now, tools and guidelines for reservoir sediment management, such as the World Bank's " RESCON" approach (*Palmieri et al.*, 2003), are still extremely focused on single reservoir sites instead of acknowledging the connected functioning of river systems, and the potential cumulative effects of dams. In addition, " RESCON"

(which is one of the few approaches that is used for reservoir sediment management) proposes using generic sediment transport values at pre-feasibility levels, and adding rigorous numerical approaches only during later stages of the project cycle (*Palmieri et al.*, 2003, p. 49). Instead, results of this research show that rigorous numerical assessments, which are now feasible on network-scales, can be relevant, and should be included already at very early, i.e., site selection, stages.

Second, a strategic, nework-scale analysis of dam sites is crucial to balance economic interest and ecosystem integrity. This resonates strongly with calls by international organizations to include strategic network/basin scale portfolia analyses into dam planning. This is both to reduce negative cumulative impacts and to include a more transparent assessment on economic benefits and environmental impacts and costs (*World Commission on Dams*, 2000; *Jager et al.*, 2015). Motivating nework-scale planning will require above all increasing the ability to monetarize impacts of sediment starvation and related losses in eco-system services in a transparent way. This is relevant for planning hydro-power in trans-national basins, but also to balance upstream and downstream interests. In future, hydro-power planning could also include other (decentral) renewable energy alternatives into the planning process. It could be speculated that there is a mixture of decentralized energy sources and hydro-power dams that minimizes lifecycle costs, maximizes energy production, and minimizes impacts on the river system. For example, in the 3S, stakeholder might have been motivated to omit dam sites that exceed the hydro-power carrying capacity of the river, if it can be shown that the resulting gap to the full hydro-power potential can be bridged with other renewable energy sources at competitive prices. As per now, the current research seems to indicate that smaller, upstream dams might present the optimal trade-off between amount and costs of hydro-electricity and sediment connectivity. Our analysis of economic data also shows that smaller dams can be relatively cheaper than larger dams. Especially as smaller dams tend to incur less cost over-runs than larger dams (*Ansar et al.*, 2014), which is not yet considered in the analysis.

7.5 Closure

Concepts of connectivity are increasingly brought forward to advance river science in biology, hydrology, and geomorphology. This research provided evidence for how the developed CASCADE framework, coupled to various parameterizations based on globally available data-sets and or model-inferred data, can progress the quantitative characterization and understanding of complex processes in poorly monitored river systems. This research put forward evidence for the connected functioning of fluvial sediment cas-

cades over large spatio-temporal scales, and for how this information can be used to develop lower-impact management strategies. This research showed potential for future modelling of connected river processes, river hydro-morphology, eco-system services, and water resources management from a network perspective. This research seems to come timely given increasing populations, energy demands, climatic changes, and thereby further increasing strains on water resources and eco-systems in many of the world's large rivers.

Bibliography

Abell, R., M. L. Thieme, C. Revenga, M. Bryer, M. Kottelat, N. Bogutskaya, B. Coad, N. Mandrak, S. C. Balderas, W. Bussing, M. L. J. Stiassny, P. Skelton, G. R. Allen, P. Unmack, A. Naseka, R. Ng, N. Sindorf, J. Robertson, E. Armijo, J. V. Higgins, T. J. Heibel, E. Wikramanayake, D. Olson, H. L. López, R. E. Reis, J. G. Lundberg, M. H. S. Pérez, and P. Petry (2008), Freshwater Ecoregions of the World: A New Map of Biogeographic Units for Freshwater Biodiversity Conservation, *BioScience*, *58*(5), 403–414, doi:10.1641/B580507.

Agency, I. E. (2012a), Technology Roadmap Hydropower, *Tech. rep.*, Paris, France.

Agency, I. E. (2015), World Energy Outlook Special Report on Southeast Asia 2015, *Tech. rep.*, International Energy Agency, Paris, France.

Agency, I. R. E. (2012b), IRENA Working paper: Hydropower, *Tech. Rep. Volume 1: Power sector, Issue 3/5*, International Renewable Energy Agency, Bonn, Germany.

Alcamo, J. M., C. J. Vörösmarty, R. J. Naiman, D. P. Lettenmaier, and C. Pahl-Wostl (2008), A grand challenge for freshwater research: Understanding the global water system, *Environmental Research Letters*, *3*(1), 010,202, doi:10.1088/1748-9326/3/1/010202.

Andrews, E. D. (1983), Entrainment of gravel from naturally sorted riverbed material, *Geological Society of America Bulletin*, *94*(10), 1225–1231, doi:10.1130/0016-7606(1983)94<1225:EOGFNS>2.0.CO;2.

Andrews, E. D. (1991), Sediment transport in the Colorado River basin, in *Colorado River Ecology and Dam Management: Proceedings of a Symposiuni May 24-25,*, pp. 54–74, Santa Fe, New Mexico.

Andrews, E. D., and R. C. Antweiler (2012), Sediment Fluxes from California Coastal Rivers: The Influences of Climate, Geology, and Topography, *The Journal of Geology*, *120*(4), 349–366, doi:10.1086/665733.

Annandale, G. (2013), A Climate Resilient Mekong: Sediment Pass-Through at Lower Se San 2, *Tech. rep.*, NHI, San Francisco.

Ansar, A., B. Flyvbjerg, A. Budzier, and D. Lunn (2014), Should we build more large dams? The actual costs of hydropower megaproject development, *Energy Policy*, *69*, 43–56, doi:10.1016/j.enpol.2013.10.069.

Anthony, E. J., G. Brunier, M. Besset, M. Goichot, P. Dussouillez, and V. L. Nguyen (2015), Linking rapid erosion of the Mekong River delta to human activities, *Scientific Reports*, *5*, 14,745, doi:10.1038/srep14745.

Archer, D. R. (1989), Flood wave attenuation due to channel and floodplain storage and effects on flood frequency, *Floods: Hydrological, Sedimentological and Geomorphological Implications. John Wiley & Sons New York. 1989. p 37-46. 5 fig, 8 ref.*

Arnaud-Fassetta, G. (2004), The Upper Rhône Delta Sedimentary Record in the Arles-Piton Core: Analysis of Delta-Plain Subenvironments, Avulsion Frequency, Aggradation Rate and Origin of Sediment Yield, *Geografiska Annaler: Series A, Physical Geography*, *86*(4), 367–383, doi:10.1111/j.0435-3676.2004.00238.x.

Asselman, N. E. M. (2000), Fitting and interpretation of sediment rating curves, *Journal of Hydrology*, *234*(3–4), 228–248, doi:10.1016/S0022-1694(00)00253-5.

Attal, M., and J. Lavé (2006), Changes of bedload characteristics along the Marsyandi River (central Nepal): Implications for understanding hillslope sediment supply, sediment load evolution along fluvial networks, and denudation in active orogenic belts, *Geological Society of America Special Papers*, *398*, 143–171.

Attal, M., and J. Lavé (2009), Pebble abrasion during fluvial transport: Experimental results and implications for the evolution of the sediment load along rivers, *Journal of Geophysical Research: Earth Surface*, *114*(F4), F04,023, doi:10.1029/2009JF001328.

Bank, T. W. (2004a), Power System Development Plan for Lao PDR. FINAL REPORT. Volume C : Project Catalogue, *Tech. rep.*, The World Bank, Washington, DC.

Bank, T. W. (2004b), Power System Development Plan for Lao PDR. FINAL REPORT. ume A : Main Report, *Tech. rep.*, The World Bank, Washington, DC.

Bank, T. W. (2016), Global Economic Prospects 2016, `http://www.worldbank.org/en/publication/global-economic-prospects`.

Barr, S. M., and A. S. MacDonald (1981), Geochemistry and geochronology of late Cenozoic basalts of Southeast Asia, *Geological Society of America Bulletin*, *92*(8 Part II), 1069–1142.

Bechtol, V., and L. Laurian (2005), Restoring straightened rivers for sustainable flood mitigation, *Disaster Prevention and Management: An International Journal*, *14*(1), 6–19, doi:10.1108/09653560510583806.

Benda, L., and T. Dunne (1997a), Stochastic forcing of sediment routing and storage in channel networks, *Water Resources Research*, *33*(12), 2865–2880, doi:10.1029/97WR02387.

Benda, L., and T. Dunne (1997b), Stochastic forcing of sediment supply to channel networks from landsliding and debris flow, *Water Resources Research*, *33*(12), 2849–2863, doi:10.1029/97WR02388.

Benda, L., N. L. Poff, D. Miller, T. Dunne, G. Reeves, G. Pess, and M. Pollock (2004a), The Network Dynamics Hypothesis: How Channel Networks Structure Riverine Habitats, *BioScience*, *54*(5), 413–427, doi:10.1641/0006-3568(2004)054[0413:TNDHHC]2.0.CO;2.

Benda, L., K. Andras, D. Miller, and P. Bigelow (2004b), Confluence effects in rivers: Interactions of basin scale, network geometry, and disturbance regimes, *Water Resources Research*, *40*(5), W05,402, doi:10.1029/2003WR002583.

Bennett, G. L., P. Molnar, B. W. McArdell, and P. Burlando (2014), A probabilistic sediment cascade model of sediment transfer in the Illgraben, *Water Resources Research*, *50*(2), 1225–1244, doi: 10.1002/2013WR013806.

Betrie, G. D., Y. A. Mohamed, A. van Griensven, and R. Srinivasan (2011), Sediment management modelling in the Blue Nile Basin using SWAT model, *Hydrol. Earth Syst. Sci.*, *15*(3), 807–818, doi:10.5194/hess-15-807-2011.

Biswas, A. K. (2004), Dams: Cornucopia or disaster?, *International Journal of Water Resources Development*, *20*(1), 3–14, doi:10.1080/0790062032000170571.

Bizzi, S., and D. N. Lerner (2013), The Use of Stream Power as an Indicator of Channel Sensitivity to Erosion and Deposition Processes, *River Research and Applications*, pp. n/a–n/a, doi:10.1002/rra. 2717.

Bizzi, S., F. Pianosi, and R. Soncini-Sessa (2012), Valuing hydrological alteration in multi-objective water resources management, *Journal of Hydrology*, *472–473*, 277–286, doi:10.1016/j.jhydrol. 2012.09.033.

Bizzi, S., Q. Dinh, D. Bernardi, S. Denaro, L. Schippa, and R. Soncini-Sessa (2015a), On the control of riverbed incision induced by run-of-river power plant, *Water Resources Research*, *51*(7), 5023–5040, doi:10.1002/2014WR016237.

Bizzi, S., L. Demarchi, R. C. Grabowski, C. J. Weissteiner, and W. V. de Bund (2015b), The use of remote sensing to characterise hydromorphological properties of European rivers, *Aquatic Sciences*, *78*, 1–14, doi:10.1007/s00027-015-0430-7.

Bogachenko, P. T., B. I. Godunov, and T. P. Ne (1984), Characteristics of the first stage of constructing the Hoa-binh dam in Vietnam, *Hydrotechnical Construction*, *18*(12), 606–613, doi: 10.1007/BF01440643.

Bracken, L. J., L. Turnbull, J. Wainwright, and P. Bogaart (2015), Sediment connectivity: A framework for understanding sediment transfer at multiple scales, *Earth Surface Processes and Landforms*, *40*(2), 177–188, doi:10.1002/esp.3635.

Brandt, S. A. (2000), Classification of geomorphological effects downstream of dams, *CATENA*, *40*(4), 375–401, doi:10.1016/S0341-8162(00)00093-X.

Bravard, J. P. (1999), Environmental and societal effects of channel incision and remedial strategies., in *Incised River Channels: Processes, Forms, Engineering, and Management*, edited by G. M. Kondolf, H. Piégay, A. Simon, and S. E. Darby, pp. 303–341, J. Wiley, Chichester; New York, oCLC: 40193495.

Bravard, J.-P., M. Goichot, and S. Gaillot (2013), Geography of Sand and Gravel Mining in the Lower Mekong River, *EchoGéo*, (26), doi:10.4000/echogeo.13659.

Bravard, J.-P., M. Goichot, and H. Tronchère (2014), An assessment of sediment-transport processes in the Lower Mekong River based on deposit grain sizes, the CM technique and flow-energy data, *Geomorphology*, *207*, 174–189, doi:10.1016/j.geomorph.2013.11.004.

Bray, D. (1987), *A Review of Flow Resistance in Gravel Bed Rivers*, Leggi Morfologichee loro verifica del Campo, Editoriale BIOS-Cosenza, Università di Calabria, Cosenza.

Brierley, G., K. Fryirs, and V. Jain (2006), Landscape connectivity: The geographic basis of geomorphic applications, *Area*, *38*(2), 165–174, doi:10.1111/j.1475-4762.2006.00671.x.

Brierley, G. J., and K. A. Fryirs (2005), *Geomorphology and River Management: Applications of the River Styles Framework*, Blackwell Pub., Malden, MA, oCLC: 55487967.

Brismar, A. (2002), River Systems as Providers of Goods and Services: A Basis for Comparing Desired and Undesired Effects of Large Dam Projects, *Environmental Management*, *29*(5), 598–609, doi:10.1007/s00267-001-0058-3.

Brown, C. B. (1943), Discussion of sedimentation in reservoirs, *Proc. Am. Soc. Civil Eng.*, *69*, 1493–1500.

Brownlie, W. R. (1982), Prediction of flow depth and sediment discharge in open channels, *Tech. Rep. Rep. No. KH-R-43A*, W. M. Keck Laboratory of Hydraulics and Water Resources, California Institute of Technology, Pasadena, Ca.

Brune, G. M. (1953), Trap efficiency of reservoirs, *Eos, Transactions American Geophysical Union*, *34*(3), 407–418.

Buffetaut, E. (2009), *Late Palaeozoic and Mesozoic Ecosystems in SE Asia*, Geological Society of London.

Buffington, J. M., and D. R. Montgomery (1997), A systematic analysis of eight decades of incipient motion studies, with special reference to gravel-bedded rivers, *Water Resources Research*, *33*(8), 1993–2029, doi:10.1029/96WR03190.

Burneikis, J., D. Streimikiene, and P. Punys (2001), Technical, economic and environmental feasibilities of Nemunas hydro energy utilization, in *Hydropower in the New Millennium: Proceedings of the 4th International Conference Hydropower, Bergen, Norway, 20-22 June 2001*, edited by B. Honningsvag, G. H. Midttomme, K. Repp, K. Vaskinn, and T. Westeren, CRC Press, google-Books-ID: nfGPXqfQ91cC.

Carbonneau, P. E. (2005), The threshold effect of image resolution on image-based automated grain size mapping in fluvial environments, *Earth Surface Processes and Landforms*, *30*(13), 1687–1693, doi:10.1002/esp.1288.

Carling, P. A. (2009), Chapter 5 - Geomorphology and Sedimentology of the Lower Mekong River, in *The Mekong*, edited by E. by and I. C. Campbell, Aquatic Ecology, pp. 77–111, Academic Press, San Diego.

Castelletti, A., F. Pianosi, and R. Soncini-Sessa (2008a), Integration, participation and optimal control in water resources planning and management, *Applied Mathematics and Computation*, *206*(1), 21–33, doi:10.1016/j.amc.2007.09.069.

Castelletti, A., F. Pianosi, and R. Soncini-Sessa (2008b), Water reservoir control under economic, social and environmental constraints, *Automatica*, *44*(6), 1595–1607, doi:10.1016/j.automatica.2008.03.003.

Castelletti, A., F. Pianosi, X. Quach, and R. Soncini-Sessa (2012), Assessing water reservoirs management and development in Northern Vietnam, *Hydrol. Earth Syst. Sci.*, *16*(1), 189–199, doi:10.5194/hess-16-189-2012.

Castelletti, A., H. Yajima, M. Giuliani, R. Soncini-Sessa, and E. Weber (2014), Planning the Optimal Operation of a Multioutlet Water Reservoir with Water Quality and Quantity Targets, *Journal of Water Resources Planning and Management*, *140*(4), 496–510, doi:10.1061/(ASCE)WR.1943-5452.0000348.

Cavalli, M., S. Trevisani, F. Comiti, and L. Marchi (2013), Geomorphometric assessment of spatial sediment connectivity in small Alpine catchments, *Geomorphology*, *188*, 31–41, doi:10.1016/j.geomorph.2012.05.007.

CGIAR (2008), SRTM 90m Digital Elevation Database v4.1 | CGIAR-CSI.

Cheung, A. K. L., D. O'sullivan, and G. Brierley (2015), Graph-assisted landscape monitoring, *International Journal of Geographical Information Science*, *29*(4), 580–605, doi:10.1080/13658816.2014.989856.

Chow, J., R. J. Kopp, and P. R. Portney (2003), Energy Resources and Global Development, *Science*, *302*(5650), 1528–1531, doi:10.1126/science.1091939.

Chow, V. T. (1959), *Open-Channel Hydraulics*, McGraw-Hill, New York.

Church, M. (2006), Bed Material Transport and the Morphology of Alluvial River Channels, *Annual Review of Earth and Planetary Sciences*, *34*(1), 325–354, doi:10.1146/annurev.earth.33.092203.122721.

Church, M., P. Biron, A. G. Roy, and P. Ashmore (2012), *Gravel Bed Rivers: Processes, Tools, Environments*, John Wiley & Sons.

Clift, P. D., G. D. Layne, and J. Blusztajn (2004a), Marine sedimentary evidence for monsoon strengthening, Tibetan uplift and drainage evolution in East Asia, *Continent-Ocean Interactions in the East Asian Marginal Seas, Geophys. Monogr. Ser*, *149*, 255–282.

Clift, P. D., G. D. Layne, and J. Blusztajn (2004b), Marine Sedimentary Evidence for Monsoon Strengthening, Tibetan Uplift and Drainage Evolution in East Asia, in *Continent-Ocean Interactions Within East Asian Marginal Seas*, edited by P. Clift, W. Kuhnt, P. Wang, and D. Hayes, pp. 255–282, American Geophysical Union.

Cormen, T. H., C. E. Leiserson, R. L. Rivest, and C. Stein (2001), *Introduction To Algorithms*, MIT Press.

Czuba, J. A., and E. Foufoula-Georgiou (2014), A network-based framework for identifying potential synchronizations and amplifications of sediment delivery in river basins, *Water Resources Research*, *50*(5), 3826–3851, doi:10.1002/2013WR014227.

Czuba, J. A., and E. Foufoula-Georgiou (2015), Dynamic connectivity in a fluvial network for identifying hotspots of geomorphic change, *Water Resources Research*, *51*(3), 1401–1421, doi:10.1002/2014WR016139.

Darby, S. E., J. Leyland, M. Kummu, T. A. Räsänen, and H. Lauri (2013), Decoding the drivers of bank erosion on the Mekong river: The roles of the Asian monsoon, tropical storms, and snowmelt: CLIMATE FLUCTUATIONS AND MEKONG RIVER BANK EROSION, *Water Resources Research*, *49*(4), 2146–2163, doi:10.1002/wrcr.20205.

de Vente, J., J. Poesen, P. Bazzoffi, A. V. Rompaey, and G. Verstraeten (2006), Predicting catchment sediment yield in Mediterranean environments: The importance of sediment sources and connectivity in Italian drainage basins, *Earth Surface Processes and Landforms*, *31*(8), 1017–1034, doi:10.1002/esp.1305.

Demarchi, L., S. Bizzi, and H. Piégay (2016), Hierarchical Object-Based Mapping of Riverscape Units and in-Stream Mesohabitats Using LiDAR and VHR Imagery, *Remote Sensing*, *8*(2), 97, doi:10.3390/rs8020097.

Dietrich, W. E., J. W. Kirchner, H. Ikeda, and F. Iseya (1989), Sediment supply and the development of the coarse surface layer in gravel-bedded rivers, *Nature*, *340*(6230), 215–217, doi:10.1038/340215a0.

Dijkstra, E. W. (1959), A Note on Two Problems in Connexion with Graphs, *NUMERISCHE MATHEMATIK*, *1*(1), 269–271.

Döll, P., F. Kaspar, and B. Lehner (2003), A global hydrological model for deriving water availability indicators: Model tuning and validation, *Journal of Hydrology*, *270*(1–2), 105–134, doi:10.1016/S0022-1694(02)00283-4.

Dudgeon, D. (2000), Large-Scale Hydrological Changes in Tropical Asia: Prospects for Riverine Biodiversity, *BioScience*, *50*(9), 793–806, doi:10.1641/0006-3568(2000)050[0793:LSHCIT]2.0.CO;2.

Elsawwaf, M., P. Willems, and J. Feyen (2010), Assessment of the sensitivity and prediction uncertainty of evaporation models applied to Nasser Lake, Egypt, *Journal of Hydrology*, *395*(1–2), 10–22, doi:10.1016/j.jhydrol.2010.10.002.

Engelund, F., and E. Hansen (1967), A monograph on sediment transport in alluvial streams, *Tech. rep.*, TEKNISKFORLAG Skelbrekgade 4 Copenhagen V, Denmark.

Evans, J. E., S. D. Mackey, J. F. Gottgens, and W. M. Gill (2000), Lessons from a dam failure, *The Ohio Journal of Science*, *5*, 121–131.

Fan, H., D. He, and H. Wang (2015), Environmental consequences of damming the mainstream Lancang-Mekong River: A review, *Earth-Science Reviews*, *146*, 77–91, doi:10.1016/j.earscirev.2015.03.007.

Fekete, B. M., B. A. Tucker, and C. J. Vorosmarty (1998), GLOBAL RIVER DISCHARGE, 1807-1991, V. 1.1 (RIVDIS), *Tech. rep.*

Ferguson, R. I., M. Church, C. D. Rennie, and J. G. Venditti (2015), Reconstructing a sediment pulse: Modeling the effect of placer mining on Fraser River, Canada, *Journal of Geophysical Research: Earth Surface*, *120*(7), 1436–1454, doi:10.1002/2015JF003491.

Ferrari, R. L. (2008), 2001 Lake Mead Sedimentation Survey, *Tech. rep.*, U.S. Bureau of Reclamation, Denver, Colorado.

Fromaget, J. (1971), Geological Map Viêt-Nam Kampuchia Làò, 1:2000000, 3rd Edition.

Fryirs, K. (2013), (Dis)Connectivity in catchment sediment cascades: A fresh look at the sediment delivery problem, *Earth Surface Processes and Landforms*, *38*(1), 30–46, doi:10.1002/esp.3242.

Fryirs, K., and G. J. Brierley (2001), Variability in sediment delivery and storage along river courses in Bega catchment, NSW, Australia: Implications for geomorphic river recovery, *Geomorphology*, *38*(3–4), 237–265, doi:10.1016/S0169-555X(00)00093-3.

Fryirs, K. A., G. J. Brierley, N. J. Preston, and J. Spencer (2007a), Catchment-scale (dis)connectivity in sediment flux in the upper Hunter catchment, New South Wales, Australia, *Geomorphology*, *84*(3–4), 297–316, doi:10.1016/j.geomorph.2006.01.044.

Fryirs, K. A., G. J. Brierley, N. J. Preston, and M. Kasai (2007b), Buffers, barriers and blankets: The (dis)connectivity of catchment-scale sediment cascades, *CATENA*, *70*(1), 49–67, doi:10.1016/j.catena.2006.07.007.

Fryirs, K. A., J. M. Wheaton, and G. J. Brierley (2016), An approach for measuring confinement and assessing the influence of valley setting on river forms and processes, *Earth Surface Processes and Landforms*, pp. n/a–n/a, doi:10.1002/esp.3893.

Gallup, J. L., J. D. Sachs, and A. D. Mellinger (1999), Geography and economic development, *International regional science review*, *22*(2), 179–232.

Gatto, M., L. Mari, E. Bertuzzo, R. Casagrandi, L. Righetto, I. Rodriguez-Iturbe, and A. Rinaldo (2013), Spatially Explicit Conditions for Waterborne Pathogen Invasion, *American Naturalist*, *182*(3), 328–346, doi:10.1086/671258.

Gilvear, D., and R. Bryant (2016), Analysis of remotely sensed data for fluvial geomorphology and river science, in *Tools in Fluvial Geomorphology*, edited by G. M. Kondolf and H. Piégay, 2 ed., J. Wiley, Hoboken, NJ, USA, oCLC: 57600569.

Gilvear, D. J., C. J. Spray, and R. Casas-Mulet (2013), River rehabilitation for the delivery of multiple ecosystem services at the river network scale, *Journal of Environmental Management*, *126*, 30–43, doi:10.1016/j.jenvman.2013.03.026.

Giuliani, M., J. D. Herman, A. Castelletti, and P. Reed (2014), Many-objective reservoir policy identification and refinement to reduce policy inertia and myopia in water management, *Water Resources Research*, *50*(4), 3355–3377, doi:10.1002/2013WR014700.

Gran, K. B., and J. A. Czuba (2015), Sediment pulse evolution and the role of network structure, *Geomorphology*, doi:10.1016/j.geomorph.2015.12.015.

Grant, G. E., J. C. Schmidt, and S. L. Lewis (2003), A geological framework for interpreting downstream effects of dams on rivers, *A peculiar river*, pp. 203–219.

Green, N., B. K. Sovacool, and K. Hancock (2015), Grand Designs: Assessing the African Energy Security Implications of the Grand Inga Dam, *African Studies Review*, *58*(1), 133–158.

Gren, I.-M., K.-H. Groth, and M. Sylvén (1995), Economic Values of Danube Floodplains, *Journal of Environmental Management*, *45*(4), 333–345, doi:10.1006/jema.1995.0080.

Grill, G., B. Lehner, A. E. Lumsdon, G. K. MacDonald, C. Zarfl, and C. Reidy Liermann (2015), An index-based framework for assessing patterns and trends in river fragmentation and flow regulation by global dams at multiple scales, *Environmental Research Letters*, *10*(1), 015,001, doi:10.1088/1748-9326/10/1/015001.

Grumbine, R. E., and J. Xu (2011), Mekong Hydropower Development, *Science*, *332*(6026), 178–179, doi:10.1126/science.1200990.

Grumbine, R. E., J. Dore, and J. Xu (2012), Mekong hydropower: Drivers of change and governance challenges, *Frontiers in Ecology and the Environment*, *10*(2), 91–98, doi:10.1890/110146.

Habersack, H., D. Haspel, and M. Kondolf (2014), Large Rivers in the Anthropocene: Insights and tools for understanding climatic, land use, and reservoir influences, *Water Resources Research*, *50*(5), 3641–3646, doi:10.1002/2013WR014731.

He, D., J. Liu, J. Hu, Y. Fen, and S. Gan (2007), Transboundary eco-security and its regulation system in the Longitudinal Range-Gorge Region, *Chinese Science Bulletin*, *52*(2), 1, doi:10.1007/s11434-007-7001-9.

Heckmann, T., and W. Schwanghart (2013), Geomorphic coupling and sediment connectivity in an alpine catchment — Exploring sediment cascades using graph theory, *Geomorphology*, *182*, 89–103, doi:10.1016/j.geomorph.2012.10.033.

Heckmann, T., W. Schwanghart, and J. D. Phillips (2015), Graph theory—Recent developments of its application in geomorphology, *Geomorphology*, *243*, 130–146, doi:10.1016/j.geomorph.2014.12.024.

Hennig, T. (2016), Damming the transnational Ayeyarwady basin. Hydropower and the water-energy nexus, *Renewable and Sustainable Energy Reviews*, *65*, 1232–1246, doi:10.1016/j.rser.2016.07.048.

Hering, D., A. Borja, J. Carstensen, L. Carvalho, M. Elliott, C. K. Feld, A.-S. Heiskanen, R. K. Johnson, J. Moe, D. Pont, A. L. Solheim, and W. van de Bund (2010), The European Water Framework Directive at the age of 10: A critical review of the achievements with recommendations for the future, *Science of the Total Environment*, *408*(19), 4007–4019, doi:10.1016/j.scitotenv.2010.05.031.

Hirsch, P., and A. Wyatt (2004), Negotiating local livelihoods: Scales of conflict in the Se San River Basin, *Asia Pacific Viewpoint*, *45*(1), 51–68, doi:10.1111/j.1467-8376.2004.00227.x.

Hoff, H. (2011), Understanding the Nexus. Background Paper for the Bonn2011 Conference: The Water, Energy and Food Security Nexus.

Hooke, J. (2003), Coarse sediment connectivity in river channel systems: A conceptual framework and methodology, *Geomorphology*, *56*(1–2), 79–94, doi:10.1016/S0169-555X(03)00047-3.

Horner, G. J., P. J. Baker, R. M. Nally, S. C. Cunningham, J. R. Thomson, and F. Hamilton (2010), Forest structure, habitat and carbon benefits from thinning floodplain forests: Managing early stand density makes a difference, *Forest Ecology and Management*, *259*(3), 286–293, doi:10.1016/j.foreco.2009.10.015.

Hsu, S., and F. J. Holly (1992), Conceptual Bed-Load Transport Model and Verification for Sediment Mixtures, *Journal of Hydraulic Engineering*, *118*(8), 1135–1152, doi:10.1061/(ASCE)0733-9429(1992)118:8(1135).

Huang, H. Q., G. C. Nanson, and S. D. Fagan (2002), Hydraulic geometry of straight alluvial channels and the principle of least action, *Journal of Hydraulic Research*, *40*(2), 153–160, doi:10.1080/00221680209499858.

Imhof, A. (2005), Making smart choices for the Mekong, *World Rivers Review*, *20*(5).

Jager, H. I., and B. T. Smith (2008), Sustainable reservoir operation: Can we generate hydropower and preserve ecosystem values?, *River Research and Applications*, *24*(3), 340–352, doi:10.1002/rra.1069.

Jager, H. I., R. A. Efroymson, J. J. Opperman, and M. R. Kelly (2015), Spatial design principles for sustainable hydropower development in river basins, *Renewable and Sustainable Energy Reviews*, *45*, 808–816, doi:10.1016/j.rser.2015.01.067.

Jain, V., and S. K. Tandon (2010), Conceptual assessment of (dis)connectivity and its application to the Ganga River dispersal system, *Geomorphology*, *118*(3–4), 349–358, doi:10.1016/j.geomorph.2010.02.002.

James, L. D. (2015), *Man and Water: The Social Sciences in Management of Water Resources*, University Press of Kentucky, google-Books-ID: heQeBgAAQBAJ.

Jansen, R. B. (1980), *Dams and Public Safety*, U.S. Department of the Interior, Water and Power Resources Service, Denver, Colorado, oCLC: 6478545.

Kareiva, P. M. (2012), Dam choices: Analyses for multiple needs, *Proceedings of the National Academy of Sciences of the United States of America*, *109*(15), 5553–5554, doi:10.1073/pnas.1203263109.

Kaygusuz, K. (2009), The Role of Hydropower for Sustainable Energy Development, *Energy Sources, Part B: Economics, Planning, and Policy*, *4*(4), 365–376, doi:10.1080/15567240701756889.

Kennedy, T. A., J. D. Muehlbauer, C. B. Yackulic, D. A. Lytle, S. W. Miller, K. L. Dibble, E. W. Kortenhoeven, A. N. Metcalfe, and C. V. Baxter (2016), Flow Management for Hydropower Extirpates Aquatic Insects, Undermining River Food Webs, *BioScience*, *66*(7), 561–575, doi:10.1093/biosci/biw059.

Khaliquzzaman, and S. Chander (1997), Network Flow Programming Model for Multireservoir Sizing, *Journal of Water Resources Planning and Management*, *123*(1), 15–25, doi:10.1061/(ASCE)0733-9496(1997)123:1(15).

Kirchner, J. W., W. E. Dietrich, F. Iseya, and H. Ikeda (1990), The variability of critical shear stress, friction angle, and grain protrusion in water-worked sediments, *Sedimentology*, *37*(4), 647–672, doi:10.1111/j.1365-3091.1990.tb00627.x.

Knighton, D. (1984), *Fluvial Forms and Processes*, E. Arnold, London; Baltimore, Md., U.S.A.

Koehnken, L. (2012a), Discharge and Sediment Monitoring Program – Program Review & Data Analysis. Part 1: Program Review & Recommendations, *Tech. rep.*, Mekong River Commission, Vientiane, Laos PDR.

Koehnken, L. (2012b), IKMP Discharge and Sediment Monitoring Program Review, Recommendations and Data Analysis Part 2: Data analysis of preliminary results, *Tech. rep.*, Mekong River Commission, Vientiane, Lao PDR.

Kondolf, G. M. (1997), PROFILE: Hungry water: Effects of dams and gravel mining on river channels, *Environmental management*, *21*(4), 533–551.

Kondolf, G. M. (2000), Assessing Salmonid Spawning Gravel Quality, *Transactions of the American Fisheries Society*, *129*(1), 262–281, doi:10.1577/1548-8659(2000)129<0262:ASSGQ>2.0.CO;2.

Kondolf, G. M., and W. V. G. Matthews (1991), Unmeasured Residuals in Sediment Budgets: A Cautionary Note, *Water Resources Research*, *27*(9), 2483–2486, doi:10.1029/91WR01625.

Kondolf, G. M., Z. K. Rubin, and J. T. Minear (2014), Dams on the Mekong: Cumulative sediment starvation, *Water Resources Research*, *50*(6), 5158–5169, doi:10.1002/2013WR014651.

Kondolf, M. G. (1994), Geomorphic and environmental effects of instream gravel mining, *Landscape and Urban Planning*, *28*(2–3), 225–243, doi:10.1016/0169-2046(94)90010-8.

Kuby, M. J., W. F. Fagan, C. S. ReVelle, and W. L. Graf (2005), A multiobjective optimization model for dam removal: An example trading off salmon passage with hydropower and water storage in the Willamette basin, *Advances in Water Resources*, *28*(8), 845–855, doi:10.1016/j.advwatres.2004.12.015.

Kummu, M., X. X. Lu, J. J. Wang, and O. Varis (2010), Basin-wide sediment trapping efficiency of emerging reservoirs along the Mekong, *Geomorphology*, *119*(3–4), 181–197, doi:10.1016/j.geomorph.2010.03.018.

Lall, U., and C. W. Miller (1988), An optimization model for screening multipurpose reservoir systems, *Water Resources Research*, *24*(7), 953–968, doi:10.1029/WR024i007p00953.

Lamb, M. P., W. E. Dietrich, and J. G. Venditti (2008), Is the critical Shields stress for incipient sediment motion dependent on channel-bed slope?, *Journal of Geophysical Research: Earth Surface*, *113*(F2), F02,008, doi:10.1029/2007JF000831.

Lane, S. N., S. C. Reid, V. Tayefi, D. Yu, and R. J. Hardy (2008), Reconceptualising coarse sediment delivery problems in rivers as catchment-scale and diffuse, *Geomorphology*, *98*(3–4), 227–249, doi:10.1016/j.geomorph.2006.12.028.

Larinier, M. (2001), Environmental Issues, Dams and Fish Migration, in *Dams, Fish and Fisheries: Opportunities, Challenges and Conflict Resolution*, edited by G. Marmulla, pp. 45–91, Food & Agriculture Organization, Rome, google-Books-ID: JpIO_ijVlWcC.

Le, T. P. Q., J. Garnier, B. Gilles, T. Sylvain, and C. Van Minh (2007), The changing flow regime and sediment load of the Red River, Viet Nam, *Journal of Hydrology*, *334*(1–2), 199–214, doi: 10.1016/j.jhydrol.2006.10.020.

Lehner, B., K. Verdin, and A. Jarvis (2008), New Global Hydrography Derived From Spaceborne Elevation Data, *Eos, Transactions American Geophysical Union*, *89*(10), 93–94, doi: 10.1029/2008EO100001.

Lehner, B., C. R. Liermann, C. Revenga, C. Vörösmarty, B. Fekete, P. Crouzet, P. Döll, M. Endejan, K. Frenken, J. Magome, and others (2011), High-resolution mapping of the world's reservoirs and dams for sustainable river-flow management, *Frontiers in Ecology and the Environment*, *9*(9), 494–502.

Lenzi, M. A., L. Mao, and F. Comiti (2003), Interannual variation of suspended sediment load and sediment yield in an alpine catchment, *Hydrological Sciences Journal*, *48*(6), 899–915, doi:10.1623/hysj.48.6.899.51425.

Lepvrier, C., N. Van Vuong, H. Maluski, P. Truong Thi, and T. Van Vu (2008), Indosinian tectonics in Vietnam, *Comptes Rendus Geoscience*, *340*(2–3), 94–111, doi:10.1016/j.crte.2007.10.005.

Ligon, F. K., W. E. Dietrich, and W. J. Trush (1995), Downstream Ecological Effects of Dams, *BioScience*, *45*(3), 183–192, doi:10.2307/1312557.

Linde, N., P. Renard, T. Mukerji, and J. Caers (2015), Geological realism in hydrogeological and geophysical inverse modeling: A review, *Advances in Water Resources*, *86, Part A*, 86–101, doi: 10.1016/j.advwatres.2015.09.019.

Liu, J., C. Zang, S. Tian, J. Liu, H. Yang, S. Jia, L. You, B. Liu, and M. Zhang (2013), Water conservancy projects in China: Achievements, challenges and way forward, *Global Environmental Change*, *23*(3), 633–643, doi:10.1016/j.gloenvcha.2013.02.002.

Liu, J. G., P. J. Mason, N. Clerici, S. Chen, A. Davis, F. Miao, H. Deng, and L. Liang (2004), Landslide hazard assessment in the Three Gorges area of the Yangtze river using ASTER imagery: Zigui–Badong, *Geomorphology*, *61*(1–2), 171–187, doi:10.1016/j.geomorph.2003.12.004.

Loucks, D., E. Stakhiv, and L. Martin (2000), SUSTAINABLE WATER RESOURCES MANAGEMENT, *Journal of Water Resources Planning and Management*, *126*(2), 43–47, doi:10.1061/(ASCE)0733-9496(2000)126:2(43).

Lu, X., M. Kummu, and C. Oeurng (2014), Reappraisal of sediment dynamics in the Lower Mekong River, Cambodia, *Earth Surface Processes and Landforms*, *39*(14), 1855–1865, doi:10.1002/esp.3573.

Lu, X. X., S. R. Zhang, S. P. Xie, and P. K. Ma (2007), Rapid channel incision of the lower Pearl River (China) since the 1990s as a consequence of sediment depletion, *Hydrol. Earth Syst. Sci.*, *11*(6), 1897–1906, doi:10.5194/hess-11-1897-2007.

Mendoza, G. A., and H. Martins (2006), Multi-criteria decision analysis in natural resource management: A critical review of methods and new modelling paradigms, *Forest Ecology and Management*, *230*(1–3), 1–22, doi:10.1016/j.foreco.2006.03.023.

Menting, F., A. L. Langston, and A. J. A. M. Temme (2015), Downstream fining, selective transport, and hillslope influence on channel bed sediment in mountain streams, Colorado Front Range, USA, *Geomorphology*, *239*, 91–105, doi:10.1016/j.geomorph.2015.03.018.

Merritt, W. S., R. A. Letcher, and A. J. Jakeman (2003), A review of erosion and sediment transport models, *Environmental Modelling & Software*, *18*(8–9), 761–799, doi:10.1016/S1364-8152(03)00078-1.

Meybeck, M. (2003), Global analysis of river systems: From Earth system controls to Anthropocene syndromes, *Philosophical Transactions of the Royal Society B: Biological Sciences*, *358*(1440), 1935–1955, doi:10.1098/rstb.2003.1379.

Meybeck, M., and C. Vörösmarty (2005), Fluvial filtering of land-to-ocean fluxes: From natural Holocene variations to Anthropocene, *Comptes Rendus Geoscience*, *337*(1–2), 107–123, doi:10.1016/j.crte.2004.09.016.

Millennium Ecosystem Assessment (2005), *Ecosystems and Human Well-Being: Synthesis*, Island Press, Washington, DC, oCLC: 59279709.

Milliman, J. D., and K. L. Farnsworth (2013), *River Discharge to the Coastal Ocean: A Global Synthesis*, Cambridge University Press, google-Books-ID: GWymw0PtH1MC.

Milliman, J. D., and R. H. Meade (1983), World-Wide Delivery of River Sediment to the Oceans, *Journal of Geology*, *91*, 1–21, doi:10.1086/628741.

Minear, J. T., and G. M. Kondolf (2009), Estimating reservoir sedimentation rates at large spatial and temporal scales: A case study of California, *Water Resources Research*, *45*(12), W12,502, doi:10.1029/2007WR006703.

Minot, N., and F. Goletti (1998), Export Liberalization and Household Welfare: The Case of Rice in Vietnam, *American Journal of Agricultural Economics*, *80*(4), 738–749, doi:10.2307/1244060.

Molinas, A., and B. Wu (2000), Comparison of fractional bed-material load computation methods in sand-bed channels, *Earth Surface Processes and Landforms*, *25*(10), 1045–1068, doi:10.1002/1096-9837(200009)25:10<1045::AID-ESP115>3.0.CO;2-X.

Montgomery, D. R., and J. M. Buffington (1997), Channel-reach morphology in mountain drainage basins, *Geological Society of America Bulletin*, *109*(5), 596–611, doi:10.1130/0016-7606(1997)109<0596:CRMIMD>2.3.CO;2.

Morris, G. L., and J. Fan (1998), *Reservoir Sedimentation Handbook: Design and Management of Dams, Reservoirs, and Watersheds for Sustainable Use*, McGraw-Hill, New York, oCLC: 36241652.

Mosegaard, K., and A. Tarantola (2002), 16 - Probabilistic Approach to Inverse Problems, in *International Geophysics*, *International Handbook of Earthquake and Engineering Seismology, Part A*, vol. 81, Part A, edited by P. C. J. William H.K. Lee and H. K. Carl Kisslinger, pp. 237–265, Academic Press.

Mousavi, H., and A. S. Ramamurthy (2000), Optimal design of multi-reservoir systems for water supply, *Advances in Water Resources*, *23*(6), 613–624, doi:10.1016/S0309-1708(99)00053-6.

MRC (2010), State of the Basin Report 2010., *Tech. rep.*, Mekong River Commission,, Vientiane, Lao PDR.

Mueller, E. R., and J. Pitlick (2013), Sediment supply and channel morphology in mountain river systems: 1. Relative importance of lithology, topography, and climate, *Journal of Geophysical Research: Earth Surface*, *118*(4), 2013JF002,843, doi:10.1002/2013JF002843.

Mueller, E. R., M. E. Smith, and J. Pitlick (2016), Lithology-controlled evolution of stream bed sediment and basin-scale sediment yields in adjacent mountain watersheds, Idaho, USA, *Earth Surface Processes and Landforms*, pp. n/a–n/a, doi:10.1002/esp.3955.

Mussgnug, F., M. Becker, T. T. Son, R. J. Buresh, and P. L. G. Vlek (2006), Yield gaps and nutrient balances in intensive, rice-based cropping systems on degraded soils in the Red River Delta of Vietnam, *Field Crops Research*, *98*(2–3), 127–140, doi:10.1016/j.fcr.2005.12.012.

Nittrouer, J. A., and E. Viparelli (2014), Sand as a stable and sustainable resource for nourishing the Mississippi River delta, *Nature Geoscience*, *7*(5), 350–354, doi:10.1038/ngeo2142.

OECD (2016), Economic Outlook for Southeast Asia, China and India 2016, *Tech. rep.*, OECD.

Opperman, J. J., G. Grill, and J. Hartmann (2015), The Power of Rivers: Finding balance between energy and conservation in hydropower development., *Tech. rep.*, The Nature Conservancy, Washington, DC.

Orr, S., J. Pittock, A. Chapagain, and D. Dumaresq (2012), Dams on the Mekong River: Lost fish protein and the implications for land and water resources, *Global Environmental Change*, *22*(4), 925–932, doi:10.1016/j.gloenvcha.2012.06.002.

Pahl-Wostl, C. (2007), The implications of complexity for integrated resources management, *Environmental Modelling & Software*, *22*(5), 561–569, doi:10.1016/j.envsoft.2005.12.024.

Palmer, M. A. (2010), Water resources: Beyond infrastructure, *Nature*, *467*(7315), 534–535, doi:10.1038/467534a.

Palmer, M. A., C. A. R. Liermann, C. Nilsson, M. Floerke, J. Alcamo, P. S. Lake, and N. Bond (2008), Climate change and the world's river basins: Anticipating management options, *Frontiers in Ecology and the Environment*, *6*(2), 81–89, doi:10.1890/060148.

Palmieri, A., F. Shah, and A. Dinar (2001), Economics of reservoir sedimentation and sustainable management of dams, *Journal of Environmental Management*, *61*(2), 149–163, doi:10.1006/jema.2000.0392.

Palmieri, A., F. Shah, G. W. Annandale, and A. Dinar (2003), Reservoir Conservation Volume I: The RESCON Approach, economic and engineering evaluation of alternative strategies for managing sedimentation in storage reservoirs, A contribution to promote conservation of water storage assets worldwide, *Tech. Rep. 34954*, Int. Bank for Reconstruction and Dev./The World Bank.

Panagos, P., A. Jones, C. Bosco, and P. S. S. Kumar (2011), European digital archive on soil maps (EuDASM): Preserving important soil data for public free access, *International Journal of Digital Earth*, *4*(5), 434–443, doi:10.1080/17538947.2011.596580.

Paola, C., P. L. Heller, and C. L. Angevine (1992), The large-scale dynamics of grain-size variation in alluvial basins, 1: Theory, *Basin Research*, *4*(2), 73–90.

Parker, C., C. R. Thorne, and N. J. Clifford (2015), Development of ST:REAM: A reach-based stream power balance approach for predicting alluvial river channel adjustment, *Earth Surface Processes and Landforms*, *40*(3), 403–413, doi:10.1002/esp.3641.

Parker, G. (1991), Selective Sorting and Abrasion of River Gravel. I: Theory, *Journal of Hydraulic Engineering*, *117*(2), 131–147, doi:10.1061/(ASCE)0733-9429(1991)117:2(131).

Parker, G., and C. M. Toro-Escobar (2002), Equal mobility of gravel in streams: The remains of the day, *Water Resources Research*, *38*(11), 1264, doi:10.1029/2001WR000669.

Parker, G., C. M. Tore-Escoba, M. Ramey, and S. Beck (2003), Effect of Floodwater extraction on mountain stream morphology, *Journal of hydraulic engineering*, *129*(11), 885–895.

Parsons, A. J., L. Bracken, R. E. Poeppl, J. Wainwright, and S. D. Keesstra (2015), Introduction to special issue on connectivity in water and sediment dynamics, *Earth Surface Processes and Landforms*, *40*(9), 1275–1277, doi:10.1002/esp.3714.

Patil, S., M. Sivapalan, M. A. Hassan, S. Ye, C. J. Harman, and X. Xu (2012), A network model for prediction and diagnosis of sediment dynamics at the watershed scale, *Journal of Geophysical Research: Earth Surface*, *117*(F4), F00A04, doi:10.1029/2012JF002400.

Patskoski, J., and A. Sankarasubramanian (2015), Improved reservoir sizing utilizing observed and reconstructed streamflows within a Bayesian combination framework, *Water Resources Research*, *51*(7), 5677–5697, doi:10.1002/2014WR016189.

Paulsen, C. M., and K. Wernstedt (1995), Cost-Effectiveness Analysis for Complex Managed Hydrosystems: An Application to the Columbia River Basin, *Journal of Environmental Economics and Management*, *28*(3), 388–400, doi:10.1006/jeem.1995.1025.

Pickup, G., and A. Marks (2001), Regional-scale sedimentation process models from airborne gamma ray remote sensing and digital elevation data, *Earth Surface Processes and Landforms*, *26*(3), 273–293, doi:10.1002/1096-9837(200103)26:3<273::AID-ESP150>3.0.CO;2-\#.

Pilarczyk, K. W., and N. S. Nuoi (2005), Experience and Practices on Flood Control in Vietnam, *Water International*, *30*(1), 114–122, doi:10.1080/02508060508691843.

Piman, T., T. A. Cochrane, M. E. Arias, A. Green, and N. D. Dat (2013), Assessment of Flow Changes from Hydropower Development and Operations in Sekong, Sesan, and Srepok Rivers of the Mekong Basin, *Journal of Water Resources Planning and Management*, *139*(6), 723–732, doi:10.1061/(ASCE)WR.1943-5452.0000286.

Piman, T., T. A. Cochrane, and M. E. Arias (2016), Effect of Proposed Large Dams on Water Flows and Hydropower Production in the Sekong, Sesan and Srepok Rivers of the Mekong Basin, *River Research and Applications*, pp. n/a–n/a, doi:10.1002/rra.3045.

Pinto, L., A. B. Fortunato, and P. Freire (2006), Sensitivity analysis of non-cohesive sediment transport formulae, *Continental Shelf Research*, *26*(15), 1826–1839, doi:10.1016/j.csr.2006.06.001.

Poff, N. L., and J. C. Schmidt (2016), How dams can go with the flow, *Science*, *353*(6304), 1099–1100, doi:10.1126/science.aah4926.

Ranzi, R., T. H. Le, and M. C. Rulli (2012), A RUSLE approach to model suspended sediment load in the Lo river (Vietnam): Effects of reservoirs and land use changes, *Journal of Hydrology*, *422-423*, 17–29, doi:10.1016/j.jhydrol.2011.12.009.

Refsgaard, J. C., J. P. van der Sluijs, A. L. Højberg, and P. A. Vanrolleghem (2007), Uncertainty in the environmental modelling process–a framework and guidance, *Environmental modelling & software*, *22*(11), 1543–1556.

Reid, H. E., and G. J. Brierley (2015), Assessing geomorphic sensitivity in relation to river capacity for adjustment, *Geomorphology*, *251*, 108–121, doi:10.1016/j.geomorph.2015.09.009.

Rice, S. (1998), Which tributaries disrupt downstream fining along gravel-bed rivers?, *Geomorphology*, *22*(1), 39–56, doi:10.1016/S0169-555X(97)00052-4.

Rice, S. P., R. I. Ferguson, and T. B. Hoey (2006), Tributary control of physical heterogeneity and biological diversity at river confluences, *Canadian Journal of Fisheries and Aquatic Sciences*, *63*(11), 2553–2566.

Rice, S. P., P. Kiffney, C. Greene, and G. R. Pess (2008), The Ecological Importance of Tributaries and Confluences, in *River Confluences, Tributaries and the Fluvial Network*, edited by S. P. Rice, A. G. Roy, and B. L. Rhoads, pp. 209–242, John Wiley & Sons, Ltd.

Richter, B. D., S. Postel, C. Revenga, T. Scudder, B. Lehner, A. Churchill, and M. Chow (2010), Lost in development's shadow: The downstream human consequences of dams, *Water Alternatives*, *3*(2), 14.

Riebe, C. S., L. S. Sklar, C. E. Lukens, and D. L. Shuster (2015), Climate and topography control the size and flux of sediment produced on steep mountain slopes, *Proceedings of the National Academy of Sciences*, *112*(51), 15,574–15,579, doi:10.1073/pnas.1503567112.

Ries, J. B., and I. Marzolff (1997), Identification of sediment sources by large-scale aerial photography taken from a monitoring blimp, *Physics and Chemistry of the Earth*, *22*(3), 295–302, doi:10.1016/S0079-1946(97)00147-X.

Rinaldi, M., B. Wyżga, and N. Surian (2005), Sediment mining in alluvial channels: Physical effects and management perspectives, *River Research and Applications*, *21*(7), 805–828, doi:10.1002/rra.884.

Rinaldo, A., G. Botter, E. Bertuzzo, A. Uccelli, T. Settin, and M. Marani (2006), Transport at basin scales: 2. Applications, *Hydrol. Earth Syst. Sci.*, *10*(1), 31–48, doi:10.5194/hess-10-31-2006.

Rosenberg, D. M., F. Berkes, R. A. Bodaly, R. E. Hecky, C. A. Kelly, and J. W. Rudd (1997), Large-scale impacts of hydroelectric development, *Environmental Reviews*, *5*(1), 27–54, doi:10.1139/a97-001.

Rubin, Z. K., G. M. Kondolf, and P. A. Carling (2015), Anticipated geomorphic impacts from Mekong basin dam construction, *International Journal of River Basin Management*, *13*(1), 105–121, doi:10.1080/15715124.2014.981193.

Sambridge, M., and K. Mosegaard (2002), Monte Carlo Methods in Geophysical Inverse Problems, *Reviews of Geophysics*, *40*(3), 1009, doi:10.1029/2000RG000089.

Schleiss, A., G. De Cesare, and J. Jenzer Althaus (2010), Verlandung der Stauseen gefährdet die nachhaltige Nutzung der Wasserkraft, *Wasser, Energie, Luft / Eau, énergie, air*, *102*(1), 31–40.

Schmidt, J. C., and P. R. Wilcock (2008), Metrics for assessing the downstream effects of dams: METRICS FOR ASSESSING EFFECTS OF DAMS, *Water Resources Research*, *44*(4), n/a–n/a, doi:10.1029/2006WR005092.

Schmitt, R., S. Bizzi, and A. Castelletti (2014), Characterizing fluvial systems at basin scale by fuzzy signatures of hydromorphological drivers in data scarce environments, *Geomorphology*, *214*, 69–83, doi:10.1016/j.geomorph.2014.02.024.

Schmitt, R. J. P., S. Bizzi, and A. Castelletti (2016), Tracking multiple sediment cascades at the river network scale identifies controls and emerging patterns of sediment connectivity, *Water Resources Research*, pp. 3941–3965, doi:10.1002/2015WR018097.

Schwanghart, W., and N. J. Kuhn (2010), TopoToolbox: A set of Matlab functions for topographic analysis, *Environmental Modelling & Software*, *25*(6), 770–781, doi:10.1016/j.envsoft.2009.12.002.

Shields, A. (1936), *Anwendung der Ähnlichkeitsmechanik und der Turbulenzforschung auf die Geschiebebewegung*, Eigenverl. der Preußischen Versuchsanst. für Wasserbau und Schiff.

Sholtes, J. S., and M. W. Doyle (2011), Effect of Channel Restoration on Flood Wave Attenuation, *Journal of Hydraulic Engineering*, *137*(2), 196–208, doi:10.1061/(ASCE)HY.1943-7900.0000294.

Showers, K. B. (2011), Beyond Mega on a Mega Continent: Grand Inga on Central Africa's Congo River, in *Engineering Earth*, edited by S. D. Brunn, pp. 1651–1679, Springer Netherlands, doi:10.1007/978-90-481-9920-4_95.

Simpson, A. (2007), The environment – Energy security nexus: Critical analysis of an energy 'love triangle' in Southeast Asia, *Third World Quarterly*, *28*(3), 539–554, doi:10.1080/01436590701192710.

Sivapragasam, C., G. Vasudevan, J. Maran, C. Bose, S. Kaza, and N. Ganesh (2008), Modeling Evaporation-Seepage Losses for Reservoir Water Balance in Semi-arid Regions, *Water Resources Management*, *23*(5), 853, doi:10.1007/s11269-008-9303-3.

Sklar, L. S., and W. E. Dietrich (2001), Sediment and rock strength controls on river incision into bedrock, *Geology*, *29*(12), 1087–1090.

Sklar, L. S., W. E. Dietrich, E. Foufoula-Georgiou, B. Lashermes, and D. Bellugi (2006), Do gravel bed river size distributions record channel network structure?, *Water Resources Research*, *42*(6), W06D18, doi:10.1029/2006WR005035.

Sklar, L. S., C. S. Riebe, J. A. Marshall, J. Genetti, S. Leclere, C. L. Lukens, and V. Merces (2016), The problem of predicting the size distribution of sediment supplied by hillslopes to rivers, *Geomorphology*, doi:10.1016/j.geomorph.2016.05.005.

Slaets, J. I. F., H.-P. Piepho, P. Schmitter, T. Hilger, and G. Cadisch (2016), Quantifying uncertainty on sediment loads using bootstrap confidence intervals, *Hydrology and Earth System Sciences Discussions*, pp. 1–32, doi:10.5194/hess-2016-264.

Stone, R. (2011), Mayhem on the Mekong, *Science*, *333*(6044), 814–818, doi:10.1126/science.333.6044.814.

Strickler, A. (1923), *Beiträge Zur Frage Der Geschwindigkeitsformel Und Der Rauhigkeitszahlen Für Ströme, Kanäle Und Geschlossene Leitungen. Mitteilungen Des Amtes Für Wasserwirtschaft.*, Eidg. Amt für Wasserwirtschaft, Bern.

Suszka, L. (1991), Modification of transport rate formula for steep channels, in *Fluvial Hydraulics of Mountain Regions*, edited by P. A. Armanini and P. G. D. Silvio, no. 37 in Lecture Notes in Earth Sciences, pp. 59–70, Springer Berlin Heidelberg.

Sutherland, A. J. (1987), Armouring Processes, in *Sediment Transport in Gravel-Bed Rivers*, edited by C. R. Thorne, J. C. Bathurst, and R. D. Hey, pp. 243–269, J. Wiley, Chichester and New York.

Syvitski, J. P. M. (2009), Sinking Deltas due to Human Activities, *Nature Geoscience*, *2*(10), doi:10.1038/ngeo629.

Syvitski, J. P. M., and J. D. Milliman (2007), Geology, Geography, and Humans Battle for Dominance over the Delivery of Fluvial Sediment to the Coastal Ocean, *The Journal of Geology*, *115*(1), 1–19, doi:10.1086/509246.

Syvitski, J. P. M., S. D. Peckham, R. Hilberman, and T. Mulder (2003), Predicting the terrestrial flux of sediment to the global ocean: A planetary perspective, *Sedimentary Geology*, *162*(1–2), 5–24, doi:10.1016/S0037-0738(03)00232-X.

Tandon, S. K., and R. Sinha (2008), Geology of Large River Systems, in *Large Rivers: Geomorphology and Management*, edited by A. Gupta, John Wiley & Sons, West Sussex, UK, google-Books-ID: gXgyHLT_hwIC.

Tarboton, D. G., R. L. Bras, and I. Rodriguez-Iturbe (1991), On the extraction of channel networks from digital elevation data, *Hydrological processes*, *5*(1), 81–100.

Trimble, S. W. (2012), Historical sources and watershed evolution, *Philosophical Transactions of the Royal Society of London A: Mathematical, Physical and Engineering Sciences*, *370*(1966), 2075–2092, doi:10.1098/rsta.2011.0606.

Trimble, S. W., and P. Crosson (2000), U.S. Soil Erosion Rates–Myth and Reality, *Science*, *289*(5477), 248–250, doi:10.1126/science.289.5477.248.

Trush, W. J., S. M. McBain, and L. B. Leopold (2000), Attributes of an alluvial river and their relation to water policy and management, *Proceedings of the National Academy of Sciences*, *97*(22), 11,858–11,863, doi:10.1073/pnas.97.22.11858.

Tucker, G. E., and R. L. Bras (1998), Hillslope processes, drainage density, and landscape morphology, *Water Resources Research*, *34*(10), 2751–2764, doi:10.1029/98WR01474.

Tunnicliffe, J., M. Church, J. J. Clague, and J. K. Feathers (2012), Postglacial sediment budget of Chilliwack Valley, British Columbia, *Earth Surface Processes and Landforms*, *37*(12), 1243–1262, doi:10.1002/esp.3229.

Tunnicliffe, J. F., and M. Church (2011), Scale variation of post-glacial sediment yield in Chilliwack Valley, British Columbia, *Earth Surface Processes and Landforms*, *36*(2), 229–243, doi:10.1002/esp.2093.

Turowski, J. M., D. Rickenmann, and S. J. Dadson (2010), The partitioning of the total sediment load of a river into suspended load and bedload: A review of empirical data, *Sedimentology*, *57*(4), 1126–1146, doi:10.1111/j.1365-3091.2009.01140.x.

UNESCO (2014), *The United Nations World Water Development Report – N° 5 - 2014: Water and Energy – Vol. 1; Facing the Challenges – Vol. 2*, UNESCO.

Vanmaercke, M., J. Poesen, J. Broeckx, and J. Nyssen (2014), Sediment yield in Africa, *Earth-Science Reviews*, *136*, 350–368, doi:10.1016/j.earscirev.2014.06.004.

Vaughan, I., M. Diamond, A. Gurnell, K. Hall, A. Jenkins, N. Milner, L. Naylor, D. Sear, G. Woodward, and S. Ormerod (2009), Integrating ecology with hydromorphology: A priority for river science and management, *Aquatic Conservation: Marine and Freshwater Ecosystems*, *19*(1), 113–125, doi:10.1002/aqc.895.

Venditti, J. G., N. Domarad, M. Church, and C. D. Rennie (2015), The gravel-sand transition: Sediment dynamics in a diffuse extension, *Journal of Geophysical Research: Earth Surface*, *120*(6), 2014JF003,328, doi:10.1002/2014JF003328.

Vinh, V. D., S. Ouillon, T. D. Thanh, and L. V. Chu (2014), Impact of the Hoa Binh dam (Vietnam) on water and sediment budgets in the Red River basin and delta, *Hydrol. Earth Syst. Sci.*, *18*(10), 3987–4005, doi:10.5194/hess-18-3987-2014.

Vogel, R. M. (2011), Hydromorphology, *Journal of Water Resources Planning and Management*, *137*(2), 147–149, doi:10.1061/(ASCE)WR.1943-5452.0000122.

Vörösmarty, C. J., M. Meybeck, B. Fekete, K. Sharma, P. Green, and J. P. Syvitski (2003a), Anthropogenic sediment retention: Major global impact from registered river impoundments, *Global and planetary change*, *39*(1), 169–190.

Vörösmarty, C. J., M. Meybeck, B. Fekete, K. Sharma, P. Green, and J. P. M. Syvitski (2003b), Anthropogenic sediment retention: Major global impact from registered river impoundments, *Global and Planetary Change*, *39*(1–2), 169–190, doi:10.1016/S0921-8181(03)00023-7.

Vörösmarty, C. J., P. B. McIntyre, M. O. Gessner, D. Dudgeon, A. Prusevich, P. Green, S. Glidden, S. E. Bunn, C. A. Sullivan, C. R. Liermann, and P. M. Davies (2010), Global threats to human water security and river biodiversity, *Nature*, *467*(7315), 555–561, doi:10.1038/nature09440.

Walling, D. E. (1977), Assessing the accuracy of suspended sediment rating curves for a small basin, *Water Resources Research*, *13*(3), 531–538, doi:10.1029/WR013i003p00531.

Walling, D. E. (1983), The sediment delivery problem, *Journal of hydrology*, *65*(1), 209–237.

Walling, D. E. (2008), The Changing Sediment Load of the Mekong River, *Ambio*, *37*(3), 150–157.

Walling, D. E., and D. Fang (2003), Recent trends in the suspended sediment loads of the world's rivers, *Global and Planetary Change*, *39*(1–2), 111–126, doi:10.1016/S0921-8181(03)00020-1.

Walling, D. E., and A. J. Horowitz (2005), *Sediment Budgets*, IAHS Press.

Walling, D. E., P. N. Owens, and G. J. L. Leeks (1998), The role of channel and floodplain storage in the suspended sediment budget of the River Ouse, Yorkshire, UK, *Geomorphology*, *22*(3), 225–242, doi:10.1016/S0169-555X(97)00086-X.

Walter, R. C., and D. J. Merritts (2008), Natural Streams and the Legacy of Water-Powered Mills, *Science*, *319*(5861), 299–304, doi:10.1126/science.1151716.

Ward, J. V., and J. A. Stanford (1995), Ecological connectivity in alluvial river ecosystems and its disruption by flow regulation, *Regulated Rivers: Research & Management*, *11*(1), 105–119, doi:10.1002/rrr.3450110109.

Warrick, J. A., J. M. Melack, and B. M. Goodridge (2015), Sediment yields from small, steep coastal watersheds of California, *Journal of Hydrology: Regional Studies*, *4, Part B*, 516–534, doi:10.1016/j.ejrh.2015.08.004.

Wilcock, P. R. (1993), Critical shear stress of natural sediments, *Journal of Hydraulic Engineering*, *119*(4), 491–505.

Wilcock, P. R. (1998), Two-Fraction Model of Initial Sediment Motion in Gravel-Bed Rivers, *Science*, *280*(5362), 410–412, doi:10.1126/science.280.5362.410.

Wilcock, P. R., and J. Crowe (2003), Surface-based Transport Model for Mixed-Size Sediment, *Journal of Hydraulic Engineering*, *129*(2), 120–128, doi:10.1061/(ASCE)0733-9429(2003)129:2(120).

Wild, T. B., and D. P. Loucks (2014), Managing flow, sediment, and hydropower regimes in the Sre Pok, Se San, and Se Kong Rivers of the Mekong basin, *Water Resources Research*, *50*(6), 5141–5157, doi:10.1002/2014WR015457, wild2014.

Wilkinson, S. N., I. P. Prosser, and A. O. Hughes (2006), Predicting the distribution of bed material accumulation using river network sediment budgets, *Water Resources Research*, *42*(10), W10,419, doi:10.1029/2006WR004958.

Willgoose, G., R. L. Bras, and I. Rodriguez-Iturbe (1991), A coupled channel network growth and hillslope evolution model: 1. Theory, *Water Resources Research*, *27*(7), 1671–1684, doi:10.1029/91WR00935.

Williams, J. C., C. S. ReVelle, and S. A. Levin (2005), Spatial attributes and reserve design models: A review, *Environmental Modeling & Assessment*, *10*(3), 163–181, doi:10.1007/s10666-005-9007-5.

Wisser, D., S. Frolking, S. Hagen, and M. F. P. Bierkens (2013), Beyond peak reservoir storage? A global estimate of declining water storage capacity in large reservoirs, *Water Resources Research*, *49*(9), 5732–5739, doi:10.1002/wrcr.20452.

Wohl, E. (2008), Hydrology and Discharge, in *Large Rivers: Geomorphology and Management*, edited by A. Gupta, John Wiley & Sons, West Sussex, UK, google-Books-ID: gXgyHLT_hwIC.

Wolman, M. G., and J. P. Miller (1960), Magnitude and frequency of forces in geomorphic processes, *The Journal of Geology*, pp. 54–74.

Wong, M., and G. Parker (2006), Reanalysis and Correction of Bed-Load Relation of Meyer-Peter and Müller Using Their Own Database, *Journal of Hydraulic Engineering*, *132*(11), 1159–1168, doi:10.1061/(ASCE)0733-9429(2006)132:11(1159).

World Commission on Dams (2000), *Dams and Development: A New Framework for Decision-Making : The Report of the World Commission on Dams.*, Earthscan, London; Sterling, VA, oCLC: 45487858.

Wu, B., A. Molinas, and A. Shu (2003), Fractional transport of sediment mixtures, *International Journal of Sediment Research*, *18*(3), 232–247.

Wyżga, B., J. Zawiejska, and A. Radecki-Pawlik (2015), Impact of channel incision on the hydraulics of flood flows: Examples from Polish Carpathian rivers, *Geomorphology*, doi:10.1016/j.geomorph.2015.05.017.

Xue, Z., J. P. Liu, and Q. Ge (2011), Changes in hydrology and sediment delivery of the Mekong River in the last 50 years: Connection to damming, monsoon, and ENSO, *Earth Surface Processes and Landforms*, *36*(3), 296–308, doi:10.1002/esp.2036.

Yalew, S., A. van Griensven, N. Ray, L. Kokoszkiewicz, and G. D. Betrie (2013), Distributed computation of large scale SWAT models on the Grid, *Environmental Modelling & Software*, *41*, 223–230, doi:10.1016/j.envsoft.2012.08.002.

Yang, S. L., J. D. Milliman, P. Li, and K. Xu (2011), 50,000 dams later: Erosion of the Yangtze River and its delta, *Global and Planetary Change*, *75*(1–2), 14–20, doi:10.1016/j.gloplacha.2010.09.006.

Yin, X.-A., Z.-F. Yang, G. E. Petts, and G. M. Kondolf (2014), A reservoir operating method for riverine ecosystem protection, reservoir sedimentation control and water supply, *Journal of Hydrology*, *512*, 379–387, doi:10.1016/j.jhydrol.2014.02.037.

Young, W. J., J. M. Olley, I. P. Prosser, and R. F. Warner (2001), Relative changes in sediment supply and sediment transport capacity in a bedrock-controlled river, *Water Resources Research*, *37*(12), 3307–3320, doi:10.1029/2001WR000341.

Zaliapin, I., E. Foufoula-Georgiou, and M. Ghil (2010), Transport on river networks: A dynamic tree approach, *Journal of Geophysical Research: Earth Surface*, *115*(F2), F00A15, doi:10.1029/2009JF001281.

Zarfl, C., A. E. Lumsdon, J. Berlekamp, L. Tydecks, and K. Tockner (2014), A global boom in hydropower dam construction, *Aquatic Sciences*, *77*(1), 161–170, doi:10.1007/s00027-014-0377-0.

Zhai, H., B. Cui, B. Hu, and K. Zhang (2010), Prediction of river ecological integrity after cascade hydropower dam construction on the mainstream of rivers in Longitudinal Range-Gorge Region (LRGR), China, *Ecological Engineering*, *36*(4), 361–372, doi:10.1016/j.ecoleng.2009.10.002.

Zheng, P. Q., B. F. Hobbs, and J. F. Koonce (2009), Optimizing multiple dam removals under multiple objectives: Linking tributary habitat and the Lake Erie ecosystem, *Water Resources Research*, *45*(12), W12,417, doi:10.1029/2008WR007589.

Ziv, G., E. Baran, S. Nam, I. Rodríguez-Iturbe, and S. A. Levin (2012), Trading-off fish biodiversity, food security, and hydropower in the Mekong River Basin, *Proceedings of the National Academy of Sciences*, *109*(15), 5609–5614, doi:10.1073/pnas.1201423109.